ISSN 0385-2520

# ROCK MAGNETISM and PALEOGEOPHYSICS

## volume 6

In Memory of the Late
Professor Naoto Kawai (1921-1979)

1979

Published by the
ROCK MAGNETISM AND PALEOGEOPHYSICS RESEARCH GROUP IN JAPAN

Professor Naoto Kawai

(1921.10.31 - 1979.7.3)

# PREFACE

The present volume of ROCK MAGNETISM AND PALEOGEOPHYSICS is dedicated to the late Professor Naoto Kawai who died on July 3, 1979. As is well known, Professor Kawai, with his bright ideas and his dedicated enthusiasm, has been a leading figure in the field of rock magnetism and plaeomagnetism in Japan, as well as in many other branches of earth sciences. Two special articles were prepared by Professors Sasajima and Domen in his memory. We also included a photograph of the late Professor.

Other parts of this volume are presented in the same format as the previous ones. This volume constitutes the annual progress report of the Rock Magnetism and Paleogeophysics Research Group in Japan for the year 1979, and consists of a collection of summaries and extended abstracts of various research works. Many of the reports contain substances which may be changed or revised as the work continues.

Except for the ones written as pure progress reports, the papers in this volume will be published in academic journals in full detail and length. This volume may be referenced, but the readers are requested to quote the full paper once the paper is published in such an academic journal. We hope that this volume is a useful source of advance information of recent works on rock magnetism and paleogeophysics in Japan.

November 1979

Masaru KONO
Editor

CONTENTS

# PROFESSOR NAOTO KAWAI

Dr. Kawai was born in Osaka on October 31, 1921. He learned a spirit of rock magnetism as a student under Dr. Matuyama, Professor of the Imperial University of Kyoto, and graduated from the university in 1945.

In 1929, Dr. Matuyama found the reverse NRM in many basaltic rocks taken from the Eastern Asia and followingly proposed a possibility of the field reversals during the Miocene and Quaternary. Unfortunately, since then no decisively supporting evidence had been appeared until 1951, when Dr. Kawai first mentioned an existence of reverse NRM in the Pleistocene sediments. This result was not merely the first step of worldwide discoveries of the reverse NRM but gave a perfect and strong support to Matsuyama's hypothesis. In discovering a truth, it must be a wonderful succession that a professor proposes a hypothesis and his student experimentally proves it.

In 1955, The Japan Society of Geomagnetism and Geoelectricity awarded the Tanakadate Prize to Dr. Kawai for his prominent contribution to palaeo- and rock magnetism.

Dr. Kawai was a man of full creative power. By a glance of statistical difference between the directions of NRM of granites collected from the northeastern and southwestern Japan, he immediately reached a famous conclusion known as "the bending of the Japanese Island" (1961). At present, this idea has widely been understood in relation to the theory of the plate tectonics.

His ingenious activities have not solely been restricted within the rock magnetism but spread over to the high pressure experiments. It is needless to emphasize here that the invention of the so-called "split-type vessel" made it possible to generate static pressure of 1 Mb in magnitude. Dr. Kawai received the Prize of Japan Academy

for his contributions to the high pressure geophysics in 1973. In the last few years, he has been trying, on the one hand, to clarify the association between the Quaternary climatic changes and frequent geomagnetic reversals using the recent sediments of lakes and oceans in the field of palaeomagnetism, on the other hand, to simulate the planets' interiors such as the cores of the Earth or the Jupiter in the field of high pressure.

It is none other than our deep regret and sorrow that we lost him and his lifeworks were interrupted halfway by his sudden death which happened on July 3, 1979.

We expect, however, that his successors will complete all the investigations which Dr. Kawai had been dreaming to finish up. The way should be the same as that Dr. Kawai had ever accomplished the masterwork of his predecessor Dr. Matuyama. History will repeat itself.

Sadao Sasajima

## List of selected papers by Dr. N. Kawai

Magnetic polarization of Tertiary rocks in Japan: J. Geophys. Res., 56, 73, (1951).

Thermal fluctuation after effect found in the natural remanent magnetic polarization of rocks: J. Geomag. Geoelectr., 5, 66, (1953).

Magnetism of rocks and solid phase transformation in ferromagnetic minerals: Proc. Japan Acad., 30, 588, (1954).

Exsolution of titanomagnetite and its time effect on rock-magnetism I – Change of exsolution phase with geological age: Proc. Japan Acad., 32, 455, (1956).

Exsolution of titanomagnetite and its time effect on rock-magnetism III – Effects of enduring temperature and slow cooling: Proc. Japan Acad., 32, 464, (1956).

Magnetism of the earth crust: J. Geomag. Geoelectr., 9, 140, (1957).

Deformation of the Japanese islands as inferred from rock magnetism: Geophys. J. 6, 124, (1961).

Magnetic minerals in black and red beds in Japan: Mem. Coll. Sci. Univ. Kyoto, Ser. B, 28, 285, (1961).

Study on magnetization of the Japanese rocks: J. Geomag. Geoelectr., 13, 150, (1965).

Archaeomagnetic studies in southwestern Japan: Ann. Geophys., 21, 574, (1965).

Counterclockwise rotation of the geomagnetic dipole axis revealed in the worldwide archaeo-secular variations: Proc. Japan Acad., 41, 398, (1965).

Effect of hydrostatic pressure on the Morin transition point of α-hematite crystal: Phys. Letters, 21, 279, (1966).

Change of the magnetic anisotropy constant $K_1$ of magnetite ($Fe_3O_4$) under hydrostatic pressure: Phys. Letters, 24 A, 503, (1967).

Wobbling motion of the geomagnetic dipole field in historic time during these 2000 years: J. Geomag. Geoelectr., 19, 217, (1967).

Low temperature melting of elements under high pressure and its progression in the periodic table: Japan. J. Appl. Phys., 7, 989, (1968).

The generation of ultrahigh hydrostatic pressures by a split sphere apparatus: Rev. Sci. Instrum., 41, 1178, (1970).

The evolution of the island arc of Japan and the formation of granites in the circum-Pacific belt: J. Geomag. Geoelectr., 23, 267, (1971).

Olivine-spinel transformation in a natural forsterite: Phys. Earth Planet. Interiors, 4, 425, (1971).

Oscillating geomagnetic field with a recurring reversal discovered from Lake Biwa: Proc. Japan Acad., 48, 186, (1972).

The magnetic control on the climate in the geologic time: Proc. Japan Acad., 48, 687, (1972).

High pressure break-down of enstatite: Proc. Japan Acad., 48, 412, (1972).

The transition of field at the Brunhes and Jaramillo boundaries in the Matuyama geomagnetic epoch: Proc. Japan Acad., 49, 820, (1973).

A new device for pressure vessels: Proc. Japan Acad., 49, 623, (1973).

A high pressure hexagonal form of $MgSiO_3$: Proc. Japan Acad., 50, 378, (1974).

Geomagnetic stage transitional from the Matuyama to Brunhes Epochs: Proc. Japan Acad., 51, 634, (1975).

Palaeomagnetism of Lake Biwa sediment: Rock Magnet. Paleogeophys., 3, 24, (1975).

Voice of geomagnetism from Lake Biwa: Paleolim. Lake Biwa Japan. Pleist., 3, 143, (1975).

Palaeomagnetism and paleoclimate: Rock Magnet. Paleogeophys., 3, 110, (1975).

A clue to the polar wandering: Proc. Japan Acad., 52, 157, (1976).

Paleomagnetic study of deep-sea sediments using thin sections: J. Geomag. Geoelectr., 28, 395, (1976).

Metallic transition of oxides, $H_2O$ and hydrogen: High Pressure Research-Applications to Geophysics, ed. M. H. Manghnani and S. Akimoto (Academic, New York) 267, (1977).

Palaeomagnetic study of deep-sea sediments from the Melanesia Basin: J. Geomag. Geoelectr., 29, 211, (1977).

Sintering of diamond with cobalt: Mater. Res. Bull., 12, 1079, (1977).

# OBITUARY TO LATE PROFESSOR NAOTO KAWAI

Haruo DOMEN

Institute of Physical Sciences, Faculty of Education,
Yamaguchi University, Yamaguchi City, 753 Japan

To my greatest saddness, Professor Naoto Kawai has passed away leaving me with many emotional effects. He was an outstanding person: the greatest "Idea Man" in his scientific field as every geoscientist knows not only in Japan but all over the world.

In the University of Kyoto, Japan, Professor Kawai was one of the last students of Dr. Matuyama, who is well known internationally these days because of the "Matuyama Reversed Epoch", and who died 21 years ago as the first president of the Yamaguchi University, West Japan (1949 - 58). There I am the last person who had his kind instructions in his whole life on paleo/rock magnetic works.

Actually I am not an ex-student of Professor Kawai, but it was through his kind and warm guidance that I was able to built my first astatic magnetometer at Yamaguchi University in 1950. While I was on leave in Professor Kawai's laboratory at Kyoto University during the period 1956 to 1957, holding a grant from the Ministry of Education, Japan, I carried out my first experimental work on the pressure effect on magnetization of rocks under his supervision and this resulted in the discovery of Piezo Remanent Magnetization (PRM), caused by one-directional high pressure. Immediately afterwards, Professor Kawai paid his visit to Europe and he kindly introduced my work on PRM to European paleo/rock magnetists so drawing their attention to my work and also PRM phenomenon earlier than Japanese scientists. Fairly later on, I was given the Tanakadate Prize from the Society of Terrestrial Magnetism and Electricity of Japan for my "Experimental Discovery of the Piezo Remanent Magnetic Phenomenon", and I owe this honour to Professor Kawai's warm but severe instructions.

Once in 1965, we, Professor Kawai and myself, took the flight from Anchorage, Alaska to Tokyo, Japan. Professor Kawai mentioned his unique idea for producing ultra high pressure during this flight. The Kawai pressure vessel seemed to me to be something like dividing a frog's egg nucleus, then I recommended to him that the apparatus might be named "Bunkatsu Kyutai; Divided Spherical Body", so he named it afterwards.

And I stayed in his laboratory at Osaka University during 1966 - 67 having been awarded a grant from the Japan Society for the Promotion of Science for the "Developemental Research of Ultra High Pressure Iquipement". I collaborated with his group and we made some rather important developements on Kawai's ultra high pressure vessel.

Kawai's secular variation curve of the geomagnetic field is very famous as "Hypotorocoidal movement". This name was also born when we, Professor Kawai and I discussed how to name such unique schematical movement of the axis of the centred geomagnetic field during my stay at Osaka University.

Anyhow he was great indeed, and I was very much obliged to him. I loved him so much not only as my teacher but also just like my elder brother, and he was so kind to me that he treated me as his real younger brother.

Alas! He has finally closed his giant life. I cannot find words to acknowledge Professor Kawai adequately. From the bottom of my heart, I earnestly dedicate my greatest thanks for his friendship and guidance to my bosom instructor, Professor Naoto Kawai.

Hoping that God lets his soul rest in peace in heaven and hoping to have him gazing on my work from there everlasting!

# MAGNETIC SURVEYING OF AN OLD IRONMAKING FURNANCE SITE

Naoto OSHIMAN and Hidehumi TANAKA

Tokyo Institute of Technology
Ookayama, Meguro, Tokyo 152

## Introduction

This paper reports the results of the magnetic survey of the old ironmaking furnance site, which Takatsuka et al.(1978) discovered in 1978 at Ozaki Maeyama in Yachiyocho, Ibaraki prefecture, and the archaeomagnetic study of the natural remanent magnetization(NRM) of the baked earth taken from the furnance site. According to Takatsuka et al.(1978), the age of the furnance is found to range from the later eighth century to the mid-nineth century. The site is on the gentle slope facing to the south. In the second excavations made at the site on August, 1979, the magnetic survey was carried out by using a proton procession magnetometer.

## Magnetic survey

The data of the measured total magnetic intensity were reduced to the differences in the simultaneous value between the respective measuring points and the Kakioka Magnetic Observatory(ΔF) in order to put away the effect of the solar daily variation on quiet days(Sq). Fig. 1(a) illustrates the magnetic contoured map of the ΔF which was obtained from the mesh points of one meter interval inside the area surrounded by the broken lines, and two meters interval outside it.

It seems that the total force gradually decreases as the measuring point becomes higher part of the slope, and that the magnetic anomaly caused by the underground ironmaking furnance superposes on this trend of the main field anomaly.

There is a high positive magnetic anomaly(+330 nT) at the the center of Fig. 1(a), but this is caused by the barbed wire wound on to a tree in the bush.

Fig. 1(b) is the area surrounded by the broken lines in Fig. 1 (a), and is carried out height revision.

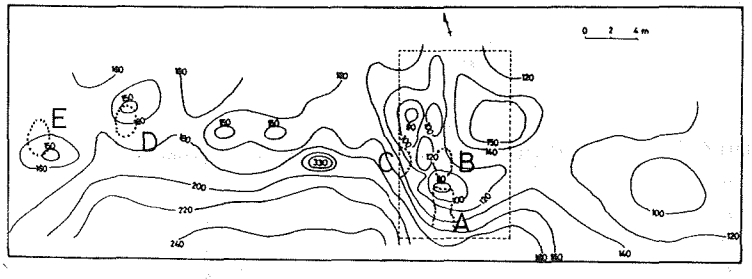


Fig. 1(a). Magnetic contoured map(unit: nT)
A: the old ironmaking furnance discovered in 1978,
B and C: the old ironmaking furnances discovered in 1979, D and E: the furnances in the Edo period.

Figs.1(a) and (b) show the good correlation of the nagative

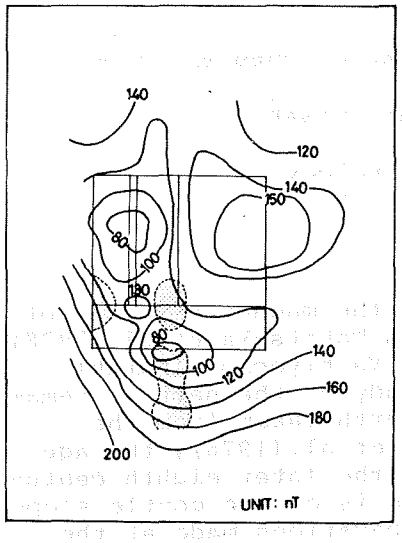


Fig. 1(b). Magnetic contoured map.

anomaly with the location of the furnance.

## Measurements of NRM's

The samples of baked earth were collected the bottom of the iron-making furnance(B in Fig. 1(a)). The direction and the intensity of NRM on the baked earth containing a few pieces of slag was measured by using an astatic magnetometer. Table 1 summarizes the results, and Fig. 2 shows the directions of NRM's.

It seems that the disagreement of the directions of NRM's is mainly caused by the poor orientation of the samples.

NRM's of several samples without orientation of the baked earth and slags were measured by using the spinner magnetometer, and the results are summarized in Tables 2 and 3, respectively.

| Samples | Jn $\times 10^{-4}$ (emu/cc) | D (°) | I (°) |
|---|---|---|---|
| MY2-1 | 7.66 | -18.7 | 41.2 |
| MY2-1-1 | 2.86 | 21.0 | 40.2 |
| MY2-1-2 | 3.48 | - 1.2 | 40.2 |

Table 1.

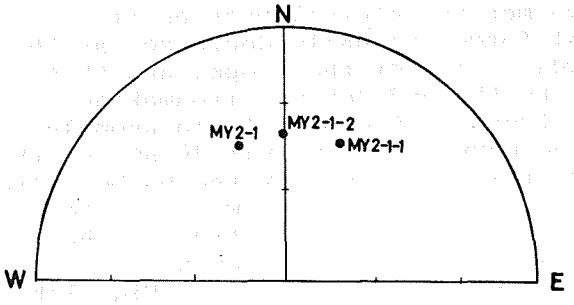


Fig. 2. The directions of NRM's

| Slag | Jn ($\times 10^{-3}$ (emu/g)) |
|---|---|
| | 3.7 |
| | 1.6 |
| | 1.2 |
| | 1.4 |
| Mean | 1.98 |

Table 2.

| Baked earth | Jn ($\times 10^{-4}$ (emu/g)) |
|---|---|
| | 1.6 |
| | 1.1 |
| | 3.2 |
| | 2.4 |
| | 2.3 |
| | 2.2 |
| | 3.0 |
| Mean | 2.26 |

Table 3.

## Discussion

If we consider an underground sphere containing uniformly magnetized matter, the anomaly of the total force on the earth's surface, $\Delta F$, is expressed as

$$\Delta F = \frac{4\ R^3 Jn}{3r^3}(3\ \sin^2 I - 1)$$

where R and r are the radius and the depth of the sphere respectively, and Jn and I are the intensity and the inclination of NRM respectively.

In the case of the sphere whose volume is the same as the underground ironmaking furnance base, the total magnetic intensity anomaly 19.1 nT is expected above the sphere when the next parameters are supposed; R=89.5 cm, r=125 cm, Jn=4.67x $10^{-4}$ emu/cc, and I=40.5°.

On the other hand, the age of the ironmaking furnance could not be determined archaeomagnetically because of the poor orientation of the samples.

## Reference

Takatsuka, H. et al.(1978) Humanities Review, Tokyo inst. of Technology 4, 147.(in Japanese)

# ARCHAEOMAGNETISM OF SOUTHWESTERN JAPAN MEASURED AND COMPILED IN OSAKA UNIVERSITY

Hidetoshi SHIBUYA and Tadashi NAKAJIMA*

Department of Physics, Faculty of Engineering Science
Osaka University, Toyonaka, Japan

In Osaka University, Archaeomagnetic studies to determine the ancient direction of the earth's magnetic line of force have been continued since 1965 (Kawai and Hirooka, 1967; Kawai et al., 1967; Kawai et al., 1968; Hirooka, 1971). All the results obtained here since 1971 are compiled. The data concerning samples from Suemura Kilns (Shibuya et al. 1979) are excluded.

The results are given in Table I. In the 6-th column of the table, the figure is the number of samples on which the average direction quoted are based. The 9-th and 10-th columns give Fisher's cone angle of confidence of 95%, and his precision parameter respectively. The 11-th column shows date which is communicated by an archaeologist who excavated the remains.

References

Hirooka, K.(1971) Mem. Fac. Sci., Kyoto Univ., Ser. Geol. & Mineral., 38, 167-207.

Kawai, N. and K. Hirooka (1967) J. Geomag. Geoelectr., 19, 217-227.

Kawai, N., K. Hirooka and K. Tokieda (1967) Earth Planet. Sci. Letters, 3, 48-50.

Kawai, N., K. Hirooka, K. Tokieda and T. Kishi (1968) 1967 Ann. Progress Rep. Palaeogeophys. Res. Japan, 81-85.

Shibuya, H., N. Natsuhara, T. Nakajima and N. Kawai (1979) Suemura IV (Report on the Research of the Cultural Properties in Osaka Prefecture), (in press) (In Japanese).

* Present address: Department of Geology, Faculty of Education, Fukui University, Fukui, Japan.

| Site | Locality | Lat(N) | Long(E) | Type of Structure | N | D(°) | I(°) | $\alpha_{95}$ | k | Archaeological date |
|---|---|---|---|---|---|---|---|---|---|---|
| Nagaike 1 | Kawachinagano-C. | 34°27' | 135°33' | Pottery Kiln | 4 | -8.6 | 55.8 | 7.7 | 142.9 | Heian Era |
| Nagaike 3-1 | Kawachinagano-C. | 34°27' | 135°33' | Pottery Kiln | 5 | -18.7 | 68.3 | 5.6 | 186.0 | 12c. |
| Nagaike 3-2 | Kawachinagano-C. | 34°27' | 135°33' | Pottery Kiln | 4 | -11.7 | 54.7 | 13.3 | 48.4 | 12c. |
| Nagaike 3-3 | Kawachinagano-C. | 34°27' | 135°33' | Pottery Kiln | 7 | -9.5 | 56.1 | 8.8 | 48.3 | 12c. |
| Nagaike 3-4 | Kawachinagano-C. | 34°27' | 135°33' | Pottery Kiln | 7 | -10.0 | 51.4 | 8.3 | 53.0 | 12c. |
| Nagaike 3-6 | Kawachinagano-C. | 34°27' | 135°33' | Pottery Kiln | 5 | -7.7 | 61.3 | 8.2 | 88.1 | 12c. |
| Nagaike 3-7 | Kawachinagano-C. | 34°27' | 135°33' | Pottery Kiln | 5 | -17.5 | 54.3 | 10.9 | 49.9 | 12c. |
| Nagaike 4-1 | Kawachinagano-C. | 34°27' | 135°33' | Pottery Kiln | 5 | -14.5 | 32.2 | 8.3 | 86.4 | Heian Era |
| Nagaike 4-2 | Kawachinagano-C. | 34°27' | 135°33' | Pottery Kiln | 5 | -13.4 | 54.2 | 5.9 | 168.1 | Heian Era |
| Nagaike 5 | Kawachinagano-C. | 34°27' | 135°33' | Pottery Kiln | 7 | -24.5 | 50.0 | 4.2 | 211.3 | Heian Era |
| Jorinji W-2 | Toki-C. | 35°24' | 137°12' | Pottery Kiln | 12 | -0.7 | 34.4 | 2.5 | 301.4 | 16-17c. |
| Jorinji W-3 | Toki-C. | 35°24' | 137°12' | Pottery Kiln | 13 | -4.8 | 39.2 | 3.6 | 135.3 | 16-17c. |
| Odo E-1 | Toki-C. | 35°20' | 137°10' | Pottery Kiln | 5 | -2.3 | 53.7 | 13.5 | 33.3 | 12c. |
| Robata 4 | Kagamihara-C. | 35°23' | 136°54' | Dwelling Pit | 7 | 8.2 | 52.2 | 5.5 | 121.7 | } Middle or Late Jomon Era |
| Robata 5 | Kagamihara-C. | 35°23' | 136°54' | Dwelling Pit | 11 | 9.4 | 62.5 | 6.2 | 55.8 | |
| Ozakidanchi 1 | Kagamihara-C. | 35°25' | 136°50' | Pottery Kiln | 10 | -6.0 | 57.8 | 4.2 | 132.4 | 550-800 |
| Ozakidanchi 2 | Kagamihara-C. | 35°25' | 136°50' | Pottery Kiln | 11 | -4.2 | 58.2 | 2.8 | 261.4 | 550-800 |
| Ozadidanchi 3 | Kagamihara-C. | 35°25' | 136°50' | Pottery Kiln | 12 | 1.7 | 48.8 | 3.2 | 181.4 | 550-800 |
| Kakishita | Kani-T. | 35°23' | 137°07' | Pottery Kiln | 15 | 4.5 | 55.2 | 1.3 | 938.0 | 12c. |
| Yabasama 1 | Kani-T. | 35°24' | 137°03' | Pottery Kiln | 15 | -6.3 | 51.9 | 1.8 | 456.4 | about 1100 |
| Yabasama 2 | Kani-T. | 35°24' | 137°03' | Pottery Kiln | 14 | 0.8 | 65.5 | 1.5 | 658.8 | Middle of 12c. |
| Mikita 1 | Sakai-C. | 35°28' | 135°30' | Tile Kiln | 11 | 1.5 | 50.9 | 3.5 | 171.5 | 11-12c. |
| Jurokusen | Seki-C. | 35°29' | 136°55' | Pottery Kiln | 7 | 6.5 | 39.5 | 3.6 | 288.7 | 17c. |
| Kuroyatanodo | Seki-C. | 35°30' | 136°56' | Pottery Kiln | 11 | -3.2 | 51.4 | 3.4 | 176.9 | Bigining of 11c. |
| Inadayama 1 | Kagamihara-C. | 35°26' | 136°54' | Pottery Kiln | 8 | -16.3 | 49.9 | 4.7 | 140.5 | 8c. |
| Inadayama 2 | Kagamihara-C. | 35°26' | 136°54' | Pottery Kiln | 11 | -13.1 | 52.4 | 3.7 | 151.5 | 8c. |
| Inadayama 3 | Kagamihara-C. | 35°26' | 136°54' | Pottery Kiln | 6 | -8.0 | 49.0 | 4.2 | 261.6 | 8c. |
| Inadayama 4 | Kagamihara-C. | 35°26' | 136°54' | Pottery Kiln | 11 | -6.0 | 57.1 | 2.1 | 464.4 | 8c. |
| Inadayama 5 | Kagamihara-C. | 35°26' | 136°54' | Pottery Kiln | 5 | 4.4 | 52.7 | 3.4 | 501.8 | End of Heian Era or |
| Inadayama 6 | Kagamihara-C. | 35°26' | 136°54' | Pottery Kiln | 12 | -15.4 | 56.6 | 4.4 | 99.4 | 8c. Kamakura Era |

Table I

| Site | Locality | Lat(N) | Long(E) | Type of Structure | N | D(°) | I(°) | $\alpha_{95}$ | k | Archaeological date |
|---|---|---|---|---|---|---|---|---|---|---|
| Inadayama 7 | Kagamihara-C. | 35°26' | 136°54' | Pottery Kiln | 9 | -25.4 | 55.7 | 4.1 | 160.8 | 8c. |
| Inadayama 8 | Kagamihara-C. | 35°26' | 135°54' | Pottery Kiln | 11 | -4.3 | 52.6 | 1.7 | 694.4 | 8c. |
| Inadayama 9 | Kagamihara-C. | 35°26' | 135°54' | Pottery Kiln | 10 | -4.0 | 61.5 | 2.4 | 394.9 | End of Heian Era or |
| Inadayama 10 | Kagamihara-C. | 35°26' | 135°54' | Pottery Kiln | 9 | -10.4 | 58.1 | 4.7 | 120.0 | 8c. Kamakura Era |
| Inadayama 11 | Kagamihara-C. | 35°26' | 135°54' | Pottery Kiln | 12 | -5.9 | 57.1 | 2.4 | 317.6 | 8c. |
| Inadayama 12 | Kagamihara-C. | 35°26' | 135°54' | Pottery Kiln | 13 | -1.8 | 57.9 | 3.0 | 193.3 | 8c. |
| Inadayama 13 | Kagamihara-C. | 35°26' | 135°54' | Pottery Kiln | 10 | -8.6 | 54.5 | 5.4 | 81.7 | 8c. |
| Inadayama 14 | Kagamihara-C. | 35°26' | 135°54' | Pottery Kiln | 6 | -1.5 | 53.1 | 6.3 | 113.5 | 8c. |
| Inadayama 15 | Kagamihara-C. | 35°26' | 135°54' | Pottery Kiln | 12 | -16.7 | 58.6 | 9.1 | 23.5 | 8c. |
| Inadayama 16 | Kagamihara-C. | 35°26' | 135°54' | Pottery Kiln | 10 | 1.3 | 60.8 | 4.0 | 150.1 | End of Heian Era or |
| Sandaseiji 1 | Sanda-C. | 34°54' | 135°14' | Pottery Kiln | 15 | -10.1 | 51.2 | 2.7 | 209.0 | 1868-1936. Kamakura Era |
| Sandaseiji 1-1 | Sanda-C. | 34°54' | 135°14' | Pottery Kiln | 10 | -8.0 | 49.2 | 3.1 | 242.4 | Meiji Era |
| Sandaseiji 2-U | Sanda-C. | 34°54' | 135°14' | Pottery Kiln | 24 | -0.8 | 46.7 | 2.7 | 124.5 | } End of Edo Era or |
| Sandaseiji 2-L | Sanda-C. | 34°54' | 135°14' | Pottery Kiln | 10 | -2.5 | 45.6 | 3.0 | 252.2 | Meiji Era |
| Sandaseiji 3 | Sanda-C. | 34°54' | 135°14' | Pottery Kiln | 19 | -3.3 | 44.5 | 2.8 | 142.8 | End of Edo Era |
| Shibatani 31 | Takatsuki-C. | 34°52' | 135°37' | Baked Earth | 6 | 23.1 | 58.9 | 5.7 | 140.7 | 380-420 |
| Tanahara 1 | Kawachinagano-C. | 34°46' | 135°33' | Pottery Kiln | 9 | -7.9 | 54.2 | 3.2 | 266.6 | 12-13c. |
| Tanahara 2 | Kawachinagano-C. | 34°46' | 135°33' | Pottery Kiln | 9 | -11.2 | 52.6 | 4.4 | 139.8 | 12-13c. |
| Tanahara 3 | Kawachinagano-C. | 34°46' | 135°33' | Pottery Kiln | 10 | -14.8 | 52.3 | 3.2 | 229.0 | 12-13c. |
| Tanahara 4 | Kawachinagano-C. | 34°46' | 135°33' | Pottery Kiln | 12 | -13.2 | 55.0 | 3.1 | 199.5 | 12-13c. |
| Tanahara 5 | Kawachinagano-C. | 34°46' | 135°33' | Pottery Kiln | 12 | -8.7 | 55.7 | 2.1 | 464.8 | 12-13c. |
| Kanaibessho | Tsuyama-C. | 35°02' | 134°03' | Kiln-like Structure | 10 | -25.5 | 61.7 | 3.6 | 182.6 | 6-12c. |
| Funagome | Tsuyama-C. | 35°06' | 134°05' | Kiln-like Structure | 8 | -10.1 | 54.7 | 4.1 | 181.4 | 1-7c. |
| Kakiemon A | Arita-T. | 33°11' | 129°52' | Pottery Kiln | 11 | 0.6 | 40.9 | 4.0 | 131.4 | Early 19c. |
| Kakiemon B | Arita-T. | 33°11' | 129°52' | Pottery Kiln | 25 | 1.7 | 39.1 | 2.6 | 125.5 | Early 19c. |
| Obo N | Arita-T. | 33°12' | 129°53' | Pottery Kiln | 12 | -6.3 | 44.6 | 2.5 | 310.4 | End of Edo Era or Meiji |
| Ryusenji 2 | Tondabayashi-C. | 34°28' | 135°36' | Tile Kiln | 7 | 3.9 | 57.2 | 2.9 | 423.5 | End of 13c. Era |
| Ryusenji 4 | Tondabayashi-C. | 34°28' | 135°36' | Tile Kiln | 9 | -5.2 | 56.3 | 3.7 | 199.3 | 10c. |
| Saka 1 | Hagi-C. | 34°25' | 131°26' | Pottery Kiln | 34 | 6.2 | 41.7 | 3.0 | 69.2 | 17c. |
| Saka 2 | Hagi-C. | 34°25' | 131°26' | Pottery Kiln | 14 | 3.3 | 38.0 | 4.0 | 99.7 | 17c. |
| Saka 3 | Hagi-C. | 34°25' | 131°26' | Pottery Kiln | 26 | 7.5 | 36.8 | 1.9 | 225.1 | 17c. |

Table I (continued)

| Site | Locality | Lat.(N) | Long.(E) | Type of Structure | N | D(°) | I(°) | $\alpha_{95}$ | k | Archaeological date |
|---|---|---|---|---|---|---|---|---|---|---|
| Sarayadani 1 | Ureshino-T. | 33°06' | 129°56' | Pottery Kiln | 14 | 2.9 | 40.1 | 4.3 | 85.4 | Early Edo Era |
| Sarayadani 3 | Ureshino-T. | 33°06' | 129°56' | Pottery Kiln | 30 | 4.2 | 36.7 | 1.9 | 187.1 | Early Edo Era |
| Suehigashi 86 | Sanda-C. | 34°56' | 135°13' | Pottery Kiln | 14 | -27.3 | 62.8 | 3.4 | 131.4 | Early Heian Era |
| Suenishi 67 | Sanda-C. | 34°57' | 135°12' | Pottery Kiln | 9 | -5.0 | 52.8 | 4.1 | 156.0 | Nara Era |
| Okawa E-3G | Mizunami-C. | 35°18' | 137°18' | Pottery Kilns | 25 | 5.3 | 40.8 | 3.2 | 85.2 | 17c. |
| Hakeue 2-U | Koganei-C. | 35°42' | 139°30' | Dwelling Pit | 4 | -11.0 | 76.4 | 5.9 | 244.2 | Middle of Jomon Era |
| Hakeue 2-L | Koganei-C. | 35°42' | 139°30' | Dwelling Pit | 6 | -1.9 | 53.8 | 6.2 | 119.1 | Middle of Jomon Era |
| Hakeue 22 | Koganei-C. | 35°42' | 139°30' | Fire Place | 5 | -4.2 | 42.0 | 4.5 | 229.4 | Middle of Jomon Era |
| Sabuta 5 | Kurashiki-C. | 34°15' | 133°40' | Pottery Kiln | 14 | -17.6 | 64.6 | 1.8 | 504.1 | Early 7c. |
| Tabuchi | Tetta-T. | 34°56' | 133°23' | Ironworks | 24 | 3.1 | 37.7 | 2.6 | 154.6 | 17-19c. |
| Saradani 1 | Wakayama-C. | 34°13' | 135°14' | Pottery Kiln | 8 | -17.7 | 45.5 | 5.9 | 89.4 | Early 9c. |
| Saradani 2 | Wakayama-C. | 34°13' | 135°14' | Pottery Kiln | 23 | -16.8 | 49.3 | 2.0 | 230.5 | Late 6c. |
| Saradani 3 | Wakayama-C. | 34°13' | 135°14' | Pottery Kiln | 13 | -1.5 | 39.1 | 4.3 | 92.6 | End of 6c. |
| Saradani 4-I | Wakayama-C. | 34°13' | 135°14' | Pottery Kiln | 12 | -8.0 | 47.3 | 3.4 | 165.4 | Late 6c. |
| Saradani 4-II | Wakayama-C. | 34°13' | 135°14' | Pottery Kiln | 12 | -14.2 | 40.9 | 4.5 | 92.0 | Early 6c. |
| Tanoso A | Mizunami-C. | 35°19' | 137°18' | Pottery Kiln | 22 | 8.4 | 43.0 | 1.6 | 399.2 | about 1700 |
| Tanoso B | Mizunami-C. | 35°19' | 137°18' | Pottery Kiln | 9 | 5.8 | 43.8 | 2.0 | 662.8 | about 1700 |
| Inkyoyama W | Toki-C. | 35°22' | 137°11' | Pottery Kiln | 18 | 7.4 | 41.2 | 1.2 | 899.5 | about 1600 |
| Hyakkengawa | Okayama-C. | 34°40' | 133°58' | Baked Earth | 8 | -26.5 | 60.5 | 15.2 | 55.3 | End of Jomon Era or Bigining of Yayoi Era |

Table I (continued)

# GEOMAGNETIC SECULAR VARIATION RECORDED IN THE STABLE MAGNETIC REMANENCE OF THE YOUNG SEDIMENTS COLLECTED FROM OSAKA BAY

Masayuki HYODO and Katsumi YASKAWA

Department of Earth Sciences
Faculty of Science
Kobe University, Kobe 657 Japan

Recently we took a core of sediments from Osaka Bay, the diameter and the length of which are 20 cm and 700 cm, respectively. The diameter of 20 cm is enough to make several specimens at any given depth level. We took out 4 to 5 specimens from every 3 cm depth level, so as to average out the error due to sampling etc.

The remanent magnetization of argillaceous sediments is known to be weak but very stable and to have kept the exact orientation of the ambient magnetic field at the time of depositions. Their magnitude of intensity of remanent magnetization is generally of the order of $10^{-6}$ emu/cc for the argillaceous sediments in the inland-sea and lake bottom, where the sedimentation rate is considerably high, and $10^{-4}$ emu/cc for the those in the ocean bottom. The sedimentation rate of the latter is almost less than a few centimeters for a thousand years and it means that we can hardly take the information about the geomagnetic secular variation of the period of several thousand years out of the deep ocean-bottom sediments.

The young argillaceous sediments in the lake or the inland sea kept those informations and are most suitable for the investigation of geomagnetic secular variation on account of their high sedimentation rate. It is necessary, however, to make considerably big specimens to carry out measurements exact enough to deduce the past geomagnetic field, say at least 10 cc, because the sensitivity of usual magnetometer is equal or less than $10^{-6}$ emu and the intensity of magnetization of those sediments is almost less than $10^{-6}$ emu/cc.

On the other hand, the diameter of core sampler is mostly between 5 and 8 cm and, because of difficulty of coring operation under the same condition, the analyses in various fields are compelled to be carried out with the extremely restricted amount of sample at each depth level of a core. Therefore, it is almost impossible to get several specimens for magnetic measurement from every depths level to be measured with such a thin core sample.

To determine the orientation and the intensity of the past geomagnetic field through the palaeomagnetic investigation of a certain volcanic rock, we usually prepare several oriented specimens, more than 4, to measure their magnetization. After measurement of their magnetization, we take a resultant vector of the magnetization vectors of all the specimens as the past geomagnetic field (Fisher; 1953 ) to average out, the error accompanied with sampling etc.

The same process should be required in case of sediments to infer correctly the past geomagnetic field from their remanent magnetization. The purpose of this short note is to report our palaeomagnetic results of young sediments collected from the bottom of Osaka Bay, which are obtained through the process mentioned above.

The magnetization of each specimen was measured with a super-conducting rock magnetometer of SCT, the sensitivity of which is $10^{-8}$emu. The output of this magnetometer is connected with a tape-puncher as well as a printer. Using this magnetometer system we obtain a punched tape for x-, y- and z- components of magnetization of each specimen, and this tape is directly used as an input of our computer, so that there is no chance to get mispunch or misreading. After computing each magnetic vector, the vectors belonging to the same depth level are gathered and are analyzed statistically by Fisher's method. The magnetization for each level thus obtained is subjected to a seven-points moving average, i.e. we get new values which are calculated by Fisher's method with every serial seven pairs of declination and inclination of magnetization for each level.

To use these values as the geomagnetic secular variations, it is necessary to know the relation between depth and age for this sediments. Fortunately we could collect pieces of shell enough to determine the age by $^{14}c$ method at three depth levels. These ages are as follows:

| | |
|---|---|
| 144 ± 27 cm | 616 ± 80 yr |
| 269 ± 15 cm | 1546 ± 80 yr |
| 357 ± 19 cm | 2896 ± 90 yr |

Assuming the relation between age (t) and depth (z) (Yaskawa, 1973) as

$$z = At + B(1 - \exp(-Ct))$$

where A, B and C are arbitrary constants, and substituting three known pairs of depth and age into this relation, we get the equation to determine the age at depth less than 7 m below sea bottom at the sampling site.

Fig.1 shows the magnetic declination and inclination versus age relations. The declination in Fig. 1 was determined in such a way that the declination of resultant vector of the vectors determined at all the depth levels was put to zero. When the core of sediments was taking out from the tube of core sampler, the core sample was scratched along a generating line of the cylinder, and the magnetic measurement of every specimen was carried out on the basis of this scratch, so that measured declination is correct only relatively in each other but it does not give the true declination. The reason why we put the declination of resultant vector to zero is that we do not find any other reasonable method to find out the original orientation of core sample at the sea bottom.

The stability of magnetization was tested by using a newly designed field rotating of demagnetizing apparatus (Matsuda et al., 1979), and the results are clearly shown that, although the intensity of magnetization gradually decreases as peak alternating field increases, the direction of magnetization scarecely changes in all the cases, in other words, the remanence of this core is quite stable and may keep original magnetization or be fossiles of the ambient geomagnetic field at the time of fixation of ferromagnetic

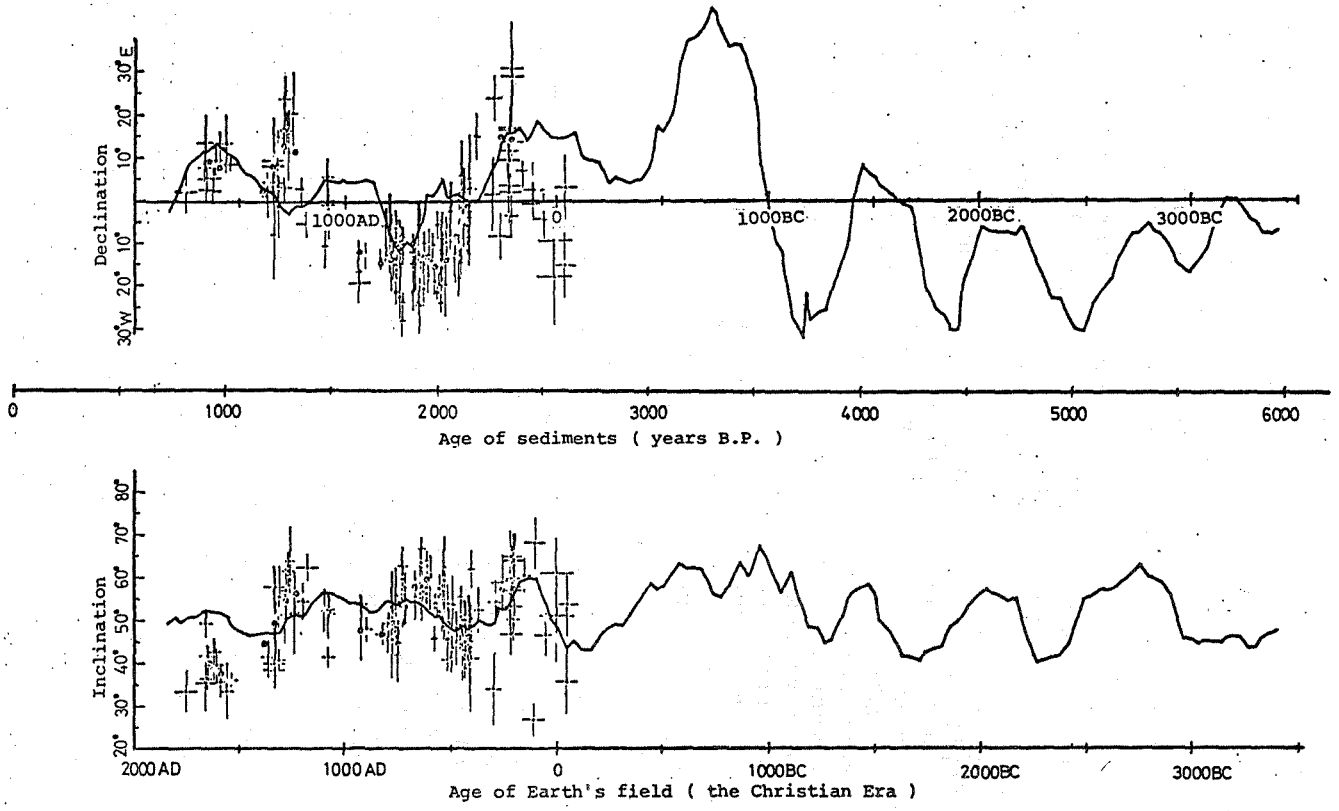


Fig. 1: Geomagnetic secular variation inferred from the vertical change of magnetization of the sediments in Osaka Bay.

minerals in the sediments.

Not so many works (Creer et al., 1972; Yaskawa et al., 1973; Yaskawa, 1974) are reported yet concerning geomagnetic secular variation through the measurement of remanent magnetization of sediments, and all of these works were based on the measurement of only one specimen for each depth level, so that the error due to sampling etc is not averaged out. We believe from any view point that the reliability of our present result is quite high. To compare the present result to that deduced from NRM of the samples collected from kilns in Kinki district, we plotted in Fig. 1 those data of both declination and inclination versus age which were compiles by Hirooka (1971), showing rather beautiful coincidence.

References

Creer, K.M., R. Thompson and L. Molyneux (1972) Earth Planet. Sci. Lett., 14, 115-127.
Fisher, R.A. (1953) Proc. Roy. Soc. London, A, 217, 295-305.
Hirooka, K. (1971) Mem. Fac. Science Kyoto University, Series of Geology and Mineralogy, 38, 167-207.
Matsuda, J. et al (1979) J.Geomag. Geoelectr., to be submitted.
Yaskawa, K. et al (1973) J.Geomag. Geoelectr., 25, 447-474.
Yaskawa, K. (1973) Rock Magnetism and paleogeophysics, 1, 39-43.
Yaskawa, K. (1974) Paleolim. Lake Biwa Japan. Pleist, 2, 77-88.

( Submitted to J. Geomag. Geoelectr. )

# ARCHAEOMAGNETIC RESULTS OF SEMPUKUJI REMAINS, THE CAVE SITE, AND THE HOLOCENE PALAEOSECULAR VARIATION IN JAPAN

Kimio HIROOKA* and Katsuyasu TOKIEDA**

*Department of Earth Sciences, Faculty of Science, Toyama University, Toyama 930.
**Department of Physics, Faculty of Science, Shimane University, Matsue, Shimane 690.

## Introduction

The secular variation of the geomagnetic field direction in Japan has been clarified for the recent 2,000 years by the archaeomagnetic studies (Yukutake, 1961; Hirooka, 1971; Watanabe, 1977). And now it becomes possible for this period to detarmine the age of archaeological sites archaeomagnetically with a good precision. For the period before 2,000 B.P., however, we have no sufficient informations about the geomagnetic field direction of known age to draw out the secular variation curves of the declination and the inclination.

Watanabe (1959) made archaeomagnetic measurements on many hearths and fireplaces which were found in the excavated archaeological sites of the Jomon period, and tried to draw the secular variation curves assuming that the inclination changed periodically between 40° and 60° with a period of 1,000 years. But the assumption is not seemed valid because the archaeomagnetic data of the recent 2,000 years tell us that the inclination did not show such a constant periodicity but showed a variable period from 400 to 600 years (Hirooka, 1971). As the direction of the geomagnetic field of a region greately changes in several hundred years, the precision of the age dating by $^{14}C$ or the other methods is still not sufficient to arrange archaeomagnetic data in the correct order of their ages. One whole cycle of the geomagnetic variation is included in the error of a determined age. This fact makes difficult to draw out the precise secular variation curves for the Jomon and the earlier periods by using the archaeomagnetic data obtained from baked clay remained in the archaeological sites.

We can trace the time variation of the geomagnetic field by palaeomagnetic study on the Recent sediments. Detailed measurements of the detrital remanent magnetization from the lower horizon to the upper of a young sediment will present us the detailed variation of the geomagnetic field. But this study can usually give us only a relative time variation of the geomagnetic field and not the variation of the absolutely known age.

If the results of the both archaeomagnetic and palaeomagnetic studies were combined in a same time span of age, the precise secular variation curves could be obtained. The both studies mutually make up their weak points each other. In this paper we will report a results of archaeomagnetic study of sediments deposited in an old cave site, Sempukuji Remains, and compare with the Holocene geomagnetic secular variation which is obtained by compiling the archaeo- and palaeo-magnetic results so far obtained in the Japanese Holocene.

## The cave site, Sempukuji Remains

Archaeomagnetic sampling was made at Sempukuji Remains which is locating in Sasebo City, Nagasaki Prefecture (129°44'E and 33°12'N).

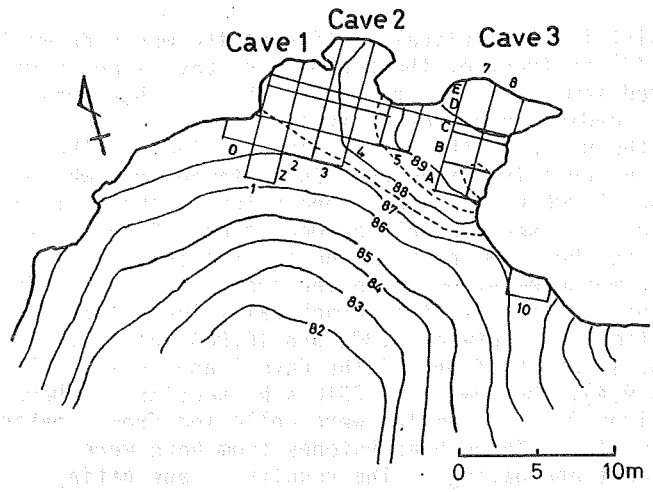


Fig. 1. Sempukuji Remains
Numerals and alphabetical letters of grids show trenches and regions respectively.

The site is being excavated by the archaeological mission directed by Dr. M. Aso of Kokugakuin University. At the site there are three caves where ancient people had been dwelling for many generations (see Fig.1). The archaeological excavation made on the sediments layer by layer which deposited on the older floor of the caves. In the uppermost horizon of the sediments were contained potsherds of the Heian period. In the middle horizon, the Jomon type earthenweres and arrowheads and spear heads made of stone were found. Potsherds of Ryūsenmon type, one of the earliest type of Japanese earthenweres were excaveted from the lower horizon and in the lowest horizon another type of earthenwere was found. It is older than the Ryūsenmon type from the stratigraphical evidence. This newly found type of earthenwere was named Tōryūmon type. This is the oldest type ever found in Japan.

Oriented samples for archaeomagnetic measurement were collected from three different places at the site. Two of them are vertical sections sediments and one is a baked sandstone which was laid under a hearth. Sand and clay deposited successively on the older floors of these caves.

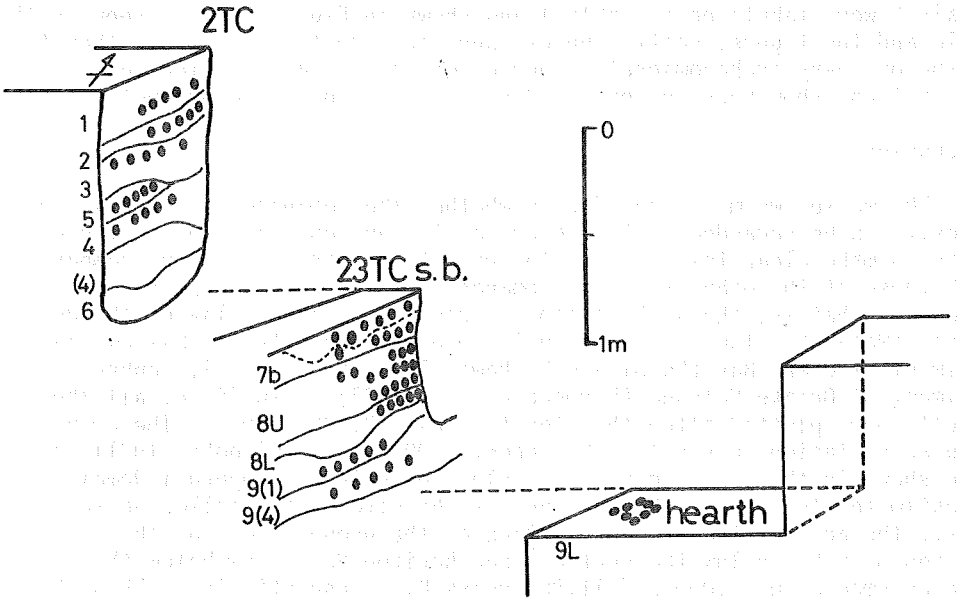


Fig. 2. A schematic illustration of sampling horizons.

Sampling horizons of three sections were illustrated schematically in Fig.2.

The first sampling point is the vertical section of the westside wall of trench 2 at C-region (2TC) in front of the boundary of Cave 1 and Cave 2. We obtained 25 oriented samples from 5 horizons, that is, horizons 1. 2, 3, 5 and 4 in the descending order respectively. This section covers the time span from the Heian to the Middle Jomon periods. The lowest two horizons, 4 and 5, contain potsherdsof Oshigatamon type which is archaeologically dated about 7,000 B.P. The second point is the vertical section at the eastside face of a section belt between trench 2 and 3 at C-region (23TC s.b.) which is about 2 m east of the first point. 41 samples for archaeomagnetic measurement we collected from 5 horizos of 7b, 8U, 8L, 9(1) and 9(4). This section is stratigraphically lower than 2TC section and may cover the time span between 8,000 and 10,000 years B.P. The third point of sampling is at the front of the Cave 3 and is a little lower horizon than horizon 9(4), the lowest of 23TC s.b. section. There found a hearth at this horizon 9L. 8 samples were collected from a baked sandstone underlying the hearth. Three hearthstones from here were also subjected to thermoluminescent age dating. The results of age dating reported were 12170 ± 1170, 11980 ± 280, and 11370 ± 760 and taking the mean of the results, the age of the hearth is 11840 ± 740 years B.P. (Ichkawa and Hagiwara, 1978). The horizon 9L belongs to the Ryusenmon type age, the age of Toryumon type earthenwere must be older than this age. Our collected samples cover the period between 1,000 to 11,800 B.P.

## Results of measurement

Although samples for archaeomagnetic study were collected from eleven horizons altogether, we could not get magnetic directions for three horizons of 1, 8U and 8L because of its very scattered direction of remanence for horizon 1, and of too weak magnetization for horizons 8U and 8L. Since horizons 3 and 5 is archaeologically and sedimentologically considered almost the same age, a mean magnetic direction was calcurated together for the both horizons.

The archaeomagnetic data thus obtaied from 8 horizons in "Sempukuji Remains" were tabulated in Table 1 and shown in Fig.3. As is seen in the table and the figure, scattering of magnetic direction is larger than that of the ordinary archaeomagnetic thermoremanence. But declinations and inclinations show very reasonable directions as for the geomagnetic field.

## Discussions

The matter we must consider is whether the remanence of such a cave deposit can be regarded as the record of the ancient geomagnetic field. So as to make clear this matter, the results obtained here were compared with those of the other types of remanence of the same age so far obtained in Japan, that is, the archaeomagnetic results of baked clay of the Jomon period (Watanabe, 1967), and the palaeomagnetic results of shallow sea sediment of Osaka Bay (Muroi and Yaskawa, 1977) and air-fall tephra sediment of Ontake Volcano (Hirooka et al., 1977). In Fig.4, all those results were plotted altogether for the last 12,000 years. The archaeo-secular variation curves for the recent 2,000 years (Hirooka, 1971) are also shown in the same figure. To plot the data of Sempukuji Remains, we estimated the age of the horizons of the site by the following way. First, the ages of the present surface of the ground floor of the caves, horizon 3 (0.5 m below the surface) and horizon 9L (2.05 m below the surface) were assumed as 0, 7,000 and 11,800 years B.P. respectively. Then the ages of horizons 7b, 9(1) and 9(4) were calcurated by interpolating the

Table 1. Results of measurement of Sempukuji Remains

| Horizon | Kind of Material | Number of Samples | Mean Declination | Mean Inclination | k | $\alpha_{95}$ |
|---|---|---|---|---|---|---|
| 2TC 1* | sand | 5 | - | - | - | - |
| 2 | sand | 5 | -3° | 55° | 30 | 14° |
| 3** | red clay | 5 | -33° | 55° | 21 | 15° |
| 5 | red clay | 5 | | | | |
| 4 | clay | 5 | -16° | 45° | 47 | 14° |
| 23TC s.b. | | | | | | |
| 7b | clay | 11 | -13° | 49° | 52 | 10° |
| 8U | clay | 15 | - | - | - | - |
| 8L | sand | 5 | - | - | - | - |
| 9(1) | sand | 5 | -17° | 36° | 55 | 12° |
| 9(4) | sand | 5 | -24° | 44° | 149 | 6° |
| Front of Cave 3 | | | | | | |
| 9L*** | baked sandstone | 8 | -13° | 66° | 54 | 9° |

* : The Jomon to the Heian Period

** : Ca 7,000 B.P. from archaeological evidence

*** : 11,840 ± 740 B.P. by thermoluminescence dating (Ichikawa and Hagiwara, 1978)

depth of the horizons from the surface and taking the sedimentation rate constant from 11,800 B.P. to 7,000 B.P. The age for horizon 2 was obtained by the same way taking the another adequate rate of sedimentaion for the last 7,000 years.

Although the scattering is large, the magnetic directions of the present study show a good agreement with the other data as is seen in Fig.4. In spite of the different mechanisms of acquiring remanence and of different accuracy of age estimation, all of the declination and inclination values obtained from the sediments of Sempukuji Remains, Osaka Bay and Ontake Tephra coincide with those of archaeomagnetic thermo-remanent magnetization of the Jomon period. From the above-mentioned fact, it is likely that the sediment of the archaeological cave site keep the record of the ancient geomagnetic field direction in their remanence. If we study more on the Holocene natural sediments, and on the baked clay and sediment of archaeologicalsites, we will get a precise secular variation curves of the geomagntic declination and inclination which enable us to carry out the archaeomagntic dating for the Japanese neolithic sites.

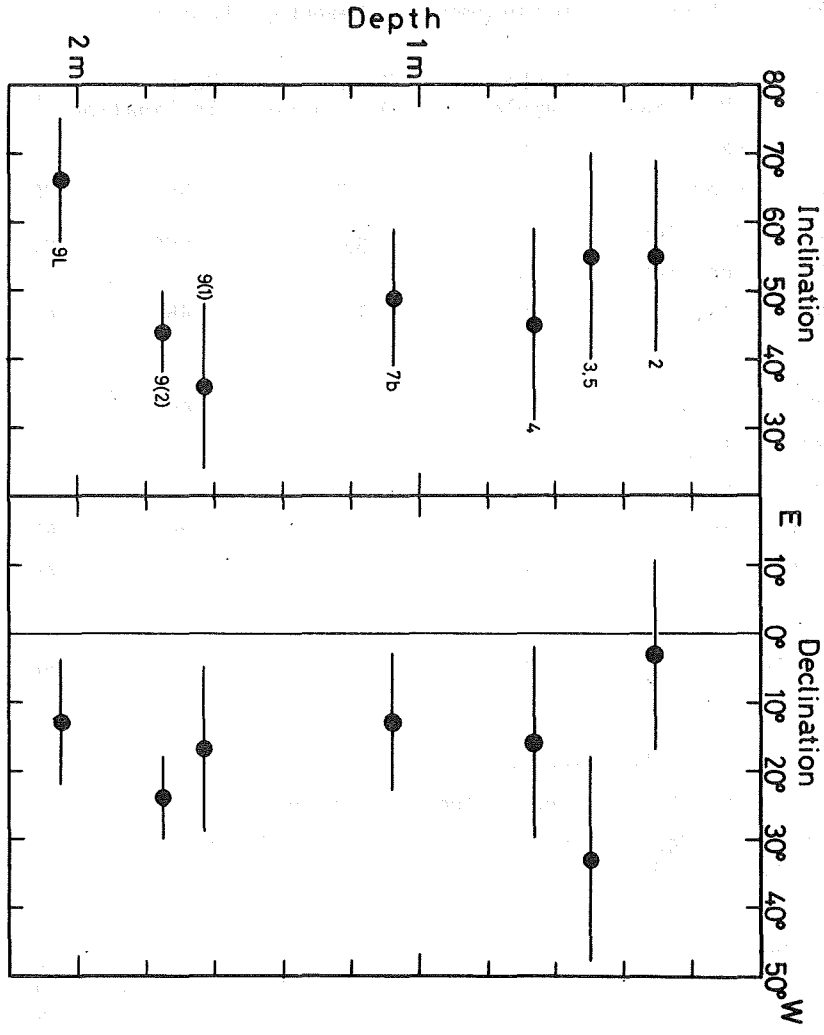


Fig. 3. Declination and inclination of each horizon in Sempukuji Remains.

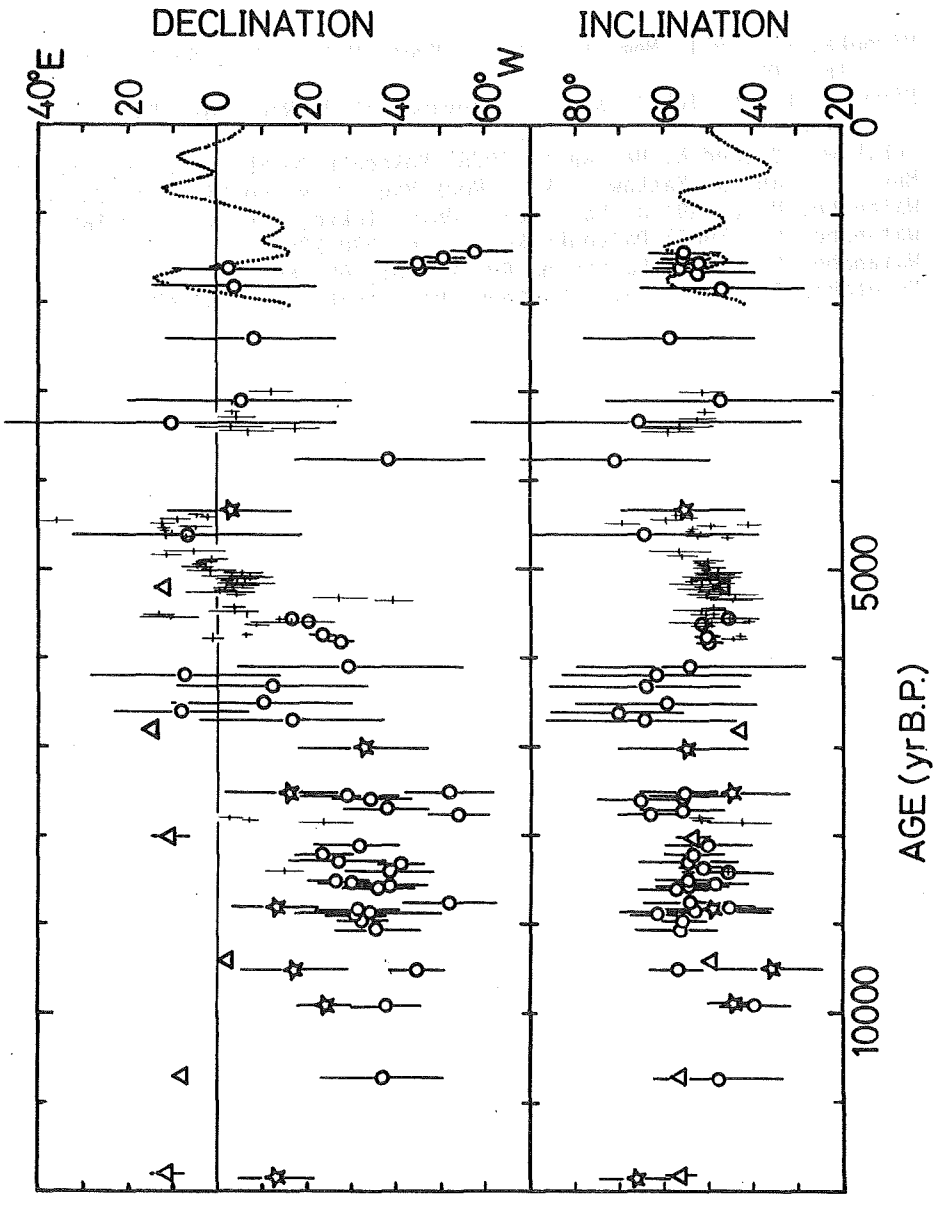


Fig. 4. The Holocene palaeosecular variation of the geomagnetic field

† : The Jomon baked clay (after Watanabe, 1967).
o : Osaka Bay sediment (after Muroi and Yaskawa, 1977).
△ : Ontake Tephra sediment (after Hirooka et al., 1977).
☆ : Sempukuji Remains (this paper).
····· : Archaeosecular variation of the recent 2,000 years (after Hirooka, 1971).

References

Hirooka, K. (1971) Mem. Fac. Sci., Kyoto Univ., Ser. Geol. & Mineral., 38, 167-207.
Hirooka, k., C. Tobita and T. Yokoyama (1977) Rock Mag. Paleogeophys., 4, 81-87.
Ichikawa, Y. and N. Hagiwara (1978) Kokogaku to Shizenkagaku, no.11, 1-7.
Muroi, I. and K. Yaskawa (1977) Rock Mag. Paleogeophis., 4, 76-80.
Watanabe, N. (1959) J. Fac. Sci., Univ. Tokyo, Sec. V, 2, 1-188.
Watanabe, N. (1967) Daiyonki Kenkyu, 6, 230-238.
Watanabe, N. (1977) Kagaku no Ryoiki, 31, 683-691.
Yukutake, T. (1961) Bull. Earthqu. Res. Inst., 39, 467-476.

# THREE PALEOINTENSITIES IN THE HOLOCENE OBTAINED FROM THE LAVA FLOWS IN ŌSHIMA ISLAND

Hidefumi TANAKA

Department of Applied Physics, Tokyo Institute of Technology, Meguro-ku, Tokyo 152

Oshima island, about 120 km south of Tokyo, has been active since the Pleiocene, and there are many volcanic ejecta. In this paper, three lava flows of the Holocene age were studied to determine the paleointensities by the Thellier's double heating method.

## Samples

One of the three lava flows is situated between the two horizons which are dated by C-14 method (Isshiki, 1976), giving the age of this flow as 8,500 $\pm$ 500 years B.P.. The other flow also lies between the two horizons which are dated by the C-14 dating and by the chronology using potteries, respectively (Isshiki, personal communication), and this fact gives the age of 4,500-1,500 years B.P. for this flow. The last one is located upper the dated horizon by the C-14 method as 10,000 years B.P., and taking it to account that the volcanic ejectas of Oshima volcano were erupted every about 150 years (Nakamura, 1964), the age of this flow is limmited to 10,000 - 5,000 years B.P.. All the three lava flows were sampled by hammer and the orientation was checked by a clinometer.

## Experiments

The Thellier's double heating method was used to determine the paleointensities using the samples taken from these three lava flows. All NRM's were stable to the laboratory heat treatment, showing the NRM directional change of less than 10 degree at higher demagnetization procedure, and 13 of 15 specimens were successful in the experiment. Results from the analysis of NRM-TRM diagrams by the least square method are summarized on the Table.

## Results

Three paleointensities of 0.77 $\pm$ 0.11 Oe (8,500 $\pm$ 500 years B.P.), 0.52 $\pm$ 0.03 Oe (10,000 - 5,000 years B.P.) and 0.66 $\pm$ 0.04 Oe (4,500 - 1,500 years B.P.) were converted to the reduced dipole moment (RDM; Smith, 1967) and are shown in the Figure (large dots with error bars) with the data of the world summarized by Kono (1972). The three data, though the errors of the age are very large except that of 8,500 years B.P., coincide with the trend of the change of the RDM in the world for the last 10,000 years. The paleointensity of 0.66 Oe for 4,500 - 1,500 years B.P. obtained in this paper also agrees with the two data of around this age reported by Nagata et al. (1963) who investigated the intensity change of the geomagnetic field during the last 5,000 years by seven historic lavas in Oshima volcano and nine baked potteries.

Table Results of the paleointensity experiment

| Age (years BP) | Specimen | $T_1$ (°C) | $T_2$ | N | -r | F (Oe) | Remarks |
|---|---|---|---|---|---|---|---|
| 1,500-4,500 | 2-1 | 20 | 500 | 9 | 0.9943 | 0.707 | |
| | 2-2 | 20 | 500 | 9 | 0.9935 | 0.617 | |
| | 2-3 | 20 | 500 | 9 | 0.9928 | 0.662 | |
| | 2-4 | 20 | 500 | 9 | 0.9923 | 0.657 | |
| | 2-5 | 20 | 460 | 8 | 0.9990 | (0.535) | abnormal NRM direction |
| | Mean : N = 4, F = 0.661 $\pm$ 0.037 Oe, RDM = 12.2 $\pm$ 0.7 x $10^{25}$ emu | | | | | | |
| 5,000-10,000 | 3-1 | 20 | 360 | 9 | 0.9987 | 0.490 | |
| | 3-2 | 250 | 360 | 5 | 0.9999 | 0.559 | |
| | 3-3 | 20 | 360 | 9 | 0.9993 | 0.535 | |
| | 3-4 | | | | | | very low r |
| | 3-5 | 250 | 440 | 7 | 0.9971 | 0.489 | |
| | Mean : N = 4, F = 0.518 $\pm$ 0.035 Oe, RDM = 9.55 $\pm$ 0.64 x $10^{25}$ emu | | | | | | |
| 8,500 $\pm$ 500 | 5-2 | 20 | 460 | 6 | 0.9962 | 0.724 | |
| | 5-3 | 20 | 460 | 6 | 0.9879 | 0.681 | |
| | 5-4 | 20 | 460 | 6 | 0.9939 | 0.683 | |
| | 5-7 | 20 | 460 | 6 | 0.9919 | 0.891 | |
| | 5-8 | 20 | 460 | 6 | 0.9895 | 0.907 | |
| | Mean : N = 5, F = 0.777 $\pm$ 0.113 Oe, RDM = 14.3 $\pm$ 2.1 x $10^{25}$ emu | | | | | | |

$T_1$, $T_2$ and N: tempwrature interval in which NRM-TRM relation is linear and the number of points in this inteval, r: correlation coefficient, F: paleointensity

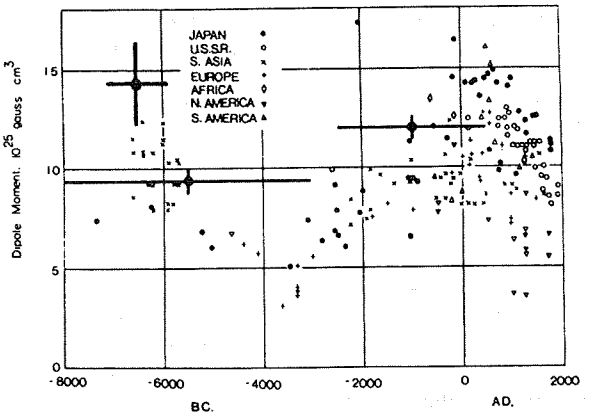


Figure
The comparison of the three RDM with other data in the world summarized by Kono (1972).

References


Isshiki,N. snd K.Matsumura (1976) The Quaternary Research,15,1.
Kono, M. (1972) Phys. Earth Planet. Interiors, 5, 140.
Nagata,T.,Y.Arai and K.Momose (1963) J. Geophys. Res., 68,5277.
Nakamura,K. (1964) Bull. Earthq. Res. Inst.,Univ. Tokyo, 42,649.
Smith,P.J. (1967) Geophys. J. R. astr. Soc., 12, 321.

# PALEOINTENSITIES FROM THE TWO DATED PYROCLASTIC FLOWS OF THE MYOKO VOLCANO

Hidefumi TANAKA

Department of Applied Physics, Tokyo Institute of Technology, Meguro-ku, Tokyo 152.

The Mt. Myoko is one of the main volcanoes of the Myoko volcanic group situated at the prefectural border region between Nagano and Niigata, Central Japan. Two pyroclastic flows of the several volcanic ejecta in the Holocene were used to determine the geomagnetic paleointensities.

## 1. Samples

Akakura and Otagirigawa pyroclastic flows are dated by C-14 method as 8,640 ± 100 and 4,790 ± 110 years B.P., respectively (Hayatsu, 1975). Several oriented essential blocks were sampled by hammer from each pyroclastic flow, but the samplings were performed at the two different sites of one flow which were about 1 km apart to ascertain the reliability of NRM directions. It is important to check the convergence of the NRM directions when pyroclastic flows are used for the paleointensity experiment. One of the five specimens taken from the each flow had an abnormally directed NRM, but NRM's of others were well converged as shown in Fig. 1, telling that the formation temperatures of these pyroclastic flows were enough

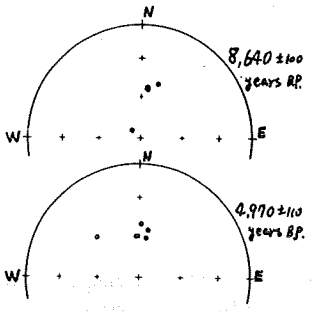


Fig. 1 NRM directions of the two pyroclatic flows of the Myoko volcano.

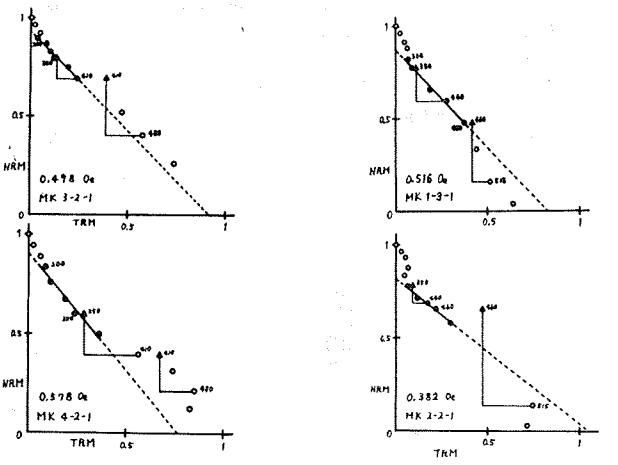


(a) (b)

Fig. 2 Examples of the NRM-TRM diagrams obtained from the Akakura pyroclastic flow of 8,640 years B.P. (a) and Otagirigawa pyroclastic flow of 4,790 years B.P. (b).

Table Results of the paleointensity experiment

| Flow, Age (years B.P.) | Sample | $T_1$-$T_2$ (°C) | N | -r | F (Oe) | Remarks |
|---|---|---|---|---|---|---|
| Akakura | 3-1 | 200-410 | 6 | 0.9977 | (0.666) | abnormal NRM direc- |
| p.f. | 3-2 | 200-410 | 6 | 0.9867 | 0.498 | tion |
| (8,640 | 4-1 | 200-350 | 4 | 0.9914 | 0.578 | |
| ± 100) | 4-2 | 200-390 | 5 | 0.9814 | 0.578 | |
| | 4-3 | 200-350 | 4 | 0.9907 | 0.528 | |
| Mean; N=4, F=0.545 ± 0.039 Oe, RDM=9.77 ± 0.70 x$10^{25}$ emu | | | | | | |
| Otagiri- | 1-1 | 300-460 | 4 | 0.9991 | 0.366 | |
| gawa p.f. | 1-2 | | | | | very low r |
| (4,970 | 1-3 | 300-460 | 5 | 0.9926 | 0.516 | |
| ± 110) | 2-2 | 350-490 | 5 | 0.9920 | 0.396 | |
| Mean; N=3, F=0.426 ± 0.079 Oe, RDM=7.63 ± 1.42 x$10^{25}$emu | | | | | | |

$T_1$, $T_2$ and N: temperature interval in which NRM-TRM relation is linear and the number of points in this interval,
r: correlation coefficient, F: paleointensity

high but not so high to form welded types. The Js-T curves of the bulk specimens of these flows were reversible and gave Curie temperatures around 500 °C.

## 2. Experiments

Eight of nine specimens were succeeded in the Thellier's double heating method and the examples of the NRM-TRM diagram are shown in Fig. 2. Deflections of the points from a straight line at the lower temperatures may be attributed to the breakdown of a secondary component such as a VRM and those at higher temperatures may be due to the change of magnetic properties of samples caused by the oxidation of magnetic minerals. Four to six points corresponding to the medium temperatures in the NRM -TRM diagram were analyzed by the least square method.

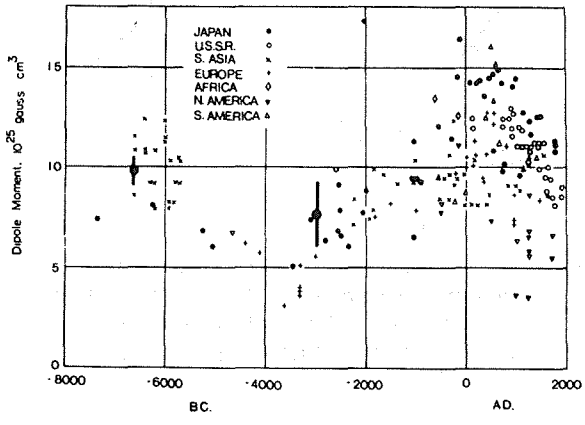


Fig. 3 The comparison of the two data obtained in this study with other data in the world summarized by Kono (1972) for the last 10,000 years.

## 3. Results

Experimental results are summarized on the Table. The mean paleointensities of 0.55 ± 0.04 Oe (8,640 years B.P.) and 0.43 ± 0.08 Oe (4,970 years B.P.) were converted to the reduced dipole moment (RDM; Smith, 1967) and plotted on the Fig. 3 which shows the change of geomagnetic dipole moment for the last 10,000 years summarized by Kono (1972). It is noticeable that these two data agree with the world-wide trend of the change of the geomagnetic dipole moment.

## References

Hayatsu,K. (1975) The Quaternary Research, 14, 1.
Kono,M. (1972) Phys. Earth Planet. Interiors, 5, 140.
Smith,P.J. (1967) Geophys. J. R. astr. Soc., 12, 321.

# FOUR PALEOINTENSITIES IN THE HOLOCENE AND THE LATEST PLEISTOCENE FROM THE HAKONE VOLCANO

Hidefumi TANAKA

Department of Applied Physics, Tokyo Institute of Technology
Meguro-ku, Tokyo 152

## 1. Introduction

Hakone Volcano, 50 km southeast of Tokyo, started its activity about 500 thousands years ago. This volcano was a huge stratovolcano in its first stage, but later, it subsided to form a large caldera and it is now in the last stage having few volcanic activities. But, for the recent last 30,000 years , several lavas and pyroclastic flows were still extruded to form the central cones (Machida, 1968, 1977). Of these flows, one lava flow and three pyroclastic flows which have radiocarbon dated ages were sampled. They are Oowakudani pyroclastic flow (HK 7) of about 3,000 years B.P., Hutagoyama lava ( HK 1; 4,500 years B.P.), and two Kamiyama pyroclastic flows ( HK 6 and HK 9; 20,000 and 30,000 years B.P.). Kanmurigatake lava dome (HK 3) was also examined which is geologically considered to be almost simultaneous formation as the Oowakudani pyroclastic flow (HK 7). This paper reports the four paleointensities determined by the Thellier's double heating method from these flows.

## 2. Samples

The ages of the four flows determined by radiocarbon dating method are listed on the Table 1. The ages of the three pyrocrastic flows were determined from carbonated woods contained in the flows, and that of one lava flow was obtained by averaging the four data determined by small carbons contained in the ash flows just under the lava flow which was formed by the heat of the lava flow.

Five block samples were collected by hand-sampling from one flow unit, and the orientation was determined by means of a magnetic compass with a level except for those from the Hutagoyama lava (HK 1) that have no orientation.

NRM directions were measured by making use of a spinner magnetometer, and results are shown on the Table 1. In this paper, it is not aimed to clarify the paleomagnetic directions, but the directional data were used only to make sure that NRM's are TRM origin because the internal consistency in NRM directions of each pyroclastic flow shows that the formation temperatures were higher than the blocking temperature of the NRM's. One sample taken from the Oowakudani pyroclastic flow (HK 7) has a reversed NRM direction, but this may be a rolled one so that the NRM direction of this sample was rejected to obtaine the mean paleodirection of this flow. Samples taken from the Hutagoyama lava flow (HK 1) and the Kanmurigatake lava dome (HK 3) have no orientation but this is no problem for the aim of this paper.

A thermomagnetic curve (Js-T curve) of bulk sample taken from each flow unit was measured in a vacuam of $10^{-5}$ Torr and

Table 1 C-14 dated ages and NRM directions of each flow

| Flow name | Age years B.P. | Specimen | NRM direction I | D | Jn emu/cc | Tc °C |
|---|---|---|---|---|---|---|
| Oowakudani p. fl. | 2,900 ± 100 | HK 7-1-1 | 58.0 | 2.2°E | $2.91 \times 10^{-2}$ | 528 |
| | | HK 7-2-1 | 50.8 | 300.8 | 0.79 | |
| | | HK 7-3-1 | (-5.4 | 278.7) | 0.17 | |
| | | HK 7-4-1 | 56.9 | 340.0 | 1.03 | |
| | | HK 7-5-1 | 50.0 | 9.0 | 4.93 | |
| Kanmurigatake l. dome | | HK 3-1-1 | | | 0.42 | |
| | | HK 3-1-2 | | | 0.48 | |
| | | Mean : I=57.1°, D=343.1°E, $\alpha_{95}$=21.4° | | | | |
| Hutago-yama l. | 4,475 ± 349 | HK 1-1-1 | | | $1.67 \times 10^{-2}$ | |
| | | HK 1-2-1 | | | 1.38 | |
| | | HK 1-3-1 | | | 0.98 | |
| | | HK 1-4-1 | | | 1.49 | 532 |
| | | HK 1-5-1 | | | 1.56 | |
| Kamiyama p. fl. | 19,640 ± 550 | HK 6-1-1 | 57.4 | 28.6 | $3.64 \times 10^{-4}$ | 493 |
| | | HK 6-2-1 | 68.9 | 35.3 | 3.08 | |
| | | HK 6-3-1 | 60.4 | 23.7 | 3.91 | |
| | | HK 6-4-1 | 60.5 | 7.2 | 3.46 | |
| | | HK 6-5-1 | 62.5 | 16.9 | 10.50 | |
| | | Mean : I=62.3°, D=21.8°E, $\alpha_{95}$=6.2° | | | | |
| Kamiyama p. fl. | 28,200 ± 1,700 | HK 9-1-1 | 64.7 | 3.2 | $2.27 \times 10^{-3}$ | 387 |
| | | HK 9-2-1 | 71.8 | 348.4 | 1.02 | |
| | | HK 9-3-1 | 57.7 | 70.1 | 0.80 | |
| | | HK 9-4-1 | 63.2 | 6.9 | 3.58 | |
| | | HK 9-5-1 | 68.3 | 353.1 | 0.59 | |
| | | Mean : I=68.4°, D=15.3°E, $\alpha_{95}$=14.4° | | | | |

p. fl.; pyroclastic flow, l.; lava, Jn; NRM intensity, Tc; Curie temperature

All the data of radiocarbon dated ages are quoted from Machida (1977).

in a magnetic field of 5 k Oe by making use of a magnetic balance. Results shown on Table 1 indicate that Oowakudani pyroclastic flow (HK 7), Kanmurigatake lava dome (HK 3) and Hutagoyama lava (HK 1) contain almost pure magnetite, and two Kamiyama pyroclastic flows (HK 6 and HK 9) contain titanomagnetite. The Js-T curve of HK 6 is irreversible, the Curie temperature (Tc) in cooling mode is about 100 degree lower than heating Tc. But, two of five samples of HK 6 was succeeded in the paleointensity experiment.

## 3. Experiments

Two specimens from the Kanmurigatake lava dome (HK 3) and five from other each flows were attributed to the ordinary Thellier's double heating method. The experiment was performed under the inducing magnetic field of 0.495 Oe and in nitrogen atmosphere when the heating temperature is higher than 200 °C.

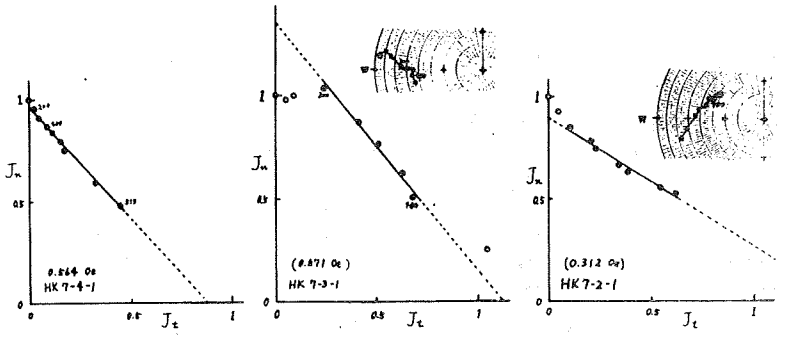


(a) (b) (c)

Fig. 1 Succeeded example (a) and rejected ones (b, c) of NRM-TRM diagram obtained from the Oowakudani pyroclastic flow (HK 7, 2,900 ± 100 years B.P.).

Experimental results were analyzed by plotting the data on the NRM-TRM diagram (Arai diagram; Arai, 1963; Nagata et al., 1963). Results of paleointensities are summarized in Table 2. 14 from 21 specimens were succeeded in the experiments.

Examples of NRM-TRM diagram obtained from the samples of Oowakudani pyroclastic flow (HK 7, 2,900 years B.P.) are shown on Fig. 1. Fig. 1 (a) is one of succeeded results. Fig. 1 (b) is rejected one because of the abnormal NRM direction of the sample although the paleointensity experiment itself is successful. This sample may be a rolled one of the same origin of others because the obtained paleointensity agrees well with other values, but there is no evidence for this supposition, so the obtained value was rejected. Fig. 1 (c) is another rejected example. NRM direction of this sample moves as the heating temperature becomes higher. This may be caused by the strong secondary remanent magnetization or the production of thermochemical remanent magnetization (TCRM). As already mentioned, there are geological evidences that the Kanmurigatake lava dome (HK 3) extruded at the same time as the formation of the Oowakudani pyroclastic flow (HK 7 ). The paleointensity value of 0.611 Oe obtained from this lava dome agrees well with four values determined from the pyroclastic

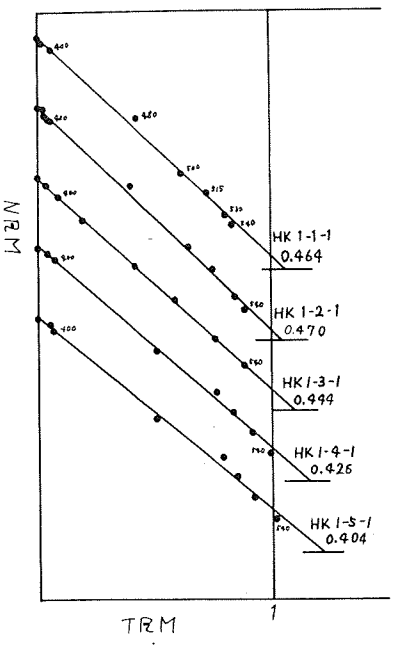


Fig. 2 NRM-TRM diagrams obtained from the Hutagoyama lava flow (HK 1, 4,475 ± 349 years B.P.).

flow. The mean paleointensity value of 0.608 ± 0.068 Oe for 2,900 years B.P. was obtained by averaging these five data.

The paleointensity experiments of the samples taken from the Hutagoyama lava flow (HK 1) were very successful as shown in Fig. 2. The NRM stability of these samples is very high and the change of NRM direction is within 10 degrees up to the high temperature of 540 °C. The paleointensity of 0.442 ± 0.027 Oe for the age of 4,475 years B.P. was obtained by averaging five results.

NRM directions of the Kamiyama pyroclastic flow (HK 6) converge well giving 6.2 degrees of $\alpha_{95}$ and this indicate that the formation temperature of this pyroclastic flow was enough high. But, the NRM stability to the progressing thermal demagnetization was not so good, and only two of five specimens were succeeded in the paleointensity experiment. Fig. 3 shows an succeeded example of the NRM-TRM diagram. Averaging the two obtained data, the paleointensity of 0.457 ± 0.047 Oe was obtained for 19,640 years B.P..

The Kamiyama pyroclastic flow (HK 9, 28,200 years B.P.) has also well converged NRM directions, but two of five specimens were unsuccessful in the paleointensity experiment as shown in Fig. 4. Two results were rejected because of a low correlation coefficient (r) of the straight line in NRM-TRM diagrams. It is noteworthy, however, that the paleointensity value, though it was rejected because of the low r, agrees well with those of the succeeded ones. According to the usual standard of analyzing the NRM-TRM diagram, the paleointensity value must be rejected that was determined from the diagram in

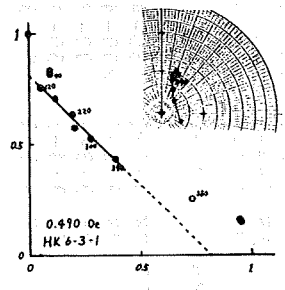


Fig. 3 An example of NRM-TRM diagram obtained from the Kamiyama pyroclastic flow (19,640 ± 550 years B.P.).

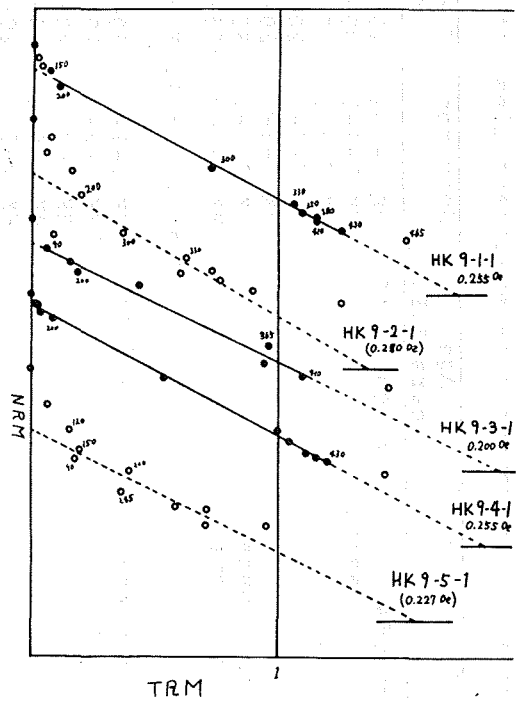


Fig. 4 NRM-TRM diagrams obtained from the Kamiyama pyroclastic flow (28,200 ± 1,700 years B.P.).

Table 2 Geomagnetic paleo-intensities determined by Thellier's double heating method

| Flow name | Age years B.P. | Specimen | $T_1$-$T_2$ °C | N | r | F Oe | Remarks |
|---|---|---|---|---|---|---|---|
| Owakudani pyroclastic flow | 2,900 ± 100 | HK 7-1-1 | 20-480 | 6 | 0.9898 | 0.554 | |
| | | HK 7-2-1 | 300-515 | 7 | 0.9886 | (0.312) | NRM direction changes |
| | | HK 7-3-1 | 300-480 | 5 | 0.9909 | (0.571) | reversed NRM |
| | | HK 7-4-1 | 20-515 | 9 | 0.9951 | 0.564 | |
| | | HK 7-5-1 | 20-515 | 8 | 0.9909 | 0.704 | |
| Kanmurigatake lava dome | | HK 3-1-1 | 365-515 | 6 | 0.9858 | 0.611 | |
| | | HK 3-1-2 | 365-515 | 6 | 0.9618 | (0.748) | low r |
| | | Mean : N = 4, F = 0.608 ± 0.068 Oe, RDM = 11.1 ± 1.2 x$10^{25}$ emu | | | | | |
| Hutagoyama lava | 4,475 ± 349 | HK 1-1-1 | 20-540 | 8 | 0.9980 | 0.464 | |
| | | HK 1-2-1 | 20-540 | 11 | 0.9988 | 0.470 | |
| | | HK 1-3-1 | 20-540 | 8 | 0.9998 | 0.444 | |
| | | HK 1-4-1 | 20-540 | 8 | 0.9987 | 0.426 | |
| | | HK 1-5-1 | 20-540 | 8 | 0.9975 | 0.404 | |
| | | Mean : N = 5, F = 0.442 ± 0.027 Oe, RDM = 8.09 ± 0.49 x$10^{25}$ emu | | | | | |
| Kamiyama pyroclastic flow | 19,640 ± 550 | HK 6-1-1 | | | | | very low r |
| | | HK 6-2-1 | 120-380 | 7 | 0.9174 | (0.484) | low r |
| | | HK 6-3-1 | 120-340 | 6 | 0.9878 | 0.490 | |
| | | HK 6-4-1 | 150-340 | 4 | 0.9581 | (0.423) | low r |
| | | HK 6-5-1 | 150-340 | 5 | 0.9908 | 0.424 | |
| | | Mean : N = 2, F = 0.457 ± 0.047 Oe, RDM = 8.36 ± 0.86 x$10^{25}$ emu | | | | | |
| Kamiyama pyroclastic flow | 28,200 ± 1,700 | HK 9-1-1 | 150-430 | 8 | 0.9980 | 0.255 | |
| | | HK 9-2-1 | 200-410 | 6 | 0.9625 | (0.280) | low r |
| | | HK 9-3-1 | 90-365 | 5 | 0.9906 | 0.200 | |
| | | HK 9-4-1 | 50-430 | 10 | 0.9991 | 0.255 | |
| | | HK 9-5-1 | 150-330 | 5 | 0.9097 | (0.227) | low r |
| | | Mean : N = 3, F = 0.237 ± 0.032 Oe, RDM = 4.34 ± 0.58 x$10^{25}$ emu | | | | | |

which little numbers of the points lie on a straight line or the correlation factor of the straight line is low. In this manner, however, it is feared that the useful data but of a little low degree of accuracy are rejected. Coe et al. (1978) proposed the method to avoid this fear which is based on the weighted mean of the paleointendity data by its degree of accuracy. But, the usual standard to accept or reject the obtained paleointensity was introduced in this paper and simple mean paleointensity of 0.24 ± 0.03 Oe was obtained for the age of 28,200 years B.P. from three of five specimens.

## 4. Discussion

Two paleointensity data in the Holocene and two in the latest Pleistocene were obtained in this research. Many paleointensity data were reported for the past 8,000 years B.P., and a sinusoidal variation of the geomagnetic intensity is supposed to have taken place (Smith, 1967; Cox, 1968; Bucha, 1970; Kono, 1972). The paleointensity data reported in this paper were converted to the reduced dipole moment (RDM; Smith, 1967) and two of them are shown in Fig. 5 with other data summarized by Kono (1972). It is noteworthy that the two data agree with the trend of the variation of the geomagnetic intensity for the past 8,000 years.

In the time range of the latest Pleistocene, very few paleointensity data are reported now. Barbetti and Flude (1979) summarized the paleointensity data for the latest Pleistocene, which are again tabulated in the Table 3 including the two data reported in this paper. He concluded that the earth's magnetic field appears to have been weaker than it is today for much of the period 50,000-10,000 years ago. The RDM of $4.3 \pm 0.6 \times 10^{25}$ e.m.u. reported in this paper for the age of 28,200 years B.P seems to agree with his conclusion but that of $8.4 \pm 0.9 \times 10^{25}$ e.m.u. for about 20,000 years B.P. does not. Their conclusion may be not reasonable because much of the ages of the flows used for the paleointensity experiment by now are restricted to around 25,000-30,000 years B.P.. The weakness of the geomagnetic field intensity around 28,000 years B.P. may be

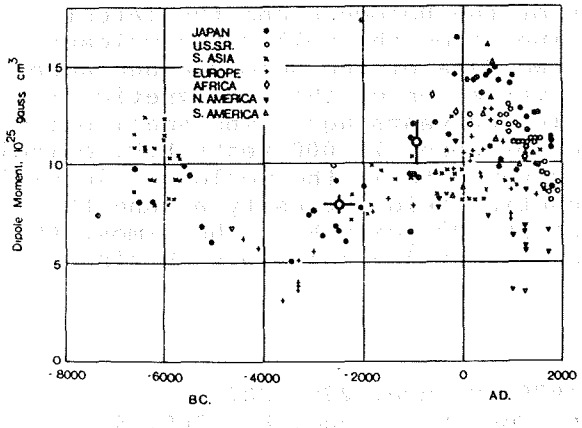


Fig. 5 The comparison of the two data obtained in this study with other data in the world summarized by Kono (1972) for the last 10,000 years.

Table 3 Summary of dipole moment data for the last 50,000 y.

| Site | Age years B.P. | Dipole moment $\times 10^{25}$ emu |
|---|---|---|
| Maniania Pali I, Hawaii | 10,140 ± 300 | 8.7 ± 1.5 |
| Maniania Pali II, Hawaii | >10,140 ± 300 | 7.6 ± 2.9 |
| Etiolles/Marsangy, France | 12,000 ± 500 | 7.6 ± 0.7 |
| Hilina Pali I, Hawaii | 17,360 ± 650 | 3.7 ± 4.4 |
| Hilina Pali II, Hawaii | >17,360 ± 650 | 4.8 ** |
| Lake Mungo(F51), Australia | 19,420 ± 360 | 5.4 ± 0.8** |
| Hakone Volcano, Japan(this work) | 19,640 ± 550 | 8.4 ± 0.9** |
| Lake Mungo(F20), Australia | 25,310 ± 810 | 5.3 ± 0.2** |
| Lake Mungo(F17), Australia | 25,570 ± 520 | 4.0 ± 1.1** |
| Lake Mungo(F6), Australia | 27,270 ± 470 | 3.8 ± 1.1 |
| Lake Mungo(F16), Australia | 28,140 ± 370 | 5.8 ± 2.1** |
| Hakone Volcano, Japan(this work) | 28,200 ± 1,700 | 4.3 ± 0.6** |
| Royat, France | 25,800 ± 2,200* | 2.4 ± 0.2 |
| Lake Mungo(F14), Australia | 31,400 ± 4,400* | 3.4 ± 0.5 |
| Dolni Vestonice, Czechoslovakia | 28,800 ± 170 | 4.2 ± 0.7** |
| Lake Mungo(F9), Australia | 27,530 ± 340 | 28.1 ±11.0 |
| Lake Mungo(F12), Australia | 28,000 ± 410 | 47.2 |
| Lake Mungo(F8), Australia | 28,310 ± 410 | 15.1 ± 1.8 |
| Lake Mungo(F7), Australia | 30,780 ± 520 | 22.8 ± 3.2 |
| Boissejour, France | ~50,000 * | 3.3 ± 0.2** |

All the data but those of this work were quated at second hand from Barbetti and Flude(1979).

* Thermoluminescence age.

** Reduced dipole moment (RDM).

valid because the seven data summarized by Barbetti and Flude (1979) and one reported in this paper coinside well, but the intensity was not always weak because the geomagnetic field intensity for the age of about 20,000 years B.P. reported in this paper is almost the same as the present day value and most of the paleointensities obtained from several lava flows of Mt. Fuji of the age around 10,000 years B.P. are larger than the present day value (Tanaka, in preparation).

## 5. Concluding remarks

Four paleointensities of the Holocene and the latest Pleistocene ages were obtained from the well dated volcanic rocks of Hakone volcano. Two data of the Holocene age agree well with the trend of the variation of the geomagnetic field intensity during the last 10,000 years ago. The small paleo-intensity value for the age of about 28,000 years B.P. coincide with the already reported seven data in the world and justifies the weakness of the geomagnetic field intensity around this time. For the age of about 20,000 years B.P. the almost the same paleointensity as the present day value was obtained.

## References

Barbetti,M. and K.Flude (1979) Nature, 279, 202.
Bucha,V (1970) Phil. Trans. Roy. Soc. Lond. A., 269, 47.

Coe,R.S., S.Gromme, and E.A.Mankinen (1978) J. Geophys. Res., 83, 1740.
Cox,A. (1968) J. Geophys. Res., 73, 3247.
Kono,M. (1972) Phys. Earth Planet. Interiors, 5, 140.
Machida,H. and A.Moriyama (1968) Geographical Review of Japan, 41, 241.
Machida,H. (1977) Kazanbai wa Kataru (in Japanese) (Soju,Tokyo) p.324.
Nagata,T, Y.Arai, and K.Momose (1963) J. Geophys. Res., 68, 5277.
Smith,P.J. (1967) Geophys. J. R. astr. Soc., 12, 321.

(In preparation for J. Geomag. Geoelectr.)

# A GEOMAGNETIC REVERSAL IN THE LATEST BRUNHES EPOCH DISCOVERED AT SHIBUTAMI, JAPAN

Hidefumi TANAKA* and Koichi TACHIBANA**

*Department of Applied Physics, Tokyo Institute of Technology, Meguro-ku, Tokyo 152
**Faculty of Education, Iwate University, Ueda, Morioka-shi, Iwate 020

## 1. Introduction

Tachibana (1977) reported the discovery of a geomagnetic reversal from the Shibutami welded tuff, and he concluded that this reversal may be related to the Laschamp event of 20,000-30,000 years B.P. (Bonhommet and Zähringer, 1967) and the Lake Mungo geomagnetic excursion around 30,000 years B.P. (Barbetti and McElhinny, 1976). In this paper, an additional paleomagnetic study is reported.

## 2. Geology

The geographical distribution of the Shibutami welded tuff is limitted around Shibutami village about 15 km north of Morioka city (Tachibana, 1971). The origin of this welded tuff is not yet fully clarified, but it is suspected that this welded tuff flowed out in the form of a pyroclastic flow from a region west of Shibutami for a short time span. The age of the formation is suspected to be very young of 20,000-30,000 years B.P. judging from many geological evidences (Tachibana, 1977). The most important example of the geological evidences is shown in the Fig. 1. Blocks of the welded tuff (E) are jammed in a sand and gravel bed (F, D), and these blocks are not roled ones because some mineralogical textures are parallel to the horizons of other beds. The upper (F) and the lower (D) sand and gravel bed are considered to be the same origin,

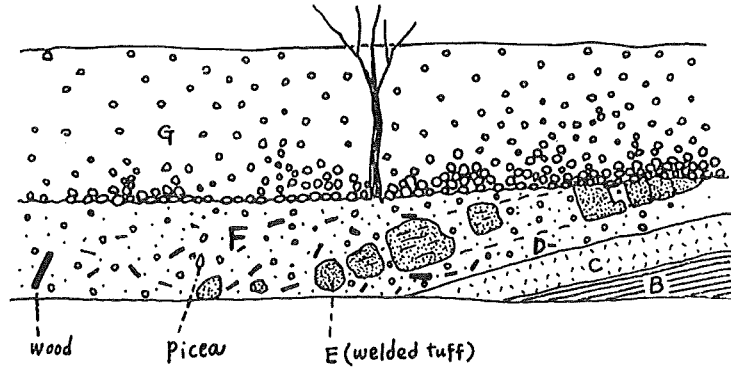


Fig. 1 One of the geological evidences showing the young age of the Shibutami welded tuff.

so the welded tuff which is situated between the two sand and gravel bed is formed at the almost same time as the sand and gravel bed. Two radiocarbon dated ages are reported as 30,780 ± 2,170 and 29,630 ± 2,130 years B.P. determined from the carbonated woods contained in the sand and gravel bed, so the age of the welded tuff amounts to about 30,000 years B.P..

## 3. Samples

Five to eight cores were sampled by engine cutter at four sites which are located with several kilometers distance (SI 1 -SI 4). The specially made instrument to determine the orientation of cores were used, and the possible orientation error may be within 1 degree.

A Js-T curve of a bulk sample taken from the second site (SI-2) was measured by a magnetic balance in a vacuum of $10^{-5}$ Torr and a magnetic field of 5 k Oe, and gave two Curie temperatures (Tc) of 534 °C and 586 °C. These values of Tc's indicate that the magnetic minerals contained in this sample are almost pure magnetite, and reject the possibility that the NRM of this sample is self-reversal.

## 4. NRM directions

Two pilot specimens were demagnetized progressively in the alternating field (A.F.) up to the peak field of 1,600 Oe. The two A.F. demagnetization curves showed an increase in NRM intensity of 10 and 50 percent around the peak field of 150 Oe. This is often the case with the reversed NRM having a secondary component which is magnetized to the present day geomagnetic field direction. The large median demagnetizing fields (MDF) of 500 and 800 Oe indicate the good stability of NRM's.

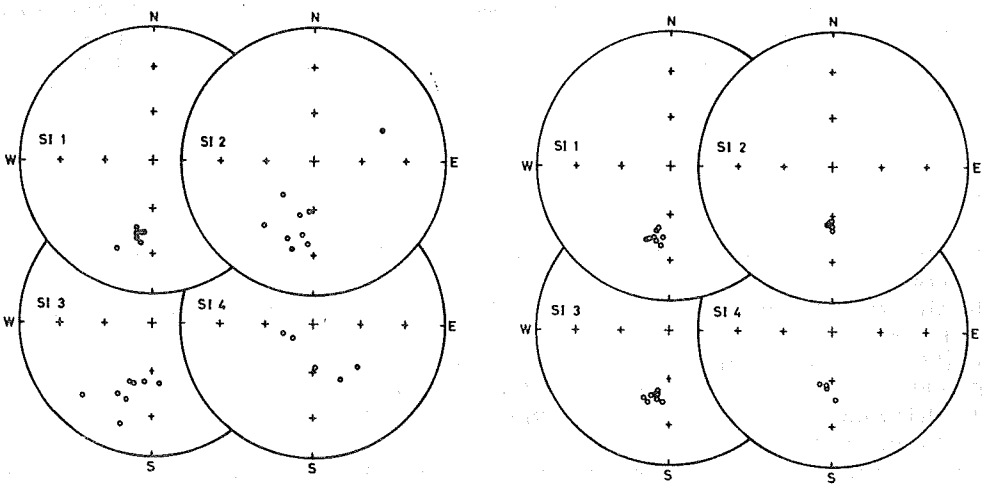


Fig. 2 Directions of NRM's (a) and the stable remanent magnetization after cleaning in the A.F. field of 150 Oe (b) plotted on the Schmidt's equal area projection net.

Table Paleodirections of the Shibutami welded tuff

| Site | N | I | D | $\alpha_{95}$ | VGP |
|---|---|---|---|---|---|
| SI 1 | 8 | -44.9 ° | 190.6 °E | 3.2 ° | |
| SI 2 | 7 | -54.3 | 182.0 | 1.9 | |
| SI 3 | 8 | -47.2 | 192.0 | 3.0 | |
| SI 4 | 5 | -55.3 | 183.8 | 5.1 | |
| Mean | | -50.5 | 187.5 | 6.8 | 79.4 °S 104.0 °E |

All the specimens were magnetically cleaned by the A.F. field of 150 Oe which may remove most of secondary components, and results are shown in Fig. 2 and on the Table. After the magnetical cleaning, good convergence of NRM directions were obtained for all the four sites.

## 5. Discussion

Mean paleodirection was determined by averaging the four mean site directions as summarized on the Table. The geomagnetic dipole moment at the age of the formation of the Shibutami welded tuff had a just reversed direction to that of the present day dipole moment, if the dipole moment at the earth's center is supposed. This indicate that the Shibutami geomagnetic reversal may not be an excursion which usually shows an abnormal paleodirection, so the reversal may not be directly related to excursion around 30,000 years B.P. such as the Lake Mungo excursion (Barbetti and McElhinny, 1976) and Mono Lake excursion (Liddicoat and Coe, 1979), but rather, has an relation to the short event known as the Lashamp event of about 20,000 years B.P. (Bonhommet and Zähringer, 1969) and the Blake event of about 110,000 years B.P. (Smith and Foster, 1969).

The age of the Shibutami welded tuff of about 30,000 years B.P. is not very decisive as mentioned already, but it is never so old as the Matsuyama reversed epoch, so it is possibly concluded that there was a reversed epoch at the latest Pleistocene in Japan.

## References


Barbetti,M.F. and M.W.McElhinny (1976) Phil. Trans. R. Soc. Lond., 281, 515.

Bonhommet,N and J.Zähringer (1969) Earth Planet. Sci. Lett., 6, 43.

Liddicoat,J.C. and R.S.Coe (1979) J. Geophys. Res., 84, 261.

Smith,J.D. and J.H.Foster (1969) Science, 163, 565.

Tachibana,K. (1971) Annual Report of the Faculty of Education, University of Iwate, 31, 37.

Tachibana,K. (1977) Annual Report of the Faculty of Education, Iwate University, 37,9.

# VARIATION OF THE GEOMAGNETIC FIELD INTENSITY IN FOUR DEEP-SEA CORES

Takaharu SATO

Department of Physics, Faculty of Engineering Science, Osaka University, Toyonaka, Japan

Kazuo KOBAYASHI

Ocean Research Institute, University of Tokyo, Nakano-ku, Tokyo, Japan

## Introduction

In recent years isotopic studies using deep-sea sediments have been extensively undertaken (Shackleton and Opdyke, 1976; Donk, 1976) and have caused a growing interest in a relationship between climate and intensity of the earth's magnetic field. Wollin et al. (1978) have suggested the existence of a relationship among climate, the magnetic field and the eccentricity of the earth's orbit. On the other hand, Chave and Denham (1979) have mentioned that no correlation is evident between climate and the paleomagnetic field intensity.

For deep-sea sediments, while a number of studies are carried out on the paleomagnetic direction, only a few studies pertinent to the paleointensity during the past 1,000,000 yr can be found. In the measurements of the paleointensity, the effect of the variation of magnetic material should be estimated. In order to eliminate the effect, it is necessary to normalize natural remanent magnetization (NRM) intensity by dividing it with the intensity of artificial remanent magnetization (Opdyke et al., 1973; Kawai et al., 1976, 1977; Kent and Opdyke, 1977; Sueishi et al., 1979). The change of deep-sea environment such as sedimentation rate should also be considered. The effect of sedimentation rate could be known by studying various cores from different sites.

In the present work specimens from three cores (KH 73-4-8, KH 72-2-2 and KH 72-2-58) are studied to clarify the change of paleointensity. The variations in the normalized intensity of the cores are compared with that of core KH 73-4-7 previously reported (Kawai et al., 1976, 1977; Sueishi et al., 1979).

Table 1. Sampling site

| Core | KH 73-4-7 | KH 73-4-8 | KH 72-2-2 | KH 72-2-58 |
|---|---|---|---|---|
| Position | 2°41.3'N<br>164°50.2'E | 1°33.2'S<br>167°38.6'E | 30°0.0'N<br>150°0.0'E | 22°53.2'N<br>129°13.2'E |
| Water depth | 4,160 m | 4,000 m | 5,800 m | 5,300 m |
| Core length | 11.27 m | 10.58 m | 6.00 m | 6.60 m |

## Sampling and Measurement

The three cores in addition to the previous one are collected by R. Hakuho-maru from the West Pacific Ocean as given in Table 1. From core KH 73-4-8 the specimens to be studied are prepared with the method described by Kawai et al. (1976). From cores KH 72-2-2 and KH 72-2-58 the specimens are obtained by enveloping the dried cores with paraffin and by slicing them into sections with a non-magnetic cutting wheel.

Natural remanent magnetization vectors are measured using a Schonstedt spinner magnetometer after AF cleaning in 100 Oe. Artificial remanent magnetization vectors are measured with an astatic magnetometer. Saturation isothermal remanent magnetization (SIRM) is generated in a field of 9,000 Oe for core KH 73-4-8. Anhysteretic remanent magnetization (ARM) is acquired in a constant field (0.83 Oe) and a peak alternating field of 1,000 Oe.

A very large values of NRM/ARM are found at the depth of 451 cm in core KH 72-2-2. The sediment of this portion was found to consist of volcanic ash.

## Results and Discussion

The results for core KH 73-4-7 (Kawai et al., 1976, 1977; Sueishi et al., 1979) are compiled in Fig. 1. For core KH 73-4-8 the results obtained from the present work are shown in Fig. 2 together with previous ones (Kawai et al., 1977; Sato et al., 1977). From the features of NRM/SIRM in Figs. 1 and 2 it is clear that both cores KH 73-4-7 and KH 73-4-8 are corresponding to each other from the portion of the Brunhes-Matuyama boundary to that of the Olduvai event. Furthermore, the two cores correspond to each other for the Brunhes epoch. In Figs. 1 and 2, the same odd numbers are labelled at the correspondent peaks which divide stages tentatively introduced here.

The correspondence seems to be supported from the micropaleontological evidence investigated by Takayanagi et al. (1979). Visual lithological description of cores on board the ship indicated that there were darkish portions in the sediment, in which SIRMs have large values. The portions are shown in Figs. 1 and 2 with the hatched lines.

Although there were no microfossils unfortunately, the variations of NRM/ARM in cores KH 72-2-2 and KH 72-2-58 correspond to those of NRM/SIRM in cores KH 73-4-7 and/or KH 73-4-8 (Figs. 3 and 4). Then, a magnetic event found at the depth of 30 cm in core KH 72-2-58 seems to coincide with that found and claimed as Biwa event in core KH 73-4-7 (Kawai et al., 1976). Moreover, the variations in NRM/ARM given by Kent et al. (1977) seem to be consistent with those shown here.

Although there remain some discrepancies such as abnormally large values in NRM/ARM at the depth of 451 cm in core KH 72-2-2 and the trends of the decrease in the normalized intensity with depth in cores KH 72-2-58 and KH 73-4-8, the present work has shown an unequivocal correspondence among the cores studied and has further elucidated the variations of the geomagnetic field intensity during the period from 1,700,000 yr to 300,000 yr.

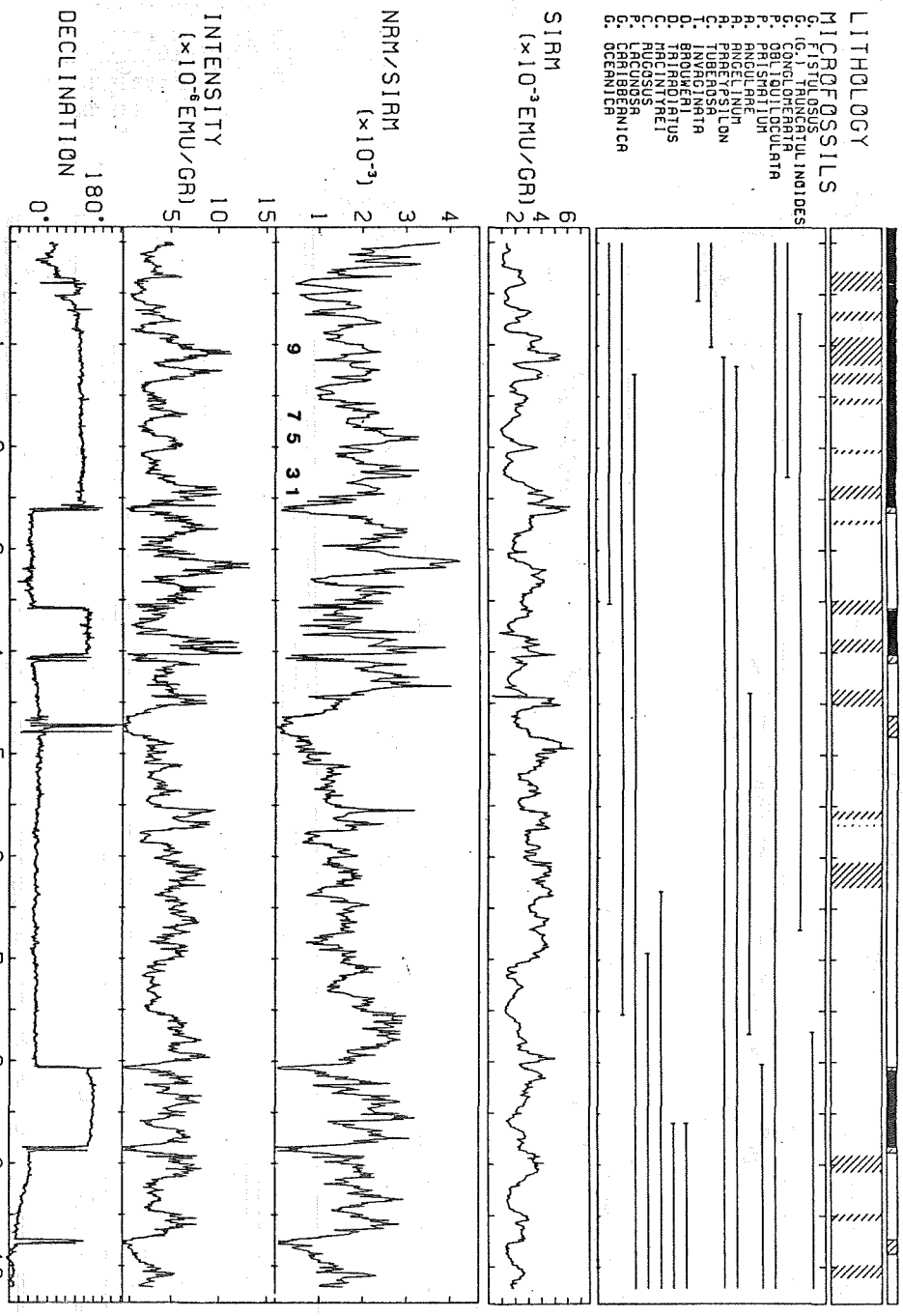


Fig. 1. The results for core KH 73-4-7. The magnetic data in region 0 to 301 cm are from Kawai et al. (1976), 301 to 449 cm from Kawai et al. (1977) and 449 to 1,027 cm from Sueishi et al. (1979). The micropaleontological results are quoted from Takayanagi et al. (1979). The numbers indicate the geomagnetic stages.

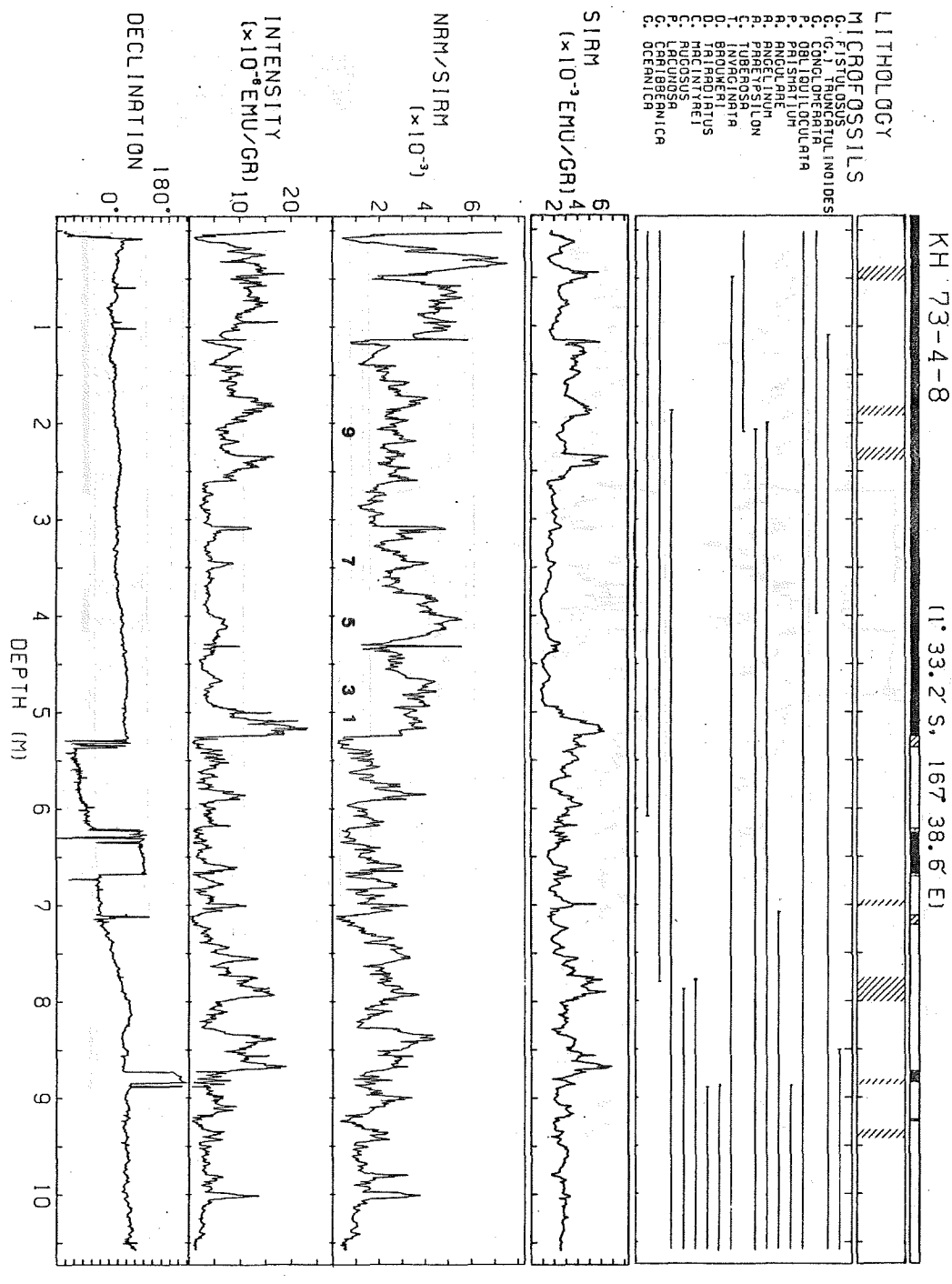


Fig. 2. The results for core KH 73-4-8. The magnetic data in region 113 to 494 cm are from Sato et al. (1977), 494 to 686 cm from Kawai et al. (1977) and 686 to 872 cm from Sueishi et al. (1979). The data in region 113 to 307 cm (Sato et al., 1977) are corrected. The micropaleontological results are quoted from Takayanagi et al. (1979). The numbers indicate the geomagnetic stages, each corresponding to that in Fig. 1.

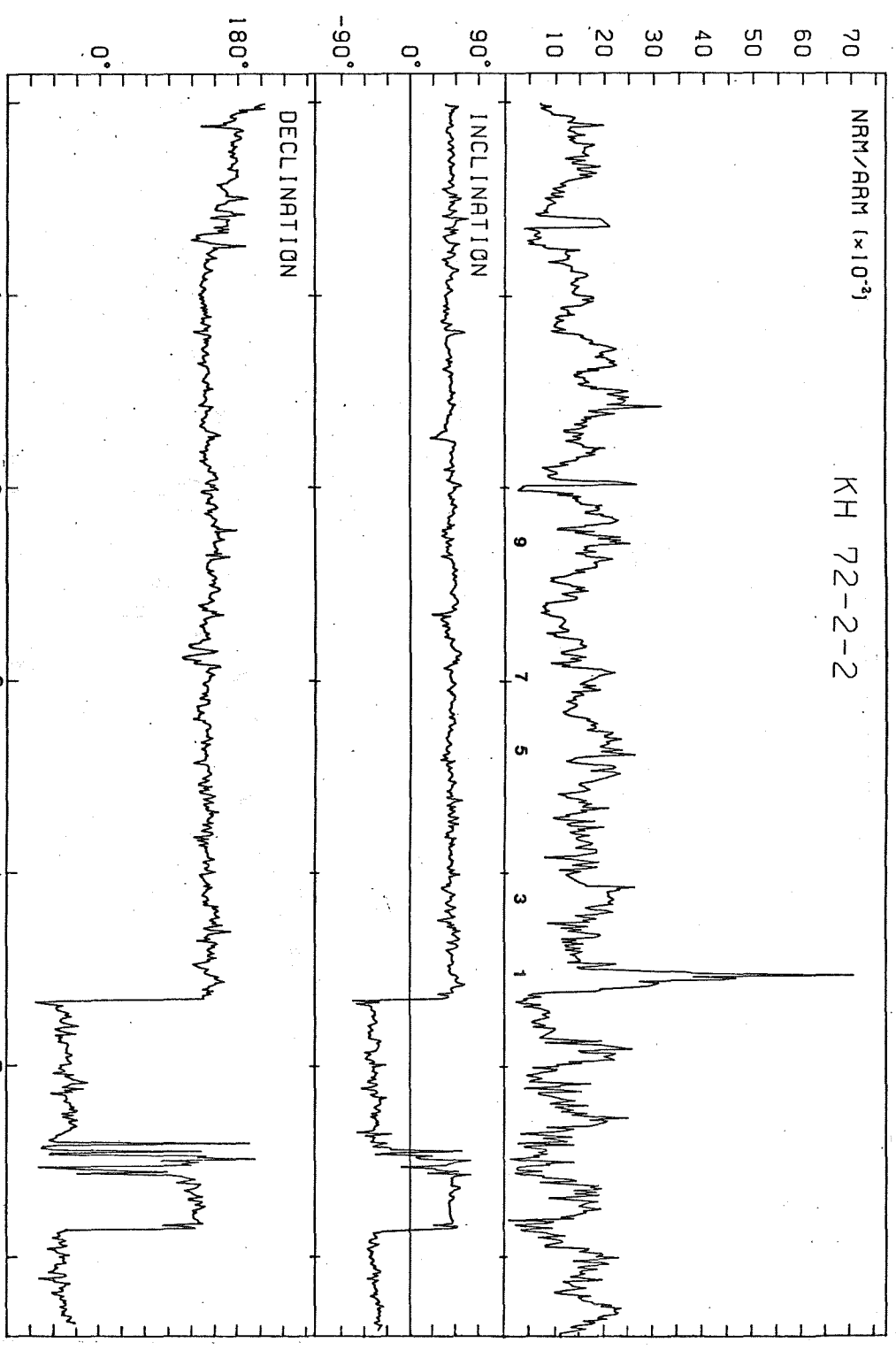


Fig. 3. The results for core KH 72-2-2. The numbers indicate the geomagnetic stages, each corresponding to that in Figs. 1 and 2.

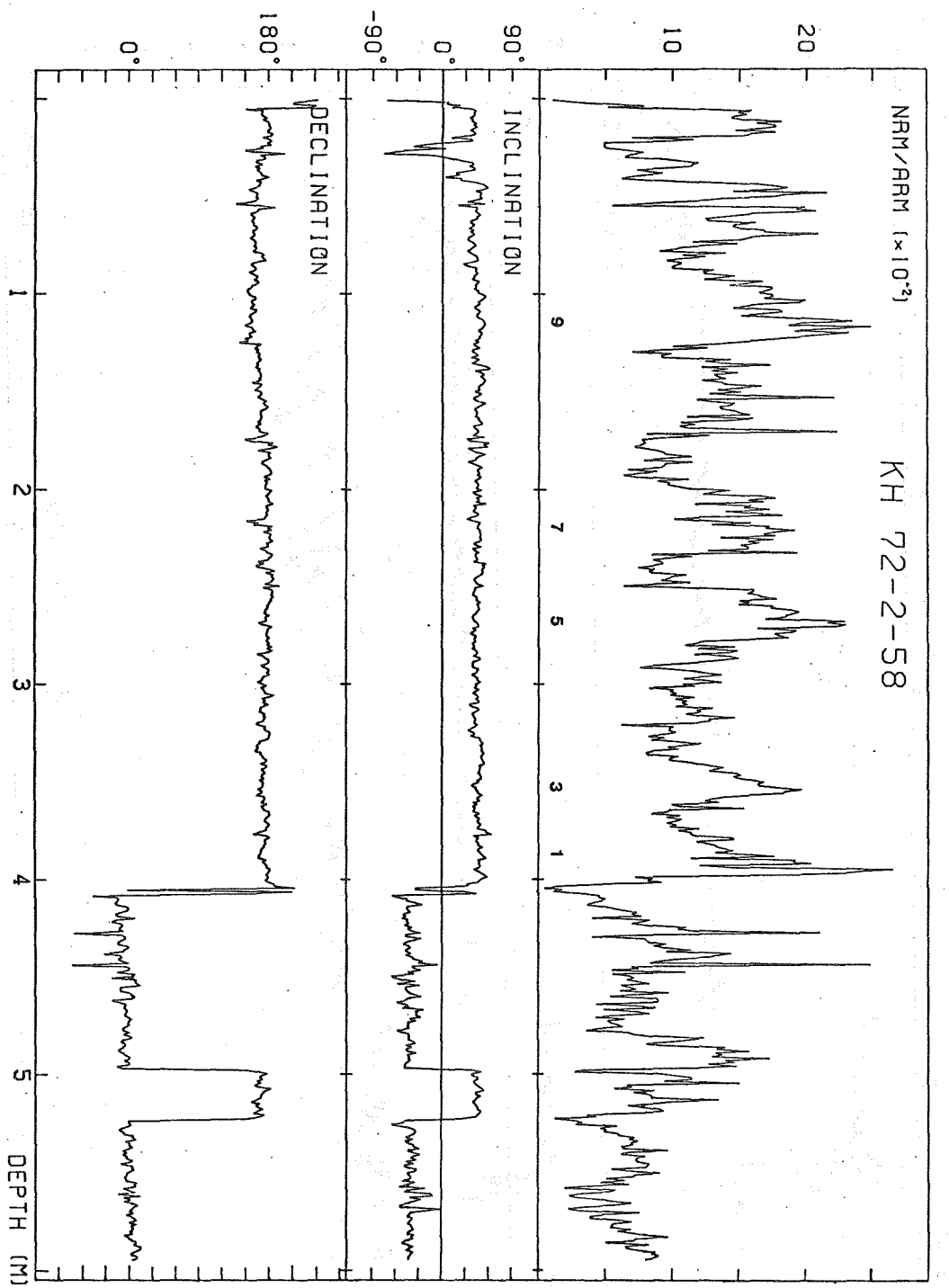


Fig. 4. The results for core KH 72-2-58. The numbers indicate the geomagnetic stages, each corresponding to that in Figs. 1 to 3.

References

Chave, A.D. and C.R. Denham (1979) Earth Planet. Sci. Lett., 44, 150-152.
Donk, J.V. (1976) Geol. Soc. Am. Mem., 145, 147-163.
Kawai, N., Y. Otofuji and K. Kobayashi (1976) J. Geomag. Geoelectr., 28, 395-412.
Kawai, N., T. Sato, T. Sueishi and K. Kobayashi (1977) J. Geomag. Geoelectr., 29, 211-223.
Kent, D.V. and N.D. Opdyke (1977) Nature, 266, 156-159.
Opdyke, N.D., D.V. Kent and W. Lowrie (1973) Earth Planet. Sci. Lett., 20, 315-324.
Sato, T., N. Kawai and K. Kobayashi (1977) Rock Mag. Paleogeophys., 4, 95-98.
Shackleton, N.J. and N.D. Opdyke (1976) Geol. Soc. Am. Mem., 145, 449-464.
Sueishi, T., T. Sato, N. Kawai and K. Kobayashi (1979) Phys. Earth Planet. Int., 19, 1-11.
Takayanagi, Y., T. Takayama, T. Sakai, M. Oda and M. Kato (1979) Tohoku Univ. Sci. Rep. 2nd ser. (Geol), 49, 71-87.
Wollin, G., W.B.F. Ryan and D.B. Ericson (1978) Earth Planet. Sci. Lett., 41, 395-397.

# PALEOMAGNETIC CHRONOLOGY OF THE PLIO-PLEISTOCENE KOBIWAKO GROUP ON THE EAST COAST OF LAKE BIWA, CENTRAL JAPAN

Akira HAYASHIDA* and Takuo YOKOYAMA**

*Department of Geology and Mineralogy, Kyoto University, Kyoto 606
**Laboratory of Earth Science, Doshisha University, Kyoto 602

## INTRODUCTION

The lacustrine deposits distributed around Lake Biwa, central Japan, are called the Kobiwako Group, and one of the typical Plio-Pleistocene strata of Japan, along with its adjacent correlatives, the Osaka Group and Tokai Group. Magnetostratigraphy of these strata were previously studied by several authors (Ishida et al., 1969; Torii et al., 1974; Maenaka et al., 1977). However, their samples were restricted to volcanic ashes which are sporadically intercalated in sediments, and the stability of remanent magnetization was not adequately examined. We attempt to establish paleomagnetic chronology for these Plio-Pleistocene Series on the basis of detailed data of local stratigraphy, providing more reliable data of paleomagnetism with alternating field and thermal demagnetizations. In this report, the results of magnetic polarity stratigraphy are described for the Kobiwako Group on the east coast of Lake Biwa.

## GEOLOGICAL SETTING AND METHODS

The Kobiwako Group is divided into the following six formations in ascending order (Yokoyama, 1969): Shimagawara, Iga-Aburahi, Sayama, Gamo, Yokaichi, and Katata formations. On the east coast of Lake Biwa, the main distributions are the Iga-Aburahi, Sayama, Gamo, Yokaichi Formations (Figure 1). Stratigraphic descriptions of these are given in Yokoyama et al.(1968), Kaigake Research Group(1972), Kobiwako Research Group(1977), Tamura et al.(1977), and Amemori et al.(1979). The Kobiwako Group in this area, which is composed of clays, sands and gravels with some volcanic ash seams, are thought to have been accumulated in the paleo-lake preceding to the present-day Lake Biwa (Yokoyama, 1969).

Most of paleomagnetic samples were collected from volcanic ashes and mud layers of the Sayama and Gamo Formations, and two from the Iga-Aburahi Formation. These samples were divided into six to eight specimens and then mounted in plastic cases of 2 cm cubes in the laboratory. Remanent magnetization of the specimen was measured with a spinner magnetometer (Schonstedt's Type SSM-1A).

One specimen from each site was chosen for progressive alternating field (AF) demagnetization in peak fields up to 400 Oe. Natural remanent magnetization of most volcanic ash samples was remarkably stable against AF demagnetization. Other specimens seem to have relatively soft components of magnetization with secondary overprints, probably originated from viscous remanent magnetization. The intensity values of most specimens were well above the intrinsic noise level of our measuring instrumentation (about $1 \times 10^{-7}$ emu/cc). Thermal demagnetization test was also performed stepwise on selected specimens. The remanent magnetization of most specimens did not show any significant changes in direction which exceed those by AF demagnetization. Consequently, AF demagnetization with a peak field of 200 or 400 Oe was applied to other

specimens for routine treatment of magnetic cleaning.

## RESULTS AND DISCUSSION

Mean direction and precision parameters of remanent magnetization were calculated for each site using the statistics of Fisher(1953). The positions of the virtual geomagnetic poles (VGP's) were also calculated to determine the magnetic polarity of each site. In that case, a few sites that have less significant concentration of magnetic directions were excluded by the guideline of the precision parameter (k) smaller than 10. Figure 2 represents a plot of the latitudes of VGP's with the stratigraphic position of sampling sites. Fission track ages of some volcanic ashes are also shown in the figure (Nishimura and Sasajima, 1970; Yokoyama et al., 1977). The accuracy of this data is estimated to be less than 20 % concerning sample errors, and the decay constant for spontaneous fission of $^{238}U$ is assumed as $6.85 \times 10^{-17}$ $year^{-1}$.

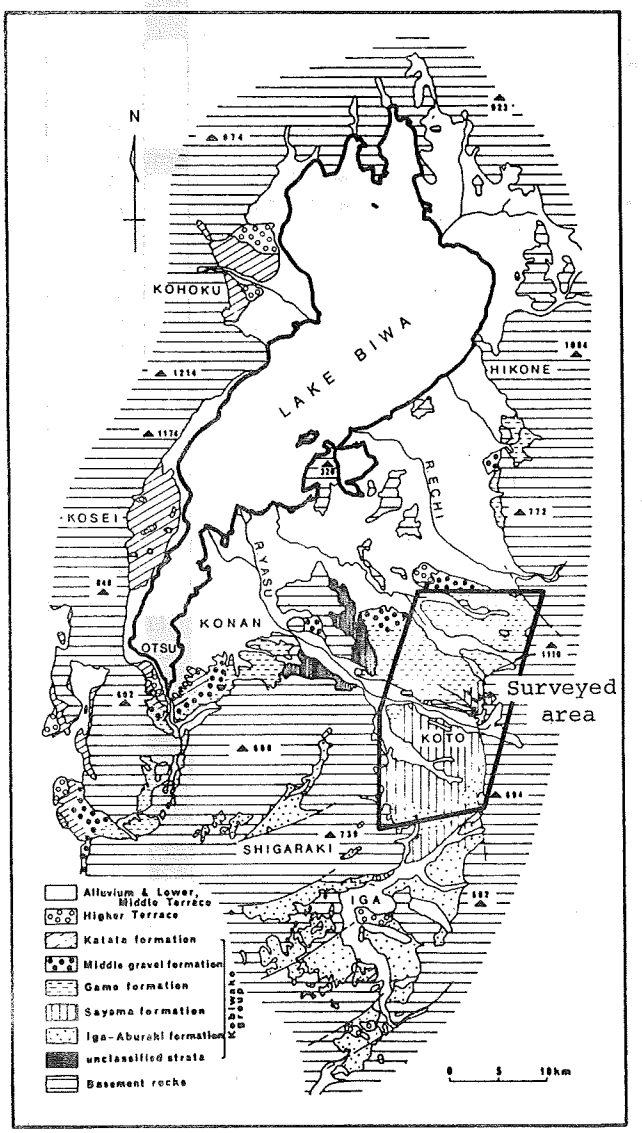


Figure 1. Map showing distribution of the Kobiwako Group and location of surveyed area. Base map from Ikebe and Yokoyama(1976).

It can be seen that at least eight transitions of magnetic polarity are recorded in the strata studied. The correlation of this polarity log to the paleomagnetic time scale of Mankinen and Dalrymple(1979) is interpreted as shown in the figure. The normal magnetozone associated with the Naka volcanic ash in the upper part of the Gamo Formation appears to represent the Olduvai normal event, which is a key character of the Pliocene/Pleistocene boundary. The exact boundary of the Carabrian stratotype in southern Italy was shown to be correlated to a level near the top of the Olduvai event by means of biostratigraphy (Haq et al., 1977). It is therefore suggested that the local Pliocene/Pleistocene boundary occurs between the Naka and Kitawaki volcanic ash layers in the Kobiwako Group. Another

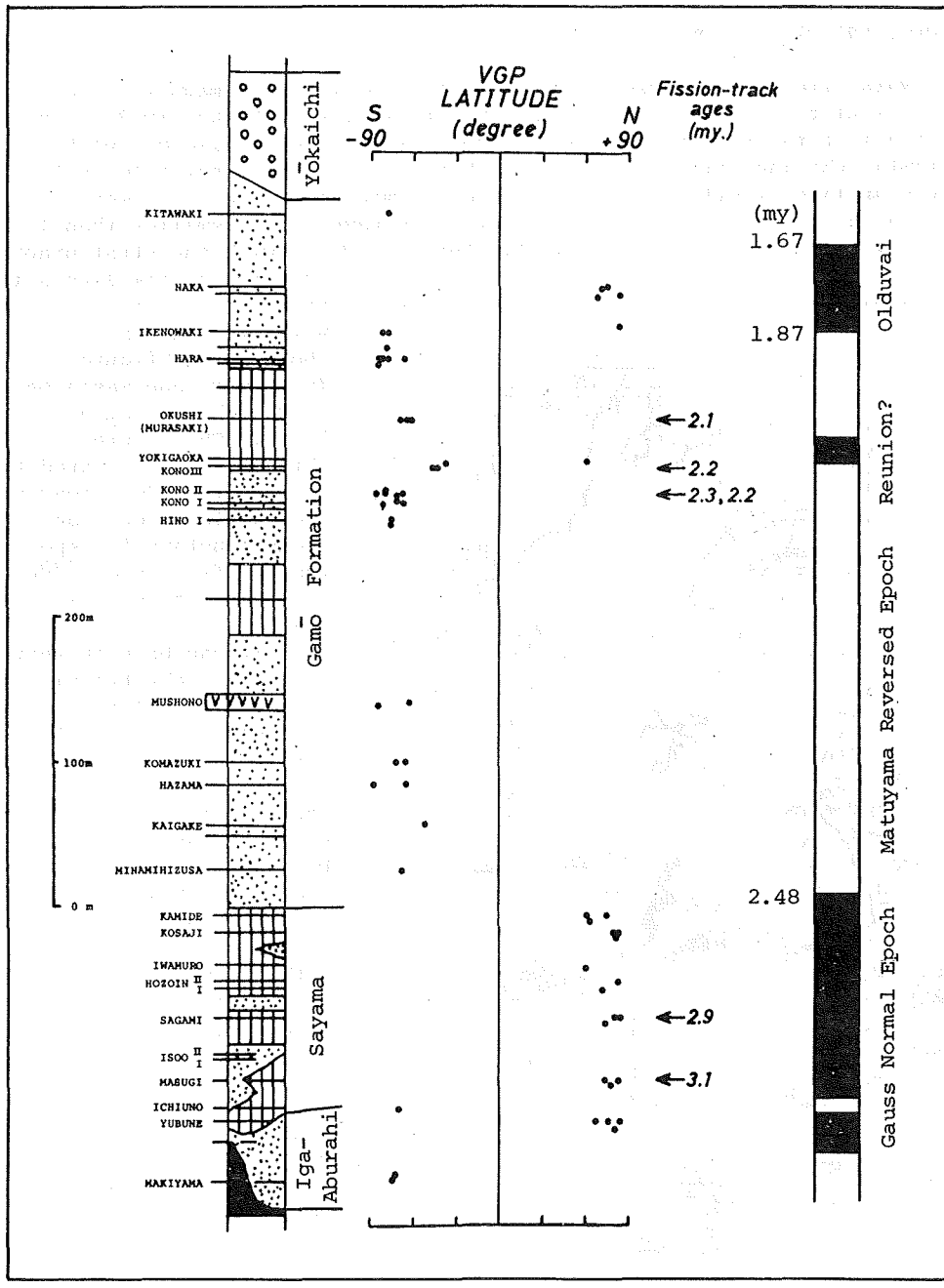


Figure 2. Plot of VGP latitudes vs. stratigraphic positions of sampling sites, and correlation of the magnetozones to paleomagnetic time scale (Mankinen and Dalrymple, 1979). Fission track ages of volcanic ashes are also shown after Nishimura and Sasajima(1970), and Yokoyama et al.(1977). Geologic columnar section(left) was compiled from Yokoyama et al.(1968), Tamura et al.(1977), and Amemori et al.(1979).

normal episode recorded by the Yokigaoka volcanic ash may be correlated to the Reunion normal event. The magnetic polarity transition detected between the Kamide and Minamihizusa volcanic ash layers is correlated to the Matuyama/Gauss Epoch boundary with age of 2.48 my. If the correlation described above is correct, it gives the sedimentation rate of 0.5 to 0.6 $m/10^3$ year for the Gamo Formation. This sedimentation rate favors the correlation of the reversely magnetized horizons in the Sayama and Iga-Aburahi Formations to the reversed events in the Gauss Epoch rather than the Gilbert Reversed Epoch.

Thus it is concluded that the Kobiwako Group on the east coast of Lake Biwa extends about 1.5 my. from the Gauss Normal Epoch to above the Olduvai normal event in the middle Matuyama Reversed Epoch. The present conclusion is in agreement with the fission track ages. It also shows no discordance with the previous result of paleomagnetic chronology (Ishida et al., 1969; Maenaka et al., 1977), while the exact horizons of the datum levels were revised.

## REFERENCES CITED


Amemori, S., Tamura, M. and T. Yokoyama(1979): in preparation.

Fisher, R.(1953): Proc. Roy. Soc. (A), 217, 295.

Haq, B. C., Berggren, W. A. and J. A. van Couvering(1977): Nature, 269, 483.

Ikebe, N. and T. Yokoyama(1976): Paleolim. Lake Biwa Japanese Pleist., 4(ed. S. Horie), 31.

Ishida, S., Maenaka, K. and T. Yokoyama(1969): Jour. Geol. Soc. Japan, 75, 183.

Kaigake Research Group(1972): Jour. Geol. Soc. Japan, 78, 601.

Kobiwako Research Group(1977): Chikyu Kagaku(Earth Sci.), 31, 115.

Maenaka, K., Yokoyama, T. and S. Ishida(1977): Quaternary Res., 7, 341.

Mankinen, E. A. and G. B. Dalrymple(1979): Jour. Geophys. Res., 84, 615.

Nishimura, S. and S. Sasajima(1970): Chikyu Kagaku(Earth Sci.), 24, 222.

Tamura, M., Matsuoka, C. and T. Yokoyama(1977): Jour. Geol. Soc. Japan, 83, 749.

Torii, M., Yoshikawa, S. and M. Itihara(1974): Rock Mag. Paleogeophys., 2(ed. M. Kono), 34.

Yokoyama, T.(1969): Mem. Fac. Sci. Kyoto Univ. (B), 36, 19.

Yokoyama, T., Danhara, T., Kobata, Y. and S. Nishimura(1977): Paleolim. Lake Biwa Japanese Pleist., 5(ed. S. Horie), 44.

Yokoyama, T., Matsuoka, C., Nasu, T. and M. Tamura(1968): Jour. Geol. Soc. Japan, 74, 327.

# PALEOMAGNETISM OF MIDDLE MIOCENE MURŌ VOLCANICS IN SOUTHWEST JAPAN

Masayuki TORII

Department of Geology and Mineralogy, Kyoto University, Kyoto 606

## INTRODUCTION

Remanent magnetization of the Murō volcanics was first measured by Hirooka (1961, MS) in a paleomagnetic reconaissance of the Neogene volcanics in southwestern Japan. He revealed an anomalous NRM direction of Murō welded tuffs. Nishiyama (1975) confirmed the direction in his paleomagnetic investigation of the Murō district. Their results suggest the low latitude pole position at Middle Miocene which was recorded in the volcanic rocks.

The present study was carried out as a preparation for a paleointensity determination on the anomalously magnetized Murō volcanics.

## GEOLOGIC SETTING

The Murō district consists of several mountains about 30 km southeast of Nara City. After Shiida et al. (1967) and Yokota et al. (1978), the basements of this area are regionally metamorphosed complex of Cretaceous age (Ryoke Complex), and is unconformably overlain by the Miocene marine sediments (Yamagasu and Yamabe Groups). The Murō Group which consists of sediments and Murō volcanics unconformably rest upon the marine sediments (Fig. 1).

The Murō volcanics have an extensive distribution of about 30 km × 15 km, and a maximum thickness of more than 400 m. The volume of volcanic products is estimated to be 50 $km^3$. Although more than ten cooling units are visible, a subdivision with the stratigraphic sequence of those units is not established.

The Murō volcanics are mainly composed of dacitic welded tuffs with subordinate amount of intercalated non-welded pyroclastics. The welded tuffs are subdivided into two types; most of them are light colored rocks with microcrystalline groundmass (w-type), and less amount of dark colored rocks with glassy groundmass like a vitrophyer (b-type). Their phenocrysts consists of quartz, plagioclase, biotite, orthopyroxene, and other minor minerals. No distinct variation of chemical and modal composition between w- and b-type was observed (Shiida et al., 1967).

K-Ar age of sanidine in the b-type rock was reported to be 13.1 ± 0.4 Ma by Hirooka and Kawai (1967).

## PALEOMAGNETIC MEASUREMENTS

Samples were collected from 33 sites which were selected to represent the specific and lithologic variations of the Murō volcanics. At each site three samples were taken as large hand samples and drilled in the loboratory. More than thirty cylindorical specimens (2.5 cm in diameter) were prepared for paleomagnetic analysis per each site.

NRM was measured using a spinner magnetometer (Schonstedt SSM-1A). Intensity of NRM was an order of $10^{-3}$cgsemu/gr for b-type, and $10^{-4}$cgsemu/gr for w-type. A few pilot specimens from each site were subjected to an alternating field demagnetization (AFD) and/or a thermal demagnetization (ThD). The progressive AFD was carried out with a three-axis tumbler in the geomagnetic field roughly reduced to one hundredth. A non-inductive

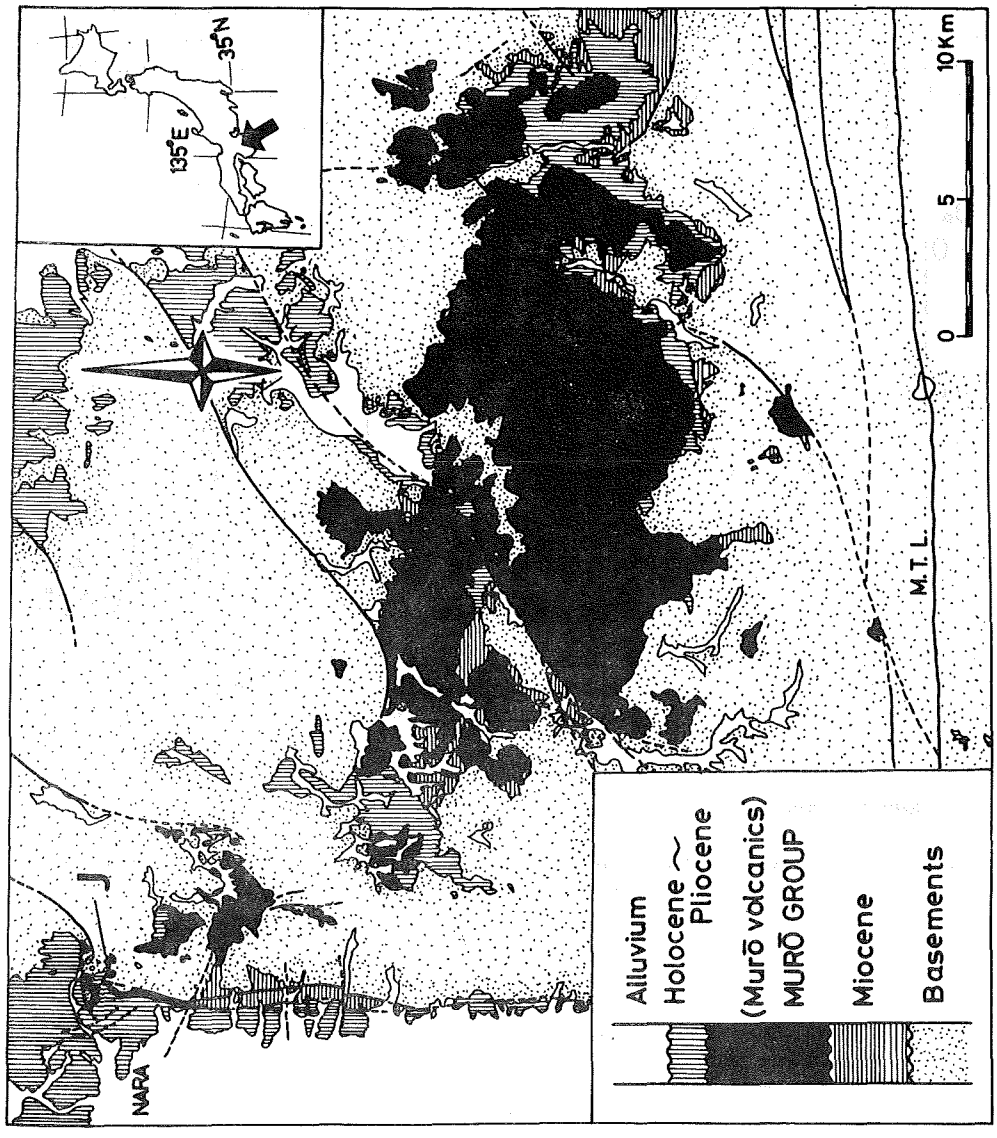


Fig. 1. Geologic map of the Murō district simplified from Shiida et al., (1967). Stratigraphic relationship are also shown in arbitrary scale. J indicates sampling locality of site "J" in the text.

electric furnace shielded by a double layered μ-metal tube and an orthogonal set of three Helmhortz coils was equipped for the partial ThD. Residual field in the furnace was about several gammas. Changes of normalized intensity to the demagnetization field and to the temperature are typically shown in Fig. 2. No significant directional change was accompanied with the progressive demagnetizations except for only a few cases of weakly welded tuffs. Most of the NRMs were verified to be stable against the demagnetizations, having little secondary magnetic components.

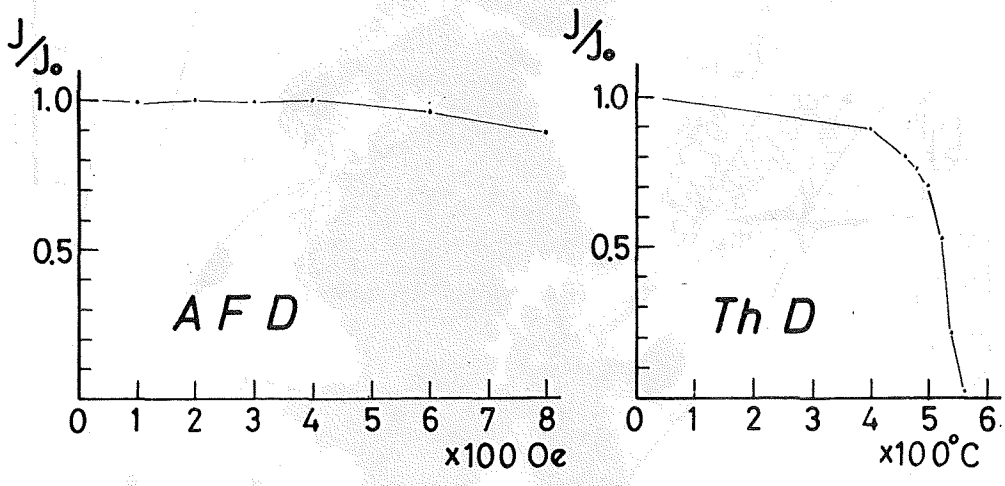


Fig. 2. Typical examples of normalized intenstiy versus progressive AFD and ThD. Signifcant directional changes are not observed for these specimens. Most of the welded tuffs show quite stable responce respect to the demagnetizations.

## RESULTS AND DISCUSSION

Mean directions of NRMs and VGPs of every site are given in Fig. 3 and Fig. 4, respectively. Both resulting field directions and pole positions are fairly concentrated. Latitudes of VGPs are restricted around 30°S which implies intermediate pole positions. These results are in accord with that of the preveous works of Hirooka (1961, MS) and Nishiyama (1975).

Fig. 5 shows the results of NRM directions from a systematic sample collection which was conducted to know the vertical variety of NRM directions. The collection was made along a trail on a cliff from the hight of 390 m to 570 m with the aid of an altimeter. This procedure covers the one half of the maximum thickness of the welded tuffs. The NRM directions on the Schmidt net tightly clustered within the limit of their error angles.

The site "J" (northwest corner of the geologic map in Fig. 1) is far apart from the Murō district. The pyroclastics exposed at the site "J" is isolated from the Murō district, but a petrographical observation reveals it to be a remainder of Murō volcanics. NRM direction from this site is as follows; D = -101.2° and I = -76.6° ($\alpha_{95}$= 8.7°). This field direction is identical with the other data. It may be said that no specific variation of the NRM directin is recognizable.

Several non-welded and water-laid tuff layers are intercalated in the welded tuffs. Paleomagneitc property was examined for some of them. Mean NRM direction of fine ash lenticular layer is plotted with that of the adjacent welded tuff in Fig. 6. Their remanent vectors point quite similar direction. Change of the normalized intensity to AFD resemble each other

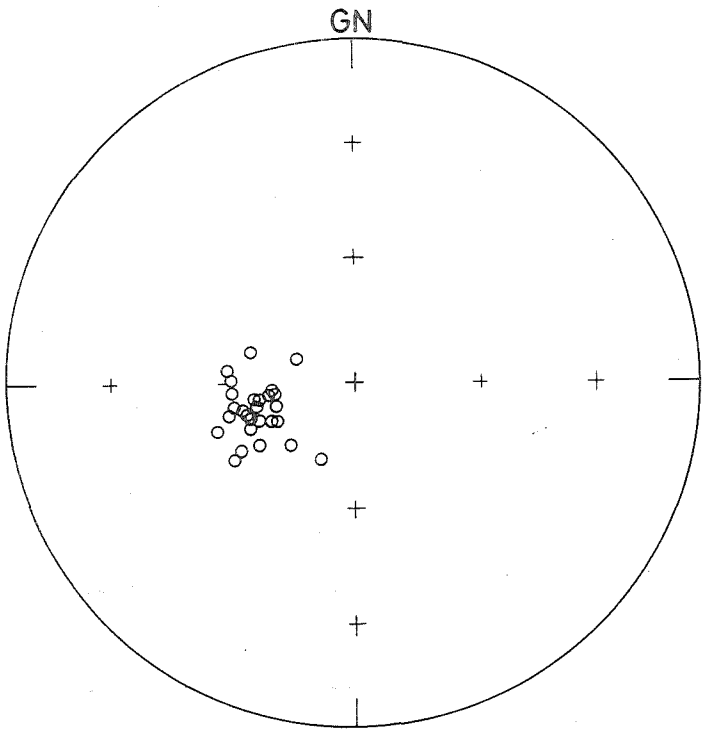


Fig. 3. Mean NRM directions of all sites plotted on the Schmidt equal area net. GN is geographic north.

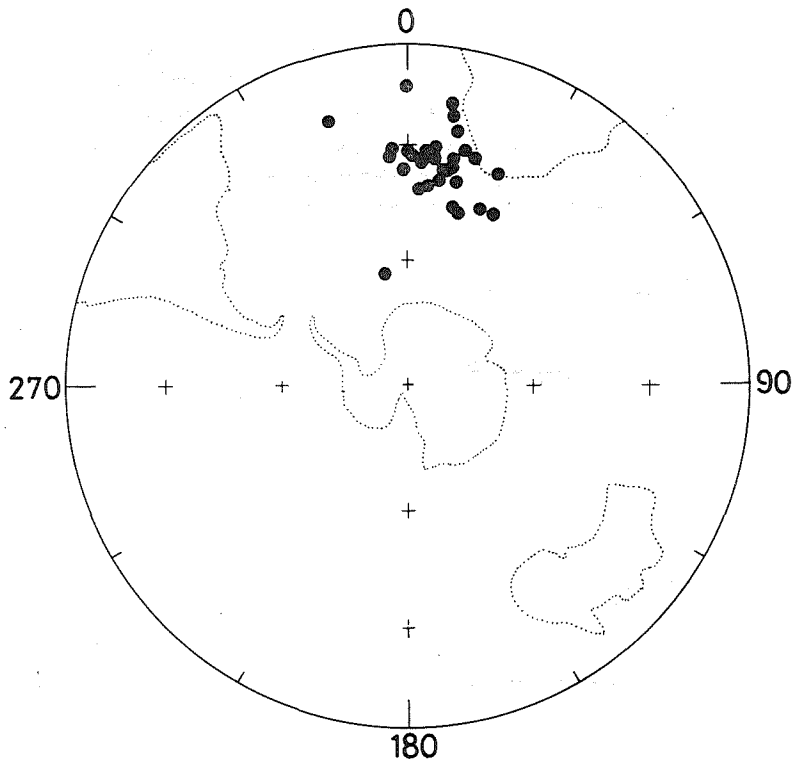


Fig. 4. VGPs plotted on the southern hemisphere. These are calculated for the mean NRM direction of each site.

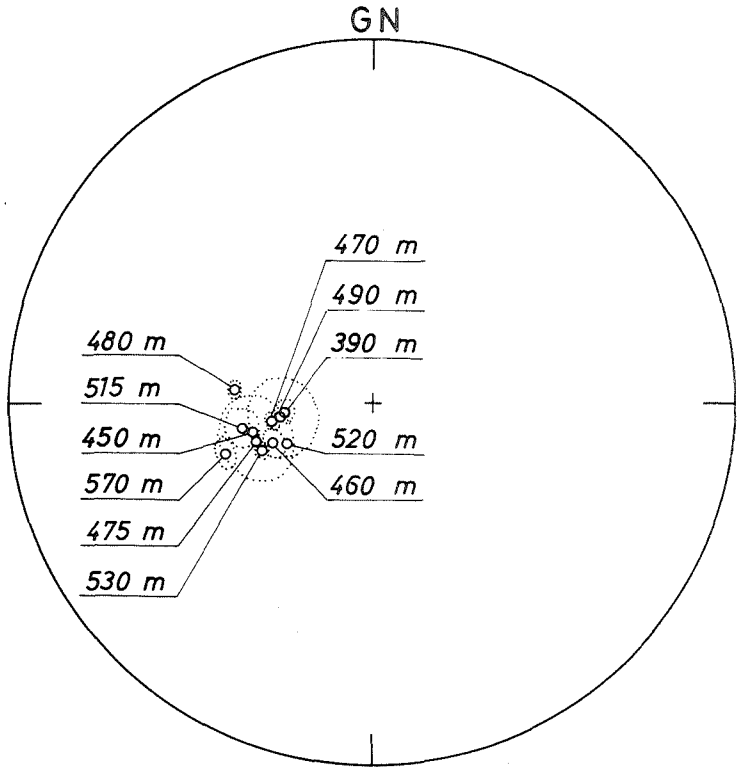


Fig. 5. Result of continueous sample collection along a trail on a cliff from the hight of 390 m to 570 m. NRM directions of each site is plotted with their error angles ($\alpha_{95}$).

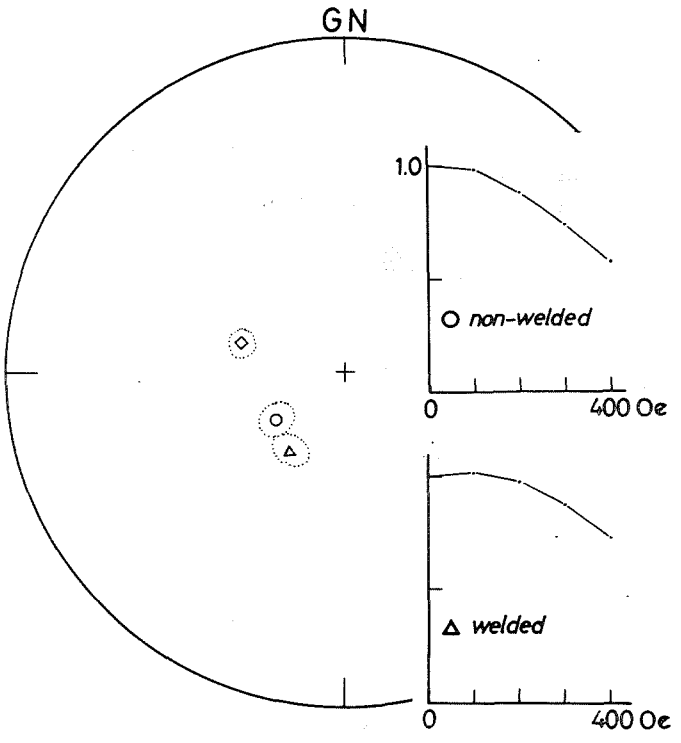


Fig. 6. NRM directions of non-welded tuff (open circle) and adjacent welded tuff (open triangle). Normalized intensity change to progressive AFD is also given. Rhombic symbole indicates NRM direction of another water-laid tuff layer.

with respect to the coercivity, but their initial intensity is $5.7 \times 10^{-6}$ cgsemu/gr for non-welded tuff and $3.8 \times 10^{-5}$cgsemu/gr for welded tuff. Another water-laid tuff layer with accretionary lapilis also gives similar mean NRM direction (rhombic symbole in Fig. 6). Consequently, these facts may imply the coincidence of TRM with DRM, because the NRM of the non-welded or water-laid tuff is regarded as DRM.

The crustal movements after the emplacement of the welded tuffs appear to be a little in this region. The welded tuff sheets gently dip north less than ten degree except for steep dipping close to the fault, judging from the tilting of the cooling unit boundaries, columner joints and eutaxitic textures. On the other hand, the least correction angle that could shift the observed intermediate pole position to the present south pole is evaluated about forty dgrees or so. This value seems considerably large compared to the tilting inferred from the geologic structure mentioned above. Therefore, it may be noted that the anomalous pole position of the Murō volcanics is not a result of the crustal movement.

The discussion may lead us to a conclusion that the anomalous pole position of the Murō volcanics is attributable to the geomagnetism. But this conclusion does not directly mean the presence of the dipole inclined at an angle of more than sixty degrees. Ito (1970) discussed on the intermediate VGPs including the data of Muro volcanics. He explained them as a characteristic route of change in geomagnetic polarity for the Mio-Pliocene period of Japan. Though his idea is convincing, a final conclusion should be reserved until we aquire the information on the magnitude of the geomagnetic field at that time. Wilson et al. (1972), Shaw (1975) and Shaw (1977) have predicted that the geomagnetic field was exceptionally large when the VGP was close to the equater. Their results, however, showed rather weak field intensity during the most of intermediate states of the pole positions. Our preliminary result on the paleointensity determination by Thellier's method suggests considerably weak intensity compared with the present field. Further experiments is in progress and we will present full data in the near future.

REFERENCES


Hirooka, K., (1961) Graduation thesis of Kyoto Unversity.

Hirooka, K. and N. Kawai (1967) Ann. Progress Rep. Paleogeophys. Res. Japan, p. 69.

Ito, H., (1970) J. Geomag. Geoelectr., 22, 273.

Nishiyama, S., (1975) *Yamato Chigaku*, 21. 1.

Shaw, J., (1975) Geophys. J. R. astr. Soc., 40, 345.

_____ , (1977) Geophys. J. R. astr. Soc., 48, 263.

Shiida, I., T. Kasama and H. Shibata (1967) Guide book for geologic excursion for annual meeting of the Geological Society of Japan at Nagoya.

Wilson, R. L., P. Dagley and A. G. McCormack (1972) Geopphys. J. R. astr. Soc., 28, 213.

Yokota, S., K. Matsuoka and M. Yashiki (1978) *Chikyu Kagaku*, 32, 133.

# PALEOMAGNETISM OF MIOCENE GRANITIC ROCKS IN THE GOTO ISLANDS

Haruaki ITO, Katsuyasu TOKIEDA
and
Yukio NOTSU

Department of Physics, Faculty of Science,
Shimane University, Matsue 690, Japan

Small stocks or dikes of Miocene granitic rocks lie scattered on Fukue-jima, Hisaga-jima, Wakamatsu-jima, Naru-jima and Nakadori-jima in the Goto Islands (33°N, 129°E), Nagasaki Prefecture. The granitic rocks have been dated as late Miocene from a geological evidence that they intruded into the Goto group and the Goto volcanic complex of early or middle Miocene (Ueda, 1961; Matsui, 1969).

About three hundred samples for paleomagnetic study were collected from twenty one sites of eleven stocks or dikes. Two or three core specimens with 23 mm in diameter and 23 mm high were drilled from each sample in the laboratory.

Stepwise alternating field (AF) demagnetization were applied to one core specimen per sample. A few core specimens of each sampling site were subjected to stepwise thermal demagnetization to 585°C. Subsequently, specimens taken from eight sites were possessed of stable directions of the NRM. The paleomagnetic data at each sampling site after AF demagnetization are summarized in Table 1. Site mean directions of the NRM after AF demagnetization to 250 oe or 300 oe are shown in Fig. 1.

Table 1

| Site | N | D | I | K | $\alpha_{95}$ | VGP | | dp | dm |
|---|---|---|---|---|---|---|---|---|---|
| 1 | 10 | 128.3° | -42.3° | 69.8 | 5.8° | 44.3°S | 137.8°W | 4.4 | 7.2 |
| 2 | 5 | 15.8° | 51.3° | 24.9 | 15.6° | 76.7°N | 142.6°W | 14.4 | 21.2 |
| 3 | 9 | 337.1° | 63.2° | 108.0 | 5.0° | 68.7°N | 79.3°E | 6.2 | 7.8 |
| 4 | 7 | 238.6° | -69.8° | 65.1 | 7.5° | 44.1°S | 6.3°W | 11.1 | 12.9 |
| 5 | 8 | 359.3° | 57.1° | 176.3 | 4.5° | 85.1°N | 122.3°E | 4.4 | 6.1 |
| 6 | 6 | 146.5° | -39.1° | 14.6 | 18.1° | 58.5°S | 152.6°W | 12.9 | 21.6 |
| 7 | 6 | 134.7° | -59.3° | 46.2 | 10.0° | 53.3°S | 116.7°W | 11.2 | 14.9 |
| 8 | 11 | 176.1° | -50.0° | 162.3 | 3.6° | 85.9°S | 174.0°W | 3.2 | 4.8 |

According to Ueda (1961) and Matsui (1969), the age of these granitic rocks is likely to correspond with granitic rocks exposed in the Soboyama area in central Kyushu dated as 21 $\pm$ 1 Ma (Miller et al., 1962) or the Omogo granitic rocks in Shikoku dated as 14 $\pm$ 2 Ma (Shibata and Nozawa, 1968). However, paleomagnetic correlation with the Goto and the Soboyama or Omogo granitic rocks is unknown, because paleomagnetic data of the Soboyama or Omogo

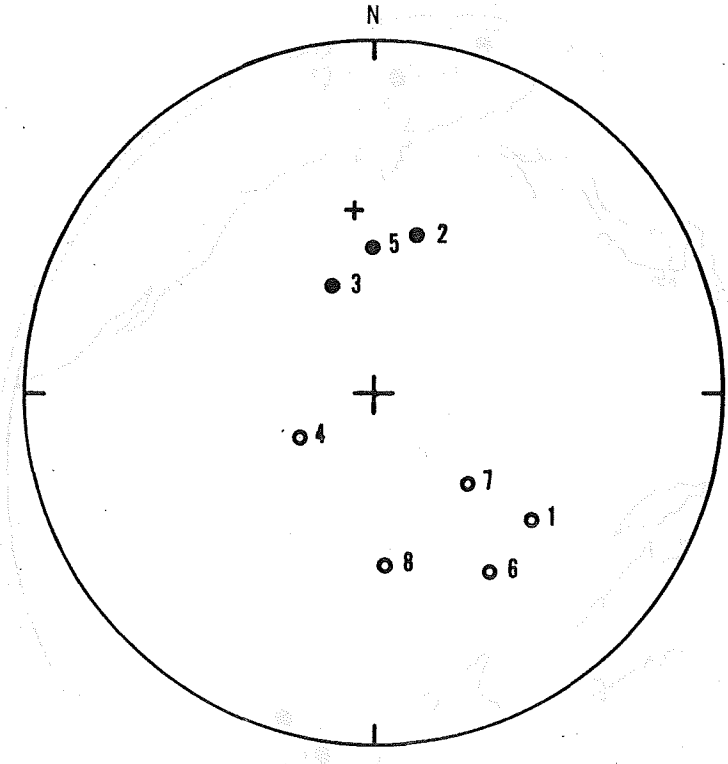


Fig. 1 Site mean directions of the NRM after magnetic cleaning. Solid circles represent positive inclinations and open circles represent negative inclinations.

granitic rocks are very few at present. On the other hand, as the NRM directions of the Goto granitic rocks are compatible with those of the Tsushima granitic rocks, it seems that these granitic rock bodies exposed in the Goto Islands and Tsushima emplaced at the same time. The K-Ar age of the Tsushima granitic rocks is 12 Ma (Kawano and Ueda, 1966). A stock in Hisaga-jima has the normal and reversed magnetization within a rock body, and a few intermediate directions of the NRM are successfully observed in other stocks. Especially, it attracts the notice of ours that intermediate NRM directions of the Goto and Tsushima granitic rocks coincided with each other.

The VGP positions from the Goto and Tsushima granitic rocks are shown in Fig. 2. As seen in the figure, the VGP positions from the intermediate NRM directions at sites 1, 6, 7 and T1 are in the Southern Pacific. This is quite different from the results obtained from Miocene or Pliocene rocks in Southwest Japan (e.g. Momose, 1958; Ito, 1970). Although only the VGP at site 4 is consistent with that for Southwest Japan, it is noted that the VGP for the Goto Islands and Tsushima (sites 1, 6, 7 and T1) is situated on a pole path obtained from the Tatoosh intrusion of the Miocene age in Western USA (Dodson et al., 1978).

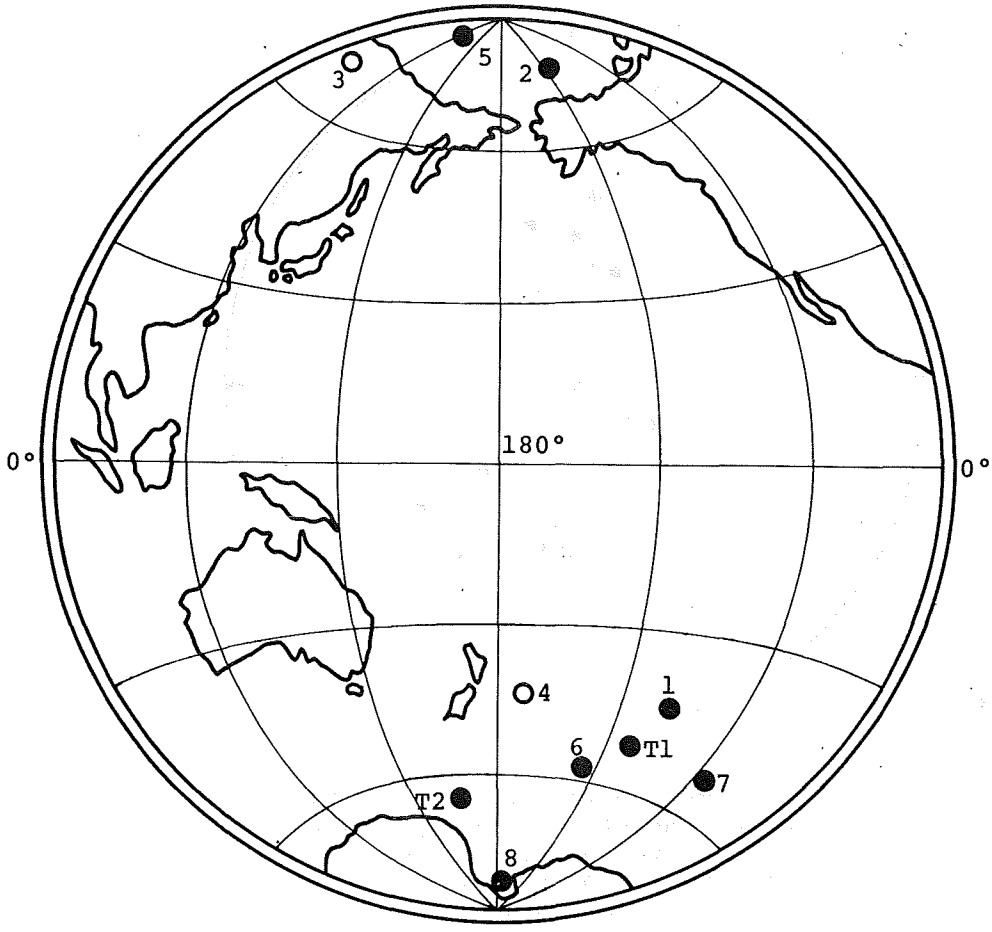


Fig. 2 VGP for the Goto Islands (1 to 8) and Tsushima (T1 and T2). Solid circles represent to be upper hemisphere and open circles to be lower hemisphere.

REFERENCES

Dodson, R., J.R. Dunn, M. Fuller, I. Williams, H. Ito, V.A. Schmidt and Yee-Ming Wu, Geophys. J. R. astr. Soc., 53, 373-412, 1978.

Ito, H., J. Geomag. Geoelectr., 22, 273-290, 1970.

Kawano, Y. and Y. Ueda, J. Jap. Assoc. Min. Petro. Econ. Geol., 56, 191-211, 1966.

Matsui, K., J. Geol. Soc. Japan, 75, 631-632, 1969.

Miller, J., K. Shibata and Y. Kawachi, Bull. Geol. Surv. Japan, 13, 70-72, 1962.

Momose, K., J. Geomag. Geoelectr., 10, 12-19, 1958.

Shibata, K. and T. Nozawa, Bull. Geol. Surv. Japan, 19, 21-24, 1968.

Ueda, Y., Res. Rep. Fac. Sci. Kyushu Univ., 5, No 2, 51-61, 1961.

# PALEOINTENSITY MEASUREMENTS ON LEG55 BASALTS IN THE EARLY CENOZOIC

Toshiyuki TOSHA and Masaru KONO

Geophysical Institute, University of Tokyo
Bunkyo-ku, Tokyo 113

## 1. Introduction

Although a number of intensive rock magnetic and paleomagnetic studies have been carried out on sea floor basalts (Lowrie,1977),paleointensity studies were relatively rare. Ozima et al. (1968) and Grommé et al. (1975;1979) applied the Thelliers' method to basaltic rocks dredged from North Pacific and to dredged fragments of submarine pillow basalts. Carmichael (1977) and Dunlop and Hale (1977) studied DSDP Leg37 basalts. In these studies samples were basaltic rocks erupted subaqueously and the common ferromagnetic minerals were titanomaghemites or low-temperature oxidized titanomagnetites.

In the Leg55 basalts, the situation was quite different. These basalts are considered to have erupted subaerially though they were drilled from submarine seamount. Most of the ferromagnetic minerals were high-temperature oxidized titanomagnetites with high Curie temperature (Fig.1a) and high median demagnetizing field (MDF) (Fig.1b). They have not been affected by the later low-temperature oxidization (Kono, 1979). So we hope that Leg55 basalts are suitable for paleointensity study about early Cenozoic.

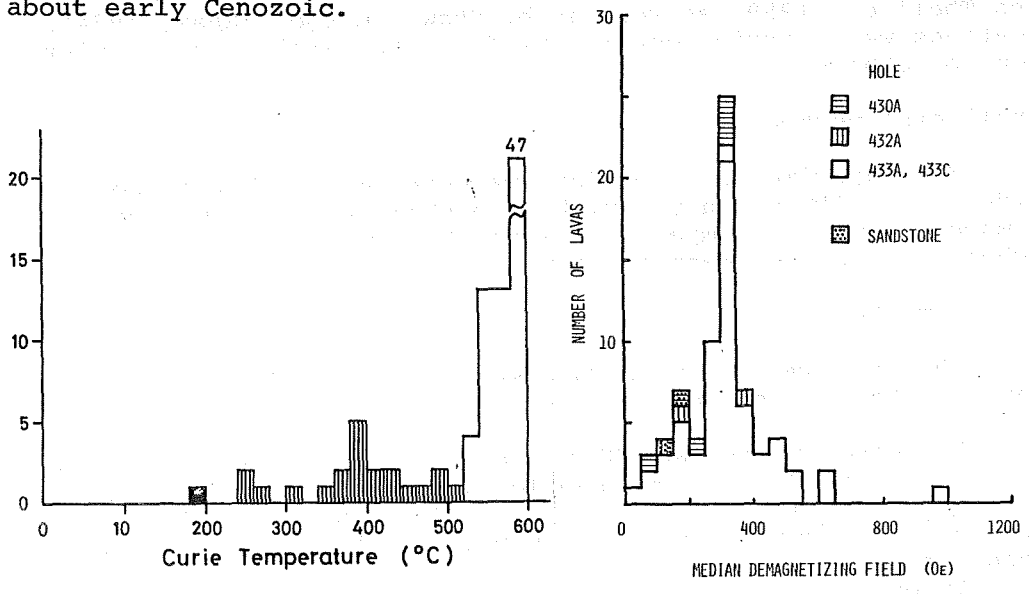


Fig.1. Histograms of magnetic properties data (a) Curie temperature (Tc) and (b) median demagnetizing field (MDF). Samples containing low-temperature oxidization phase are indicated by hatchures; reprinted from Kono(1979).

## 2. Samples

The samples used in this study were drilled in Leg55 of the DSDP at Sites 430 (Ojin), 432 (Nintoku), and 433 (Suiko) located near the middle of the Emperor Seamounts in the North Pacific. The basaltic rocks from these seamounts are dated at 55.2 Ma, 56.2 Ma, and 64.7 Ma, respectively (Dalrymple et al., 1979).

From the paleomagnetic data, it was inferred that at a latitude of about 25° these seamounts erupted (Kono and Morgan, 1979). Petrographically, samples drilled from Holes 430 and 432 and from the upper layers of Hole 433 are alkalic basalts, while the lower parts of Hole 433 are tholeiitic. Of these holes, Hole 433C penetrated 390 meters and recovered 250 meters of basaltic layer and 66 flow units with various inclinations ( Kono and Morgan, 1979). So we concidered the rocks of Hole 433C as a good recorder in secular variation and studied more samples.

Though Smith (1967) adopted three criteria as necessary for Thelliers' method in Js-T curve, Coe and Grommé (1973) showed that a good reliable paleointensity was obtained from samples which would be rejected according to Smith's criteria. So samples for paleointensity studies were selected mostly based on thermomagnetic analyses; samples with relatively high Curie temperatures and reversible Js-T curves were preferred. Samples used in this study are listed in Table 1.

## 3. Experimental method

Paleointensity was studied by Thelliers' method (Thellier and Thellier, 1959) as well as by Shaw's method (Shaw, 1974). Heatings were carried out in air for some samples and in nitrogen for others.

### Thelliers' method

The experimental procedure was similar to that of Coe (1967). A pTRM was given with a constant field of 0.5 Oe. The remanence at room temperature after heating was measured by a Schonstedt spinner magnetometer.

### Shaw's method

The experimental procedure was similar to that of original author (Shaw, 1974) and the results were classified (Kono, 1978 ).

In some samples, an ARM was given with a direct field of 1.74 Oe ( 0.84 Oe for some samples), and a TRM was given with 0.44 Oe by heating to 590°C in air. The remanence after each step of A.F. demagnetization was measured by a Digico spinner magnetometer.

In others, an ARM was given 2.0 Oe, and a TRM was given with 0.495 Oe by heating in nitrogen to the temperature which was about 20°C higher than its Curie temperature. the remanence after each step of A.F. demagnetization was measured by a Schonstedt spinner magnetometer.

| SAMPLE NUMBER | | | ROCK TYPE | Tc (°C) | METHOD | | FLOW UNIT | INCLI (°) |
|---|---|---|---|---|---|---|---|---|
| 430A | 4-3 | 80-90 | ALK | --- | S | A | 1 | -18.1 |
| | 5-2 | 21-23 | ALK | --- | S | A | 1 | |
| | 5-2 | 30-32 | ALK | 520 | T | A | 1 | |
| | 5-3 | 107-109 | ALK | 503 | T,S | N | 1 | |
| | 5-4 | 132-134 | ALK | --- | S | A | 2 | -17.4 |
| | 5-5 | 44-46 | ALK | 575 | T | A | 2 | |
| | 5-5 | 76-78 | ALK | --- | S | A | 2 | |
| | 5-5 | 103-105 | ALK | 583 | T,S | N | 2 | |
| | 6-1 | 67-69 | ALK | 575 | T,S | N | 2 | |
| | 6-2 | 54-56 | ALK | 582 | T | A | 3 | -22.4 |
| | 6-2 | 74-76 | ALK | --- | S | A | 3 | |
| | 6-2 | 122-124 | ALK | 576 | T,S | N | 3 | |
| | 6-3 | 55-57 | ALK | --- | S | A | 3 | |
| | 6-4 | 15-17 | ALK | 577 | T,S | N | 4 | -18.8 |
| 432A | 2-1 | 107-109 | ALK | 364 | T,S | N | 1 | -65.2 |
| | 2-1 | 113-115 | ALK | --- | S | A | 1 | |
| | 2-1 | 115-117 | ALK | --- | S | A | 1 | |
| | 2-2 | 66-68 | ALK | --- | S | A | 2 | -66.4 |
| | 2-2 | 72-74 | ALK | 572 | T | A | 2 | |
| | 2-3 | 2-4 | ALK | --- | S | A | 2 | |
| | 2-3 | 12-14 | ALK | 457 | T,S | N | 2 | |
| | 3-3 | 92-94 | ALK | --- | S | A | 3 | -28.6 |
| | 4-1 | 64-66 | ALK | 550 | T | A | 3 | |
| | 4-1 | 69-71 | ALK | --- | S | A | 3 | |
| | 4-1 | 71-73 | ALK | 579 | T,S | N | 3 | |
| | 4-2 | 41-43 | ALK | --- | S | A | 3 | |
| | 4-2 | 80-82 | ALK | 577 | T,S | N | 3 | |
| 433A | 20-2 | 2-4 | ALK | 581 | T,S | N | 1 | -39.0 |
| | 20-2 | 14-16 | ALK | 580 | T,S | N | 1 | |
| | 20-2 | 24-26 | ALK | 580 | T | A | 1 | |

| SAMPLE NUMBER | | | ROCK TYPE | Tc (°C) | METHOD | | FLOW UNIT | INCLI (°) |
|---|---|---|---|---|---|---|---|---|
| 433C | 10-2 | 21-23 | THO | --- | S | A | 4 | -43.0 |
| | 10-3 | 145-147 | THO | 569 | T | A | 4 | |
| | 11-1 | 139-141 | THO | 573 | T,S | N | 6 | -43.0 |
| | 11-3 | 84-86 | THO | 579 | T,S | N | 7 | -44.3 |
| | 11-3 | 112-114 | THO | 582 | T | A | 7 | |
| | 11-4 | 58-60 | THO | --- | S | A | 8 | -53.0 |
| | 11-5 | 36-38 | THO | 539 | T | A | 8 | |
| | 13-2 | 103-105 | THO | 543 | T | A | 10 | -28.5 |
| | 14-2 | 37-39 | THO | 574 | T | A | 11A | -33.4 |
| | 15-4 | 48-50 | THO | 551 | T | A | 12 | -18.5 |
| | 19-3 | 74-76 | THO | 574 | T | A | 15A | -44.3 |
| | 21-3 | 7-9 | THO | 532 | T | A | 17 | -61.2 |
| | 25-2 | 27-29 | THO | 570 | T | A | 20 | -40.1 |
| | 27-5 | 41-43 | THO | 541 | T | A | 24 | -36.2 |
| | 28-4 | 121-123 | THO | 580 | T | A | 26A | -68.9 |
| | 31-4 | 83-85 | THO | 562 | T | A | 28A | -57.0 |
| | 35-6 | 48-50 | THO | 557 | T | A | 35 | -49.6 |
| | 36-1 | 45-47 | THO | 576 | T,S | N | 36 | -50.9 |
| | 36-4 | 56-58 | THO | 528 | T | A | 39 | -55.3 |
| | 36-5 | 29-31 | THO | 540 | T,S | N | 40 | -50.4 |
| | 38-1 | 57-59 | THO | 577 | T | A | 45 | -47.3 |
| | 38-5 | 119-121 | THO | 364 | T | A | 47 | -5.4 |
| | 39-6 | 78-80 | THO | 573 | T | A | 48 | -44.1 |
| | 42-1 | 68-70 | THO | --- | T | A | 52 | -13.6 |
| | 42-2 | 136-138 | THO | 573 | T | A | 53 | -25.8 |
| | 43-1 | 33-35 | THO | 578 | T | A | 54 | -33.9 |
| | 44-1 | 41-43 | THO | 553 | T | A | 56 | -42.5 |
| | 44-4 | 108-110 | THO | 553 | T | A | 58 | -47.2 |
| | 45-2 | 45-47 | THO | 555 | T | A | 59 | -45.0 |
| | 47-1 | 26-28 | THO | 579 | T | A | 63 | -40.0 |
| | 48-3 | 30-32 | THO | 575 | T | A | 64 | -68.1 |
| | 49-1 | 142-144 | THO | 577 | T | A | 66 | -65.4 |

Table 1. Sample list ROCK TYPE ALK-alkalic basalt, THO-tholeiitic basalt: METHOD T-Thellier' method S-Shaw's method, A-heated in air N-heated in nitrogen: INCLI a flow mean inclination (Kono and Morgan, 1979) : Tc-Curie temperature (Kono, 1979)

## 4. Result and Discussion

### Thelliers' method

Eight out of 32 samples heated in air (Fig.2a) and six out of 16 samples heated in nitrogen (Fig.2b; marked '*' in the last column in Table 2) gave paleointinsity estimates in Thelliers' method experiments. The criteria of success in this study were similar to those used by Kono (1974) ; namely, (1) six or more points in the linear portion, and (2) a correlation coefficient of linear regression between NRM and TRM components equal to or greater than 0.98.

In most samples the direction of the NRM component did not change much up to 500°C or more. But the NRM-TRM linear relation line did not extend

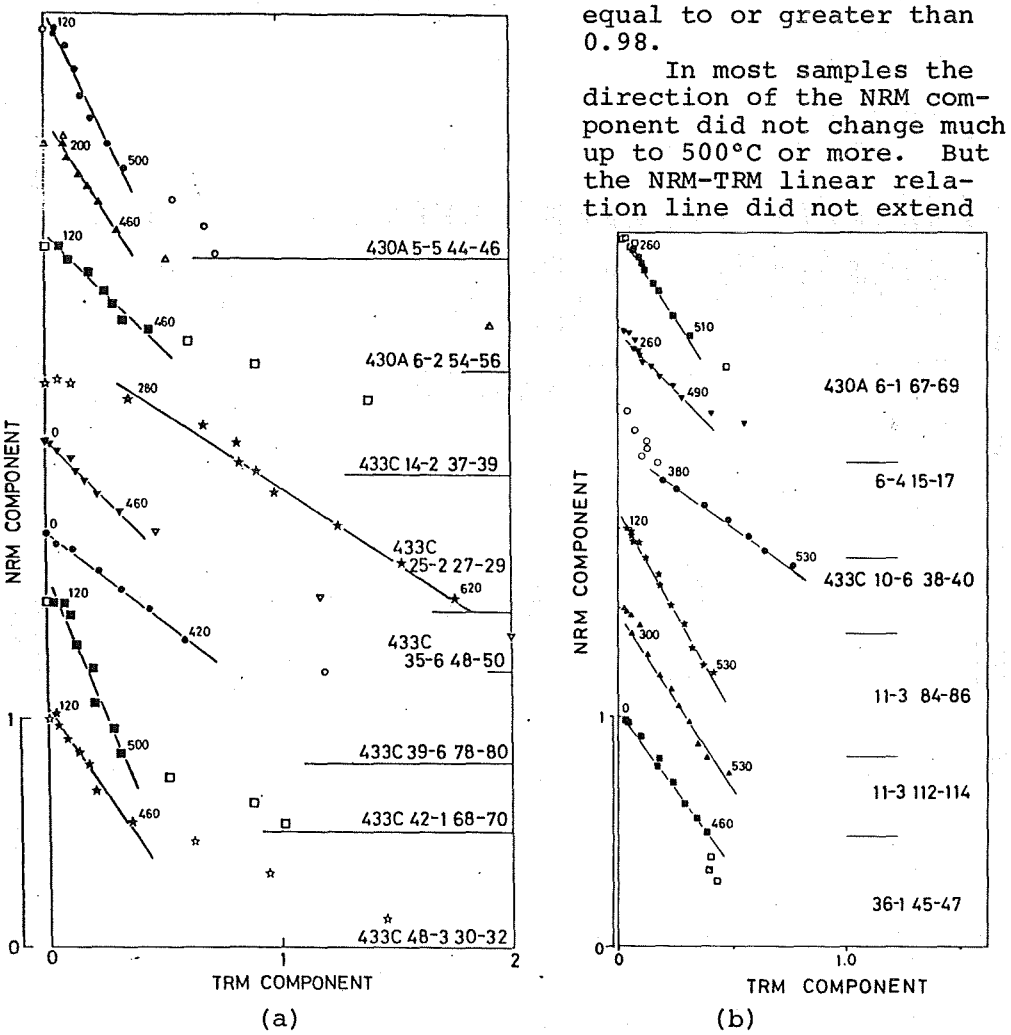


Fig.2. The NRM-TRM curves of successful samples by Thelliers' method in air (a) and in nitrogen (b). Intensities are normalized by those of NRM of individual samples. The horizontal lines are the TRM axed for individual samples. Some of heating temperatures are indicated in the figure (°C). Open symbols are the data excluded from linear regression analyses.

up to 500°C. Changes in magnetic properties caused by heating are very common in volcanic rocks, and most of the high temperature points deviates from the straight lines even in successful samples (e.g., Coe and Grommé, 1973). Samples heated in nitrogen, however, showed less changes to higher temperatures.

At the low temperature end, most of the results show that the points lie below the straight lines. Since all the Leg55 basalts were reversely magnetized, this may be a result of superposition of a VRM component in the present field.

Shaw's method

For the most samples the gradients in ARM1-ARM2 diagrams were not one but significantly lower even for the ones heated in nitrogen. Apparently the magnetic minerals have been affected by heating. Therefore all the results obtained by Shaw's method were rejected following the criteria by original author Shaw (1974). Kono (1978) showed that some samples gave results which were agreed with those obtained by Thelliers' method when gradients in ARM1-ARM2 diagrams were taken into account. The results obtained by Shaw's method were different from those by Thelliers' method even for the samples with gradient close to one. Comparing Shaw's method with Thelliers', it seems that the results by Thelliers' are more reliable because paleointensity estimates can be determined from experimental data below the temperature where chemical changes occurred by heating. So we discarded all the results obtained by Shaw's method as unreliable.

It is said that magnetic remanences with higher coercivity are less affected by heating. A higher alternating field may be needed to obtain reliable paleointensity results by Shaw's method. But at higher alternating fields the signal to noise ratio becomes worse. So a similar method introduced by Rigotti (1978), which uses ARM's aquisition before and after heating, may be useful.

Paleointensities in the Early Cenozoic

From the paleointensity estimates obtained by Thelliers' method, we calculated virtual dipole moments (VDMs) with a mean of $15 \times 10^{25}$ $Gcm^3$, which is much larger than the present value of $8.0 \times 10^{25}$ $Gcm^3$. Paleointensities of geomagnetic field at nearly the same ages are only available from Deccan Trap basalts with a mean VDM of $7.2 \times 10^{25}$ $Gcm^3$ (Kono, 1974). Difference between holes is not very clear, but it seems that VDMs in Hole 430 are somewhat higher than those in 433 (a mean in 430 and 433 are $19 \pm 6$ (s.d.) $\times 10^{25}$ $Gcm^3$ and $14 \pm 8$ (s.d.) $\times 10^{25}$ $Gcm^3$, respectively).

In Hole 433, the mean inclination (-45.7°) probably corresponds to the dipole field direction as the secular variation is adequately sampled (Kono and Morgan, 1979). Therefore if a flow mean inclination is quite different from the hole mean, it indicates either a time when non-dipole field was large at the sampling site or a time when the field was different from the dipole regime; ie., geomagnetic reversal or excursion.

When the inclination was smaller, the intensity of geomagnetic field seemed to be larger (Fig.3). Such a phenomenon in

| Sample Number | | Flow Unit | Incli (°) | T (°C ) | N | -r | F (Oe ) | VDM (x $10^{25}$ $Gcm^3$) | |
|---|---|---|---|---|---|---|---|---|---|
| 430A | 5-5 44-46 | 2 | -17.4 | 120-500 | 8 | .987 | 1.07 ± 0.07 | 26.7 ± 1.8 | |
| | 6-1 67-69 | 2 | -17.4 | 260-510 | 9 | .997 | 0.77 ± 0.03 | 19.2 ± 0.8 | * |
| | 6-2 54-56 | 3 | -22.8 | 200-460 | 6 | .996 | 0.81 ± 0.04 | 19.6 ± 0.9 | |
| | 6-4 15-17 | 4 | -18.8 | 260-490 | 8 | .987 | 0.48 ± 0.03 | 11.9 ± 0.7 | * |
| 433C | 10-6 38-40 | 5 | -43.0 | 380-510 | 7 | .997 | 0.35 ± 0.01 | 7.29 ±0.22 | * |
| | 11-3 84-86 | 7 | -44.3 | 120-530 | 13 | .995 | 0.88 ± 0.03 | 18.1 ± 0.6 | * |
| | 11-3 112-114 | 7 | -44.3 | 300-530 | 9 | .980 | 0.77 ± 0.03 | 15.8 ± 1.2 | * |
| | 14-2 37-39 | 11A | -33.4 | 120-460 | 7 | .981 | 0.50 ± 0.05 | 11.4 ± 1.0 | |
| | 25-2 27-29 | 20 | -40.1 | 280-580 | 8 | .985 | 0.33 ± 0.03 | 7.03 ±0.50 | |
| | 35-6 48-50 | 35 | -49.6 | 120-460 | 7 | .987 | 0.52 ± 0.04 | 10.2 ± 0.7 | |
| | 36-1 45-47 | 36 | -50.9 | 0-460 | 11 | .991 | 0.69 ± 0.03 | 13.5 ± 0.6 | * |
| | 39-6 78-80 | 48 | -44.1 | 0-420 | 7 | .997 | 0.39 ± 0.02 | 7.99 ±0.26 | |
| | 42-1 68-70 | 52 | -13.6 | 120-500 | 8 | .988 | 1.33 ± 0.09 | 33.6 ± 2.2 | |
| | 48-3 30-32 | 64 | -68.1 | 120-460 | 7 | .980 | 0.73 ± 0.07 | 11.3 ± 1.0 | |

Table 2. Successful results of Thelliers' method. Incli, flow mean inclination (Kono and Morgan, 1979). T and N, blocking temperature interval where NRM and TRM component are linear and points in this interval. r, correlation coefficient of the linear regression. F, paleointensity. VDM, virtual dipole moment. Mark '*' indicates that heating was done in nitrogen.

changing polarity has been reported by Wilson et al. (1972) and Shaw (1975). We have to have much more data before we conclude about the intensity variation in the early Cenozoic.

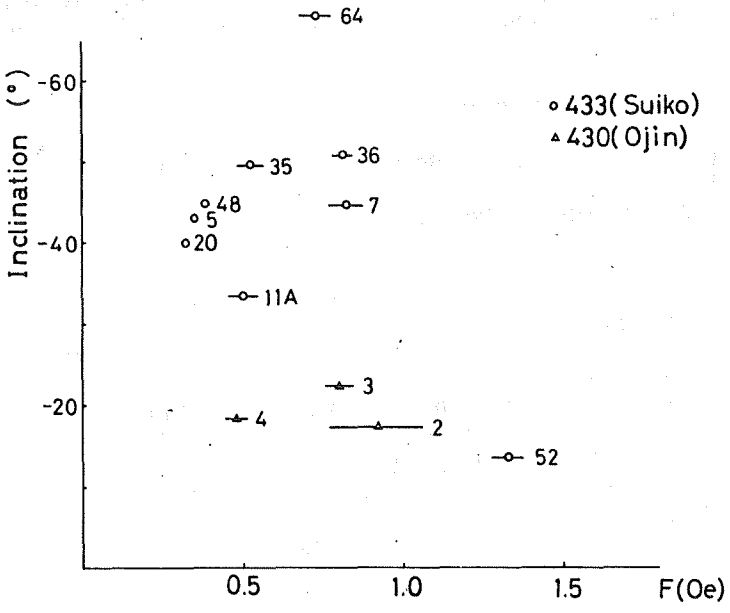


Fig.3. A graph of flow mean inclinations against successful paleointensity results by Thelliers' method. For some flows symbols are located at a mean of two results (430A Flow 2,433C Flow 7).

## 5. Conclusion

Both Thelliers' and Shaw's method were applied to samples of Leg55 basalts to determine paleointensity of geomagnetic field in the early Cenozoic. The heatings were done in air or in nitrogen. Effects of different heating conditions were not clear in both methods. But Thelliers' method, the linearity between NRM decayed and TRM acquired seems to extend to higher temperature in samples heated in nitrogen. Comparison of data obtained by two heating conditions cannot be performed because only one paleointensity estimate is available from flow unit 2 of Ojin (430).

For some samples deviation from the linear line at low temperature is a result of superposed VRM component in the present field direction. Deviation at high temperature is probably caused by some change in chemistry or grain size distribution of ferromagnetic minerals.

The rate of success in Thelliers' method was 8/32 (in air) and 6/16 (in nitrogen). All the results from Shaw's method were not satisfactory in that some change occurred in ARM spectrum by heating even in nitrogen.

The mean and standard deviation of VDMs calculated from the present paleointensity results are $19 \pm 6 \times 10^{25}$ $Gcm^3$ for

Ojin (430) and 14 ± 8 x $10^{25}$ $Gcm^3$ for Suiko(433). For Nintoku (432) reliable paleointensity estimates were not obtained. The mean VDM of 15 ± 8 x $10^{25}$ $Gcm^3$ is much larger than the corresponding value of similar ages obtained from the Deccan basalts, 7.2 ± 3.0 x $10^{25}$ $Gcm^3$ and the present value, 8.0 x $10^{25}$ $Gcm^3$.

## References


Carmichael, C.M. (1977) Initial Reports of DSDP, vol.37, p.481.

Coe, R.S. (1967) J. Geophys. Res., 72, 3247

Coe, R.S. and C.S. Grommé (1973) J. Geomag. Geoelectr., 25, 415.

Dalrymple, G.B. et al. (1979) Initial Reports of DSDP, vol.55, in press.

Dunlop, D.J. and C.J. Hale (1977) Initial Reports of DSDP, vol.37, p.457.

Grommé, C.S. et al. (1975) IAGA Bull., No.36, p.160.

Grommé, C.S. et al. (1979) J. Geophys. Res., 84, 3553.

Kono, M. (1974) J. Geophys. Res., 79, 1135.

Kono, M. (1978) Geophys. J. R. astr. Soc., 54, 241.

Kono, M. (1979) Initial Reports of DSDP,vol.55, in press.

Kono, M. and W.J. Morgan (1979) Initial Reports of DSDP, vol.55, in press.

Lowrie, W. (1977) J. Geol. Soc. Lond., 133, 61.

Wilson, R.L. et al. (1972) Geophys. J. R. astr. Soc., 28, 213.

Ozima, M. et al. (1968) J.Geophys. Res., 73, 711.

Rigotti, P.A. (1978) Earth Planet. Sci. Lett., 39, 417.

Shaw, J. (1974) Geophys. J. R. astr. Soc., 39, 133.

Shaw, J. (1975) Geophys. J. R. astr. Soc., 40, 345.

Smith, P.J. (1967) Geophys. J. R. astr. Soc., 12, 239.

Thellier, E. and O. Thellier (1959) Ann. Géophys., 15, 285.

# PALEOMAGNETIC EVIDENCE FOR THE PALEOPOSITION OF SUMBA ISLAND, INDONESIA

Yo-ichiro OTOFUJI*, Sadao SASAJIMA*, Susumu NISHIMURA**,
and
Fred HEHUWAT***

*Department of Geology and Mineralogy, Kyoto University, Kyoto 606, Japan
**Institute of Earth Science, Kyoto University, Kyoto 606, Japan
***National Institute of Geology and Mining-LIPI, Jl. Cisitu No. 21, Bandung, Indonesia

## 1. Introduction

The Banda Arc is a double arc of which the inner one is a typical volcanic island arc and the outer one a non-volcanic arc (Fig. 1). Because of the complex geological history of this area, several scientists have advocated conspicuously different hypotheses on the evolution of the Indonesian Archipelago (Katili, 1971, 1973; Hamilton, 1972, 1973; Audley-Charles, 1975). According to Audley-Charles(1975), the plate boundary of Australia in eastern Indonesia is between the Inner and the Outer Banda Arcs, and the Outer Arc, including Sumba, has been detached from Australian continent. The paleomagnetic results from the Banda Arc (Chamalaun, 1977) indicates that Timor formed part of the Australian margin at least during the Late Permian.

During the course of an expedition of Sumba, Sumbawa and Flores, the sample collection for paleomagnetism was undertaken in 1979. The purpose of the present paper is to discuss the paleoposition of Sumba on the standpoint of paleomagnetism.

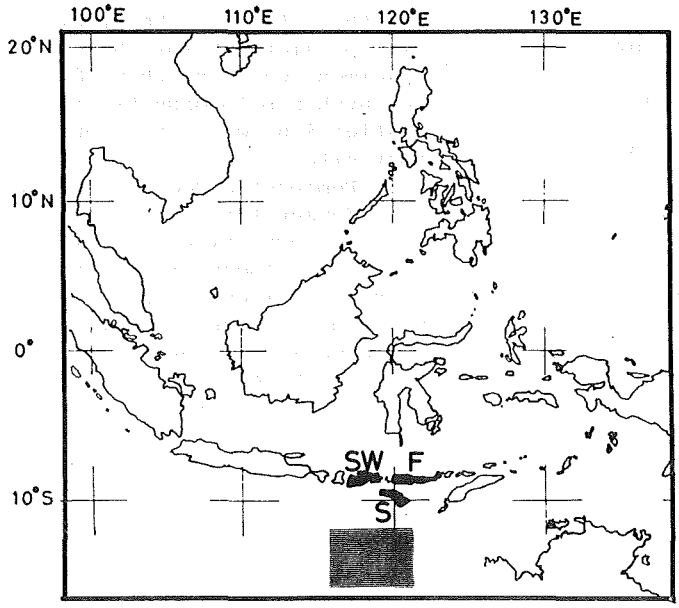


Fig. 1. Map showing the configuration of the Indonesian Archipelago with position of Sumba, Sumbawa and Flores. S=Sumba, SW=Sumbawa and F=Flores. The shaded area shows the Argo Abyssal Plain where the M-Series of marine magnetic anomalies are observed.

## 2. Geological outline

### Sumba

The rocks of West and Central Sumba is subdivided into the Pre-Tertiary rocks of the central and southern mountains and the Tertiary and Quaternary rocks, which extend over the rest of the island (Laufer and Kraëff, 1957). The Tertiary and Quaternary strata mostly consist of shelf sediments which show little or no deformation. Pyroclastic rocks only occur at the early Neogene (Miocene). The Pre-Tertiary can be divided into two formations, a slate formation with subordinate quartz-sandstones and quarzites, and a volcanic formation built up mainly of basaltic rocks. Based on poorly preserved fossils in the slate formation a Jurassic age has been assigned to the Pre-Tertiary (Van Bemmelen, 1970).

### Sumbawa and Flores

Geology of these islands of the volcanic arc show relatively simple structural style. Since the Early Miocene volcanic activity has contributed to the rock-sequence on these islands, and the stratigraphy shows an alternation of volcanic rocks and marine deposits from the Early Miocene to the Recent.

## 3. Paleomagnetic results

Rocks collected at fifteen sites in Sumba cover their ages from the Jurassic to the Miocene. Rocks of the Miocene were obtained from five sites in Flores and four sites in Sumbawa. Sampling localities are listed in Table 1. About ten hand samples were collected in each site. A specimen 2.5 cm in diameter and 2.5 cm long were cut from each samples in the laboratory.

Three specimens were randomly picked up from each site and they were demagnetized in alternating fields (a.f.) in steps with peak fields of 50, 100, 150, 200 and 300 Oe. The remanence was measured by a spinner magnetometer (Schonstedt, SSM-1A). The a.f. value where the precision parameter k (Fisher, 1953) for three specimens reached a maximum was adopted as the most suitable demagnetization field for the site. If the precision parameter k for three specimens was less than 10.0, no further paleomagnetic investigations were made for that site.

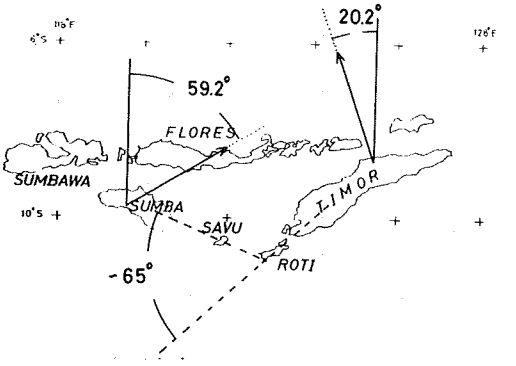


Fig. 2. Comparison of the rotation of Sumba relative to Timor presumed from geomorphological and paleomagnetic viewpoints. The bending angle of 65 degrees is presumed from geomorphological configuration.

Remanent directions after a.f. demagnetization with tilting correction are listed in Table 1 together with their virtual geomagnetic pole (VGP) positions. Mean directions are also listed for the Miocene of three islands and for the Jurassic of Sumba.

The Miocene rocks of each island have an almost same directions of remanent magnetism to the axial dipole field, although the remanent directions from Flores show a considerable scattering.

Table 1. Results of paleomagnetic measurement

| Site | Locality | | Estimated Age | Rock Type | N | a.f. (Oe) | D | I | $\alpha_{95}$ | k | V G P North pole | |
|---|---|---|---|---|---|---|---|---|---|---|---|---|
| [Sumba] | | | | | | | | | | | | |
| IS 135 | 09°35'S | 119°19'E | Miocene | Tuff breccia | 8 | 300 | 3.0 | -20.0 | 9.2 | 37.2 | 87.0N | 223.5E |
| IS 137 | 09°41'S | 119°25'E | " | Tuff | 13 | 300 | 17.6 | 16.0 | 11.1 | 15.0 | 65.0N | 164.5E |
| IS 142 | 09°42'S | 119°27'E | " | Mudstone | 4 | 150 | -1.3 | -26.9 | 9.1 | 103.4 | 85.3N | 315.0E |
| IS 141 | 09°45'S | 119°27'E | Tertiary | Dyke | 6 | 300 | 177.0 | 35.7 | 10.6 | 41.2 | 79.6N | 315.2E |
| Mean | | | | | 4 | | 4.6 | -17.1 | 28.4 | 11.5 | 85.4N | 198.0E |
| IS 143 | 09°42'S | 119°27'E | Jurassic | Shale | 11 | 150 | 63.8 | -43.1 | 8.6 | 29.3 | 27.7N | 232.8E |
| IS 144 | 09°42'S | 119°27'E | Jurassic | Shale | 12 | 50 | 59.2 | -45.9 | 4.4 | 101.0 | 31.7N | 235.6E |
| IS 146 | 09°39'S | 119°42'E | Jurassic | Shale | 9 | 300 | 234.5 | 43.3 | 20.6 | 7.2 | 36.1N | 234.0E |
| Mean | | | | | 3 | | 59.2 | -44.2 | 5.7 | 465.1 | 31.8N | 234.1E |
| [Sumbawa] | | | | | | | | | | | | |
| IS 201 | 08°39'S | 117°27'E | Miocene | Tuff | 10 | 50 | -1.3 | -25.8 | 6.9 | 49.7 | 84.9N | 311.8E |
| IS 203 | 08°39'S | 117°26'E | " | Lava flow | 9 | 300 | -1.8 | 0.8 | 4.9 | 109.4 | 80.8N | 106.1E |
| Mean | | | | | 2 | | -1.7 | -12.4 | | | 87.1N | 81.9E |
| [Flores] | | | | | | | | | | | | |
| IS 205 | 08°37'S | 122°24'E | Miocene | Lava flow | 11 | 200 | -3.9 | -19.8 | 3.5 | 171.5 | 85.8N | 9.7E |
| IS 208 | 08°42'S | 122°06'E | " | Taff breccia | 8 | 150 | 218.4 | 8.9 | 6.4 | 76.3 | 51.6N | 208.3E |
| IS 209 | 08°42'S | 122°08'E | " | Tuff breccia | 8 | 200 | -29.1 | -37.5 | 8.2 | 46.3 | 59.4N | 5.2E |
| Mean | | | | | 3 | | 3.9 | -24.6 | 57.1 | 5.7 | 84.3N | 260.1E |

N = number of specimens, (a.f.) = demagnetization field, D = declination, I = inclination,
$\alpha_{95}$ = radius of 95% confidence circle, k = precision parameter.

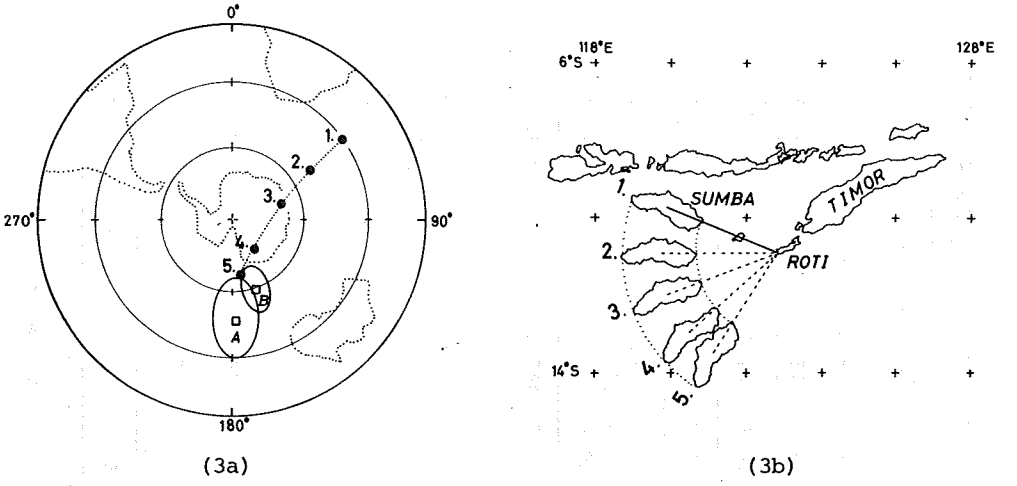


(3a) (3b)

Fig. 3. Comparison of pole positions from Sumba, Timor and Australia. "A" and "B" correspond to the Early Jurassic pole from Australia and the Late Permian pole from Timor, respectively. Poles from Sumba are drawn by closed circles in (3a). The numberd pole corresponds to the VGP evaluated for the rotated position of Sumba with the same number of (3b). The present position of Sumba is drawn by configuration 1 in (3b).

One of the Jurassic data reveals a reversed polarity and the paleomagnetic directions of the Jurassic in all have become to be tightly clustered after tilting correction. These facts suggest great reliability of the Jurassic paleomagnetic direction.

## 4. Discussion

The mean directions of the Miocene from three islands are almost same to the axial dipole field and they show considerably similar value each other. This data imply that three islands have been situated at the present position since the Miocene.

As already shown, the mean declination of Sumba of the Jurassic rocks points to 59.2 degrees eastward from the geographic noth. The only other paleomagnetic results reported from the Banda Arc (Chamalaun, 1977) show the declination of Timor in the Permian is 20.2 degrees westward from the geographic north. As the difference of VGP positions of the Mesozoic (Triassic to Jurassic) and the Permian-Carboniferous estimated from Australia is considerably small (10.7°), the Jurassic magnetic direction of Sumba is allowed to be compared with the Permian direction of Timor. Compared with these directions, the clockwise rotation of Sumba is expected to have occurred by 79.4 degrees relatively to Timor. From a viewpoint of geomorphological configuration, the trend of Sumba and Savu islands chain seems to be undergone a clockwise bending of about 65 degrees relative to the trend of Timor and Roti islands chain (see Fig. 2). A fair agreement between geomorphological and paleomagnetic views lends strong support to the hypotheses that Sumba and Timor had formed the unique island chain till the Jurassic and that Sumba had rotated clockwise through roughly 70 degrees about a pole of rotation just west of Roti island since the Jurassic. The discrepancy of 14.4 degrees may be attributed to the difference in age of rocks from both islands. The clockwise rotation of Sumba in the Jurassic is consistent with the pattern of the magnetic anomaly in the Argo Abyssal

Plain to the southwest of Sumba (see Fig. 1). Larson(1975) identified the Argo set as part of the M-series of anomalies which have a basement age of 150 m.y. and Flavey and Veevers(1974) pointed out that the pattern of anomalies indicated a pole of rotation in the vicinity of east Timor.

In Fig. 3 are shown the VGPs for Australia and Timor together with their error circles. Pole "A" and "B" correspond to the Early Jurassic basalt (Schmidt, 1975) and the Late Permian red bed (Chamalaun, 1977), respectively. These are far away from the VGP obtained from Sumba which is shown by pole 1. This difference may be caused by the clockwise rotation of Sumba after the fixation of the Jurassic magnetization. In order to evaluate the VGPs for restored positions, Sumba was rotated counter-clockwise through 0°, 23°, 43°, 65° and 79.4° about a pole of rotation just east of Roti island (cf Fig. 3b). The VGPs from Sumba in Fig. 3a is numbered in order of increasing rotational angle. It is clearly seen that the VGPs of Sumba is gradually approaching to the poles of Australia and Timor as the rotation progresses. The VGP of Sumba is not statistically distinguished from both of Australian and Timor, when Sumba is rotated by 79.4 degrees that is presumed from the paleomagnetic view as a probable angle of rotation for Sumba. It may lead us to a conclusion that Sumba was situated near the Australian margin with the counter-clockwise rotated position in the Jurassic as well as Timor.

The paleoposition of Sumba relative to Antarctica was estimated by the inclination value of Sumba together with the sea floor spreading of the south eastern Indian Ocean. The inclination of -44.2° of Sumba indicates the paleolatitude of 25.9°S. The position of the Jurassic geomagnetic north pole is different from that of the present pole because the polar wondering is clearly identified from the Jurassic to the present (McElhinny, 1973). The Jurassic VGP of 53°N, 35°E is known from Antarctica. Combining the paleolatitude of Sumba with the VGP from Antarctica, we can depict the paleolatitude of 29.5°S by dotted line in Fig. 4 on which Sumba was situated at the Jurassic.

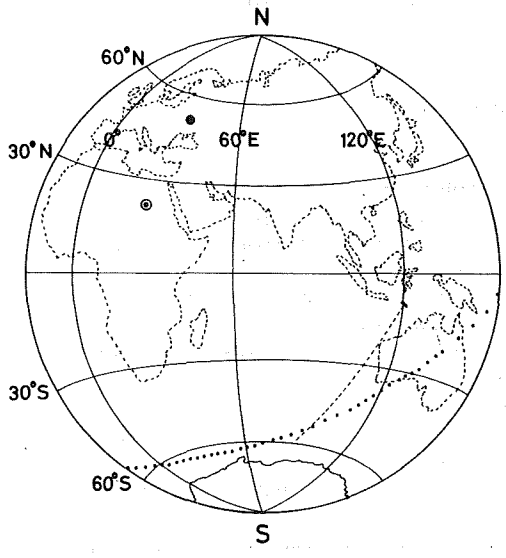


Fig. 4. A presumable paleoposition of Sumba relative to Antarctica. Sumba is situated at a point of the intersection between paleo-latitudinal line(dotted line) and the circular arc through Sumba about a pole of rotation of the Indian Ocean(dashed line).
● = Jurassic VGP from Antarctica.
◉ = Pole of rotation inferred from the magnetic lineation of the southwest Indian Ocean.

Two sets of marine magnetic anomaly patterns with different period to the south of Sumba are reported; M-series in Argo Abyssal Plain (Larson, 1975) and Indian Ocean magnetic anomalies 1 to 17 (Le Pichon and Heirtzler, 1968). The opening of the southeast Indian Ocean is regarded as a main cause of the drift of Sumba island from Antarctica. The pole of rotation of the Indian Ocean floor is obtained at 26°N, 21°E from the fracture zone method by Heirtzler et al.

(1968). Sumba could have lain on the locus drawn by dashed line in Fig. 4 which describes the path of the restoring rotation of Sumba. The Paleo-position of Sumba relative to Antarctica is assumed to lie at a point of intersection between paleolatitudinal line and the locus of the drift (Fig. 4).

It is noted that there is distinct difference between VGPs obtained from Antarctica and Asian continent. The Jurassic data from Russian Platform and China indicate the VGPs of 65°N, 138°E and 55°N, 149°E, respectively (McElhinny, 1973). The difference is mainly due to the difference of longitude values of both VGPs. The both latitudes, on the other hand, have almost the same value. The agreement of the latitudes suggests that Antarctica and Asian continent have exhibited almost the same geographical display on the earth as that at the present although a significant rotation had occurred between them around the present spin axis, and that Antarctica have never approached to Asian continent since the Jurassic. We, therefore, conclude that during the Jurassic Sumba was situated far away from Asian continent, at fairly high latitude of southern hemisphere of the present geographical coordinate system.

## 5. Conclusive remarks

Based on the paleomagnetic study of Sumba together with the marine magnetic anomaly pattern, it is inferred that Sumba have formed marginal part of the Australian continent at the counter-clockwise rotated position with a considerably high latitude in the southern hemisphere till the Late Jurassic.

## References


Audley-Charles, M. G., (1975) Tectonophysics, 26, 213.
Chamalaun, F. H., (1977) Earth Planet. Sci. Lett., 34, 107.
Flavey, D. A. and J. J. Veevers, (1974) Marine Geology, 17, 21.
Fisher, R., (1953) Proc. Roy. Soc. London, A217, 295.
Hamilton, W. (1972) U. S. Geol. Surv. Open File Rep., 3 sheets.
Hamilton, W. (1973) Bull. Geol. Soc. Malaysia, 6, 3.
Heirtzler, J. R., G. O. Dickson, E. M. Merron, W. C. Pitman III and X. Le pichon (1968) J. Geophys. Res., 73, 2119.
Katili, J. A. (1971) Earth Sci. Rev., 7, 143.
Katili, J. A. (1973) The western Pacific, P. J. Coleman, ed. (Univ. of Western Australia Press, Perth, W. A.), pp287.
Laufer, F. and A. Kraëff (1957) Geol. Surv. Ind., Pablikasi Keilmuan 33.
Larson, R. L., (1975) Geology, 3, 69.
Le Pichon, X. and J. R. Heirtzler (1968) J. Geophys. Res., 73, 2101.
McElhinny, M. W. (1973) Paleomagnetism and plate tectonics (Cambridge Univ. Press, London).
Schmidt, P. W. (1976) Tectonophysics, 33, 1.
Van Bemmelen, R. W. (1970) The geology of Indonesia, 2nd ed. (Govet. Printing Office, Hargue).

# REMANENT MAGNETIZATION OF LATE PRECAMBRIAN ROCKS IN MALAWI AND KENYA, AFRICA

Haruaki ITO and Katsuyasu TOKIEDA
Department of Physics, Faculty of Science, Shimane University, Matsue 690, Japan

Kanenori SUWA
Department of Earth Science, Faculty of Science, Nagoya University, Nagoya 464, Japan

Shoichi KUME
College of General Education, Osaka University, Toyonaka 560, Japan

Late Precambrian rocks were collected from two rock bodies in Africa. One is the Linthipe anorthosite body exposed near Linthipe (14°07'S, 34°E) in central Malawi (Suwa et al., 1979b). The other is a body of the granitoid gneisses in the Machakos area (1°30'-1°45'S, 37°25'-37°30'E) in central Kenya (Suwa et al., 1979a). The sampling sites are shown in Fig. 1.

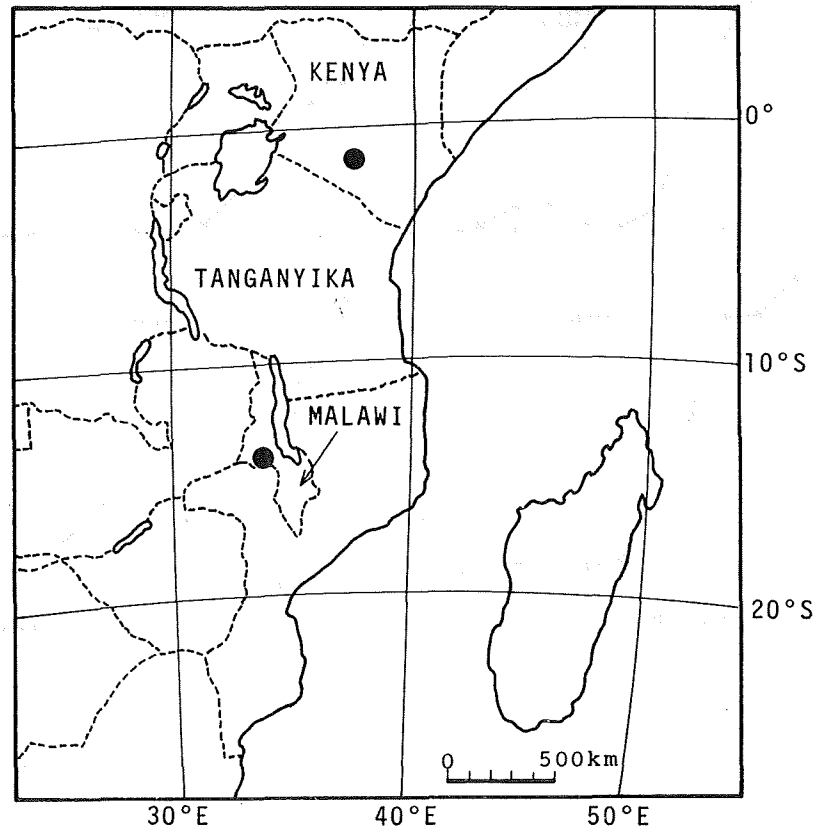


Fig. 1 Sampling localities (solid circles)

Eleven hand samples for paleomagnetic study were collected from five sites of the Linthipe anorthosite body and eight from eight sites in the Machakos area by one of the authors (K. Suwa). The weight of each sample was about 2.5 kg. Five or six core specimens with 23 mm in diameter and 23 mm high were drilled from each sample.

The K-Ar dating was also carried out for the same samples. The K-Ar age of the Linthipe anorthosite body is 670 Ma (Okano, personal communication) and that of the Machakos area is 766 ± 29 Ma (Rb-Sr age) and 528 ± 16 Ma (K-Ar age) by Shibata and Suwa (1979) and 550 Ma (K-Ar age) by Okano (personal aommunication).

The NRM of all specimens were measured with an spinner magnetometer. After the measurements of NRM, one or two specimens per sample were subjected to stepwise thermal demagnetization to 586°C. Stepwise AF demagnetization were applied to the remaining specimens. Subsequently, Six hand samples of the Linthipe anorthosite body and two of the Machakos area were confirmed to have the stable NRM.

Typical demagnetization curves of the thermal treatment of the Linthipe anorthosite samples are shown in Fig. 2. The stable NRM of the granitoid gneisses of the Machakos area had no change in direction and intensity to about 550°C

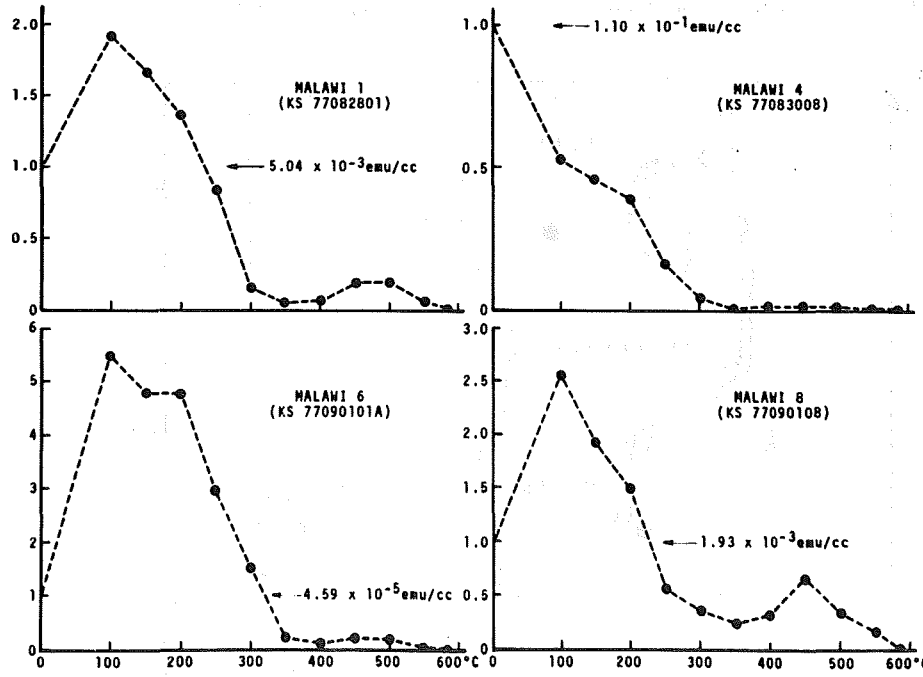


Fig. 2 Typical thermal demagnetization curves of the Linthipe anorthosite samples.

Thermal demagnetization tests on specimens of the Linthipe anorthosite body (samples of Malawi 1, 4, 6 and 8) showed the presence of two components of magnetization as seen in Fig. 3. One is a remanent vector remaining stable in temperature between 100°C and 300°C. The other is a vector being stable in temperature

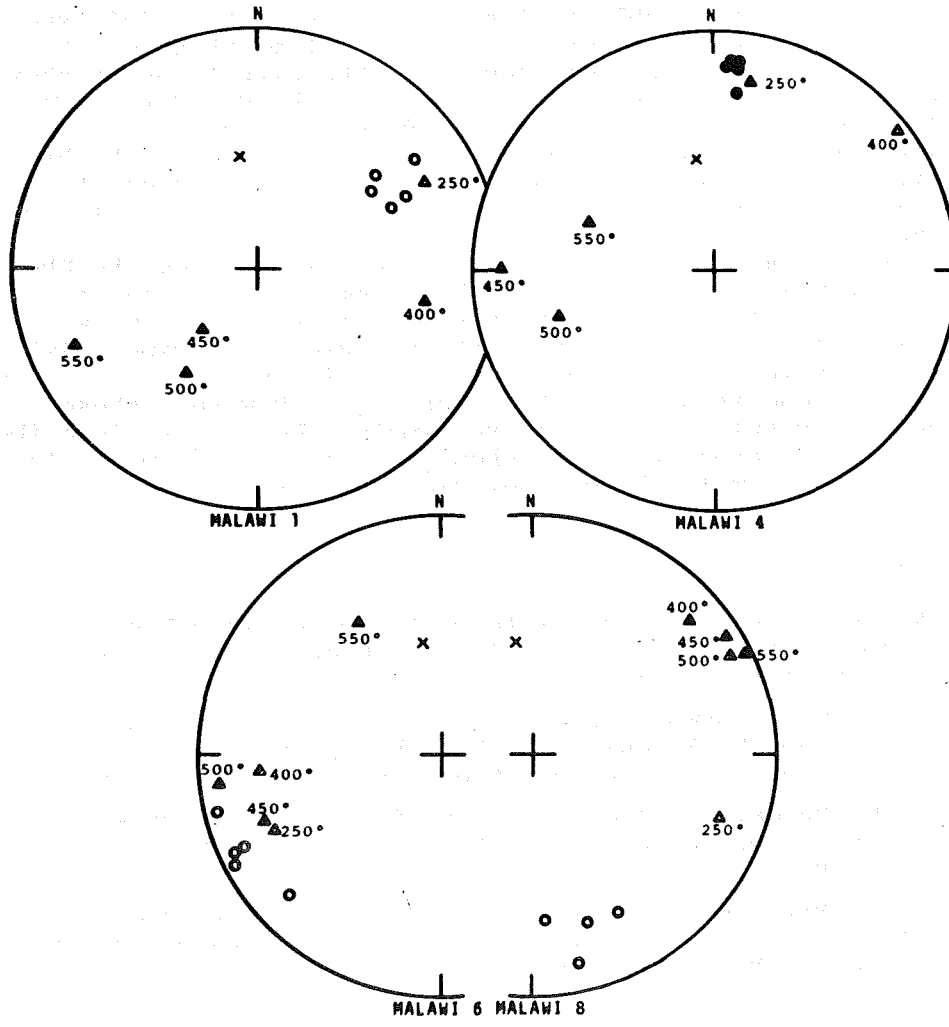


Fig. 3 Change in direction during thermal demagnetization (triangles) and NRM directions after AF demagnetization to 100 oe (circles). Solid triangles and circles represent positive inclinations and open triangles and circles represent negative inclinations. Cross mark is the present field direction at sampling site.

between 400°C and 550°C. The remanent vector of samples Malawi 1, 4 and 8 abruptly changed its direction in temperature range of about 300°C and 400°C. In that case, change in intensity of magnetization is about one tenth at 350°C. The existence of remanent vectors being stable in temperature less than 300°C suggests to be affected by lower temperature metamorphism of the anorthosite body after the emplacement. The directions of these remanent vectors are nearly consistent with the NRM directions after AF demagnetization to 75 oe or 100 oe as seen in Fig. 3.

Directions of remanent vector remaining stable in the high temperature demagnetization range (400°C to 550°C) appear to be nearly close to a point that suggests a direction of primary remanent magnetization.

Virtual geomagnetic pole positions estimated from the NRM directions remaining stable in the high temperature range are close to those obtained from the Bukoban intrusives or Gagwe amygdaloidal lavas dated at about 800 Ma (Brock and Piper, 1972), and also the pole positions are nearly consistent with that from the granitoid gneisses in the Machakos area. However, these paleomagnetic results may not be so simple. We plan to describe these results in greater detail when petrological and mineralogical studies of samples have progressed further.

REFERENCES

Brock, A. and J. A. D. Piper, Interpretation of late Precambrian palaeomagnetic results from Africa, Geophys. J. R. astr. Soc., 28, 139-146, 1972.

Shibata, K. and K. Suwa, A geochronological study on granitoid gneiss from the Mbooni Hill, Machakos area, Kenya, 4th Prelim. Rept. Afr. Studies, Nagoya Univ., 163-167, 1979.

Suwa, K., T. Nureki, H. Inoue, K. Biyajima and K. Miyakawa, Geology and petrology of the Machakos area, Kenya, 4th Prelim. Rept. Afr. Studies, Nagoya Univ., 3-20, 1979.

Suwa, K., K. Miyakawa, T. Nureki, Y. Yusa, T. Miyata and K. Suzuki, Geological and petrological notes on the Linthipe anorthosite, 4th Prelim. Rept. Afr. Studies, Nagoya Univ., 21-40, 1979.

# RARE GAS ISOTOPES AND MASS FRACTIONATION

Ichiro KANEOKA

Geophysical Institute, University of Tokyo, Tokyo 113, Japan

Rare gases are characterized by their chemical inertness. This characteristic permits their use as a tool to investigate the physical processes which govern their elemental and isotopic distribution in nature. Thus, rare gases observed in volcanic materials may reflect the physical conditions which produced these volcanic materials.

The elemental distribution of rare gases is governed by such processes as diffusion through solids and/or liquids, solubility in magma, partitioning between silicate melt and minerals, adsorption on rock or mineral surfaces, and so on. Isotopic composition is also changed by these processes, but generally to a lesser degree. However, when a limited exchange is involved, where no equilibrium is reached, mass fractionation among the isotopes will occur. For example, when volcanic gases come from a magma reservoir through a very narrow conduit to the surface, mass fractionation among isotopes will be observed. When some parts of the minerals in the upper mantle are at an elevated temperature, and a portion of rare gases in them are removed from their original site into other phases, isotopic mass fractionation is also expected.

On the other hand, some rare gases show differences in isotopic composition apart from those produced by mass fractionation. For example, the $^{3}He/^{4}He$ ratio observed in submarine pillow basalts (Krylov et al., 1974; Lupton and Craig, 1975), volcanic gases (ex. Mamyrin et al., 1974) and ultramafic rocks (Tolstikhin et al., 1974) are an order of magnitude higher than that of the atmosphere, suggesting the occurrence of primordial $^{3}He$. The value of the $^{3}He/^{4}He$ ratio seems to have regional differences (Craig et al., 1978), and thus gives us a key to identify different magma sources. The occurrence of excess $^{129}Xe$ in terrestrial rocks (Hennecke and Manuel, 1975) and $CO_2$ well gases (ex. Boulos and Manuel, 1971) may also provide us another anomaly which can be used to identify the magma source. Other radiogenic components, such as $^{4}He$ and $^{40}Ar$, directly reflect the state of the distribution of their parent elements. They also characterize the properties of the magma source. Hence, noble gases may be profitably used as a tool to identify the characteristics of the magma source.

Although information from rare gases will not always provide a unique solution, it will give us many important constraints on the physical processes in volcanic phenomena and the identity of possible magma sources (Kaneoka and Takaoka, 1978). However, we must always be careful to distinguish the effect of isotopic mass fractionation from other isotopic anomalies.

When gases enter and/or degas from a magma source through a very narrow conduit, it is expected that the rare gases are mass fractionated. Such mass fractionated rare gases have been found in volcanic materials (Krummenacher, 1970; Nagao et al.,

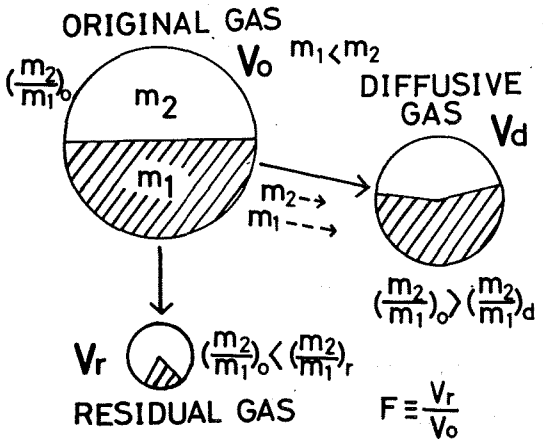


Fig. 1. A model adopted in this study. A part of gas is lost from the original gas causing mass fractionation and the diffusive gas is kept as another phase.
V : volume of each gas phase.
$m_1$, $m_2$ : atomic masses of two isotopes $M_1$ and $M_2$, respectively.
Suffixes, o, d, r indicate the factors related to the original, the diffusive and the residual gas phases, respectively. F is defined as the ratio of the volume of the residual gas to that of the original one.

1979). We will consider a very simple model to characterize the effect. Even if it is too simplified, it will demonstrate the general characteristics of fractionation processes which affect rare gases during volcanic processes.

We define a case where a part of gas is lost from an original reservoir, causing mass fractionation, and the diffusive gas is retained in another phase. Hence, after some time, two gas phases exist (Fig. 1).

We assume that the original gas contain two isotopes, $M_1$ and $M_2$, where atomic mass of $M_2$ ($\equiv m_2$) is greater than that of $M_1$ ($\equiv m_1$). In this case, the lighter isotope will be enriched in the diffusive gas. As a result, the residual gas will be enriched in heavier isotope. We designate here the volume of a gas by V and the original gas, the residual gas and the diffusive gas by suffixes, o, r and d, respectively. Then, the enrichment factor of the isotopic ratio R ($\equiv (m_2/m_1)_r/(m_2/m_1)_o$) in the residual gas can be expressed as follows (Aston, 1933):

$$R = F^{-\frac{m_2-m_1}{m_2+m_1}} , \qquad (1)$$

where F is defined as $V_r/V_o$. Conversely, the depletion factor of the isotopic ratio R' ($\equiv (m_2/m_1)_d/(m_2/m_1)_o$ in the diffusive gas can be easily deduced from the equation (1), and is expressed as follows:

$$R' = \frac{1-RF}{1-F} . \qquad (2)$$

Although this is a very simple case, it will give us useful information. In Fig. 2, R and R' are plotted against F for He and Ne isotopes. It should be noted that the isotopes are normalized to the heaviest isotope according to convention, which makes the variation of R and R' for residual and diffusive gases against F in Fig. 2 the reverse of that in the model described above. As shown in Fig. 2, the $^3He/^4He$, $^{20}Ne/^{22}Ne$ and $^{21}Ne/^{22}Ne$ ratios have the highest value in the diffusive gas when only a slight amount of gas is lost from the original reservoir. The maximum value for the enrichment factor R' in the diffusive gas is very close to that expected from a dynamical

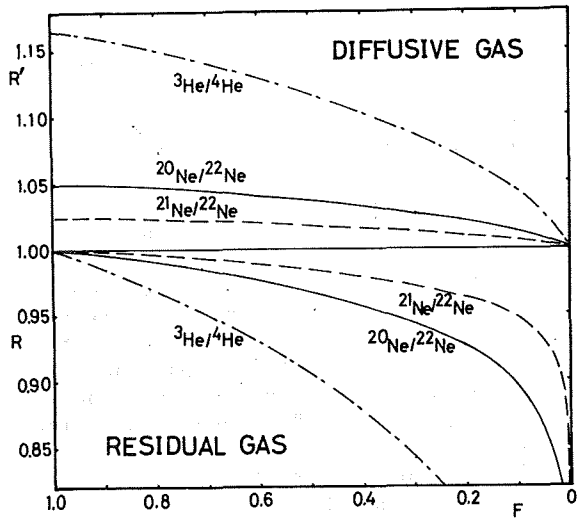


Fig. 2. The change of R and R' (defined in the text as (1) and (2)) as a function of F. Since the heaviest isotope is taken as a denominator conventionally for He and Ne, R' indicates the enrichment factor and R the depletion factor for these ratios. Note that the upper limits for R' exist for the $^{3}He/^{4}He$, the $^{20}Ne/^{22}Ne$ and the $^{21}Ne/^{22}Ne$ ratios in the diffusive gas phase, but no lower limits for them in the residual gas phase.

model expressed as $(m_2/m_1)^{1/2}$. If most gases are removed from the original reservoir, the isotopic ratios in the diffusive gas become close to those of the original gas. It is easily understood that when all gas is transfered from the original one, the ratio should be the same as that of the original gas reservoir. However, the isotopic ratios in the residual gas decrease with increasing loss of gas. Mathematically, the isotopic ratios in the residual gas approach zero when most of the gas is lost from the original reservoir. In practice, however, we may not be able to detect the small amount of residual gas and other factors may limit the value of the ratio.

From Fig. 2, we can infer that when mass fractionation occurs during gas transfer from one phase to another one, the maximum enrichment factor for the $^{3}He/^{4}He$, $^{20}Ne/^{22}Ne$ and $^{21}Ne/^{22}Ne$ ratios is governed dynamically. Even for the $^{3}He/^{4}He$ ratio, the maximum enrichment factor is less than 16%. Hence, it is difficult to explain the high $^{3}He/^{4}He$ ratio observed in the pillow basalts and volcanic gases by mass fractionation of atmospheric He. Since the former has nearly ten times higher $^{3}He/^{4}He$ ratio than the atmospheric He, multi-enrichment processes of more than fifteen stages would be required to explain the enrichment. On the other hand, a decrease in the $^{3}He/^{4}He$ ratio by more than fifty percent is possible in the residual gas by the mass fractionation process. So long as we observe only the $^{3}He/^{4}He$ ratio, we cannot unambiguously identify the effects of isotopic mass fractionation. Hence, care should be exercised in interpreting the $^{3}He/^{4}He$ ratios in volcanic materials which may show the effects of isotopic mass fractionation.

In the case of Ne, however, we can check the occurrence of isotopic mass fractionation by plotting the $^{20}Ne/^{22}Ne$ ratio against the $^{21}Ne/^{22}Ne$ ratio. In Fig. 3, Ne isotopes which have been observed in terrestrial volcanic materials are plotted. They include the data on pillow basalts and Kilauea fumarolic gases (Craig and Lupton, 1976), volcanic rocks from New Mexico (Hennecke and Manuel, 1975a) and others. As shown in Fig. 3, most data approximately lie on the mass fractionation line which goes through the atmospheric Ne values. If only a single mass

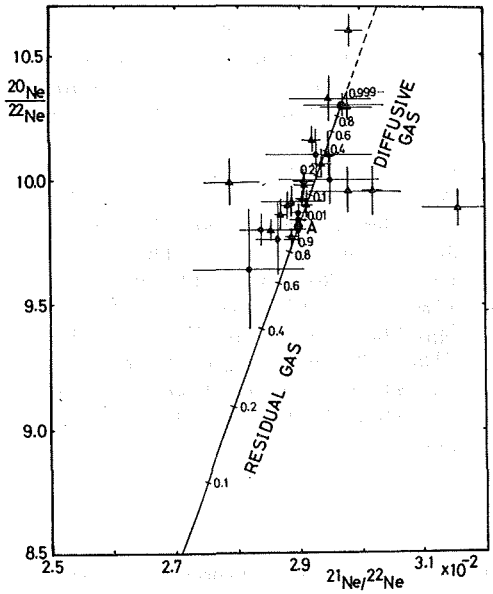


Fig. 3. The $^{20}Ne/^{22}Ne$ ratio versus the $^{21}Ne/^{22}Ne$ ratios observed in volcanic materials.
● : volcanic rock
▲ : gas from the thermal area including fumarolic gas.
The mass fractionation line through the atmospheric Ne is drawn as a solid line. Dotted line means its extension in the case of multiple stage mass fractionation. The numerical figures on the mass fractionation line correspond to F in Fig. 1, in the case of single mass fractionation from the atmospheric Ne. "A" denotes the atmospheric values.
Data sources : Anufriev et al. (1976) Bochsler and Mazor (1975), Craig and Lupton (1976), Hunnecke and Manuel (1975a, c), Kaneoka and Takaoka (unpublished, 1977), Nagao et al. (1979).

fractionation process controls the trend, the results shown in Fig. 2 suggest that the $^{20}Ne/^{22}Ne$ and $^{21}Ne/^{22}Ne$ ratios in a volcanic material should have the maximum values of about 10.3 and 0.0297, respectively, assuming that the original Ne has atmospheric isotopic compositions ($^{20}Ne/^{22}Ne$ = 9.81, $^{21}Ne/^{22}Ne$ = 0.0290 (Eberhardt et al., 1965)). Except for one sample, values of the $^{20}Ne/^{22}Ne$ ratios observed in most seriously fractionated volcanic materials show approximately the values expected for single stage fractionation. In the case of the $^{21}Ne/^{22}Ne$ ratio, however, the addition of a nuclear component at $^{21}Ne$, produced by the $^{18}O$ ($\alpha$, n) $^{21}Ne$ reaction may produce higher values of $^{21}Ne/^{22}Ne$ than expected from simple fractionation.

To explain such a trend for terrestrial Ne isotopes, a mixing between solar wind Ne B and Ne E has been suggested (Tolstikhin, 1978). Since the mixing line is close to that expected from fractionation, and the analytical uncertainty in Ne isotopes is relatively large, it is difficult to identify which mechanism is more reasonable from the trend in the Ne isotopic ratios alone. However, when Ar isotope data are available for a sample whose Ne isotopes deviate from the atmospheric values, Ar isotopes may also show the deviation expected from mass fractionation (Nagao et al., 1979). Hence, although a mixture of solar Ne and Ne E or the occurrence of excess $^{20}Ne$ (Craig and Lupton, 1976) cannot always be excluded as a possible explanation for high $^{20}Ne/^{22}Ne$ ratios, we can also explain the observed data by a simple mass fractionation process.

For Ar isotopes, a similar trend is expected. Starting with atmospheric Ar, the lower limits for the $^{40}Ar/^{36}Ar$ and $^{38}Ar/^{36}Ar$ ratios in the diffusive gas are expected to be about 280 and 0.182, respectively, assuming a single mass fractionation process. In Fig. 4, Ar isotope data on recent volcanic rocks are shown, together with the mass fractionation line. They approximately lie on the mass fractionation line. Furthermore, it is noteworthy that the lowest $^{40}Ar/^{36}Ar$ ratio observed

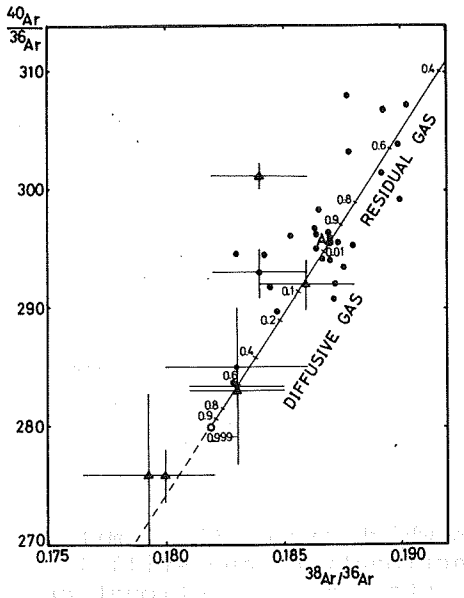


Fig. 4. The $^{40}Ar/^{36}Ar$ ratio versus the $^{38}Ar/^{36}Ar$ ratios observed in recent materials.

Symbols are the same as those in Fig. 3. The mass fractionation line through the atmospheric Ar is drawn as a solid line. The meanings of the dotted line and the numerical figures on the mass fractionation line are the same as described in the caption of Fig. 3.

Data sources : Krummenacher (1970), Hennecke and Manuel (1975a), Nagao et al. (1979), Kaneoka and Takaoka (unpublished data, 1977), Honda, Nagao and Takaoka (unpublished data, 1978).

in these rocks is around 280, the value predicted for single stage fractionation. Although a few samples show a slightly lower value, about 276, the difference between this and the predicted value is insignificant because of the large experimental uncertainties. Hence, as suggested by Krummenacher (Krummenacher, 1970), Ar isotope data observed in recent volcanic materials can often be explained by mass fractionation of atmospheric argon.

By the same procedure, we can also calculate the limit values for Kr and Xe isotopes in the diffusive gas phases, assuming single stage mass fractionation of originally atmospheric composition. The calculated results for typical rare gas isotope ratios are compared with those observed in the extremely mass fractionated rare gas isotope ratios in the volcanic materials (Table 1). As shown in Table 1, the calculated values are similar to those observed in some soil gases in geothermal area, Japan (Nagao et al., 1979), except for the $^{3}He/^{4}He$ ratio. In the case of the Kilauea gas (Craig and Lupton, 1976), the $^{20}Ne/^{22}Ne$ ratio is the same as that calculated for fractionation, but the $^{3}He/^{4}He$ ratio is much higher than the calculated value. This indicates that the high $^{3}He/^{4}He$ ratio cannot be explained by mass fractionation, but the other ratios in the recent volcanic materials are mostly the result of mass fractionation. If we assume atmospheric composition for the original gas and the single stage fractionation process described in Fig. 1, we may estimate the fraction of gas that escaped into the diffusive gas phase. However, we cannot unambiguously separate the mass fractionation trend from all possible mixing trends. However, the limiting value of each isotopic ratio poses a constraint on their origin. For example, if the value for each isotopic ratio in a sample is close to that predicted for the limiting value in the diffusive gas, then it may imply that the observed rare gases represent only a small portion of the original rare gases in the source of atmospheric composition.

Table 1. Examples of extremely mass fractionated rare gas isotope ratios in the volcanic materials

| Sample | $^{3}He/^{4}He$ ($\times 10^{-6}$) | $^{20}Ne/^{22}Ne$ | $^{38}Ar/^{36}Ar$ | $^{40}Ar/^{36}Ar$ | $^{78}Kr/^{86}Kr$ | $^{124}Xe/^{136}Xe$ | Reference |
|---|---|---|---|---|---|---|---|
| Observed values | | | | | | | |
| A-15 (soil gases in geothermal area) | 3.00 ±0.15 | 10.29 ±0.06 | 0.180 ±0.002 | 276 ± 2 | 0.02108 ±0.00027 | 0.0114 ±0.0004 | Nagao et al. (1979) |
| A-31 (soil gases in geothermal area) | 4.38 ±0.29 | 10.33 ±0.10 | 0.179 ±0.002 | 276 ± 7 | 0.02096 ±0.00036 | 0.0114 ±0.0004 | Nagao et al. (1979) |
| Kilauea gas (fumarolic gas) | 20.9 ±1.1 | 10.3 ±0.04 | ——— | ——— | ——— | ——— | Craig and Lupton (1976) |
| Calculated values as the limit in the diffusive gas phase * | 1.63 | 10.3 | 0.182 | 279.9 | 0.0213 | 0.0114 | This study |
| Air | 1.40 | 9.81 | 0.187 | 295.5 | 0.0204 | 0.0108 | |

* The limit value is calculated in the case of a single mass fractionation process, based on an assumption that the original rare gas has of atmospheric composition.

If a sample shows isotopic ratios which exceed the limit value expected from a single stage fractionation, and still lie on a mass fractionation line, multiple-stage mass fractionation is suggested. However, most reported values lie within the limit expected for each isotopic ratio. This suggests that even if multiple-stage mass fractionation processes may occur in nature, they are not a common occurrence in most volcanic materials.

In terrestrial volcanic materials, however, there are some isotopic ratios which deviate from this scheme and cannot be explained by the presence of radiogenic components. The $^{3}He/^{4}He$ ratio is one of the typical examples (ref. Table 1). Thus, we can use rare gas isotope data in volcanic materials for different purposes; the observation of mass fractionation from atmospheric values may suggest a relatively shallow physical process, whereas difference in the isotopic ratios of rare gases in volcanic materials, other than those due to radiogenic components, may reflect the properties of a magma source of greater depth.

References


Anufriev, G.S., I.L. Kamenskii and V.P. Pavlov (1976) Dokl. Akad. Nauk USSR, 231, 1454.

Aston, F.W. (1933) Mass-Spectra and Isotopes, Edward Arnold & Co., London, 248p.

Bochsler, P. and E. Mazor (1975) Nature, 257, 474.

Boulos, M.S. and O.K. Manuel (1971) Science, 174, 1334.

Craig, H. and J.E. Lupton (1976) Earth Planet. Sci. Lett., 31, 369.

Craig, H., J.E. Lupton and Y. Horibe (1978) in Terrestrial Rare Gases, ed. by E.C. Alexander, Jr. and M. Ozima, Cent. Acad. Publ. Japan, Tokyo, 3.

Eberhardt, P., O. Eugster and K. Marti (1965) Z. Naturforsch., 20, 623.

Hennecke, E.W. and O.K. Manuel (1975a) Nature, 256, 284.

Hennecke, E.W. and O.K. Manuel (1975b) Nature, 257, 778.

Hennecke, E.W. and O.K. Manuel (1975c) Earth Planet. Sci. Lett., 27, 346.

Kaneoka, I. and N. Takaoka (1978) Earth Planet Sci. Lett., 39, 382.

Krummenacher, D. (1970) Earth Planet. Sci. Lett., 8, 109.
Krylov, A. Ya., B.A. Mamyrin, L.V. Khabarin, T. I. Mazina and Y.A. Silin (1974) Geokhimiya, No. 8, 1221.
Lupton, J.F. and H. Craig (1975) Earth Planet. Sci. Lett., 26, 133.
Mamyrin, B.A., V.I. Gerasimovsky and L.V. Khabarin (1974) Geokhimiya, No. 5, 693.
Nagao, K., N. Takaoka and O. Matsubayashi (1979) Earth Planet. Sci. Lett., 44, 82.
Tolstikhin, I.N. (1978) in Terrestrial Rare Gases, ed. by E.C. Alexander, Jr. and M. Ozima, Cent. Acad. Publ. Japan, Tokyo, 33.
Tolstikhin, I.N., B.A. Mamyrin, L.V. Khabarin and E.N. Erlikh (1974) Earth Planet. Sci. Lett., 22, 75.

# THE ORIGIN OF RARE GASES IN THE EARTH ATMOSPHERE

Minoru OZIMA[1] and Kiyoshi NAKAZAWA[2]

1) Geophysical Institute, University of Tokyo, Tokyo 113, Japan
2) Department of Physics, Kyoto Univeristy, Kyoto 606, Japan

Because of the similarity in the rare gas elemental abundance pattern between the terrestrial atmosphere and chondrites, the terrestrial rare gases are generally assumed to have been derived from the planetary type rare gases, that is, the rare gases trapped in chondrites. However, there are large differences in the isotopic compositions of Xe and Ne. It is clearly not possible to derive the atmospheric Xe and Ne simply from the planetary type rare gases. Hence, the origin of the terrestrial rare gases must be sought in the pre-planet conditions rather than in the chondritic materials.

During the fragmentation process (e.g. Safronov, 1969) which formed numerous planetesimals ranging from $10^{18}$ to $10^{25}$ g, some of the solar nebula must have been captured within the planetesimals. The solar nebula thus captured is fractionated due to the gravitation field of the planetesimals, in that the degree of the fractionation depends both on the mass number of the rare gas and the size of the planetesimals. This is shown in Figure 1, where the fractionation pattern is calculated with the use of a hydrostatic equilibrium equation for the planetesimals of a variable size (R).

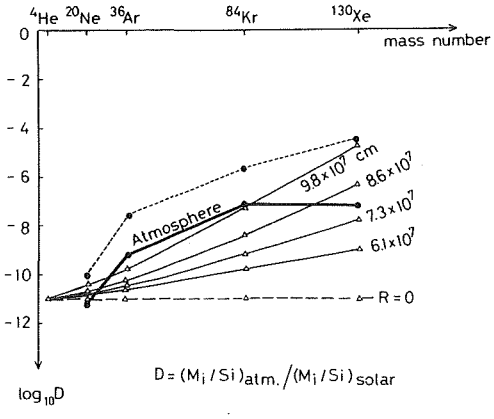


Fig. 1. Rare gas elemental abundance ($\log_{10} D$) relative to the solar abundance in planetesimals fo various sizes (R) are plotted against a mass number. The amount of rare gases is normalized to Si. In the case of the atmospheric values (thick line), $M_i$ stands for the rare gases in the atmosphere and Si in the whole earth. Note that the mixing of the gravitationally fractionated planetesimal type (thin lines) and the planetary type rare gases (dotted line) would approximate the atmospheric pattern.

The isotopic compositions are also gravitationally fractionated within the planetesimals, which can be calculated similary with the use of the hydrostatic equilibrium equation. The isotopic fractionation is most conspicuous in the heaviest rare gas, i.e. Xe. Figure 2 shows the isotopic fractionation factor $\delta$ (see Figure 2 for the definition) for the case of Xe. The fractionation factor shows nearly a linear mass dependence in accordance with the observation.

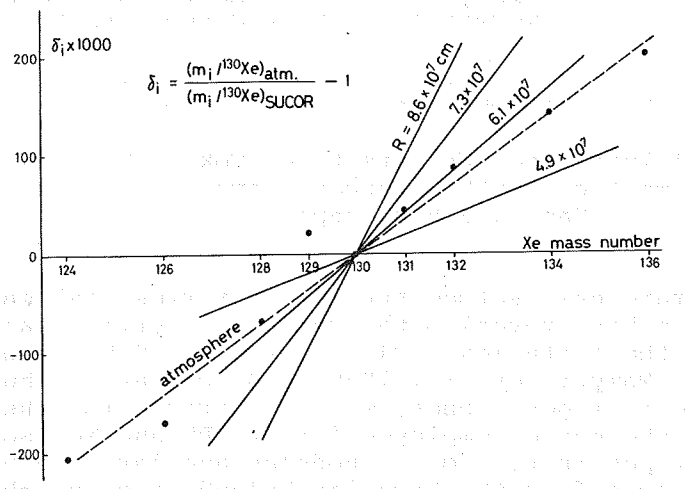


Fig. 2. Isotopic fractionation pattern for Xe in planetesimals of various sizes relative to SUCOR Xe (SUCOR designates Surface-Correlated gas in lunar soil, which is regarded to be close to the solar composition). Lines indicate the fractionation for a planetesimal with a radius R(cm), which resulted from the gravitational fractionation in the planetesimal.

We propose that the terrestrial rare gases are the mixture of the planetary type rare gases which were added to the earth via the chondritic materials and the rare gases captured by the planetesimals which accreted the earth. The atmospheric rare gases were later degassed from the solid earth. The model can explain, (i) the enormous depletion of the rare gases and (ii) heavier rare gas enrichment relative to the solar abundance. The model can also explain, (iii) the large Xe isotopic fractionation ($\sim$ 4% / a.m.u.) with nearly a linear mass dependence, (iv) the difference in Ne isotopic compositions and (v) similar isotopic compositions of Ar and Kr among the terrestrial, planetary and solar type rare gases, for which no satisfactory explanations have so far been offered. The model fits quite nicely to the general frame work of the astrophysics on the origin of the solar system (e.g., Hayashi et al., 1977).

References

Hayashi, C., K. Nakazawa and I. Adachi (1977) Pub. Astr. Soc. Japan, 29, 163.
Safronov, V.S. (1969) NASA, TFF-677 (English translation).

(Submitted to IUGG Inter-disciplinary symposia "Chemical evolution of the atmosphere, oceans and crust" at Camberra, 1979.)

# RARE GAS ISOTOPES IN HAWAIIAN ULTRAMAFIC NODULES AND VOLCANIC ROCKS : A CONSTRAINT ON THEIR GENETIC RELATIONSHIPS

Ichiro KANEOKA[1] and Nobuo TAKAOKA[2]

1) Geophysical Institute, University of Tokyo, Tokyo 113, Japan
2) Department of Earth Sciences, Yamagata University, Yamagata 990, Japan

Recent rare gas isotope studies in terrestrial materials of deep origin have revealed the remains of primordial components within the earth (ex. Clarke et al., 1969; Hennecke and Manuel, 1975; Mamyrin et al., 1969). By comparing the components and the radiogenic ones, we can characterize the source materials in the manner employed for Sr, Pb and Nd isotopes. Rare gas isotopes in ultramafic nodules and large phenocrysts of volcanic rocks from the Hawaiian Islands suggest that they were derived from different source materials : The former from ones similar to those of the oceanic tholeiites, whereas the latter from ones of a more primitive nature.

Concerning the origin of Hawaiian volcanic rocks, there are many investigations, including petrographical, mineralogical and geochemical studies (ex. Jackson and Wright, 1970; Wright, 1971). In these studies, it is often assumed that the ultramafic nodules included in Hawaiian volcanic rocks represent the source materials or cumulates for these volcanic rocks (ex. Jackson, 1968; Kuno and Aoki, 1970). However, no definite evidence has been found that they have a common genetic relationship. Even isotope studies have not yet settled the problem, since most studies are mainly concerned with volcanic materials of different types. The few isotopic investigations on ultramafic nodules had insufficient analytical precision to settle the problem (Stueber and Ikuramuddin, 1974). In the present study, we have attempted to resolve this problem by using rare gas isotopes.

Three ultramafic nodules (two spinel-lherzolites and one garnet-pyroxenite) from the Salt Lake Crater, Oahu Island and three large phenocryst samples (one olivine and two augite samples) from the Haleakala Volcano, Maui Island were analysed in the present study. Two dunite nodules from Hualalai and one olivine phenocryst sample of the Kapoho lava, Hawaii Island were previously analysed (Kaneoka and Takaoka, 1978), and the results are included in the present figures for discussion. Olivine and augite phenocrysts were handpicked under a microscope. Their grain size ranges from about one to 5 mm. One pair of olivine and augite phenocrysts was separated from an ankaramite from the Haleakala Volcano to check the equilibrium state of rare gas isotopes between the two phases. The reasons that we have used large phenocrysts instead of volcanic rock itself to observe rare gas isotopes are as follows. Since volcanic rocks solidify at the surface of the earth, original gases of the magma may be lost or exchanged with atmospheric gases. Oceanic pillow basalts can trap the original gases to some degree due to their rapid cooling and the circumstantial hydrostatic pressure (ex. Dymond and Hogan, 1973). However, it is not easy to find such materials in the subaerial condi-

tion. Furthermore even in glassy materials, we cannot exclude the possibility of atmospheric contamination. On the other hand, large phenocrysts are considered to have solidified at depth in a magma reservoir, where no serious atmospheric contamination occurs. Since they are formed in situ in a magma reservoir, the isotopic compositions of rare gases in phenocrysts should represent those of the magma as long as an isotopic equilibrium of rare gases is kept in the magma reservoir. Olivine is expected to be suitable for the present purposes because of its good retentivity of rare gases and relatively deep origin. Present results also support the usefulness of large augite phenocrysts for rare gas studies.

To measure all rare gas isotopes including the $^3He/^4He$ ratio, a Nier-type mass spectrometer equiped with a secondary multiplier was used. This instrument has a resolving power of about 600 and can separate $^3He$ from $HD + H_3$. All vacuum lines are made of stainless steel except for the sample holding part (Takaoka, 1976). To examine the effect of surface atmospheric contamination, two stage (700 and 1800°C, 30 min.) stepwise heating was employed for some of the samples. Samples were melted in a Ta crucible with a resistance heater, and the temperature was measured with an optical pyrometer.

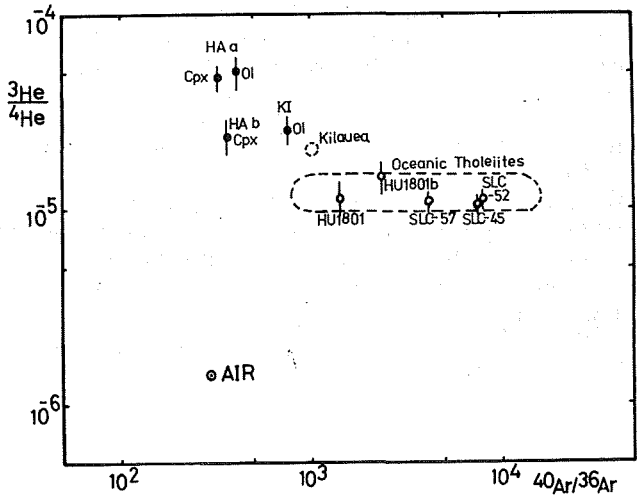


Fig. 1. The $^3He/^4He$ ratio versus the $^{40}Ar/^{36}Ar$ ratio for Hawaiian ultramafic nodules (open symbols) and phenocrysts of volcanic rocks (closed symbols).
Ol : olivine phenocrysts, Cpx : augite phenocrysts,
HU : Hualalai, Hawaii Is., SLC : Salt Lake Crater, Oahu Is.,
KI : Kilauea, Hawaii Is., HA : Haleakala, Maui Is.
Dotted area designated as Kilauea is represented as the combination of data on the $^3He/^4He$ ratios of fumarolic gases (Craig and Lupton, 1976) and the maximum $^{40}Ar/^{36}Ar$ ratio observed in pillow basalts from the East Rift zone (Dalrymple and Moore, 1968). The oceanic area is also defined by the combination of the published data. When stepwise heating was done, the data in the higher temperature fraction are plotted.

Our results indicate that the ultramafic nodules and phenocrysts of volcanic rocks have different isotopic compositions. As shown in Fig. 1, the difference is especially clear in the $^{3}He/^{4}He$ and $^{40}Ar/^{36}Ar$ ratios. Ultramafic nodules from Hualalai and Salt Lake Crater show high $^{40}Ar/^{36}Ar$ ratios ( $>1000$) and relatively constant $^{3}He/^{4}He$ ratios of (1.0-1.4) x $10^{-5}$. Both ratios are quite similar to those observed in the oceanic tholeiites (ex. Dymond and Hogan, 1978; Lupton and Craig, 1975). Olivine and augite phenocrysts from Kilauea and Haleakala Volcanoes show, however, lower $^{40}Ar/^{36}Ar$ ratios ( $<1000$) and higher $^{3}He/^{4}He$ ratios ( $>2 \times 10^{-5}$). Since the atmospheric $^{40}Ar/^{36}Ar$ and $^{3}He/^{4}He$ ratios are 295.5 and $1.4 \times 10^{-6}$, respectively, it is impossible to explain the difference by atmospheric contamination. Fig. 1 rather shows a mixing trend between two possible source materials. One is represented by the sample HA a with the $^{40}Ar/^{36}Ar$ ratio of about 400 and the $^{3}He/^{4}He$ ratio of around $5 \times 10^{-5}$, and the other is represented by the oceanic tholeiites with the $^{40}Ar/^{36}Ar$ ratio of about 16000 and the $^{3}He/^{4}He$ ratio of (1.0-1.4) x $10^{-5}$. It is noteworthy that Kilauea fumarolic gases also show high $^{3}He/^{4}He$ ratios of about $1.9 \times 10^{-5}$ (Craig and Lupton, 1976). Such high $^{3}He/^{4}He$ ratios ( $>1.9 \times 10^{-5}$) are typically observed in Hawaii, Iceland (Mamyrin et al., 1972) and Yellowstone (Craig et al., 1978) and are interpreted to be characteristic of a hot spot area (Craig et al., 1978). It is almost impossible to relate such a hign $^{3}He/^{4}He$ ratio to that of the oceanic tholeiites by a simple mass fractionation process, unless more than ten mass fractionation processes occur. The Ne and Ar isotope data do not support such multiple mass fractionation processes for present samples. In Fig. 1, it seems that olivine and augite phenocrysts from the sample HA a show a similar $^{3}He/^{4}He$ ratio, but different $^{40}Ar/^{36}Ar$ ratios.
However, this can be explained by the difference in the analytical procedures. Olivine phenocrysts were analysed by the two stage stepwise heating and the values for 1800°C fraction are shown in Fig. 1, but augite phenocrysts were analysed as a total melt. In effect, their total isotopic values are similar both in the $^{3}He/^{4}He$ and $^{40}Ar/^{36}Ar$ ratios. Hence, we may argue that an isotopic equilibrium occurred between the two phases. On the

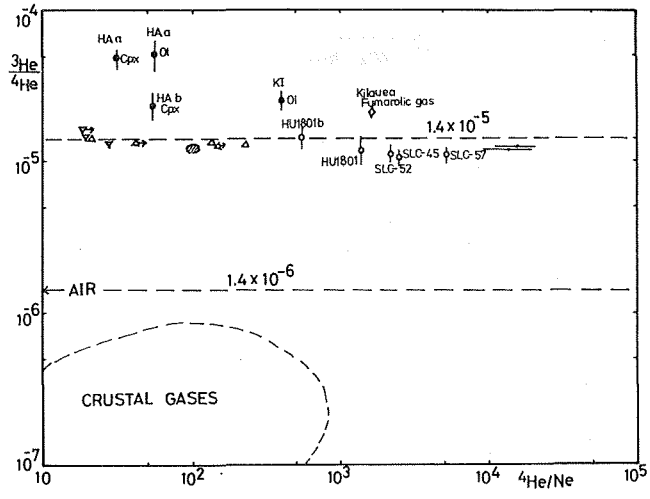


Fig. 2. The $^{3}He/^{4}He$ ratio versus the $^{4}He/Ne$ ratio. Symbols without any designation indicate the data for the oceanic tholeiites analysed by Lupton et al. (1977). The legends for Hawaiian samples are same with those of Fig. 1. The data for Kilauea fumarolic gases are taken by Craig and Lupton (1976).

other hand, the sample HA b shows lower $^{3}He/^{4}He$ and $^{40}Ar/^{36}Ar$ ratios than those of the sample HA a even in the 1800°C fraction. This may reflect either the heterogeneity of source materials and/or slight introduction of atmospheric components into the magma reservoir at a relatively shallow depth from which the sample HA b was derived. However, the $^{3}He/^{4}He$ ratio for this sample is still higher than those of ultramafic nodules from the Hawaiian Islands, suggesting different source materials between them.

In Fig. 2, the $^{3}He/^{4}He$ ratios are plotted against the $^{4}He/Ne$ ratios. The data for the oceanic tholeiites are taken from Lupton et al. (1977) for comparison. The $^{3}He/^{4}He$ ratios for the oceanic tholeiites from quite separated regions such as the East Pacific Rise and the Mid-Atlantic Ridge are rather uniform in spite of very large variation in the $^{4}He/Ne$ ratios. The variation in the $^{4}He/Ne$ ratios probably reflects the difference of the mobility for each element during geological processes. However, the uniformity of the $^{3}He/^{4}He$ ratios over large areas requires a special condition for He to be equilibrated. A simple estimation suggests that it is difficult for He to be equilibrated over such large distance by diffusion through solids. Hence, it seems likely that equilibration occurred through liquids. Accordingly, the partial melting zone in the asthenosphere would probably play an important role for the equilibrium of He isotopes. Slight differences in the $^{3}He/^{4}He$ ratios among different regions may correspond to the state of local equilibrium, reflecting different degree of partial melting. Ar may follow a similar trend, though to a much less degree than He. The occurrence of excess $^{129}Xe$ in Hawaiian ultramafic nodules and no definite evidence for it in the recent oceanic tholeiites may be also explained by a very limited local equilibrium for Xe isotopes.

Accordingly, the rare gas isotopes do not support the genetic relationships between Hawaiian volcanic rocks and ultramafic nodules found in Hualalai, Hawaii Is. and Salt Lake Crater, Oahu Is. Since garnet lherzolite is not analysed in this study, one may argue that it is of different origin from the other kinds of nodules. From the occurrences of nodules, however, we think the probability for it small. The similarity of rare gas isotopes between Hawaiian ultramafic nodules and the oceanic tholeiites implies that the lithosphere under the Hawaiian Islands are composed of such ultramafic rocks and were formed from similar source materials to those of the oceanic tholeiites. We suppose that the uniformity of the $^{3}He/^{4}He$ ratios observed in the oceanic tholeiites occurs due to the existence of partial melting zone in the asthenosphere. Seismologically, the partial melting zone is estimated to exist under the lithosphere. Thus, if we take this model, the asthenosphere should be the source region for the production of the oceanic tholeiites.

The formation mechanism of the Hawaiian Chain can be well explained by a hot spot hypothesis (Morgan, 1972) and the present results are compatible with this. It requires that a mantle plume should arise at least from a deeper part than the lithosphere. As revealed in the present study, the source materials of the Hawaiian volcanic rocks are different from those of the oceanic tholeiites which might be derived from the asthenosphere. This leads us to a conjecture that mantle plume(s) should arise from a deeper part than the asthenosphere.

Hence, the difference in the rare gas isotopes between the two sources, the one for the Hawaiian mantle plume and the other for the oceanic tholeiites, may give us significant information concerning the evolution of the erath. As shown in Table 2 and Fig. 1, the source materials for the Hawaiian volcanic rocks have higher $^{3}He/^{4}He$ and lower $^{40}Ar/^{36}Ar$ ratios than those of the oceanic tholeiites. To explain the difference, one of the interpretations is that the radiogenic components such as $^{4}He$ and $^{40}Ar$ are relatively enriched compared to primordial components such as $^{3}He$ and $^{36}Ar$ in the source region of the oceanic tholeiites. However, this is incompatible with the concept of "depleted mantle" deduced from the other isotopic and geochemical data for it (ex. Kay and Hubbard, 1978). Alternatively, if we consider that the primordial components of rare gases are depleted in the source region of the oceanic tholeiites, we can also explain the isotopic differences between the two sources. The latter is compatible with the concept of "depleted mantle". In this case, the source region from which a mantle plume arises still retain a relatively primordial character, though its degree of primitiveness is very model dependent. Our results imply that a model on the evolution of the earth should not be based only on information derived from ultramafic nodules and oceanic tholeiites.

Finally, our results support a view of mixing between the mantle plume and the source materials of the oceanic tholeiites (materials of the asthenosphere and/or lithosphere) as observed in the Hawaiian volcanic rocks. The Sr, Pb and Nd isotopes in the Hawaiian volcanic rocks may be also interpreted in this way. Such a mixing between the non-depleted and depleted mantle materials may be more common than has been considered.

References and Notes


Clarke, W.B., M.A. Beg, H. Craig (1969) Earth Planet. Sci. Lett., 6, 213.

Craig, H., and J.E. Lupton (1976) Earth Planet. Sci. Lett., 31, 369.

Craig, H., J.E. Lupton, J.A. Welhan, R. Poreda (1978) Geophys. Res. Lett., 5, 897.

Dalrymple, G.B. and J.G. Moore (1968) Science, 161, 1132.

Dymond, J. and L. Hogan (1973) Earth Planet. Sci. Lett., 20, 131.

Dymond, J. and L. Hogan (1978) Earth Planet. Sci. Lett., 38, 117.

Hennecke E.W. and O.K. Manuel (1975) Nature, 257, 778.

Jackson, E.D. (1968) Proc. 23rd Internat. Geol. Congr., 1, 135.

Jackson, E.D. and T.L. Wright (1970) Jour. Petrology, 11, 405.

Kaneoka, I. and N. Takaoka (1978) Earth Planet. Sci. Lett., 39, 382.

Kay, R.W. and N.J. Hubbard (1978) Earth Planet. Sci. Lett., 38, 95.

Kuno, H. and K. Aoki (1970) Phys. Earth Planet. Interiors, 3, 273.

Lupton, J.E. and H. Craig (1975) Earth Planet. Sci. Lett., 26, 133.

Lupton, J.E., R.F. Weiss and H. Craig (1977) Nature 266, 244.

Mamyrin, B.A. and I.N. Tolstikhin, G.S. Anufriyev, and I.L. Kamenskiy (1969) Doklady Acad. Nauk USSR, 184, 1197.

Mamyrin, B.A., I.N. Tolstikhin, G.S. Anufriev, and I.L. Kamenskiy (1972) Geokhimiya, No. 11, 1396.
Morgan, W.J. (1972) Am. Ass. Petrol. Geol. Bull., 56, 203.
Stueber, A.M. and M. Ikuramuddin (1974) Geochim. Cosmochim. Acta, 38, 207.
Takaoka, N. (1976) Mass Spectroscopy, 24, 73.
Wright, T.L. (1971) Geol. Surv. Prof. Paper, 735.

# RADIOMETRIC AGES OF METEORITES

Frank A. PODOSEK

Dept. Earth and Planetary Sciences, Washington Univ.
St. Louis, MO 63130

More than twenty years ago the Pb-Pb analyses of Patterson and others led to the plausible argument that there was a defineable time of formation for at least the planetary objects in the solar system some 4.5 Ga ago. Subsequent work has led to greater precision in this age, has indicated that the solar system as a whole must be characterized by this age, and has shed some light on the nature of events near the "beginning" of the solar system.

At present, the strongest evidence for a well-defined beginning — a short time scale for planet-forming events — is the prior existence of short-lived (now extinct) radionuclides in meteorites. Assuming such radionuclides were indeed synthesized in other stars, their presence in meteorites demands a short time scale between presolar nucleosynthesis and the formation of solids within the solar system. On the basis of $^{129}I$ and $^{244}Pu$, the indicated time scale is of the order of $10^8$ yr. A much shorter scale is similarly indicated by the shorter-lived and more recently discovered nuclides $^{107}Pd$ and $^{26}Al$. The most stringent limits follow from $^{26}Al$ : no more than a few Ma between nucleosynthesis and the formation of solids (refractory inclusions in carbonaceous chondrites) and, if $^{26}Al$ is adopted as the heat source for achondrite igneous processes and chondrite metamorphism, no more than an additional 2-3 Ma for the formation of planet-sized ( $\gtrsim$ 50 km) objects. Even without this assumption, the presence of $^{107}Pd$ in iron meteorites sets the time scale for planetary differentiation in the $10^7$ yr range.

The most precise absolute chronology for meteorites is the $^{207}Pb$-$^{206}Pb$ age, both because of the inherent precision of isotopic (as opposed to elemental) measurements and because the parent U decay constants are more precisely known than are other decay rates (the decay constant uncertainty is only 5 Ma for a $^{207}Pb$-$^{206}Pb$ age). The best age for the solar system is accordingly 4.54 - 4.57 Ga, following from $^{207}Pb$-$^{206}Pb$ ages of Allende refractery inclusions and some Pb-poor achondrites, notably Angra dos Reis. The event dated is chemical differentiation, enrichment of U relative to Pb, and is probably the most likely candidate for the time of condensation of solids.

This range is larger than statistical uncertainty in individual determinations. Other meteorites, including chondrites, give a larger range (also beyond individual uncertainties), down to 4.50 Ga and below but not significantly above 4.57 Ga. It remains to be resolved whether this range reflects experimental problems or ambiguity in age assignments for discordant U/Pb systems, or whether it is a real spread of ages for parent body formation, igneous differentiation, or metamorphism.

Precise recent Rb-Sr analyses indicate a common chondrite whole rock isochron of age $\sim$ 4.50 Ga, with which other meteorite

classes are compatible. This also indicates the time of macroscopic chemical differentiation, enrichment of Sr relative to Rb, and should be the age most nearly comparable to Pb-Pb ages. The significance of the difference between, say, 4.50 (Rb-Sr) and 4.56 (Pb-Pb) remains to be clarified; it is worth noting, however, that this difference is within the uncertainty in the $^{87}Rb$ decay rate.

Excepting a few young non-chondrites, Rb-Sr internal isochron ages of individual meteorites are compatible, within rather larger errors, with the whole rock isochron age. More significant, it now appears that chondrites in general have initial $^{87}Sr/^{86}Sr$ ratios which are elevated above those in Rb-poor objects like Allende inclusions or Ca-rich achondrites. These are generally interpreted to represent parent-body metamorphism, so that Sr isotopic closure was not achieved until some $10^8$ yr after parent-body formation.

$^{40}Ar-^{39}Ar$ ages for a number of chondrites fall in the range $\sim$4.38-4.52 Ga, and again the range is larger than individual nominal uncertainties. It could be maintained that the ages are actually isochronous, that the mean absolute age differs from the Rb-Sr and Pb-Pb ages because of $^{40}K$ decay constant uncertainty, and that the age spread reflects a combination of experimental uncertainty (typically $\sim$0.03 Ga) and ambiguity in the interpretation of apparent age release patterns. This is not necessary, however, and the ages may be acceptable at face value as metamorphism ages. The time scale is the same $10^8$ yr range suggested by initial $^{87}Sr/^{86}Sr$, and follows plausibly from surprisingly low estimated Ar closure temperatures ($\sim$200-300°C) and slow cooling rates (frequently $\sim$1°C/Ma) inferred from metallographic and differential fission track retention studies.

$^{129}I-^{129}Xe$ retention times for chondrites in general and many non-chondrites are not known as absolute ages but fall within a fairly narrow range of 20-30 Ma age difference. It might be expected that Xe retention times should be the same as Ar retention times, but the $^{129}I-^{129}Xe$ age range would then be incompatible with the $^{40}Ar-^{39}Ar$ age range. Since Xe closure temperatures are apparently substantially higher than Ar closure temperatures, however, it is plausible to suppose that Xe and Ar ages are significantly decoupled by slow cooling. A consistent view is then that I-Xe ages also reflect relaxation of metamorphic conditions some time after parent-body formation but at a higher temperature and an earlier time than the corresponding K-Ar ages.

Reservations must arise in the acceptance of the usual chronological interpretations because of the possibility of isotopic heterogeneity. Reinterpretations of Pb-Pb and U-Pb ages must be made in response to recent evidence for $^{235}U/^{238}U$ variation, for example, but clarificaiton of this situation is needed. Even excluding isotopically pathological cases such as C1 and EK1-4-1, there is evidence for systematically different O (and perhaps volatiles such as C, N and noble gases) compositions in various classes of solar system material. Such variations could - and should - have sizeable effects on chronological schemes. Permil variations in $^{87}Sr$ and $^{147}Nd$, for example, would be quite prominent. For low-abundance short-lived nuclides, such as $^{129}I$ and $^{40}K$ for example, recently synthesized and nonuniformly distributed components should make

a much larger relative contribution than for stable species. Thus, for example, a $^{40}Ar$-$^{39}Ar$ age $\sim 5$ Ga for an Allende inclusion might indicate $^{40}K$ enhancement. K in this inclusion was found to be isotopically normal, however, so this case remains an enigma. More generally, evidence for chronological misinterpretation because of unrecognized heterogeneity seems conspicuously absent, in that no organized schemes have emerged for clarification of chronological puzzles by invocation of isotopic heterogeneity in any systematic fashion.

# Sr ISOTOPE STUDIES OF MAFIC AND ULTRAMAFIC INCLUSIONS FROM ITINOME-GATA, JAPAN

Shigeo ZASHU, Ichiro KANEOKA[1)]
and
Ken-ichiro AOKI[2)]

1) Geophysical Institute, University of Tokyo, Tokyo 113, Japan
2) Institute of Mineralogy, Petrology and Economic Geology, Tohoku University, Sendai 980, Japan

## Introduction

It is well known that a lot of mafic and ultramafic inclusions are observed in basalts erupted at Itinome-gata, located at the Japan Sea coast of northeast Japan (ex. Kuno and Aoki, 1970). Petrologically, they are estimated to have been derived from the upper mantle and lower crust.

Since these inclusions are derived from different depths, there is no guarantee that they are isotopically homogeneous one another. Even a mantle-derived lherzolite may have different isotopic ratio with that of its host rock. If so, the isotopic difference in these samples may suggest different genetic relationships among these samples and/or different history. In this respect, Sr isotopes in the ultramafic and mafic inclusions from Itinome-gata will give us significant information to understand the characteristics of the upper mantle and lower crust in this region. The comparison of $^{87}Sr/^{86}Sr$ ratio between inclusions and host rocks will clarify the petrogenetic relationships between them. Furthermore, samples derived from different depths make it possible to evaluate the isotopic homogeneity of the upper mantle, and lower crust vertically. To investigate this, we have analysed mafic and ultramafic inclusions derived from different depths and their host rocks. In this note, we report the results on Rb, Sr contents and $^{87}Sr/^{86}Sr$ ratios for them.

## Samples

Various types of inclusions from Itinome-gata were originally described by Hayashi (1955) and Kuno (1967) in brief. Later, Kuno and Aoki (1970), Aoki (1971) reported the petrology of the ultramafic and mafic inlusions in greater detail. $^{14}C$ dating results suggest that host rocks were extruded about 10000 years ago (Aoki, 1971). Host rocks were first described as alkali basalts (Kuno, 1967). However, recent work has revealed that most ultramafic inclusions were carried out in calcalkalic andesites (Katsui et al., 1978). Rock types of investigated samples and the derived depths estimated petrologically are shown schematically in Fig. 1.

## Experimental procedures

Samples were analysed as total rock. To remove xenolithic contamination, groundmass samples of host basalts were purified by handpicking under a microscope.

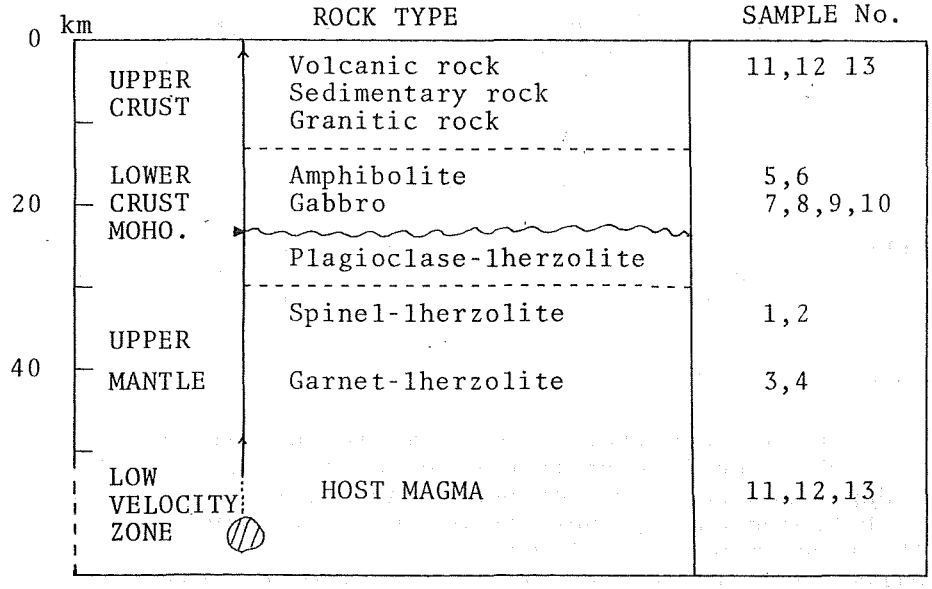


Fig.1 The schematic diagram of the vertical relationship for each sample from the Itinome-gata region.

Analytical procedures in this study are identical to those described by Matsuda et al. (1977). Five determinations of $^{87}Sr/^{86}Sr$ ratio on the Eimer and Amend $SrCO_3$ standard carried out during the present study gave a mean value of 0.7080 ± 0.0002 (2σ). The $^{87}Sr/^{86}Sr$ ratios of the samples were measured in duplicate, including chemical processing of the samples. From them, an experimental error (2σ) of about 0.0004 ∿ 0.0005 was estimated for lherzolites and of about 0.0001 ∿ 0.0002 for mafic inclusions and basaltic rocks. Rb and Sr contents were analysed in duplicate by isotope dilution method, using $^{87}Rb$ and $^{86}Sr$ enriched spikes. These determinations are usually precise to about ± 2%. Blanks for Rb and Sr determinations were estimated to be 0.005 μg and 0.03 μg, respectively. These blanks were applied for correction in the determination of Rb and Sr contents.

## Results and Discussion

The Rb and Sr contents and the $^{87}Sr/^{86}Sr$ ratios in the inclusions and host basaltic rocks are presented in Table 1.

The data show some characteristic features. Both Rb and Sr contents in lherzolites are similar to those of Alpine-type peridotites rather than those ultramafic inclusions in volcanic rocks from other areas (Faure and Powell, 1972). As compared with the ultramafic inclusions in alkali basalts from the Oki-Dōgo Island, southwestern Japan, our samples are more depleted in Rb except for sample 4. This may suggest that the upper mantles from which these rocks were derived may have different properties each other. In effect, although host volcanic rocks from the two regions have identifal Rb contents (40 - 90 ppm), Sr contents are different (Oki-Dōgo samples : 800 - 900 ppm). Hence, the uppermost part of the mantle may be chemically different between the northeast and southwest of Japan.

Our results show that the host basalt and andesite from Itinome-gata have $^{87}Sr/^{86}Sr$ ratios ranging from 0.7031 to 0.7033.

Table 1. Rb,Sr and $^{87}Sr/^{86}Sr$ ratios of inclusions and host basaltic rocks

| No. | Rock type | $Rb_{(ppm)}$ | $Sr_{(ppm)}$ | Rb/Sr | $^{87}Sr/^{86}Sr$ |
|---|---|---|---|---|---|
| 1 | Lherzolite | 0.052 | 2.04 | 0.025 | 0.7053 |
| 2 | Lherzolite | 0.137 | 11.0 | 0.012 | 0.7044 |
| 3 | Lherzolite | 0.087 | 1.87 | 0.047 | 0.7030 |
| 4 | Lherzolite | 0.406 | 55.5 | 0.007 | 0.7045 |
| 5 | Amphibolite | 1.75 | 310 | 0.006 | 0.7032 |
| 6 | Amphibolite | 1.31 | 725 | 0.002 | 0.7030 |
| 7 | Hornblendite | 0.49 | 285 | 0.002 | 0.7041 |
| 8 | Hornblende gabbro | 0.26 | 94.5 | 0.003 | 0.7048 |
| 9 | Pyroxene gabbro | 0.28 | 253 | 0.001 | 0.7039 |
| 10 | Pyroxene gabbro | 0.26 | 336 | 0.002 | 0.7035 |
| 11 | Basalt | 39.0 | 462 | 0.084 | 0.7031 |
| 12 | Andesite | 87.1 | 428 | 0.202 | 0.7033 |
| 13 | Basalt | 65.5 | 582 | 0.109 | 0.7030 |

N.B. Each value in the content and $^{87}Sr/^{86}Sr$ ratio is given as an averaged one for at least replicate analyses. Sample Nos. 1–12 are collected from Itinome-gata, and No. 13 is from Sannome-gata.

Although the former seems slightly less radiogenic than the latter, we cannot give much weight on the apparent difference due to the overlap of experimental uncertainties for each values. Furthermore, no difference cannot be found in the $^{87}Sr/^{86}Sr$ ratios for host basaltic rocks between Itinome-gata and Sannome-gata. Hedge and Knight (1969) reported a $^{87}Sr/^{86}Sr$ ratio as high as 0.7058 for Middle Miocene rhyodacite from Itinome-gata, together with the lower $^{87}Sr/^{86}Sr$ ratios (0.7031, 0.7032) for two andesites from the Kampu-zan which is located about 20 km east of Itinome-gata. Our preliminary result for the sample from the Kampu-zan supports the low $^{87}Sr/^{86}Sr$ ratio. These results suggest that recent basaltic rocks from Itinome-gata are probably isotopically similar to the samples from the Kampu-zan and the $^{87}Sr/^{86}Sr$ ratio of the source materials for recent volcanic rocks in this region probably has low values of $0.7030 \sim 0.7033$ as represented in the present study and the results of the andesite from the Kampu-zan.

It is worthwhile to note that three of four ultramafic inclusions show significantly higher $^{87}Sr/^{86}Sr$ ratios than those of host basaltic rocks, which exceed the range of $2\sigma$ experimental uncertainties. If ultramafic inclusions are cumulates from a magma, they will have identical $^{87}Sr/^{86}Sr$ ratio with the magma. The same Sr isotopic ratios are also expected if the host basalt is the partial fusion product of the ultramafic inclusions. However, the Sr isotope results for these lherzolites do not support any genetic relationships

with their host rocks and they must be of 'accidental' origin, having been caught in the ascending magma. This means that these lherzolite inclusions might represent old remains of the uppermost part of the mantle which had different history from the underlying part. To explain the apparent high $^{87}Sr/^{86}Sr$ ratios of lherzolites by aging effect, we need to assume that the lherzolites should have kept the closed system for more than 2 b.y. with an initial ratio of 0.703. Hence, there might have been a process by which the $^{87}Sr/^{86}Sr$ ratio was increased to the value observed in these ultramafic inclusions. From these discussions, we can see that xenolithic ultramafic inclusions do not always directly represent the upper mantle materials which relate to the recent magma genesis, but may rather reflect to those of the old different volcanic activity. It is noteworthy to point out, however, that one lherzolite (sample 3) shows almost an identical $^{87}Sr/^{86}Sr$ ratio to that of the host rocks. Hence, it is isotopically possible that this sample may be related to the recent magma genesis in this region.

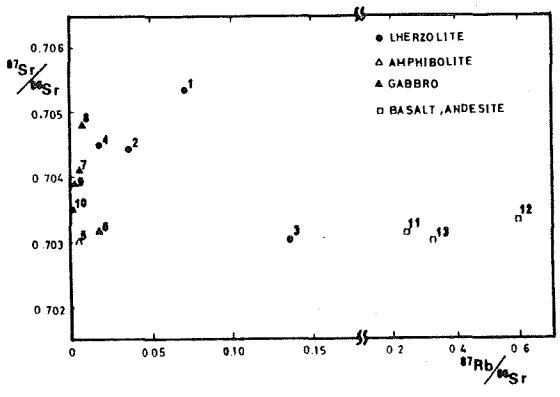


Fig.2 $^{87}Rb/^{86}Sr$ versus $^{87}Sr/^{86}Sr$ diagram for ultramafic, mafic inclusions and host basaltic rocks

Among gabbroic rock group, however, they have slightly different $^{87}Sr/^{86}Sr$ ratios one another. As shown in Fig. 2, it seems difficult to explain such differences in the $^{87}Sr/^{86}Sr$ ratio by the aging effect.

In Fig. 3, $^{87}Sr/^{86}Sr$ ratios are plotted against Sr content. In this figure, gabbroic rocks seem to show a reverse correlation between the $^{87}Sr/^{86}Sr$ and Sr content. This may be interpreted as the effect of contamination by materials with high $^{87}Sr/^{86}Sr$ ratios. However, we cannot designate the proper candidate for this which satisfy both the high $^{87}Sr/^{86}Sr$ ratio and reasonable Sr content. Hence, the $^{87}Sr/^{86}Sr$ ratios of gabbroic rocks may reflect the primary values.

These results have revealed that the vertical inhomogeneity of the $^{87}Sr/^{86}Sr$ ratio exists in the uppermost part of the mantle and lower crust in the Itinome-gata region and most ultramafic inclusions are not equilibrated with the host magma with respect to Sr isotopes.

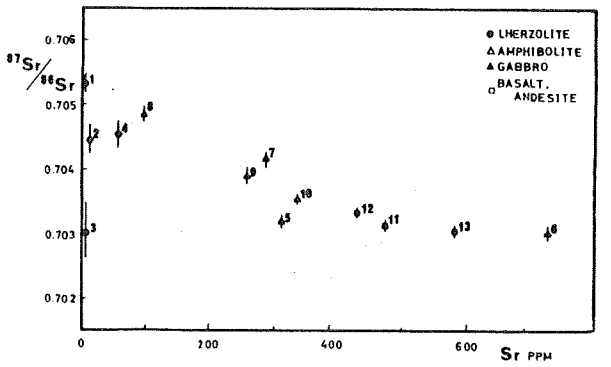


Fig. 3
Sr content versus $^{87}Sr/^{86}Sr$ diagram for ultramafic, mafic inclusions and host basaltic rocks

References

Aoki, K., (1971) Contr. Mineral. Petrol., 30, 314
Faure, G. and Powell, J. L., (1972) Strontium Isotope Geology. ( Springer Verlag, Berlin.)
Hayashi, H., (1955) J. Geol. Soc. Japan 61, 240
Hedge, C. E. and Knight, R. J., (1969) Geochem. J., 3, 15
Katsui, Y. et al., (1978) In: Abstract for Internat. Geodyn. Conf. Western Pacific and Magma Genesis. 266
Kuno, H., (1967) In: Ultramafic and Related Rocks ( Wiley, New York ) 337
Kuno, H., and Aoki, K., (1970) Phys. Earth Planet. Interiors, 3, 273
Matsuda, J. et al., (1977) Tectonophys., 37, 141

# REMANENT MAGNETIZATION OF SAKI WELDED TUFFS

Hideo Sakai

Department of Physics, Faculty of Engineering Science
Osaka University, Toyonaka, Japan

Tadashi Nakajima

Department of Geology, Faculty of Education,
Fukui University, Fukui, Japan

## Introduction

In recent decades a method to demagnetize specimens by etching them with HCl has been successfully employed by several researchers. The method, referred to as either chemical demagnetization or etching demagnetization, has been applied to detect self-reversals (Merrill and Kawai, 1969) and further to find the three magnetic components in sedimentary rocks (Roy and Park, 1972). This paper is concerned with an application of the chemical demagnetization method to Pliocene welded tuffs. Comparison is made on the magnetic property of the tuff before and after etching.

## Measurements of NRMs and the results of a.f. demagnetization

Samples were collected from the outcrop at Saki, Mikuni-cho, Fukui Prefecture. The NRM directions of these samples are divided into two groups; reverse group and intermediate group. By the intermediate group it is meant that NRMs are distributed in the northern upper hemisphere of the net. As shown in Fig. 1, the samples classified in reverse group have such stable NRMs that directions were changed very little after a.f. demagnetization (peak field is 150 Oe). On the contrary, the directions of the samples in intermediate group changed over 50 degrees after a.f. demagnetization and the terminal directions were almost identical to those of reverse group. Fig.2 shows the typical change of direction after a.f. demagnetization applied to the intermediate sample. It shoud be noted that the change of the direction lies along the long circle of the net.

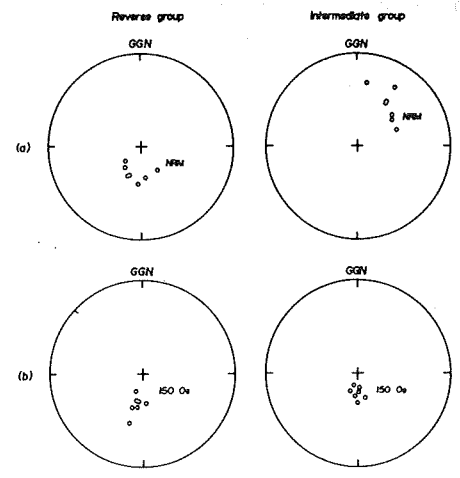


Fig.1. Directions of NRMs (a) and those of remanent magnetization after a.f. cleaning at 150 Oe (b).

## Chemical demagnetization

Samples cubical in shape and 1.5 cm in edge length were used. Since the samples were quite porous (mean porosity is 0.32), liquids could easily

penetrate into them. First, the samples were soaked in the oxidizing agent ($H_2O_2$) and the reducing agent ($NaHSO_3$) besides HCl. As the magnetization of the sample was not affected at all by any of the above acids except HCl, the magnetic change of the sample caused by HCl is interpreted not as the effect of chemical reaction but as the loss of magnetic minerals by etching .* Since the magnetic change of the sample soaked in HCl was quite rapid, the concentration of HCl and the etching time were modulated so that we could follow the change gradually.

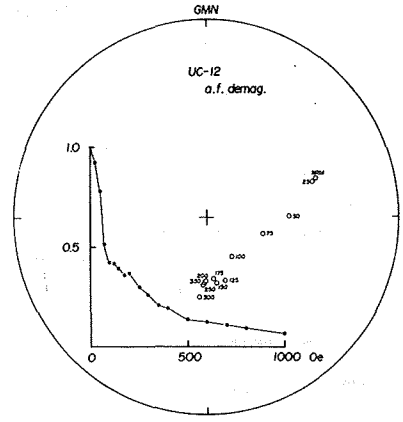


Fig.2. Progressive a.f. demagnetization applied to a sample of intermediate polarity.

The concentrations of HCl used were changed from 4N to 10N.

The samples were demagnetized as follows.

1 The sample was soaked in HCl.
2 It was then washed with water for 10 minutes.
3 Magnetization was measured with astatic magnetometer.

The whole process was repeated untill the magnetization of the sample disappeared. All the samples became discoloured from brown to grey by HCl.

Magnetic properties in the samples of intermediate group

Etching, a.f. and thermal demagnetization method were applied to the sample of intermediate group and the results are shown in Fig.3. The three demagnetization curves are along the large circle of the net. Similar results are obtained from all the samples studied. Thus, it can be concluded that the NRMs of intermediate polarity each consists of two components, and one of them is demagnetized quickly. On the left half of Fig.3, the change of the remanent intensity is plotted against the directional change measured from the NRM direction. The diagram gives the efficiency of demagnetization by three methods, respectively. There

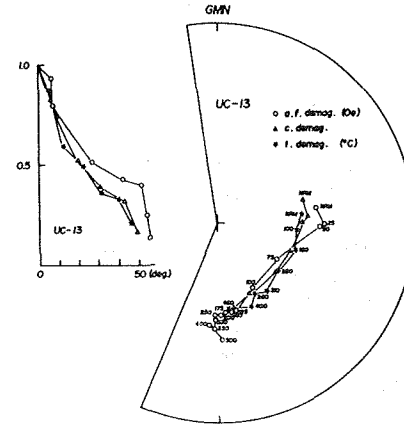


Fig.3. Results of demagnetization applied to the sample of intermediate polarity.
△ chemical demagnetization
○ a.f. demagnetization
☆ thermal demagnetization

* Though a change of magnetization up to 10% was recognized after the sample was exposed to $O_3$ (ozon gas), the change was not systematic.

appears no appreciate difference among three methods.

Fig.4 shows the a.f. demagnetization curves of NRM and ARM. For both NRM and ARM, the residual magnetization after etching has higher coercivity than the magnetization prior to etching. Fig.5 shows the thermal demagnetization curves of NRM before and after etching, respectively. As seen from Fig.5, the residual magnetization after etching has a higher blocking temperature than the magnetization before etching. It can be seen from these figures, that the residual magnetization after etching is considered to be more stable than the magnetization diminished by etching.

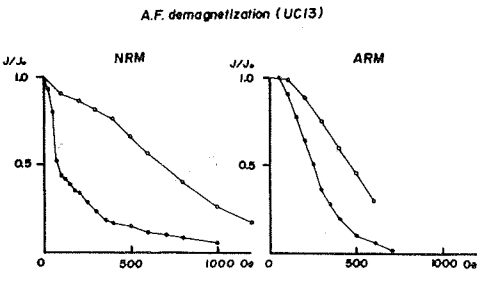


Fig.4. A.f. cleaning of NRM and ARM in the sample of intermediate group. Closed circles represent the data of pre-etched sample and open circles are obtained from the sample after etching. ARM is produced in a 1 Oe static field and peak alternating field in 1,000 Oe.

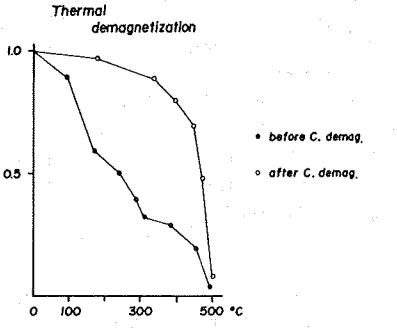


Fig.5. Thermal demagnetization of NRM in the sample of intermediate polarity. Closed circles represent the data of pre-etched sample and open circles are obtained from the etched sample.

## Results of Thelliers' method

Fig.6 gives the results of Thelliers' method for the sample of intermediate polarity. As shown in this figure, as long as the heating temperature in the experiment is below 300°C, TRM acquired is quite small in comparison to NRM's decrease. The Thelliers' method was also applied to an etched sample. The result is shown in Fig.7b. This figure shows that there is a linear relation between NRM and TRM as long as the heating temperature is up to 450°C. The geomagnetic intensity was estimated from the relation, and the obtained value (about 0.450e) is a little smaller than the present value.

The Thelliers' method was applied to the sample of reverse group also, and the results are

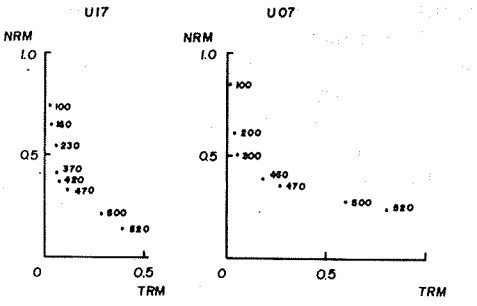


Fig.6. Examples of NRM-TRM diagram for the pre-etched samples of intermediate polarity

shown in Fig.8. In Fig.8b is shown the result of the etched sample. As NRM-TRM plots up to 400°C seem to be on a straight line in this figure, the geomagnetic intensity was estimated from the slope of the line. The estimated intensity was about 0.41 Oe and is nearly the same value as the intensity obtained from the etched sample of intermediate group. The directions of the etched samples of both intermediate and reverse polarities were also nearly same. Then, from the results that the etched magnetizations of both polarities have such similar properties, it can be suggested that these residual magnetizations after etching were probably acquired in the same condition.

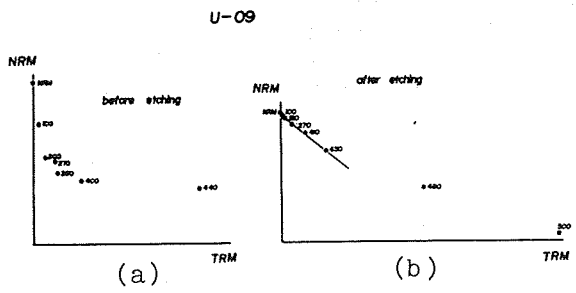


Fig.7. Results of Thelliers' method applied to the sample of intermediate group
(a) the sample before etching
(b) the sample after etching

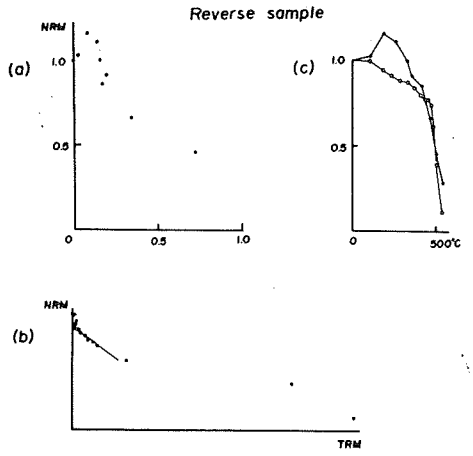


Fig.8. Results of Thelliers' method applied to the sample of reverse group
(a) the sample before etching
(b) the sample after etching
(c) thermal demagnetization results, open circles show the data of etched sample and closed circles represent the data of pre-etched sample.

## Discussion

It was shown before that the curves of direction change on the Schmidt's net obtained by each three cleaning methods are almost identical and lie along the long circle. From these results, it is indicated that there are two components of magnetization in the each samples of intermediate group. In the following, the discussion is about the kind of magnetizations which contribute to these components.

The magnetic component demagnetized easily by each cleaning methods is rather strong. As a sort of such the unstable magnetization either IRM or CRM is examined. According to Kodama et al. (1973), andesites of Oshima in Fukui Prefecture whose sampling site is not far from ours, have IRMs caused by thunder. Then, there is a possibility that our welded tuffs also have such IRMs. To examine that, artificial IRMs are added to the welded tuffs and they are demagnetized by three methods.

As there is no clear tendency that IRMs are demagnetized quickly by chemical or thermal demagnetization, it is scarcely possible that the unstable components of our welded tuffs are IRMs. From the preliminary microscopic observasions maghaemite particles are recognized in some pre-etched sample. Then, it is suggested that the unstable magnetizations in the samples of intermediate group are CRMs, but further microscopic observations are neccessary.

The other component of intermediate group is such a stable magnetization that is residued in the fairly demagnetized sample. Using the residual magnetization in the chemically demagnetized sample, the geomagnetic intensity was estimated as 0.45 Oe, before. That value is in a reasonable agreement with the intensity obtained from our experiments using Pliocene andesites in Fukui Prefecture (unpublished data). Therefore, the residual magnetization after each demagnetization is considered to be TRM acquired in a cooling process of welded tuff at deposition.

References

Kodama, K., S. Tsuda and K. Horii (1973) Graduate Thesis of Osaka University.

Merrill, R.T. and N. Kawai (1969): J. Geomag. Geoelec. 21, 507.

Roy, J.L. and J.K. Park (1972): Earth Planet. Sci. Letters 17, 211.

# IDENTIFICATION OF TEPHRAS BY MAGNETIC MEASUREMENT (1)

Mio YOSHIDA

Kyushu Agricultural Experiment Station, Chikugo, Fukuoka, 833

An area nearly 9000 km wide is covered with varieties of tephras in Kyushu and the greater part of the area is used as an agricultural field and is provided peculiar problems to soils derived from tephras. Knowledges of distribution and properties of tephras are, therefore, problems of much consequence not only in the field of geology or tephrochronology but also in the field of agriculture. Detailed stratigraphic survey of the area and description and the dating of individual tephras has already been achieved and reported frequently. Numbers of tephras are, however, remained unidentified despite of these efforts.

Momose et al. (1968) developed an identification method of tephras by thermomagnetic analysis and reported that ferromagnetic minerals separated from Pleistocene pumice layers show specific thermomagnetic properties pertinent to each pumice layer and thermomagnetic examination could be highly helpful for pumice identification. There are several advantages in Momose et al's method : Ferromagnetic minerals are common in most tephras and are highly stable against weathering (Aomine and Wada,1962) ; They can easily separated with a hand magnet and only a few milligrams of specimens are needed for the analysis ; The determination can be carried out by a simple thermomagnetic balance with fairly high sensitivity ; Ferromagnetic minerals included in the same tephra has been proved to have homogeneous composition also chemically (Kohn,1970; Shoji et al.,1974; Nagatomo et al., 1976).

I have been trying to apply Momose et al's method (ibid) together with some magnetic hysteresis, X-ray and chemical analyses for identification of tephras distributed in southern Kyushu. First, influence of grain size of tephras will be discussed as problems of sampling and selection of samples in the present note.

## Materials

Akahoya of Yokoichi, Miyakonojo, A-1, which is highly glassy volcanic ash erupted from Kikai caldera (Machida and Arai,1978) about 5000 y.B.P. (Wada,1967) and Miike pumice of Fukuhira, Miyakonojo, Mp-1u, erupted from Miike, Kirishima about 3000 y.B.P. (Matsui and Wajima,1961) were used. The layer of Akahoya has an ash part, A-1a, at the upper part and a pumice part, A-1p, at the bottom in one fall unit.

A-1a and A-1p were sieved into four size fractions, i.e. $<0.1$ mm, 0.1-0.25 mm, 0.25-0.5 mm and 0.5 mm$<$ in diameter in water. Ferromagnetic fractions were separated with a hand magnet from water suspension of each size fraction and pulverized with an agate mortar. Magnetic separation was repeated several times for purification and the fractions were washed with 99 % ethanol and dried. Mp-1u was air dried and sieved into three size fractions, $<2$ mm, 2-4 mm and 4 mm$<$. Each fraction was pulverized with a ball mill and magnetic separation and purification were done in the same manner as Akahoya.

For microscopic determination of grain size distribution of opaque minerals, crude ferromagnetic fractions magnetically separated from air dried A-1a and A-1p and thin sections of Mp-1u fixed in resin were used.

## Results and discussions

X-ray diffraction analysis show that all the ferromagnetic minerals are

titanomagnetite of cubic spinel structure. Though difference of the lattice constant values (Table 1) between A-1 and Mp-1u may be seen by careful determination, no significant difference in the values among the different grain size fractions of the same tephra is seen.

Table 1 Lattice constant, a(Å) and magnetic properties of ferromagnetic minerals from different grain size fractions

| Specimens | | a(Å) | Js (emu/g) | Jr (emu/g) | Jr/Js | Hc (Oe) | Tc (°C) |
|---|---|---|---|---|---|---|---|
| A - 1a | < 0.1 mm | 8.431 | 40.2 | 2.35 | 0.058 | 49 | 330 , 505 |
| | 0.1 - 0.25 | 8.434 | 38.1 | 2.02 | 0.055 | 39 | 315 , 495 |
| | 0.25 - 0.5 | 8.437 | 37.0 | 2.05 | 0.055 | 49 | 316 , 506 |
| | 0.5 < | 8.433 | 38.6 | 2.90 | 0.075 | 55 | 316 , 504 |
| A - 1p | < 0.1 mm | 8.436 | 36.8 | 2.30 | 0.063 | 50 | 325 , 490 |
| | 0.1 - 0.25 | 8.432 | 38.3 | 1.85 | 0.048 | 35 | 325 , 496 |
| | 0.25 - 0.5 | 8.435 | 39.0 | 2.40 | 0.062 | 43 | 320 , 492 |
| | 0.5 < | 8.433 | 39.0 | 2.30 | 0.059 | 43 | 318 , 490 |
| Mp - 1u | < 2 mm | 8.439 | 32.3 | 3.98 | 0.123 | 75 | 270 , 510 |
| | 2 - 4 | 8.442 | 30.9 | 3.71 | 0.120 | 83 | 275 , 505 |
| | 4 < | 8.445 | 31.7 | 3.94 | 0.124 | 78 | 270 , 513 |

a(Å) : lattice constant, Js(emu/g) : saturation magnetization, Jr(emu/g) : remanent magnetization, Hc(Oe) : coercive force, Tc(°C) : Curie temperature

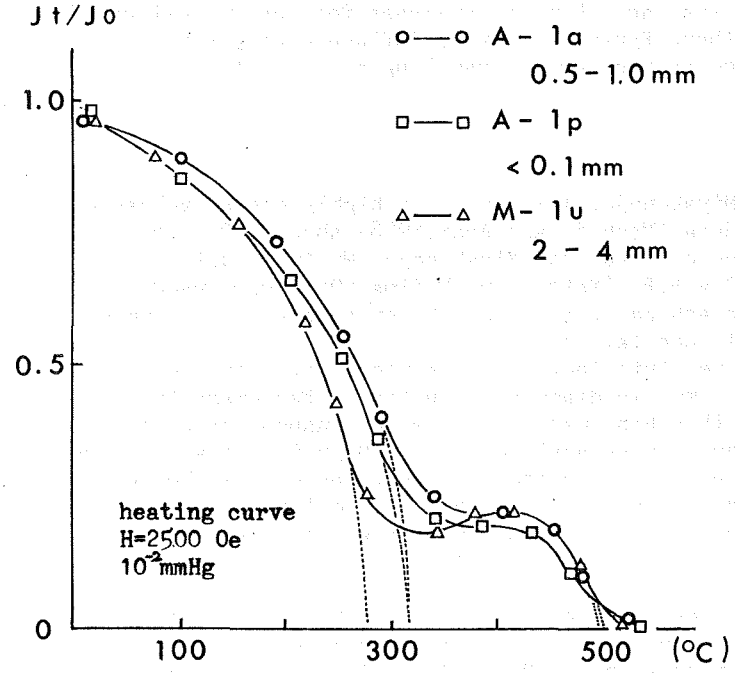


Fig. 1 Normalized Js-T curves of ferromagnetic minerals.

A few examples of Js-T curves are shown in Fig.1, which show that the specimens invert to another phase while heating up to 500°C. Ferromagnetic minerals extracted from the other size fractions of each tephra showed the curves similar to the corresponding examples. Curie temperature, Tc obtained from the curves are also shown in Table 1.
The average values of a low temperature phase are about 320°C for A-1 and 270°C for Mp-1u. Though any significant difference of the values cannot be seen among ferromagnetic minerals extracted from different size groups of

tephras, the values of A-1 and Mp-1u are clearly different and the discrimination of these tephras can easily be achieved despite of the grain size of tephras. So long as the stoichiometric composition is assumed, ulvöspinel content of titanomagnetite of A-1 is 40-45 % and that of Mp-1u is 45-50 % by referring Akimoto et al's equal a(Å) diagram (1957). When their equal Tc(°C) diagram is referred, ulvospinel % of A-1 is 45 % and that of Mp-1u is about 50 %.

Three major components of titanomagnetite, FeO, $Fe_2O_3$ and $TiO_2$ were determined and the compositions are plotted in the ternary diagram in Fig.2.

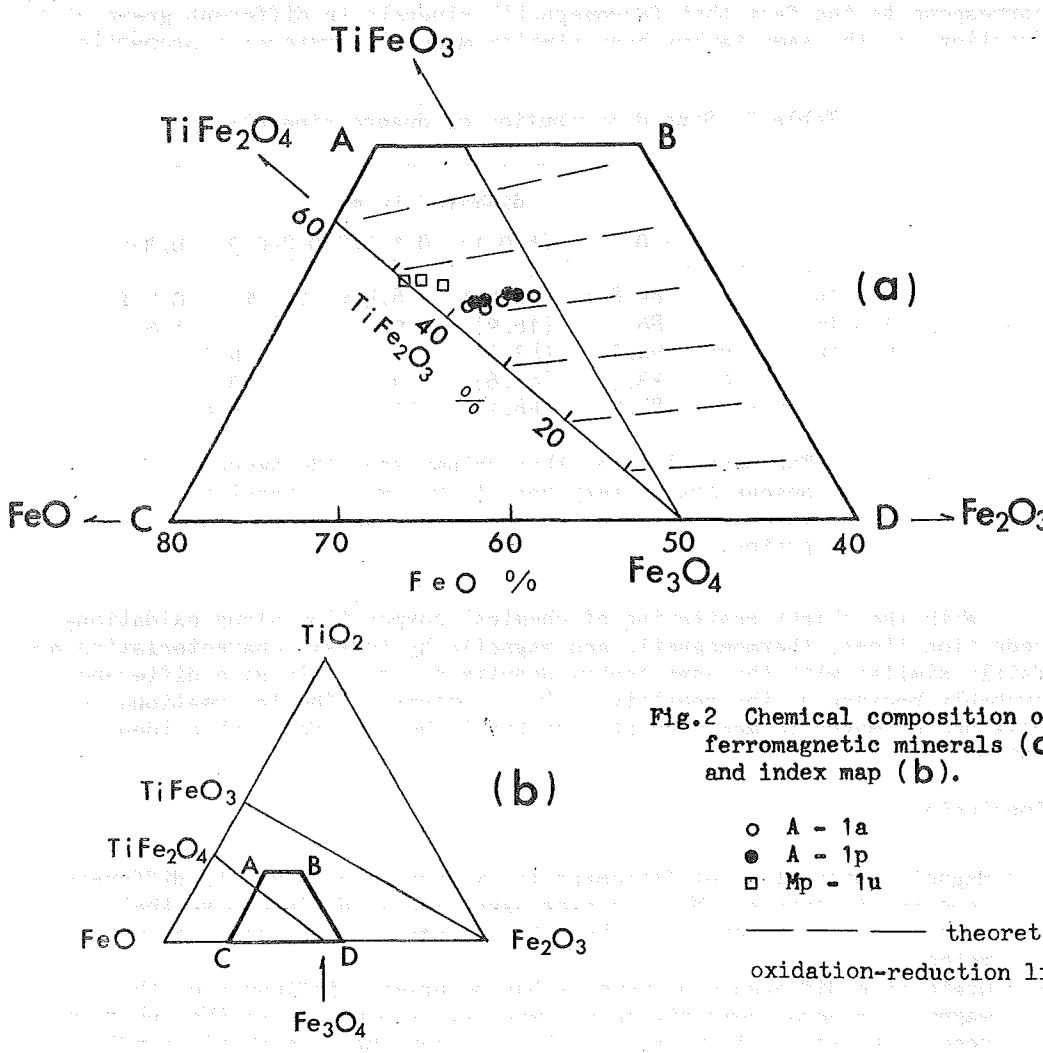


Fig.2 Chemical composition of ferromagnetic minerals (a) and index map (b).

o A - 1a
● A - 1p
□ Mp - 1u

—— —— —— theoretical oxidation-reduction lines

Both A-1 and Mp-1u have compositions near to magnetite-ulvöspinel line and ulvöspinel content of the former is about 40 % and that of the latter is 50 %. In both tephras, $TiO_2$ content is fairly equal respectively even though the grain size of tephras is different and the scattering of the composition is seen along the theoretical oxidation-reduction lines. Titanomagnetite in tephras might have been suffered from oxidation while falling and after deposition or while storage of specimens even though they

are said to be highly stable.

Fairly clear difference of hysteresis parameters (Table 1) can be seen between A-1 and Mp-1u, i.e. Jr/Js values of Mp-1u are about twice as large as those of A-1 and Hc values of Mp-1u are 1.5 times as large as A-1. No noticeable difference in the magnetic properties is seen between A-1a and A-1p and among different size fractions of each tephras.

Size distribution of opaque minerals were also determined (Table 2) and it was known that grain size of individual opaque minerals is quite similar in all the specimens despite of the size of the tephras and more than 85 % of opaque grains are smaller than 0.1 mm in diameter, which may correspond to the fact that ferromagnetic minerals in different grain size fractions of the same tephra have similar magnetic hysteresis properties.

Table 2 Size distribution of opaque minerals

| | | diameter in mm | | | | |
|---|---|---|---|---|---|---|
| | | < 0.1 | (≒ 0.1) | 0.1-0.2 | 0.2-0.3 | 0.3< |
| A - 1a | | 89.8 % | (18.4 %) | 8.4 % | 1.5 % | 0.2 % |
| A - 1p | | 86.2 | (16.9) | 9.4 | 2.8 | 1.6 |
| M - 1u | < 2 mm | 94.2 | (43.0) | 1.7 | 4.0 | |
| | 2 - 4 | 93.3 | (61.6) | 3.2 | 3.4 | |
| | 4 < | 84.5 | (48.1) | 11.1 | 6.4 | |

( ) : The percentage of this column show the amount of opaque grains very near to 0.1 mm in diameter, which is included in the percentage of < 0.1 mm grains.

With the slight scattering of chemical composition along oxidation-reduction lines, thermomagnetic and magnetic hysteresis characteristics are fairly similar with the same tephra despite of the grain size difference probably because of the equality of TiO content. The informations obtained by magnetic measurements are highly helpful for tephra identification.

## Conclusion

(1) Magnetic properties of ferromagnetic minerals contained in different tephras, Akahoya and Miike pumice, are clearly different so that discrimination of one from the other is easily achieved by magnetic method.
(2) Grain size difference of tephras has no primary influence on the ferromagnetic mineral composition and magnetic properties so that we do not need to be too cautious with grain size sorting in magnetic studies.

## References


Akimoto,S. et al. (1957) J.Geomag. Geoelectr., 9, 165
Aomine,S. and Wada,K. (1962) Am. Mineral., 47, 1024
Kohn,B.P. (1970) Lithos, 3, 361
Machida,H. and Arai,F. (1978) Quat. Res., 17, 143
Matsui,T. and Wajima,S., (1961) Misc. Rep. Research Inst. for Natural Resources, 54-55, 161

Momose,K. et al. (1968) Bull. Earthq. Res. Inst., 46, 1275
Nagatomo,Y. et al. (1976) J.Sci. Soil Manure, Japan, 47, 25
Shoji,S. et al. (1974) J.Jap. Assoc. Mineral. Petrol. Econ. Geol., 69, 110

# IDENTIFICATION OF TEPHRAS BY MAGNETIC MEASUREMENT (2)

Mio YOSHIDA

Kyushu Agricultural Experiment Station, Chikugo, Fukuoka, 833

The previous paper (Yoshida,1979) described that grain size difference of tephras has scarce influence on magnetic properties of ferromagnetic minerals in tephras so that it is not necessary to be too cautious with grain size sorting in magnetic studies. In the present report, magnetic properties and chemical compositions of ferromagnetic minerals contained in pumices erupted from Sakurajima, Miike (kirishima) and Ikedako (Kaimon) are compared. Samples were taken at different distances from the sources.

Identification of ferromagnetic minerals and lattice constant calcuration by means of X-ray diffraction analysis and chemical and thermomagnetic analyses were carried out.

## Materials

The following pumices were sampled at the sites shown in Fig.1 and the samples are listed in Table 1 together with the ages after Matsui and Wajima (1961). Fig.1 also contains the lines of distribution limit of each pumice (Matsui and Wajima, ibid).

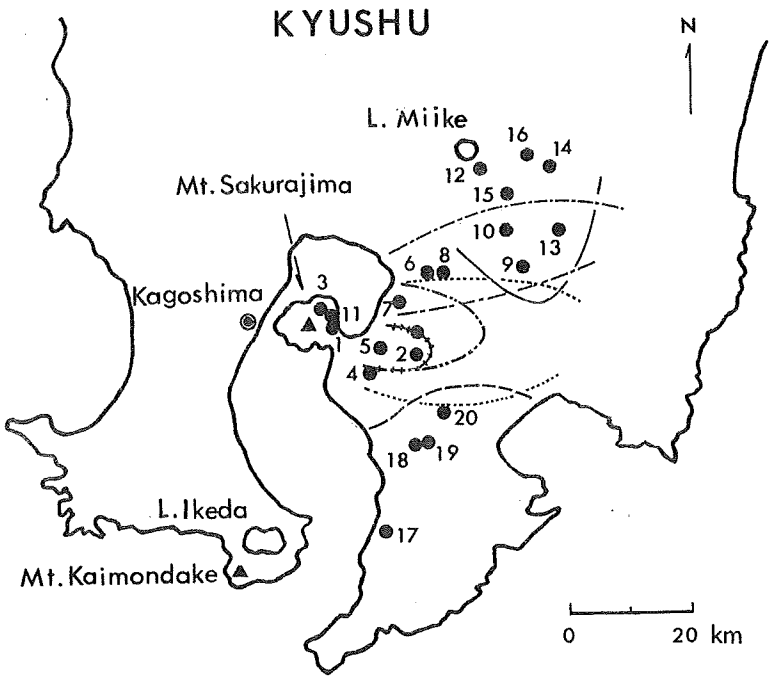


Fig.1 Sampling sites and distribution limit of pumices.

Tp
Anp
Bp
Xp
Mp
KmC

Site names are shown in Table 1.

(i) Sakurajima pumices

Taisho pumice, Tp : This is extremely fresh and hard two-pyroxene andesite pumice of light gray color. At Kurokami, Sakurajima, Tp is laid over An-ei pumice with a thickness of 2 m. At Mobiki, about 20 km apart from the source, the layer of Tp has a thickness of about 45 cm.

An-ei pumice, Anp : This pumice is grayish yellow orange with slight stain but still fairly fresh and hard. The profile at Komen consists of

Table 1 Samples and sampling sites

| Source | Tephra name | Site No. | Sampling site | Sample No. |
|---|---|---|---|---|
| Sakurajima | Taisho pumice | 1 | Kurokami, Kagoshima | Tp - 1 |
| | | 2 | Mobiki, Kihoku | - 2 |
| | 1914 A.D. | 3 | Komen, Kagoshima | - 3 |
| | | 4 | Onobaru, Tarumizu | - 4 |
| | | 5 | Dakeno, Kihoku | - 5 |
| | An-ei pumice | 3 | Komen | Anp - 1u |
| | | | | - 1m |
| | 1778-1780 A.D. | | | - 11 |
| | | 6 | Makinohara, Fukuyama | - 2 |
| | | 7 | Kawachiyama, Fukuyama | - 3 |
| | | 8 | Obino, Takarabe | - 4 |
| | | 9 | Umekita, Miyakonojo | - 5 |
| | | 10 | Yokoichi, Miyakonojo | - 6 |
| | Bunmei pumice | 2 | Mobiki | Bp - 1 |
| | | 11 | Uto, Kagoshima | - 2 |
| | 1471-1476 A.D. | 5 | Dakeno | - 3 |
| | Unidentified pumice | 5 | Dakeno | Xp - 1u |
| | | | | - 1m |
| | unidentified age in Holocene | | | - 11 |
| Miike, Kirishima | Miike pumice | 12 | Fukuhira, Miyakonojo | Mp - 11 |
| | | 10 | Yokoichi | - 2 |
| | 3000 y.B.P. | 9 | Umekita | - 3 |
| | | 13 | Katsuoka, Mitsumata | - 4 |
| | | 14 | Ishiyama, Takajo | - 5 |
| | | 15 | Ofurukawa, Yamada | - 6 |
| | | 16 | Tanaka, Takasaki | - 7 |
| Ikedako, Kaimon | Kaimon C pumice | 17 | Atsugase, Onejime | KmC - 1u |
| | | | | - 1m |
| | older than 3000 y.B.P. | 18 | Oji, Kanoya | - 11 |
| | | 18 | Oji, Kanoya | - 2 |
| | | 19 | Fudamoto, Kanoya | - 3 |
| | | 20 | Hosoyamada, Kanoya | - 4 |

( ) : eruption age after Matsui and Wajima (1961)

at least six fall units of Anp with a thickness of about 5 m. At Yokoichi, Miyakonojo, about 40 km apart from the source, it forms lenticular deposits at about 50 cm below the surface.

Occurrence of these two pumices are described by Kobayashi and Shinagawa (1964), Kobayashi (1968), Matsui (1960) and Nagatomo et al. (1976) in detail.

Bunmei pumice, Bp : Though it is still in discussion if pumice was erupted during Bunmei eruption, Matsui and Wajima (ibid) considered their Sz-c pumice as an ejecta during Bunmei period. After them, I adopted the term, Bunmei pumice in the present report. This is fairly fresh and dull brown in color.

Pumice oc unidentified age, Xp : At Dakeno, this pumice consists of a fer fall units with a total thickness of about 50 cm at the depth of about 2 m below the surface. This is slightly weathered and yellow orange and occurs as mixtures of pumice and sand there. Samples, Xp-1u, -1m and

-11, were taken from the upper to lower of three fall units. Matsui and Wajima (ibid) considered this pumice as an ejecta at unknown old age in Holocene.

Detailed description of the above two pumices can be found in Matsui and Wajima (ibid).

(ii) Pumices of Kaimon and Kirishima

Miike pumice, Mp : This is yellowish brown to orange pumice with less hardness. At Fukuhira, 3 km south of Miike, the pumice forms a layer of a thickness of about 2.5 m consisting of three fall units. Thickness of a layer of this pumice at Umekita, about 25 km south from the source, is about 30 cm.

Kaimon C pumice, KmC : At Atsugase, this light yellowish brown pumice forms a layer with a thickness of about 1.3m. The layer of this pumice at Kanoya is about 10 cm in thickness and contains much stain of humus.

Table 2 Lattice constant, a(Å) and Curie temperature, Tc(°C) of ferromagnetic minerals

| Sample No. | a(Å) | Tc(°C) | |
|---|---|---|---|
| Tp - 1 | 8.430 | 290 | (486) |
| - 2 | 8.437 | 298 | (485) |
| - 3 | 8.432 | 300 | (485) |
| - 4 | 8.426 | 300 | (490) |
| - 5 | 8.435 | 290 | (490) |
| Anp - 1u | 8.452 | 220 | - |
| - 1m | 8.455 | 215 | - |
| - 1l | 8.445 | 215 | - |
| - 2 | 8.455 | 216 | (500) |
| - 3 | 8.453 | 220 | (500) |
| - 4 | 8.453 | 223 | (500) |
| - 5 | 8.454 | 220 | (500) |
| - 6 | 8.453 | 220 | (505) |
| Bp - 1 | 8.443 | 255 | (485) |
| - 2 | 8.441 | 259 | (485) |
| - 3 | 8.446 | 252 | (495) |
| Xp - 1u | 8.428 | 310 | 490 |
| - 1m | 8.430 | 305 | 500 |
| - 1l | 8.433 | 310 | 495 |
| Mp - 1l | 8.448 | 270 | 500 |
| - 2 | 8.444 | 270 | 505 |
| - 3 | 8.444 | 275 | 510 |
| - 4 | 8.446 | 270 | 510 |
| - 5 | 8.448 | 265 | 510 |
| - 6 | 8.447 | 268 | 515 |
| - 7 | 8.446 | 270 | 500 |
| KmC - 1u | 8.426 | 500 | 515 |
| - 1m | 8.421 | 500 | 513 |
| - 1l | 8.420 | 500 | 517 |
| - 2 | 8.427 | 503 | 520 |
| - 3 | 8.421 | 505 | 520 |
| - 4 | 8.422 | 505 | 517 |

Results and discussions

Diffraction peaks only due to cubic spinel titanomagnetite were identified for all the specimens by X-ray diffraction analysis. The values of lattice constant are shown in Table 2. Values are different among pumices of different ages of Sakurajima with an exceprion of Tp and Xp which show almost the same value, 8.43 Å. Specimens from three different fall units of Anp-1 and Xp-1 show values close to each other. The values of KmC are specifically low, but those of Mp are close to the values of Bp.

Examples of Js-T curves are shown in Fig.2. Curie temperatures, Tc, are also listed in Table 2. Mean values of Tc of the low temperature phase of Sakurajima specimens are 300°C for Tp, 220°C for Anp, 255°C for Bp and 308°C for Xp. The average values of Mp is 270°C and that of KmC is about 500°C. Similarities of the values are again seen between Tp and Xp and between Bp and Mp. The curves of Xp and Mp, however, show clearer increase in magnetization at high temperature than the curves of the others indicating that the titanomagnetite has inverted to a new phase with high Tc values to greater extent.

When the stoichiometric composition of titanomagnetite is assumed and Akimoto et al's (1957) equal a(Å) diagram is referred, ulvöspinel contents of the minerals are 40 % for Tp and Xp, 50 % for Anp, 45-50 % for Bp and Mp and 30 % for KmC. Similarly, ulvöspinel contents are

50 % for Tp and Xp, 60 % for Anp, 55 % for Bp and Mp and 15 % for KmC when their equal Tc diagram is referred.

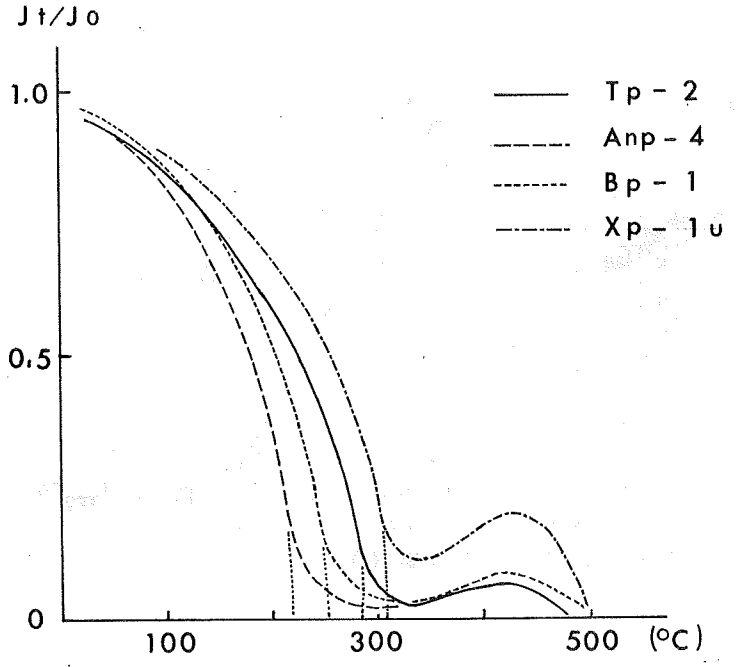


(a)
Sakurajima pumices

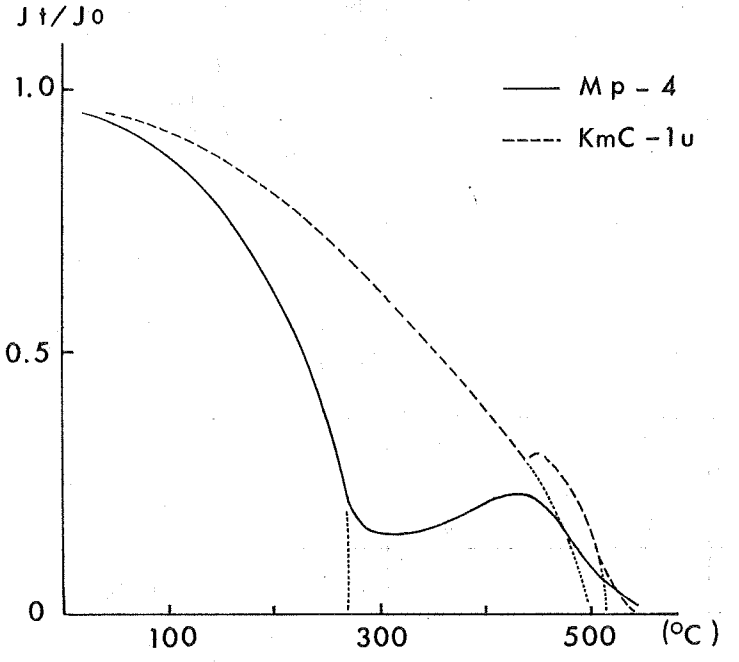


(b)
Pumices of Kirishima and Kaimon

Fig.2 Normalized Js-T curves of ferromagnetic minerals.
heating curve, H=2500 Oe, $10^{-2}$ mmHg

Three major components of titanomagnetite, FeO, $Fe_2O_3$ and $TiO_2$ were determined and plotted in the ternary diagram in Fig.3.

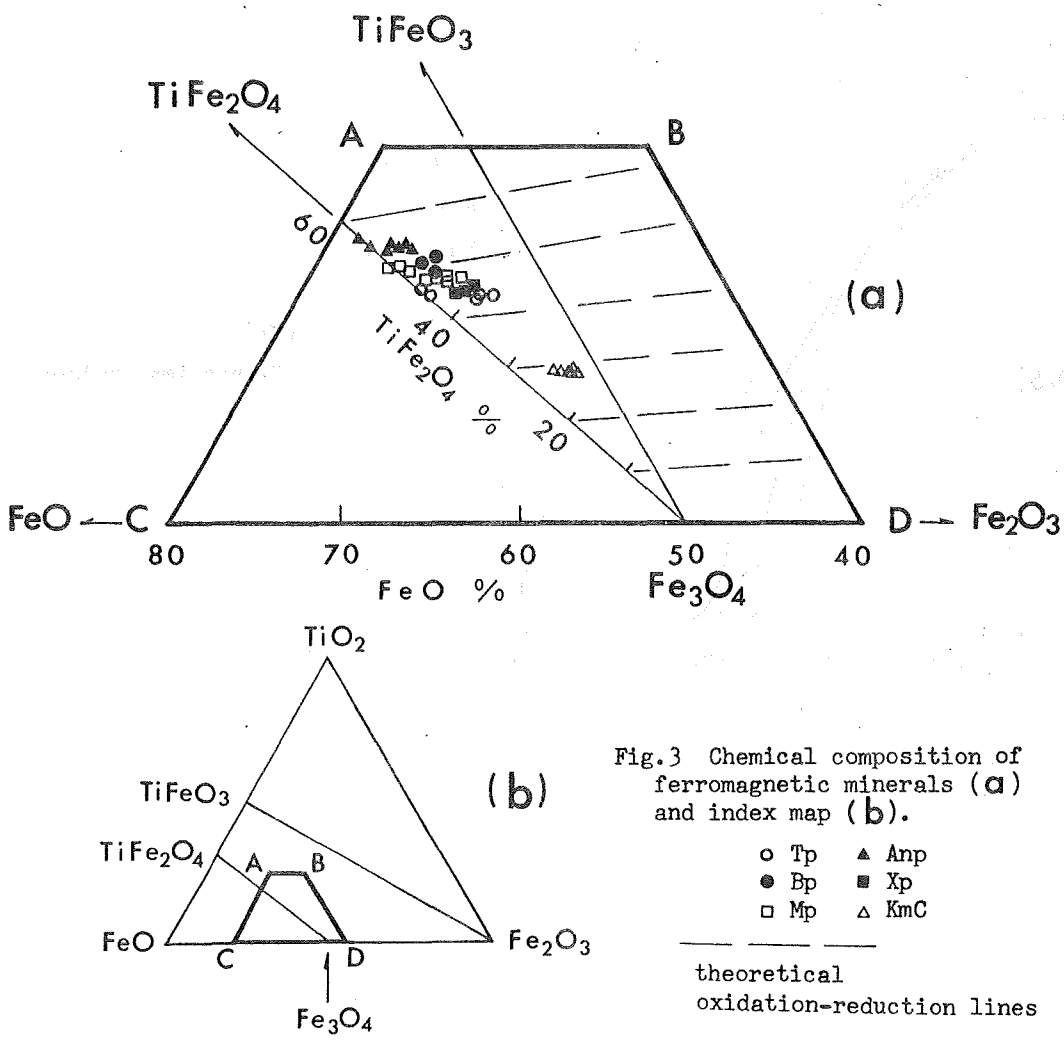


Fig.3 Chemical composition of ferromagnetic minerals (a) and index map (b).

o Tp ▲ Anp
● Bp ■ Xp
□ Mp △ KmC

——— ——— ———
theoretical oxidation-reduction lines

All the specimens have compositions near to magnetite-ulvöspinel line and composition of each pumice group is concentrated in a narrow range in the diagram, while compositions of different pumices are more or less apart. Tp and Xp, and Bp and Mp having similar a(Å) and Tc values respectively, however, have also similar chemical compositions each other. The plots among specimens of a same pumice group scatter nearly along the theoretical oxidation-reduction lines indicating that the dispersion of the composition is only caused by oxidation of $Fe^{3+}$ in titanomagnetite. $TiO_2$ content of titanomagnetite in each pumice group is fairly uniform.

Similarity of ferromagnetic mineral composition of Tp and Xp among pumices of Sakurajima was shown as hitherto described. It is known that $SiO_2$ content of Sakurajima lavas of different ages has changed gradually (Taneda,1977) and periodically between 59 and 67 % (The Volcanological Society of Japan,1935). Magma properties might have been similar at the eruption stages of Tp and Xp. Apparently, however, Tp is more fresh than Xp and Tp appears at the upper horizontal position in a profile and we will

be able to distinct these two pumices by careful field survey.

Conclusions

(1) Ferromagnetic minerals in pumices of different stages of Sakurajima show different properties in X-ray crystallography, magnetics and chemistry except that Tp and Xp have ferromagnetic minerals with similar properties.
(2) Ferromagnetic minerals separated from different fall units of Anp and Xp show the same properties respectively.
(3) KmC contains very specific ferromagnetic minerals and is clearly distinguishable from others among the present specimens.

References

Akimoto,S., et al. (1957) J.Geomag. Geoelect., 9, 165
Kobayashi,T. and Shinagawa,A. (1964) Bull Fac. Agr. Kagoshima Univ.,14,85
Kobayashi,T. (1968) ibid, 18, 71
Matsui,T. (1960) Misc. Rept. Research Inst. for Natural Resources, 52-53, 115
Matsui,T. and Wajima,S. (1961) ibid, 54-55, 161
Nagatomo,Y. et al. (1976) J.Soi. Soil Manure, Japan, 47, 25
Taneda,S. (1977) Bull. Volcanological Soc. of Japan (II), 22, 61
The Volcanological Soc. of Japan ed. (1935) ibid (I), 2, 226
Yoshida,M. (1979) under contribution to Quat. Res.

# IDENTIFICATION OF TEPHRAS BY MAGNETIC MEASUREMENT (3)

Mio YOSHIDA

Kyushu Agricultura Experiment Station, Chikugo, Fukuoka, 833

"Akahoya" is highly glassy rhyoritic volcanic ash deposit with yellowish orange in color and mainly distributes from southern islands of Kyushu to Shikoku island. It is known as one of the most wide spread tephras in Japan and has several local names as "Onji" or "Imogo" etc. Many tephrochronologists and soil scientists have repeatedly discussed about the distribution, the source, age and properties of Akahoya because it is one of a few good key layers in Kyushu and it gives specific problems to agricultural fields. Several investigators have considered that there are two or more sources for Akahoya, while others have deduced one volcano as its source. Recently, Nagatomo and Shoji (1977) have considered the source as Kikai caldera based both on the uniform distribution of ratios of certain elements in ferromagnetic minerals involved in Akahoya and on the results of detailed field survey. Independently of them, Machida and Arai (1978) have also considered Kikai caldera as the source according to the survey covering wide-spread district and the fact that the refractive indices of glass shards or hypersthene included in Akahoya concentrate in very narrow range despite that the sampling places are far off each other.

Judging from their results that Akahoya has fairly homogeneous mineralogical properties, the opinion that every Akahoya belongs to the same tephra is to be endorced. In the present paper, I am going to presemt the results of X-ray mineralogical, thermomagnetic and chemical analyses on ferromagnetic fractions of Akahoya to certify the identity of the tephra.

While, there are two other glassy volcanic ashes known to have similar apparent features to Akahoya ; Aira Tn ash erupted from Aira caldera 2.1-2.2 $\times 10^4$ y.B.P. (Machida and Arai,1976) and Akahoya-like ash (Matsui,1960 ; Matsui,1963 ; Gohara,1964) which have been considered to be marginal facies

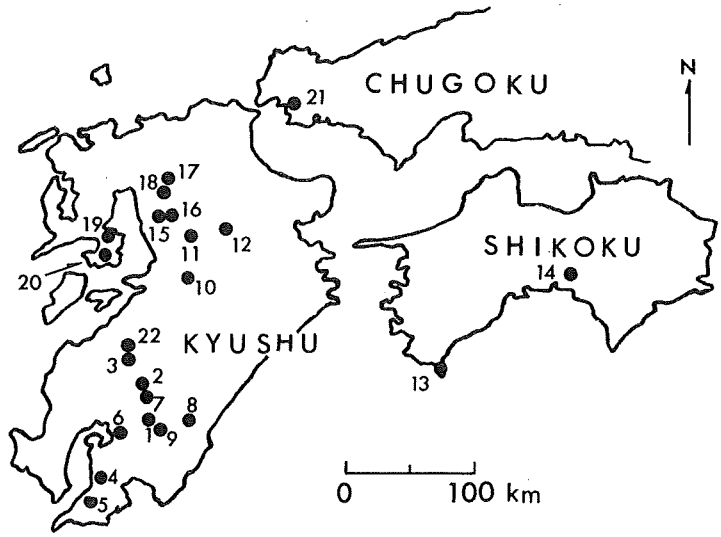


Fig.1 Sampling sites

of welded tuff of Aso (Matsui,1963,ibid) with the age of about $3.3 \times 10^4$ y. B.P. (Ariake Bay Res. Group,1965). The former is wider-spread tephra than Akahoya and has been revealed to have glass shards and hypersthenes with different refractive indices (Machida and Arai,1976,ibid). The latter has been considered to correspond to Tosu-, Ube- and Akiyoshi loams (Gohara et al.,ibid ; Matsui and Kato,1965 ; Domen et al.,1970). Techniques which make up for the deficiency of the field survey are especially needed for more satisfactory identification of these three tephras. I have carried out thermomagnetic analysis also on these two tephras and the results will be given hereafter.

Materials

(i) Akahoya, A

Sampling sites are shown in Fig.1 and samples are listed in Table 1. Akahoya samples include ash, -a, and pumice, -p, parts in one fall unit in some cases.

(ii) Akahoya-like ash (pseudo Akahoya), PA, and Aira Tn ash, AT

These ashes were sampled and named as shown in Fig.1 and Table 1. Ferromagnetic fraction was magnetically separated and purified.

Table 1 Samples and sampling sites

| Site No. | Tephra name | Site No. | Site name |
|---|---|---|---|
| 1 | Akahoya | A - 1a,p | Yokoichi, Miyakonojo |
| 2 | | - 2a,p | Minaminishikata, Kobayashi |
| 3 | | - 3 | Kodonbaru, Hitoyoshi |
| 4 | | - 4a,p | Oji, Kanoya |
| 5 | | - 5a,p | Atsugase, Onejime |
| 6 | | - 6 | Obino, Takarabe |
| 7 | | - 7 | Takabaru |
| 8 | | - 8 | Saginose, Tano |
| 9 | | - 9 | Umekita, Miyakonojo |
| 10 | (Imogo) | -10 | Ushigase, Yabe (Imogo) |
| 11 | ( " ) | -11 | Aso ( " ) |
| 12 | ( " ) | -12 | Hanamure, Kokonoe ( " ) |
| 13 | (Onji) | -13 | Ashizuri (Onji) |
| 14 | ( " ) | -14 | Tosashimizu ( " ) |
| 15 | Pseudo-Akahoya | PA - 1 | Kamenoko, Yame |
| 16 | | - 2 | Yoshida, Yame |
| 17 | (Tosu loam) | - 3 | Akasaka, Tosu |
| 18 | ( " ) | - 4 | Nagano, Kiyama |
| 19 | | - 5 | Ariake, Shimabara |
| 20 | | - 6 | Minamiarima |
| 21 | (Ube loam) | - 7 | Sanyo, Asa |
| 22 | Aira Tn | AT - 1 | Takanbaru, Hitoyoshi |

Results and discussions

According to X-ray identification of the minerals, all the specimens contain only titanomagnetite with cubic spinel structure.

(i) Akahoya, A

Lattice constant, a(Å), of some specimens are shown in Table 2. The values range between 8.430 Å and 8.440 Å and the average is 8.435 Å.

Examples of Js-T curves and Curie temperature, Tc, are shown in Fig.2 and Table 2 respectively. The values of Tc range between 315°C and 335°C and the average is 323°C.

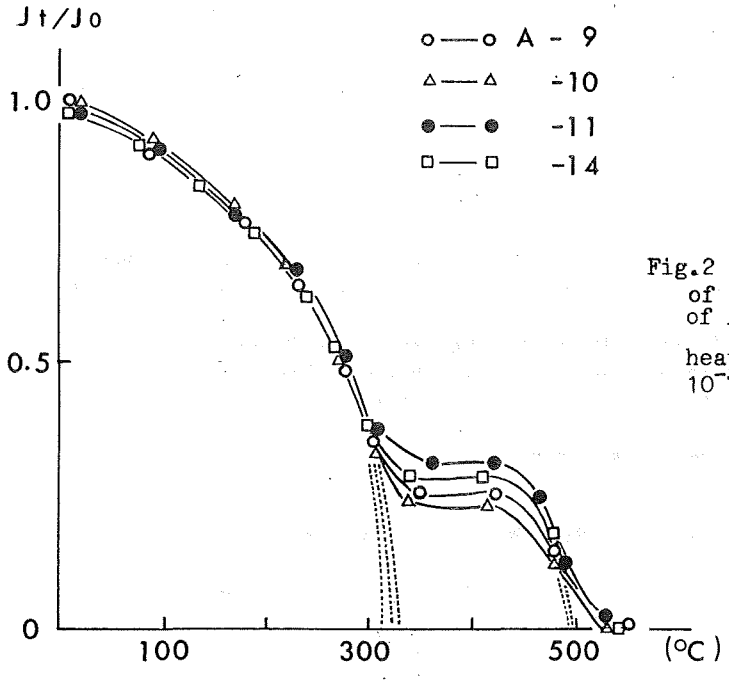


Fig.2 Normalized Js-T curves of ferromagnetic minerals. of Akahoya.

heating curve, H=2500 Oe, $10^{-2}$ mmHg

Table 2 Lattice constant, a(Å) and Curie temperature, Tc(°C) of ferromagnetic minerals of Akahoya

| Sample No. | a(Å) | Tc(°C) | |
|---|---|---|---|
| A - 1a | 8.429 | 320 | 502 |
| - 1p | 8.431 | 325 | 492 |
| - 2a | 8.437 | 325 | 500 |
| - 2p | 8.436 | 320 | 490 |
| - 3 | 8.438 | 320 | 500 |
| - 4a | 8.435 | 322 | 500 |
| - 4p | 8.440 | 321 | 500 |
| - 5a | 8.436 | 325 | 500 |
| - 5p | 8.435 | 325 | 495 |
| - 6 | 8.437 | 325 | 500 |
| - 7 | 8.440 | 335 | 495 |
| - 8 | 8.435 | 325 | 495 |
| - 9 | 8.433 | 331 | 497 |
| - 10m | 8.432 | 320 | 500 |
| - 11 | ND | 325 | 500 |
| - 12 | ND | 325 | 500 |
| - 13 | ND | 315 | 498 |
| - 14 | ND | 315 | 498 |

Assuming that the titanomagnetites have stoichiometric composition, they have 35 % ulvöspinel by referring Akimoto et al's (1957) equal a(Å) diagram and 45 % ulvöspinel by using their equal Tc diagram.

Three major components of titanomagnetite, FeO, $Fe_2O_3$ and $TiO_2$ , were determined and plotted on the ternary diagram as shown in Fig.3. They are considered to be solid solution of 45 % ulvöspinel and 55 % magnetite and its oxidized forms because the plots lie along theoretical oxidation-reduction lines. $TiO_2$ content is fairly equal in almost all specimens, which might have caused the coincidence of thermomagnetic properties.

(ii) pseudo Akahoya, PA, and Aira Tn ash, AT

Though the sample numbers are still a few, thermomagnetic data of PA and AT are shown in Fig.4 and Table 3. All the specimens

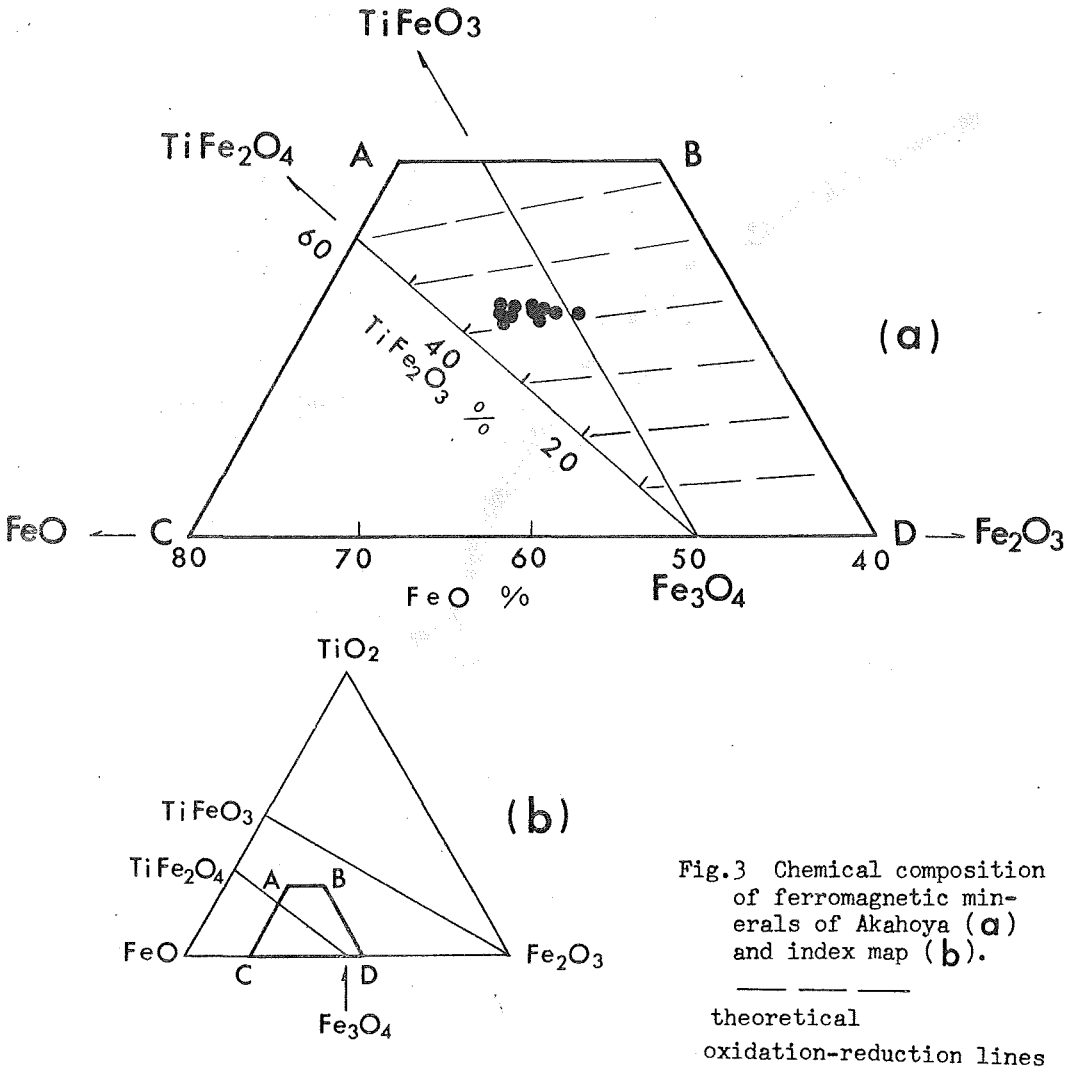


Fig.3 Chemical composition of ferromagnetic minerals of Akahoya (a) and index map (b).

— — — theoretical oxidation-reduction lines

of PA have Tc at around 500°C and their Js-T curves are quite different from those of Akahoya. Stoichiometrically, PA has about 15 % ulvöspinel. Though the specimen is only one at present, thermomagnetic features of AT are different from both Akahoya and PA. Determination of Tc values from the curve has still problems, but three phases might be involved in this specimen. Detailed study is needed on AT. Thermomagnetic measurement thus gave noticeable difference among the three tephras.

Table 3 Curie temperature, Tc(°C) of ferromagnetic minerals of Pseudo-Akahoya and Aira Tn ash

| Sample No. | Tc(°C) |
|---|---|
| Pa - 1 | 503 |
| - 2 | 508 |
| - 3 | 500 |
| - 4 | 495 |
| - 5 | 493 |
| - 6 | 495 |
| - 7 | 500 |
| AT - 1 | 375 465 495 |

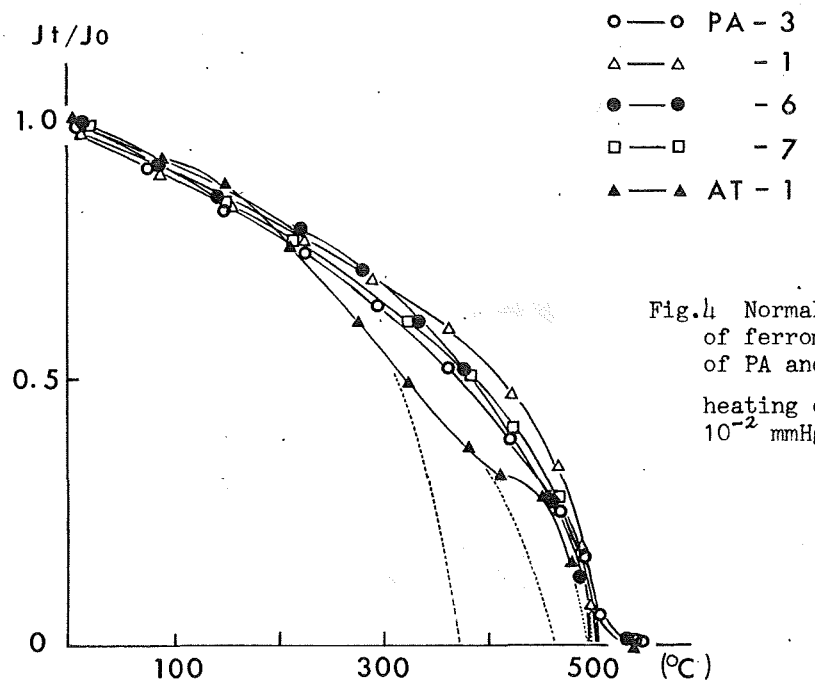


Fig.4 Normalized Js-T curves of ferromagnetic minerals of PA and AT.

heating curve, H=2500 Oe, $10^{-2}$ mmHg

Conclusions

Akahoya, highly glassy vocanic ash sampled in southern and middle parts of Kyushu and Shikoku island was revealed to have titanomagnetite whose thermomagnetic properties are in good accordance with each other. This will support the conclusions of Nagatomo and Shoji (ibid) and Machida and Arai (1978,ibid) that every Akahoya is the same tephra erupted from one source.

Akahoya-like glassy ash considered to be marginal facies of welded tuff of Aso and Aira Tn ash erupted from Aira caldera showed different thermomagnetic properties from each other and also from Akahoya though their apparent feature is very much a-like.

References

Akimoto,S. et al. (1957) J.Geomag. Geoelect., 9, 165
Ariake Bay Res. Group (1965) Monograph/11 The Association for the Geological Collaboration in Japan.
Domen,H. et al. (1970) Bull Fac. Educ., Yamaguchi Univ., 19, Pt.2, 23
Gohara,Y. et al. (1964) Misc. Rept. Research Inst. for Natural Resources, 62, 83
Machida,H. and Arai,F. (1976) Kagaku, 46, 339
Machida,H. and Arai,F. (1978) Quat. Res., 17, 143
Matsui,T. (1960) Misc. Rept. Research Inst. for Natural Resources, 52-53, 115
Matsui,T. (1963) ibid, 60, 1
Matsui,T. and Kato,Y. (1965) ibid, 64, 31
Nagatomo,Y. and Shoji,S. (1977) J.Sci. Soil Manure, Japan, 48, 1

# EFFECTS OF A PLASTIC DEFORMATION ON A REMANENT MAGNETIZATION OF Cu-Co ALLOY

Minoru OZIMA

Geophysical Institute, University of Tokyo, Tokyo 113, Japan

## Introduction

Although there are a number of reports on the effects of stress on a remanent magnetization of rocks, these studies were mostly carried out for applied stresses below the elastic limit of the rocks and only a few studies have been made to examine the effects of a plastic deformation on a remanent magnetization. Since deep-sea sediments which have been yielding the major paleomagnetic information of the oceanic crust must have undergone some degree of a deformation under burial compression, it is vital to study the latter effect for the meaningful paleomagnetic information.

Recently Kodama and Cox (1978) presented experimental results on the effect of a constant volume deformation on a remanent magnetization. They found that 33.1/3 % shortening of the axis of maximum compression did not result in significant change in the direction of magnetization (ARM produced at DC field = 1 Oe with peak AF field = 1,000 Oe). They concluded that a continuous deformation model in which the magnetic needles were embeded in a plastically deforming linearly homogeneous medium does not explain the results, but that a discontinuous deformation model, where deformation occurs mainly in shear zones bounding blocks which translate along the shears, better explains the results. If deep-sea sediments behave in the similar way as in the above discontinuous deformation model under the burial compression, the inclination of the remanent magnetization of the sediments would not change, therefore assuring useful information about the paleolatitude of the oceanic crust. On the contrary to the results by Kodama and Cox (1978), Blow and Hamilton (1978) concluded from their redeposition experiments of deep-sea sediments that post depositional compaction is a major factor in shallowing the inclination of the DRM. Their results suggest that a plastic deformation affects the inclination of the DRM. Since unless both polar wandering and crustal movements are specified, it would be difficult to elucidate uniquely the compaction effects on a natural DRM, a model experiment may be an useful approach to this problem. Below I present the results on the compression effects on a remanent magnetization of Cu-Co alloy. I hope that the results can be instructive for the better understanding of the plastic deformation effects on a remanent magnetization or the compaction effects on the ocean sediment remanent magnetization.

## Experimental results

I studied the effects of a plastic deformations on a remanent magnetization (IRM, at H = 1,000 Oe) imposed on Cu-Co alloy, in which 2 % (wt) of Co was precipitated to have formed ferromagnetic particles in the Cu matrix. I estimated from

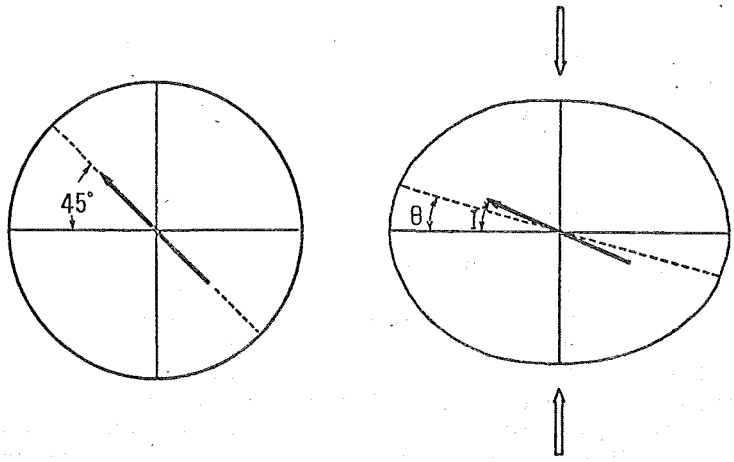


Fig. 1. Rotation of a body vector (dotted line) drawn on the surface of a plastically deforming Cu-Co alloy and an IRM vector (thick arrow). Notice that both the body vector and the IRM vector rotate away from the compressional axis (white arrow). Left : before deformation and right : after deformation.

the annealing time of the Cu-Co alloy that the Co-particles range from submicron to a few tens of microns. I feel that the Cu-Co alloy in which rigid Co-particles were precipitated in the relatively soft Cu matrix may not be unrealistic simulation of the magnetite grains in deep-sea sediments. The procedure to make the Cu-Co alloy was described by Kobayashi (1961). The Cu-Co alloy was then shaped in a disk (0.38 cm radius and 0.31 cm thickness) and IRM (H = 1,000 Oe, J = 2.1 x $10^{-2}$ emu/g) was imposed on the disk plane (Figure 1). Compression was then applied to the disk along the vertical direction, in which the axis of the compression was at an angle of 45° from the IRM direction. The disk was bound at the both faces in a stainless steel container, so that the plastic deformation could occur only in the disk plane. A line (a body vector) was marked initially on the disk plane along the direction of the IRM (Figure 1). With the increasing compression, the circular disk was flattend and the angle θ between the body vector and the horizontal axis decreased (Figure 1). With the decreasing θ, the magnetization vector also rotated away from the axis of the compression giving shallower inclination (Figure 1). Table 1 gives θ and I as well as the relative intensity of the magnetization with the deformation.

Table 1.

| | | | | |
|---|---|---|---|---|
| θ | 45° | 39° | 31° | 24° |
| I | 45° | 38° | 33° | 26° |
| $M/M_0$ | 1.0 | 0.92 | 0.83 | 0.77 |

The experimental results show that the magnetization vector rotated almost in the same way as the body vector did during the plastic deformation. The results are contrary to those which Kodama and Cox (1) observed in the case of the artificial sediment.

To examine further the mechanism of the ortation of the remanent magnetization during the plastic deformation, I measured saturation magnetization anisotropy (H = 15,000 Oe) on the original undeformed sample and the most deformed sample. The experimental procedures for the anisotropy measurement were described previously (Ozima, Kinoshita, 1964). The results are shown in Figure 2. For the undeformed sample, the anisotropy was almost negligible and a sin 4θ component was the most prominent in the torgue curve. For the deformed

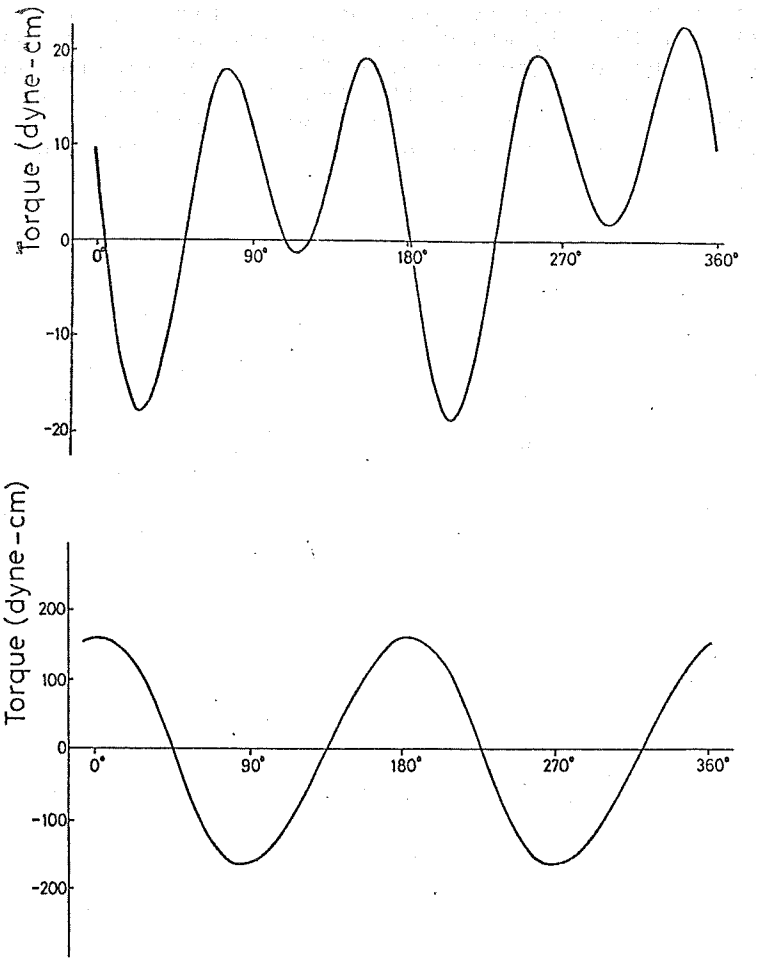


Fig. 2. Saturation magnetization torque curves before deformation (above) and after deformation (below). Notice that after the deformation a large anisotropy appeared with a predominant sin 2θ component.

one, sin 2θ became the most predominant component and the absolute value of the anisotropy was about an order of a magnitude larger than that for the undeformed sample. It is well known (Stacey, 1960) that the sin 4θ component in the torque curve corresponds to the crystalline alignment in the case of a cubic crystal (Co has a cubic crystallographic structure), whereas the sin 2θ component indicates that the anisotropy is essentially due to shape alignment; elongated ferromagnetic particles were aligned statistically in some prefered direction. For the deformed sample, the easy axis of the anisotropy (sin 2θ component) was perpendicular to the axis of the compression.

From the above experimental results I propose a model to explain the effects of the plastic deformation on the remanent magnetization of the Cu-Co alloy. I first assume that the precipitated Co-particles have generally an ellipsoidal form. When magnetic field was applied to the Cu-Co alloy, each Co-particle must heve acquired the magnetization along the long axis of the ellipsoid, which was then the nearest to the direction of the applied magnetic field. During the subsequent plastic deformation, the long axis of the Co-particles rotated away from the axis of the compression, therefore giving the observed anisotropy and the shallowing of the magnetic inclination.

## Discussion

Although it is generally regarded that inclination error may not occur in deep-sea sediments (Opdyke and Henry, 1969), the recent report by Carlson and Christensen (1979) seems to call for further examination of this problem; they found a systematic increase in compressional-wave velocity anisotropy with the subbottom depth of the sediments, higher velocities in the bedding plane than these in the vertical direction in calcareous deep-sea sediment cores. Carlson and Christensen suggested the mechanisms for the produced fabric anisotropy : (1) the alignment of certain microfossils such as Discoaster during compaction, (2) epitaxial growth of aligned forms during diagenesis and (3) recrystallization of calcite. If (1) is the case, we should expect the magnetic grains also align themselves in the bedding plane, resulting in a shallower magnetic inclination.

To resolve whether magnetic minerals in deep-sea sediments behave in a similar way to Co-particles precipitated in the Cu-matrix under compression or if the behavior is much closer to that of the magnetic needles embedded in the artificial sediments studied by Kodama and Cox (1978), saturation magnetic anisotropy measurement would be most promising. If the former is the case we would expect a systematic increase of the magnetic anisotropy (sin 2θ component) with increase of the subbottom depth in deep-sea sediment core.

References

Blow, R.A. and N. Hamilton (1978) Geophys. J.R. astr. Soc., 52, 13.
Carlson, R.L. and N.I. Christensen (1979) J. Geophys. Res., 84, 205.
Kobayashi, K. (1961) J. Geomag. Geolelectr., 12, 148.
Kodama, K.P. and A. Cox (1978) Earth Planet. Sci. Lett., 38, 436.
Opdyke, N.D. and K.W. Henry (1969) Earth Planet Sci. Lett., 6, 139.
Ozima, M. and H. Kinoshita (1964) J. Geomag. Geoelectr., XVI, 194.
Stacey, F.D. (1960) J. Geophys. Res., 65, 2429.

(Submitted to Earth Planet. Sci. Lett.)

# GRAIN SIZE EFFECT ON THE LOW-TEMPERATURE OXIDATION OF TITANOMAGNETITES

Tadashi NISHITANI

Geophysical Institute, University of Tokyo,
Bunkyo-ku, Tokyo 113, Japan

## 1. Introduction

The intensity and the direction of natural remanent magnetization of a rock are important in investigating the pole position and the magnetic field of the earth when the rock was cooled from its Curie temperature. Titanomagnetite is a principal carrier of a remanent magnetization. The cubic titanomagnetite solid solution series lies along the line joining magnetite($Fe_3O_4$) with ulvospinel($Fe_2TiO_4$) in the ternary system $FeO$-$Fe_2O_3$-$TiO_2$. Any member of this series can be represented by the following formula

$$xFe_2TiO_4 \cdot (1-x)Fe_3O_4,$$

where x means ulvospinel molar ratio. Titanomagnetite is sometimes found in an oxidized state in continental basalts (Akimoto and Katsura, 1958)or in a soil(Katsura et al.,1962). However, cation-deficient titanomagnetite (titanomaghemites) are frequently observed in oceanic basalts(e.g., Marshall,1978). In continental basalts high-temperature oxidation occurs frequently (Buddington and Lindsley, 1964). This process of high-temperature oxidation was actually observed in Hawaiian lava lake (Grommé et al., 1969). In oceanic basalts high-temperature oxidation is seldom observed and low-temperature oxidation process prevails (Lowrie, 1974). The oxidation parameter z is defined as follows.

$$Fe^{2+} + \frac{z}{2}O \longrightarrow zFe^{3+} + (1-z)Fe^{2+} + \frac{z}{2}O^{2-} \qquad (0 \leq z \leq 1)$$

z = 0.0 stands for stoichiometric titanomagnetite and z = 1.0 for fully oxidized state.

Akimoto et al.(1957) investigated magnetic properties of titanomagnetites in air at temperatures of 400° ∿ 500°C. Ozima and Larson(1970) pointed out that they did not produce pure titanomaghemite because their samples had contained an amount of the high-temperature oxidation product. Sakamoto et al.(1968) demonstrated that titanomaghemites could be produced when titanomagnetites were ground in water and heated in air at temperatures below 300°C. Ozima and Sakamoto(1971) performed oxidation experiments for titanomagnetites of high ulvospinel ratio (x = 0.7, 0.9 and 1.0), and reported parameters such as lattice constants and Curie temperatures. Readman and O'Reilly(1972) examined titanomaghemite with four compositions (x = 0.0, 0.4, 0.7 and 1.0), however, their results did not always agree with those of Ozima and Sakamoto(1971). As for the oxidation state reached under laboratory condition, Ozima and Sakamoto(1971) concluded that z ∿ 0.3 was the maximum, after which the unmixing of titanomagnetites proceeded, while

Readman and O'Reilly(1972) claimed that titanomagnetite could be completely oxidized.

It is necessary to remove the discrepancies between these two works. Changes in magnetic properties associated with oxidation must also be examined precisely. In this study magnetic properties were investigated for three titanomagnetite compositions, x = 0.3, 0.5 and 0.7, During low-temperature oxidation. The relationship between oxidation state and time and temperature of heating was made clear. Through oxidation experiments with titanomagnetite of controlled grain size, it is clearly shown that the results of the two experiments, Ozima and Sakamoto(1971) and Readman and O'Reilly(1972), can be explained in terms of difference in particle size.

The magnetic minerals were separated from the DSDP samples and heated in air. As a result of heating the oxidation proceeds in submarine basalts, but it does not proceed in subaerially erupted basalts and unmixing process occurs. This can also be explained in terms of grain size.

## 2. Experimental procedure

Synthetic samples were prepared as follows. To produce titanomagnetite of composition x, pure $TiO_2$ and $Fe_2O_3$ were mixed in the stoichiometric proportion, and well ground in an agate mortar for several hours. The mixtures were then sintered in air at 1200°C for an hour. After that they were well ground and sintered again. Sintered material was crushed into the size of about 2 mm and kept at 1200°C in a furnace with controlled ozygen fugacity($PO_2$) for several hours. The samples were quenched to about 0°C and determined the lattice constant using X-ray diffractometer to ascertain that a single phase titanomagnetite was formed. Heatings were repeated until the two peaks of $FeK\alpha_1$ and $FeK\alpha_2$ in (511) and (400) reflections were seen clearly. Titanomagnetite samples were prepared five or six times for the same x values. Their lattice constants and Curie temperatures coincide within ranges of ±0.001 A and ±2°C.

Titanomagnetite samples were ballmilled in a slurry of high purity ethyl alcohol. Alumina balls($Al_2O_3$) were used. After ballmilling titanomagnetites were collected with a hand magnet from a slurry of ethyl alcohol. The oxidation state can be monitored accurately observing lattice parameter and Curie temperature. The ballmilled samples show a slight decrease in lattice parameter and a slight increase in Curie temperature. This indicates that these samples are slightly oxidized in the process of ballmilling. Oxidation parameter of these samples are $z \lesssim 0.1$. Therefore we may consider that the process of ballmilling caused no great change in the properties of titanomagnetites.

Samples ballmilled in ethyl alcohol were heated in an electric furnace in air. Samples were put in the furnace which was preheated and kept at a setting temperature. The temperature fluctuations in the furnace was controlled within ±1°C of the fixed oxidizing temperature. A small amount of samples (∿50 mg) was placed in a small basket and oxidized at various

temperatures for different intervals. Some samples were prepared in a batch of about 1 g to be used in chemical analysis.

Lattice constants and Curie temperatures are sensitive to small changes in composition and oxidation state. These two parameters has extensively been used in rock magnetism. In this experiment, measurements of lattice constant and Curie temperature were made much of and these parameters were used to estimate an oxidation state(z). In order to determine lattice constant X-ray diffractometer(RIGAKU 2035) with Fe target and Mn filter was used under a condition of 30 kV and 10 mA. The angles (2θ) between 100° and 20° were scanned. Instrumentation errors were calibrated by measuring the diffraction angles of the silicon powder. Curie temperature was measured using magnetic balance in a vacuum (below $1\times10^{-5}$ Torr) under the magnetic field of 5.5kOe.

The compositions of starting materials and oxidation products were determined by wet chemical analysis.

## 3. Results

Lattice constants and Curie temperatures as a function of oxidation parameter are represented in Fig.1 and Fig.2. All the data in Fig.1 are chemically analyzed samples. Oxidation state of a sample which was not analyzed chemically can be obtained from Fig.1 if lattice constant and ulvospinel ratio(x) of the sample are known. In Fig.2, samples which were analyzed chemically are represented by double circles. Lattice constants and Curie temperatures vary smoothly and continuously with z values and no other phases are seen in X-ray analyses. This means that the oxidation state from z = 0.0 to 1.0 are obtained in this study.

Relation between oxidation state and heating time and temperature is made clear only for titanomagnetites with the size of 0.3 ∿ 0.6 μm. This size of titanomagnetites can be obtained as a result of ballmilling for 40 ∿ 100 hours.

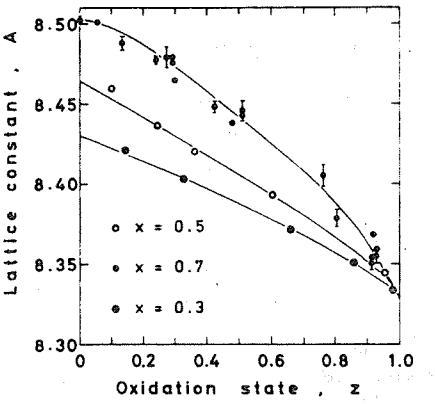


Fig.1 Lattice constant against oxidation state.

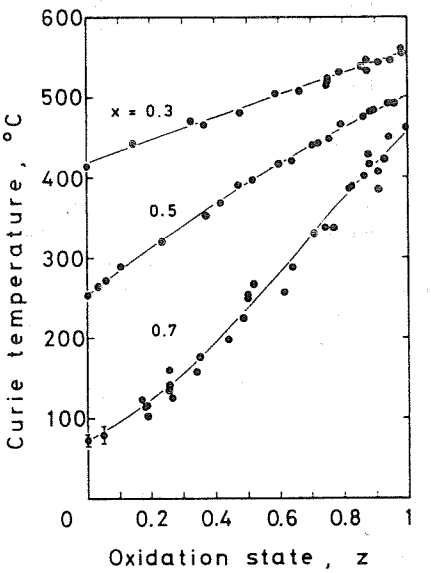


Fig.2 Curie temperature against oxidation state.

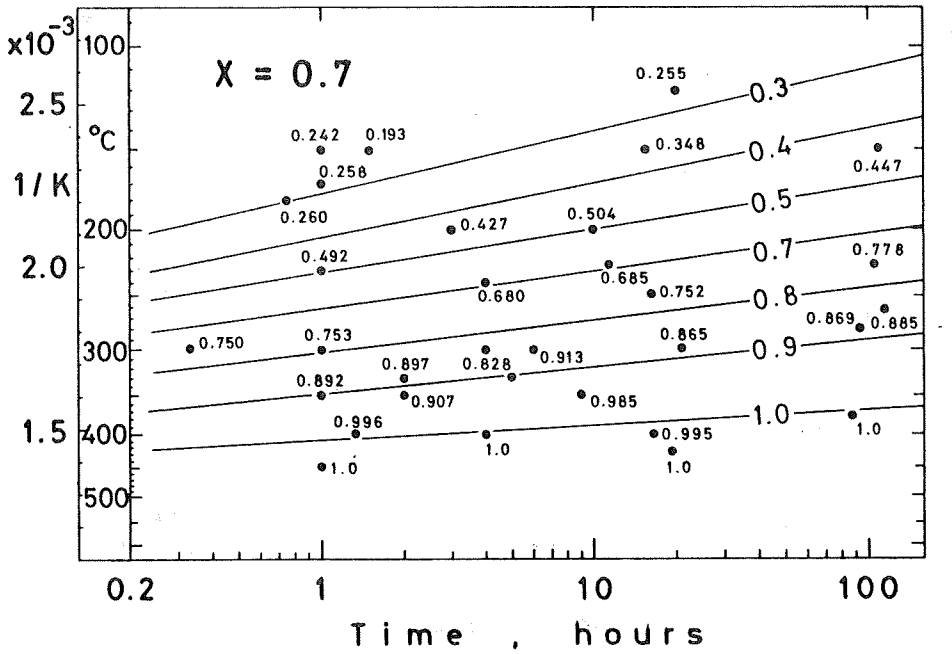


Fig. 3 Relationship between reciprocal absolute temperature (1/T) and time for x = 0.7 ballmilled titanomagnetite.

Fig.3 represents the relation between oxidation parameter and heating time and temperature for x = 0.7 titanomagnetite. In this figure the abscissas represent logarithms of heating time and the ordinates represent the reciprocal of absolute temperature. The temperature in °C is also shown in this figure for convenience. Solid circles stand for experimental points and added numbers are oxidation parameter z which were determined by chemical analysis or by interpolation using the data of lattice constant and Fig.1. Conditions of equal oxidation states are well expressed by the solid lines. If x = 0.7 ballmilled titanomagnetite is heated for 100 hours at 200°C, for example, the oxidation state of the sample is z = 0.69. The same oxidation state can also be obtained by heating 1 hour at 260°C or 10 hours at 230°C. Another state can be assessed easily using Fig.3.

The relation between lattice constant and Curie temperature for x = 0.7 is shown in Fig.4. Solid circles represent experimental points while the solid line was constructed from the general trend. The results of Ozima and Sakamoto(1971) and Readman and O'Reilly(1972) are also shown in Fig.4. As this figure clearly shows that the starting materials, ballmilled titanomagnetites which were used by them, show about 50°C lower temperature and 0.01 A smaller lattice constant than those of the present experiment. The deviation is much greater for high z values than for low z ones. Considering the results of wet chemical analysis and other experimental data (Katsura et al., 1976; Nishitani,1979), 8.502 A and 75°C seem the most suitable value for x = 0.7 titanomagnetite.

Low-temperature oxidation line and contours of equal oxidation state are summarized in Fig.5. This figure can be

used to determine the oxidation states of natural and synthetic samples.

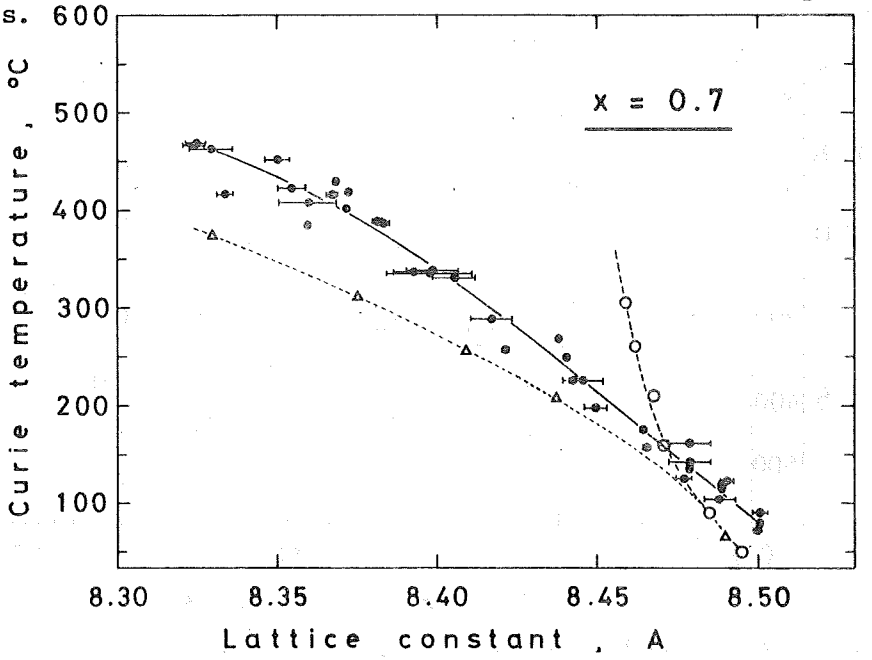


Fig.4 Relation between lattice constant and Curie temperature for x = 0.7 titanomagnetite. Solid circles represent experimental points in this study. Results of Ozima and Sakamoto (1971) are shown in open circles and those of Readman and O'Reilly(1972) in open triangles for x = 0.7 titanomagnetite.

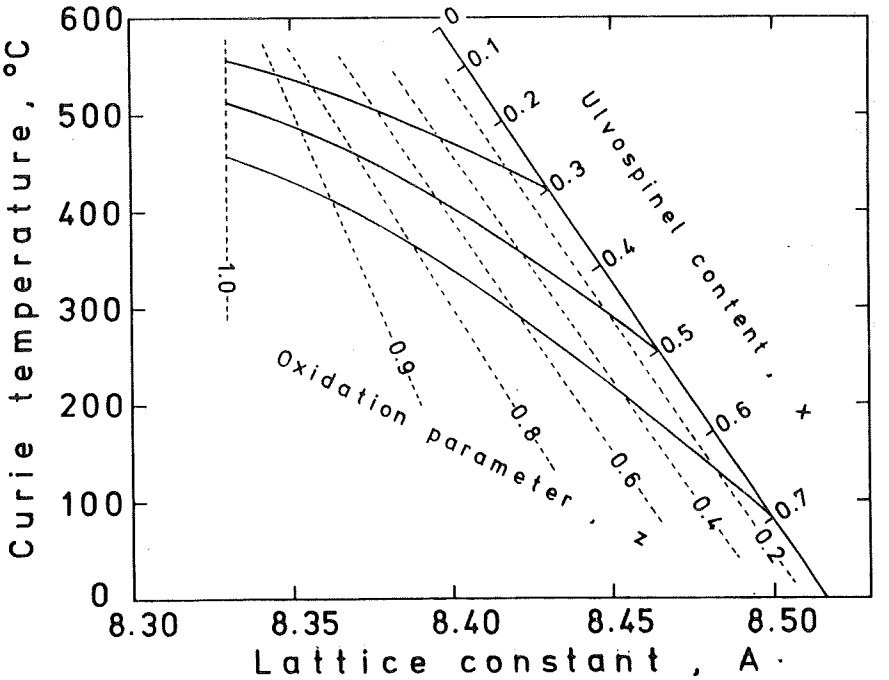


Fig.5 Relationship between lattice constant and Curie temperature. Contours of equal oxidation state are shown.

## 4. Discussion

Ozima and Sakamoto(1971) used titanomagnetites which were ground in an agate mortar, while Readman and O'Reilly(1972) used ballmilled titanomagnetites. Other experimental conditions were almost the same between these two experiments. The difference in Fig.4, namely, Ozima and Sakamoto's(1971) experiment shows a sharp rise in Curie temperature with oxidation, while Readman and O'Reilly's(1972) does not, may be originated from the grain size of titanomagnetite. The grain size may control the state of low-temperature oxidation and this effect may appear in the differences between the oxidation states of oceanic basalts and those of continental basalts. Consequently, it is important to investigate the effect of grain size on low-temperature oxidation.

Titanomagnetite samples which cover the particle size from 0.57 ± 0.33 μm to 300 μm were prepared. They were heated in air in the same condition; the temperature was 300°C and heating time was 300 minutes. Their lattice constants and Curie temperatures after the heating were measured. These values are represented in Fig.6. In this figure as the number increases the grain size of titanomagnetite is smaller. The broken line stands for the oxidation line obtained by the present work (x = 0.7). The result of Ozima and Sakamoto(1971) for x = 0.7 is shown in the same figure. Their trend, sharp rise in Curie temperature, coincides with the trend of the samples No.1 to no.8. They are almost on the stoichiometric titanomagnetite solid solution line, so that they are

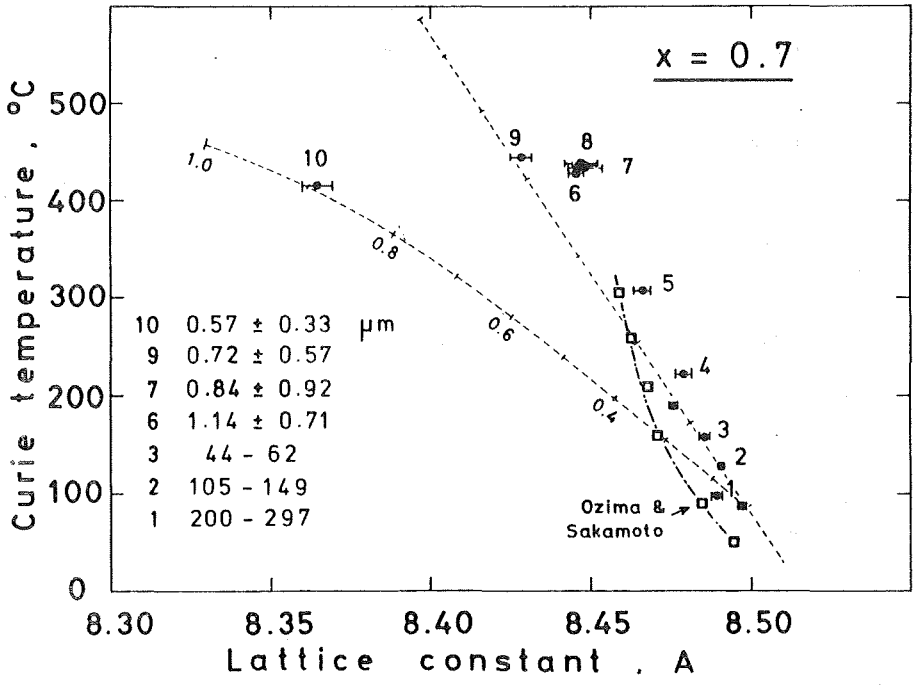


Fig.6 Relationship between lattice constant and Curie temperature when different sizes of titanomagnetites(x = 0.7) are heated 300 minutes at 300°C. The results of Ozima and Sakamoto(1971) for x = 0.7 are represented by open squares.

considered to be the phase of decomposition of titanomagnetite associated with oxidation. As is evident from Fig.6, there is a critical grain size in low-termperature oxidation. The critical size is about 0.7 ∿ 0.8 μm in case of x = 0.7 titanomagnetite in the laboratory condition. The ballmilled titanomagnetite and that ground in an agate mortar behave in a quite different way when they are heated in air. To ascertain this fact more clearly, two samples were prepared, one was ballmilled and the other was ground in an agate mortar for x = 0.7 titanomagnetite. They were heated in air under the condition of 250°C for 15 hours, 300°C for 5 hours and 400°C for 469.5 hours. The results are shown in Fig.7. The ballmilled samples were oxidized along the oxidation line. However, samples which were ground in an agate mortar decomposed or unmixed to an iron-rich stoichiometric titanomagnetite (spinel structure) and a hemo-ilmenite (rhombohedral structure) by heating. Rhombohedral phases are clearly seen in a chart of X-ray diffractometer. It can be determined either low-temperature oxidation process or decomposition process dominates if lattice constant and Curie temperature of titanomagnetite are observed before and after heating.

Ozima and Sakamoto(1971) prepared titanomagnetite samples using an agate mortar and their grain size is probably greater than 0.7 ∿ 0.8 μm. So that decomposition process dominates over low-temperature oxidation process and a sharp rise in Curie temperature occurs as in Fig.4. The grain size of a sample which was used by Readman and O'Reilly(1972) was reported to be about 0.1 μm. Therefore generally the same trend of oxidation process as in the present experiment was obtained.

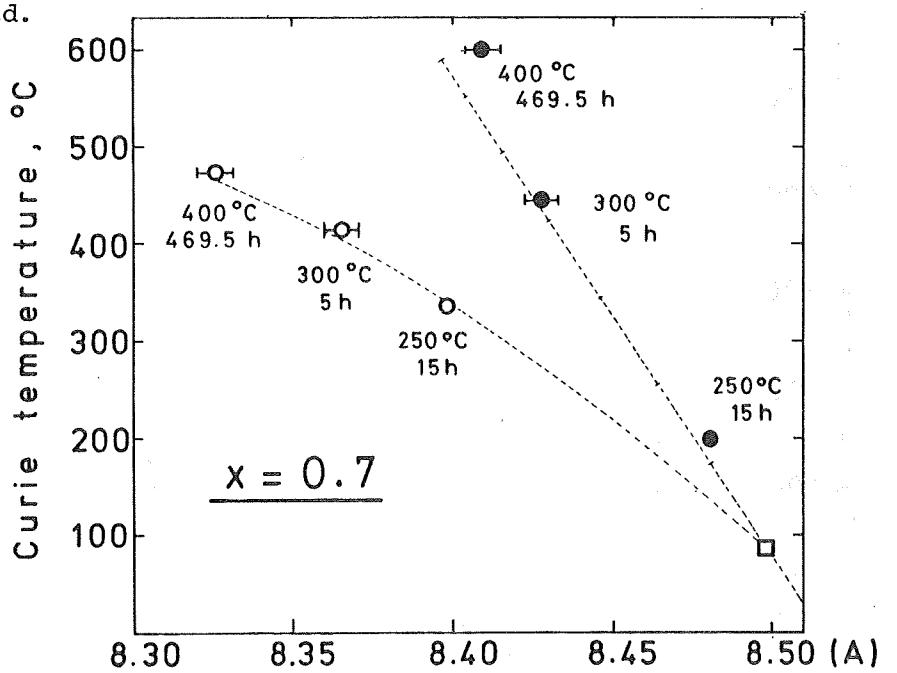


Fig.7 Results of heat treatment in air for x = 0.7 titanomagnetite. Two samples, one is ballmilled (open circles) and the other is ground in an agate mortar (solid circles), were heated.

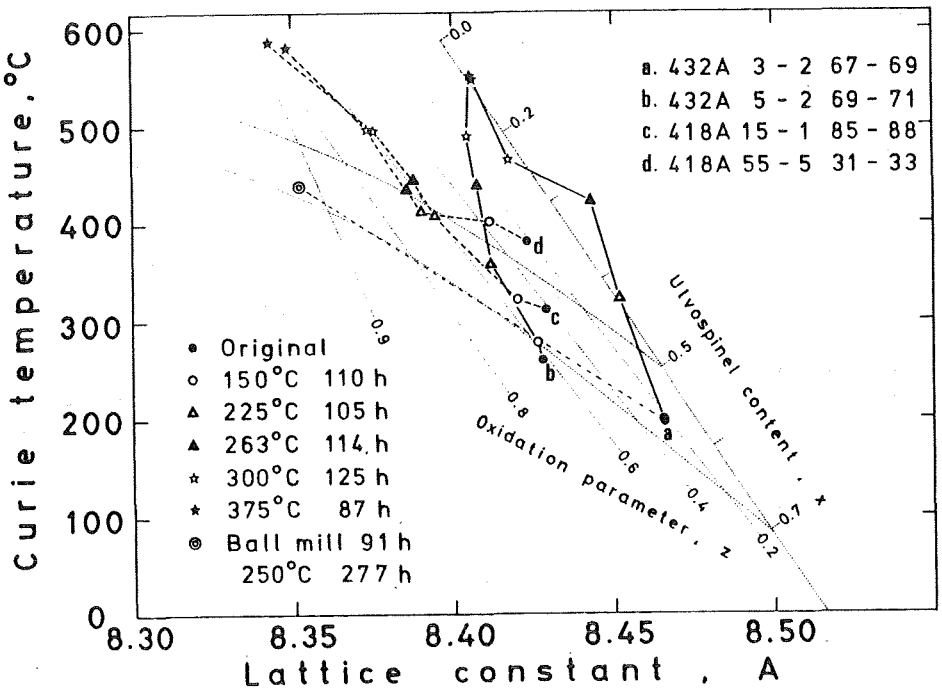


Fig.8 Results of heat treatment of magnetic minerals of submarine basalts(418A) and subaerially erupted basalts (432A).

Magnetic minerals were separated from basaltic samples of the Deep Sea Drilling Project(DSDP) legs 51, 52, 53 and 55. Four samples were selected and heated in a laboratory condition. As subaerially erupted basalts(Leg 55) 432A 3-2 67-69 and 432A 5-2 69-71 and representatives of submarine basalts(Legs 51, 52 and 53) 418A 15-1 85-88 and 418A 55-5 31-33 were chosen. These magnetic minerals were heated in air for about 100 hours at various temperatures. The change of lattice constants and Curie temperatures as a result of heating were summarized in Fig.8. The tendency of the change of experimental points of 432A and 418A are different as the treatment temperature increases. 432A samples show a sharp rise in Curie temperature, indicating that they are decomposed into Fe-rich titanomagnetite and hemo-ilmenite. 418A samples show rather the same trend as the ballmilled samples, that is, low-temperature oxidation process seems dominant. Low-temperature oxidation occurs at the grain size of the magnetic minerals of 418A, but it does not occur at the grain size of those of 432A under a laboratory condition. If small grain size is essential for low-temperature oxidation to occur, 432A samples may also be low-temperature oxidized when their grain size is small enough. The sample 432A 3-2 is ballmilled for 91 hours and heated for 277 hours at 250°C in air. Result of this heating is also shown by double circle in Fig.8. It is evident from this figure that low-temperature oxidation occurred on above condition because the particle size is now smaller than before.

It can be concluded from above experiment that the grain size of magnetic minerals is one of the important controlling factor of low-temperature oxidation.

References

Akimoto,S. and T.Katsura (1958) J. Geomag. Geoelectr.,10, 69.
Akimoto,S., T.Katsura and M.Yoshida (1957) J. Geomag. Geoelectr. 9, 165.
Buddington,A.F. and D.H.Lindsley (1964) J. Petrology, 5, 310.
Grommé,C.S., T.L.Wright and D.L.Peck (1969) J. Geophys. Res., 74, 5277.
Katsura,T., I.Kushiro, S.Akimoto, J.L.Walker and G.D.Sherman (1962) J. Dedimentary Petrology, 32, 299.
Lowrie,W. (1974) J. Geophys., 40, 513.
Marshall,M. (1978) J. Geophys. Res., 83, 289.
Nishitani,T. (1979) Accepted to J. Geomag. Geoelectr.
Ozima,M. and E.E.Larson (1970) J. Geophys. Res., 75, 1003.
Ozima,M. and N.Sakamoto (1971) J. Geophys. Res., 76, 7035.
Readman,P.W. and W.O'Reilly (1972) J. Geomag. Geoelectr., 24, 69.

(To be published in Earth Planet. Sci. Lett.)

# MAGNETIC HISTERESIS PROPERTIES OF x = 0.5 TITANOMAGNETITE

Yozo HAMANO

Geophysical Institute, University of Tokyo, Tokyo 113, Japan

## 1. Introduction

The hysteretic properties of pure magnetites have been studied (Parry, 1965; Dunlop, 1972), and can be used to estimate magnetite grain sizes contained in rocks and sediments. Little is known, however, of the properties in magnetite-ulvöspinel solid solutions. Day et al. (1976) compared the hysteretic properties of fine grain ($\sim$ 0.1 μm) particles with those of coarse grain ($\sim$ 150 μm) particles of titanomagnetite. But magnetic carriers observed in natural rocks and sediments have particle sizes between the above two extremes. Thus, the variations of the hysteretic properties within this range of the particle size are important to discremenate the magnetic carriers.

The experimental work described in this paper observed the variation of the hysteretic properties as a function of the particle size using titanomagnetite samples of a fixed composition.

## 2. Sample description

Synthetic titanomagnetite with a composition of 0.5 $Fe_3O_4$ 0.5 $Fe_2TiO_4$ (x = 0.5) was used in the present experiment. The titanomagnetite powders were synthesized at 1200°C temperature under a controlled oxygen fugacity. The intrinsic properties of this titanomagnetite, i.e., Curie temperature, saturation magnetization, and lattice parameter are 250°C, 32 emu/g, and 8.46 A respectively.

The sample sintered under the above condition was weakly ground with an agate mortar before being sieved with micropore filters made of polycarbonate. Three fractions with different size distributions were obtained by this procedure. The smallest fraction was prepared by ball-milling the sample powder for about 24 hours. Because the sizes of the sieved magnetic powders are always substancially smaller than the aperture of the sieves (Levi and Merril, 1978), the size distribution in each fraction was measured by grain counting on electron and optical microscope pictures. These pictures indicated that the particles have nearly equi-dimensional shape.

The observed size distributions for the four fractions of the titanomagnetite are shown in Fig. 1. The wide distribution of the size in each fraction and probable artificial filters in the counting of grains make it very difficult to obtain the mean grain sizes. Some consideration might be necessary to circumvent this difficulty.

In powder technology many empirical distribution functions have been invented. Among them the Rosin-Rammler equation (Rosin and Rammler, 1923) can satisfactorily approximate the size distributions of crushed materials. The equation is expressed as

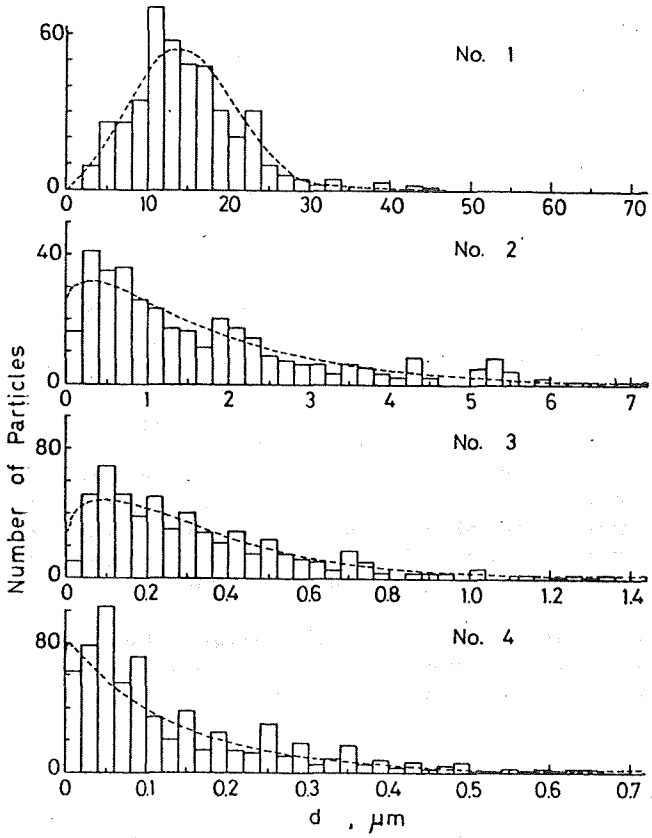


Fig. 1. Particle size distributions of the four fractions of the x = 0.5 titanomagnetite. Dotted lines represent the Rosin-Rammler distribution functions fitted to the observation.

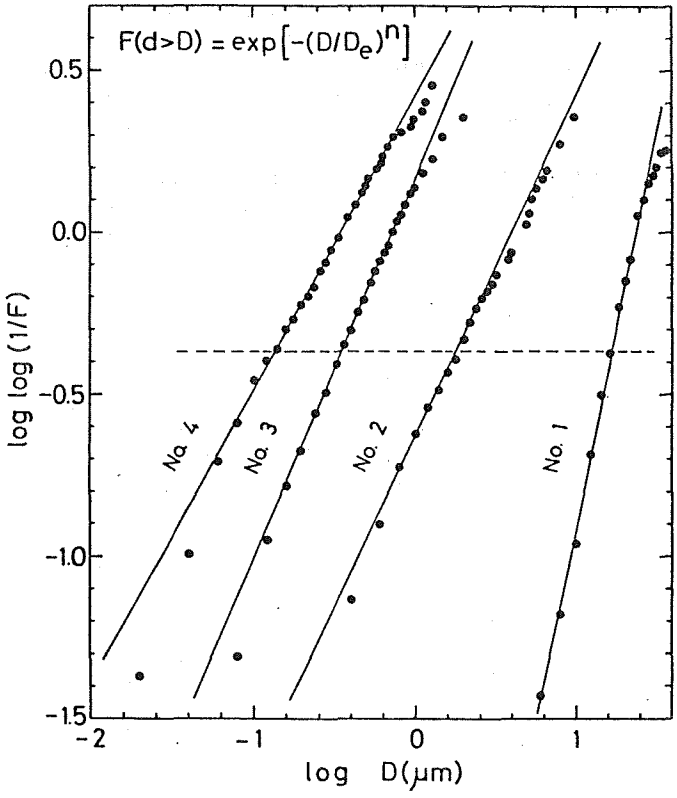


Fig. 2. Rosin-Rammler plotts for the present titanomagnetite samples.

$$F(d > D) = \exp\left[-(D/D_e)^n\right]$$

where $F(d > D)$ is the proportion of the number of grains which have diameters greater than D, and $D_e$ and n are the two parameters characterizing the distribution. It is easily shown that the distribution can be expressed as a straight line in a loglog $F(d > D)$ vs. log D diagram. The Rosin-Rammler plotts for the present four fractions of the present titanomagnetite sample, shown in Fig. 2, indicate that the size distributions of these powder assemblages can be well approximated by this equation. The deviations in the larger and the smaller sizes can be attributed to the finiteness of the number of the counted grains and some artificial filters in the counting.

Once the parameters of the Rosin-Rammler equation are known, the mean diameter in any meanings can be calculated. For the present purpose the volume or mass distribution is important. Thus, the mean grain sizes averaged in the volume distribution and the ranges of the particle size which contain more than 80% of the powder volume are calculated and listed in Table 1.

## 3. Experiments and Results

The observed hysteresis properties are coercivity $H_c$, remanence coercivity $H_{rc}$, saturation remanence $J_{rs}$, and $J_{rs}/J_s$ ratio. The measurements were made with a PAR vibration magnetometer. The magnetic field of as much as 13 KG was applied to obtain the hysteresis curves.

For the measurement cylindrical rods with 3 mm diameter and about 5 mm length were used. The rods consist of mixture of the titanomagnetite powders described above and non-magnetic alumina cement with a mixing weight ratio of 1 : 100.

The observed hysteresis properties for four fractions of the present $x = 0.5$ titanomagnetite are listed in Table 1. The variations of coercivity $H_c$ and $J_r/J_s$ ratio as a function of particle size are shown in Figs. 3 and 4 respectively. In these figures available data on Ti-free magnetite are also plotted for comparison.

The $J_r/J_s$ ratio and the coercivity increases with decreasing of the particle size both in the titanomagnetite and the Ti-free magnetite. The trends are reasonably explained by the variation of the magnetic domain state with the particle size. The $J_r/J_s$ ratio in the smaller two fractions of the titanomagnetite are very high and exceed 0.5. Stoner and Wohlfarth

Table 1. Magnetic hysteresis properties observed in $x = 0.5$ titanomagnetite.

| Sample No. | Range of the grain size (μm) | mean size (μm) | $H_c$ (Oe) | $H_{rc}$ (Oe) | $H_{rc}/H_c$ | $J_{rs}/J_s$ |
|---|---|---|---|---|---|---|
| 1 | 14 ∿ 27 | 22 | 65 | 275 | 4.23 | 0.09 |
| 2 | 2 ∿ 8 | 5 | 270 | 835 | 3.09 | 0.27 |
| 3 | 0.4 ∿ 1.4 | 0.9 | 2000 | 2250 | 1.13 | 0.51 |
| 4 | 0.2 ∿ 0.8 | 0.5 | 2100 | 2550 | 1.20 | 0.58 |

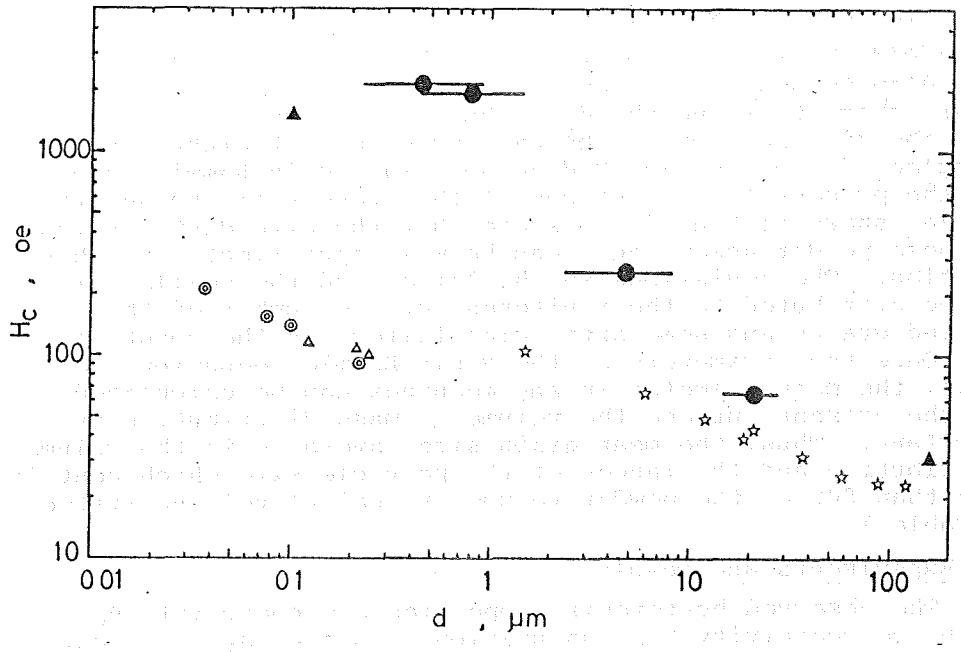


Fig. 3. Coercivity, Hc, versus particle size. ● ; present result, ▲ ; Day et al. (1976) for x = 0.5 titanomagnetites : ☆ ; Parry (1965), ◎ ; Dunlop (1972), Δ ; Levi and Merril (1978) for Ti-free magnetites.

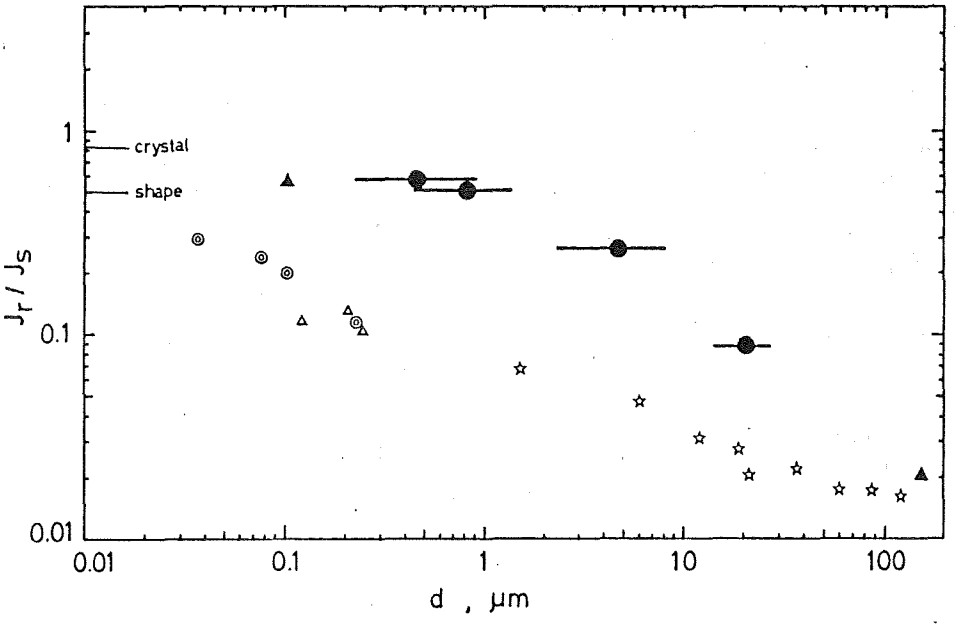


Fig. 4. $J_r/J_S$ ratio versus particle size. Symbols are the same as in Fig. 3.

(1948) calculated the hysteresis properties of single domain spheroidal particles. According to their calculation the $J_r/J_s$ ratio can be greater than 0.5 when the cubic crystalline anisotropy controls the magnetic coercive force in the grain. Therefore the above results suggest that single domain particles are dominant in the smaller two fractions, and that the crystalline anisotropy control the coercive force in these particles. The high $H_c$ and $H_{rc}$, and the small $H_{rc}/H_c$ ratio in these fractions are consistent with the above interpretation.

In single domain grains coercivities due to shape anisotropy and crystalline anisotropy can be expressed as

$$H_c^{shape} = \frac{1}{2} (N_b - N_a) I_s$$

$$H_c^{crystal} = \frac{4}{3} \frac{|K_1|}{I_s}$$

respectively (Stacey and Banerjee, 1974), where $N_a$, $N_b$ are the demagnetizing factors, $K_1$ is the anisotropic constant, and $I_s$ is the spontaneous magnetization in the grain. Because the anisotropic constants in Ti-free magnetite and $x = 0.5$ titanomagnetite are mutually comparable with a value of about $-10^5$ erg/cm$^3$ (Syono, 1965), the coercivity is inversely proportional to the spontaneous magnetization, $I_s$. On the other hand, the coercivity due to shape anisotropy is proportional to $I_s$. These facts explain the high contribution of the crystalline anisotropy in $x = 0.5$ titanomagnetite.

The present result suggests that the single domain to multidomian transition in $x = 0.5$ titanomagnetite occures around the particle diameter of 1 μm. This larger transition diameter in $x = 0.5$ titanomagnetite than Ti-free magnetite are consistent with the observation by Soffel (1971), who examined the domain structure in titanomagnetite grains with a wide range of sizes and constant composition ($x = 0.55$), and estimated the transition diameter between 0.7 to 1 μm. Theoretical calculation by Butler and Banerjee (1975) also indicates the increase of the critical size with the increase of Ti content.

The higher coercivity and the larger $J_r/J_s$ ratio in $x = 0.5$ titanomagnetite compared to Ti-free magnetite with the same size, can be partly explained by this increase of the single domain threshold size. The larger effect of the crystalline anisotropy in the titanomagnetite may also contribute this result.

## 4. Conclusion

Hysteresis properties in $x = 0.5$ titanomagnetite were examined with various sizes of grains. The present result combined with the measurement by Day et al. (1976) can give the variation of the hysteresis properties in a wide range of the grain size (0.1 μm ∿ 100 μm). Coercivity, remanence coercivity and $J_{rs}/J_s$ ratio in $x = 0.5$ titanomagnetite are much higher than those of Ti-free magnetite when their grain sizes are the same. Because titanomagnetites with a composition of $x = 0.5 \sim 0.7$ are commonly observed in basaltic rocks, the present result provides a basis to understand the magnetic properties in these rocks.

## 5. References

Butler, R.F., and S.K. Banerjee (1975) J. Geophys. Res., 80, 4049.
Day. R., M.D. Fuller, and V.A. Schmidt (1976) J. Geophys. Res., 81. 873.
Dunlop, D.J. (1972) Science, 176, 41.
Levi, S., and R.T. Merrill (1978) J. Geophys. Res., 83, 309.
Parry, L.G. (1965) Phil. Mag., 11, 303.
Rosin, P., and E. Rammler (1923) J. Inst. Fuel., 7, 29.
Soffel, H. (1971) Z. Geophys., 37, 451.
Stacey, F.D., and S.K. Banerjee (1974) "The Physical Principles of Rock Magnetism", Elsevier, Chap. 4.
Stoner, E.C., and E.P. Wohlfarth (1948) Phil. Trans. Roy. Soc. London, Ser. A, A240, 599.
Syono, Y. (1965) Japan J. Geophys., 4, 71.

(to be submitted to J. Geophys. Res.)

# A COMPUTER CONTROLLED ASTATIC MAGNETOMETER

Yoshiki FUJIWARA and Mitsuo YOSHIDA

Department of Geology and Mineralogy, Hokkaido University
Sapporo 060, JAPAN

A computer controlled automatic astatic magnetometer system was developed in the palaeomagnetic laboratory of the Department of Geology & Mineralogy, Hokkaido University. The objects of this development were to obtain reliable magnetic directions from very weak magnetized samples such as sedimentrary rocks and to achieve an automatic instrument of rapid and multi range measurements for various types of rock samples.

A schematic representation of this system is given in Fig.1. The magnet system suspended by 10 micron nylon fiber is covered by 3 layered mu-metal shield in order to adopt a various sources of magnetic noise. The specimen holder is located underneath the magnet system and rotate co-axially with system at a rate of 1 sec/rev. The specimen rotates evry 90° and stand still for a given moment in proportion to the sensitivity setting of this system for reorientation and reading command. As the specimen holder is placed below the magnet system at a fixed distance, the sensitivity of this instrument is able to vary in 7 ranges (Fig.2). In Fig. 2, the ranges of measurable intensities at different sensitivity settings are represented. Solid lines indicate ranges of sensitivity at the center of Helmholtz coil. Shaded lines

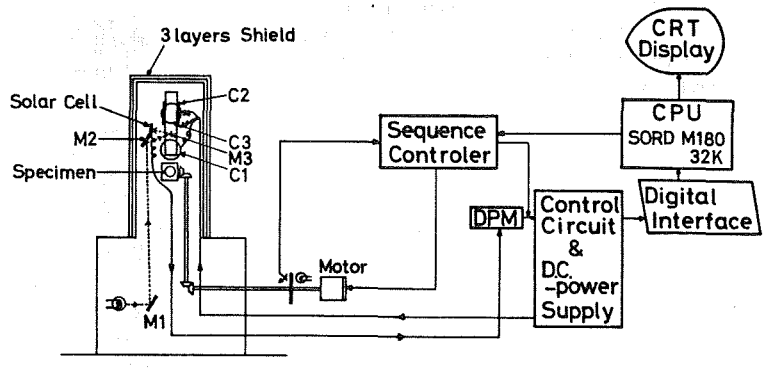


Fig.1 Shematic diagram of the automatic astatic magnetometer.

indicate ranges of magnetization intensities measurable at the corresponding sensitivity settings. For this purpose two small Helmholtz coils centered on and co-axial with each of the magnets are mounted.

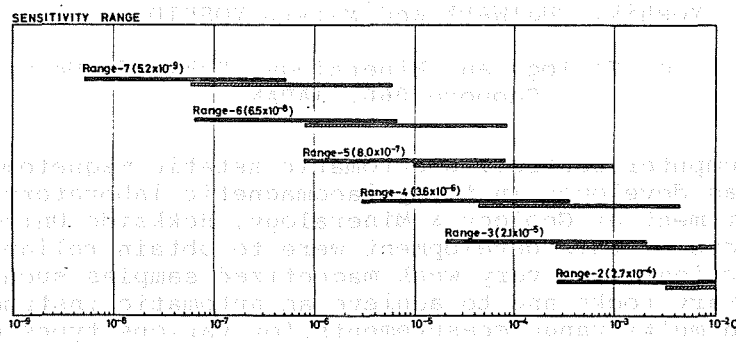


Fig.2 Ranges of measurable intensities at different settings.

The angular of deflections of the magnet system are determined optically. A light beam reflected from a small mirror attached on the magnet system is converted to analogue electric signal through a wedge shaped solar cell. The output voltage of the solar cell is read to degital binary coded singnal by A-D converter and send to the 32K bite microcomputer system. The magnetometer operation and signal read strobe are controlled by given program stored in a core memory of the sequence control system. The sequencial operation is shown in the flow chert of Fig.3.

Fig.3 Sequencial operation flow chert. S1-S5 mean sensitivity select switch on the central control unit.

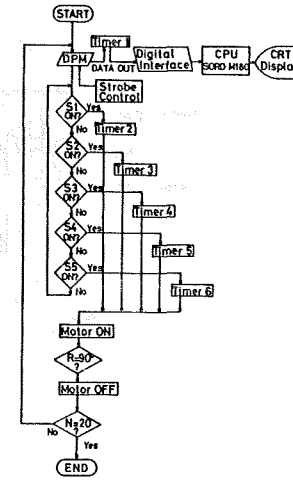

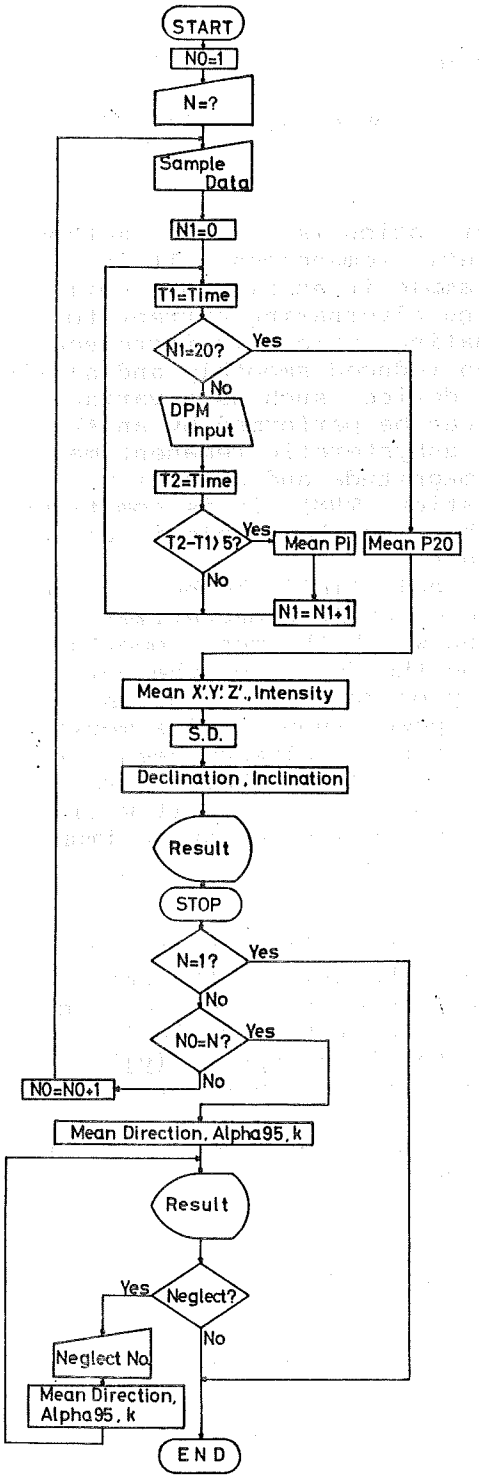


Measurements repeated 20 times for one specimen after which the specimen reoriented and are read out as the corresponding singnals of each position. The signals are stored in the memories of the computer. The direction of magnetization, each axis' intensity and total intensity obtained from the mounted speciem are calculated in accordance with stored program. The results of calculations are displayed on the CRT terminal of the computer system. Calculation and statistics flow chert is illustrated in Fig.4.

The time required to obtain the directions and intensity of a specimen magnetized to an intensity of $10^{-7}$ emu/cc is about 25 min., and to an intensity of $10^{-4}$ emu/cc is about 5 min.

(Submitted to Jour. Fac. Sci. Hokkaido University)

Fig.4 Flow chert of caluculation and statistics.

# OPTIMUM DESIGN OF COILS FOR AF DEMAGNETIZATION

Masaru KONO

Geophysical Institute, University of Tokyo, Tokyo 113, Japan

## 1. Introduction

Alternating field (AF) demagnetization is a useful method in assessing the stability of magnetic remanences. It is usually carried out by placing a sample in an air-core coil in a nonmagnetic space and supplying alternating current to the coil. The amplitude of alternating current is increased to a predetermined maximum and then reduced smoothly and slowly to zero by some voltage regulating device such as a variac. Another important experiment that can be performed by an AF demagnetizer is the acquisition of anhysteretic remanent magnetization (ARM). As the ARM has magnitude and stability similar to thermoremanent magnetization (TRM), it is sometimes used as a substitute for TRM when heating the sample is undesirable because of chemical changes.

Naturally, the higher the available field the better the AF demagnetizer. The maximum field of an AF demagnetizer is determined by several factors, among which the most important are the capacity of power supply and the design of the coil. In this paper, I shall outline the procedure to design an optimum shape of a coil for a given power supply and a working space (inner cavity). Similar analysis has already been carried out by Roy et al. (1973). They concluded that H/R rather than H should be maximized in an AF coil. However, it will be shown below that the quantity to be maximized for an optimum design is $H/\sqrt{R}$.

## 2. Variational Problem

Let the inner and outer radii of the coil be $y_1(x)$ and $y_2(x)$ where x is the coordinate along the axis of the coil, and let $y_1$ and $y_2$ be symmetric about the origin. We require $y_2(x)$ which maximizes the magnetic field at the origin for a given power supply ($V_{max}$, $I_{max}$) and the inner cavity ($y_1$).

The total resistance of the coil with a length of 2h is

$$R = \frac{4\pi\varepsilon\rho}{S^2}\int_0^h dx \int_{y_1}^{y_2} y\, dy = \frac{32\varepsilon\rho}{\pi D^4}\int_0^h (y_2^2 - y_1^2)\, dx \qquad (1)$$

the magnetic field at the center is

$$H = (\varepsilon I/S)\int_0^h dx \int_{y_1}^{y_2} y^2 (x^2 + y^2)^{-3/2}\, dy$$

$$= \frac{4\varepsilon I}{\pi D^2}\int_0^h \left[\frac{y_1}{\sqrt{x^2+y_1^2}} - \frac{y_2}{\sqrt{x^2+y_2^2}} + \log\frac{y_2 + \sqrt{x^2+y_2^2}}{y_1 + \sqrt{x^2+y_1^2}}\right] dx \qquad (2)$$

where $\rho$, $\varepsilon$, S, D and h are resistivity, packing factor, cross section and diameter of the wire and h the half length of the coil. For a given power supply, the resistance should take

a value so as the relation $I_{max} = V_{max}/R$ is satisfied. Therefore, we have a variational problem of finding the shape of the coil $y_2(x)$ which produces maximum field (H) for given in $y_1$ and R. The Euler's equation is

$$\frac{\partial}{\partial y_2}\left[-\frac{y_2}{\sqrt{x^2+y_2^2}} + \log\left|y_2 + \sqrt{x^2 + y_2^2}\right| + \frac{1}{2}\lambda(y_2^2 - y_1^2)\right] = 0,$$

which is reduced to

$$y_2^2(x^2 + y_2^2)^{-3/2} + \lambda y_2 = 0$$

Considering the boundary condition that $y_2 = b$ at $x = 0$, we obtain the equation specifying the outer shape of the coil

$$x = \sqrt{(b^2 y_2)^{2/3} - y_2^2} \quad . \tag{3}$$

## 3. Evaluation of Coil Performance

Actually, the maximum we obtained by (3) is not so pronounced and coils of other shapes can produce nearly as large magnetic fields. The capacity of a coil is more strongly influenced by the shape of inner cavity ($y_1$) and by the length/diameter ratio than by the outer shape.

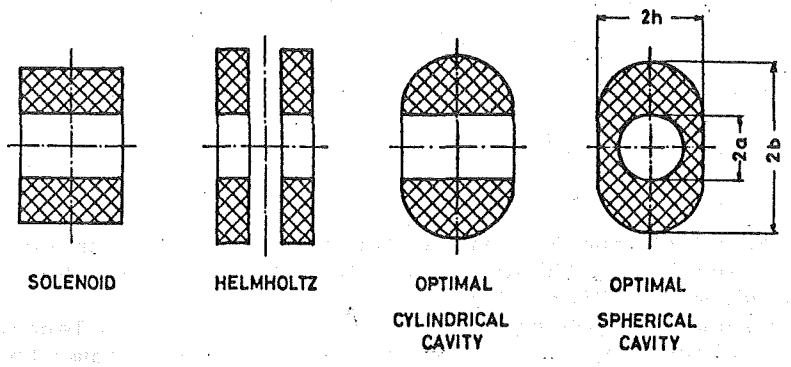


Fig. 1. Cross sections of four types of coils. In each case, inner and outer diameter are a and b, and length is 2h.

Fig. 1 shows sections of the four types of coils investigated below. In all cases, the inner and outer diameters at center and half the length are taken as a, b, and h, respectively. The "Helmholtz" type coil has a gap of width a at center and total length $2h = b$. Optimum-shaped coils has either a cylindrical or spherical cavity and an outer shape described by (3), with $h/b \leqq (4/27)^{1/4} = 0.6204$.

To fully utilize a given power supply the total resistance should satisfy

$$R = V_{max}/I_{max} \quad . \tag{4}$$

Referring to eq. (1), (3) can be satisfied by using a wire with a proper diameter,

$$D = \left[\frac{32\varepsilon\rho}{\pi R}\int_0^h (y_2^2 - y_1^2)\, dx\right]^{1/4} \quad . \tag{5}$$

Inserting this in eq. (2), we obtain

$$H = \left(\frac{\varepsilon R I^2}{2\pi}\right)^{1/2} \frac{\int_0^h \left\{\frac{y_1}{\sqrt{x^2+y_1^2}} - \frac{y_2}{\sqrt{x^2+y_2^2}} + \log \frac{y_2 + \sqrt{x^2+y_2^2}}{y_1 + \sqrt{x^2+y_1^2}}\right\} dx}{\left[\int_0^h (y_2^2 - y_1^2)\,dx\right]^{1/2}} \quad (6)$$

As wires are available only at discrete intervals, (6) is the upper limit of the magnetic field produced. Magnetic field can be inceased (at first) by making outer dimensions (b, h) larger. However, as the weight of a coil increases roughly as $b^2h$, it is unpracticable to make coils with too large dimensions. Let us take the following units to make the equations non-dimensional,

| | |
|---|---|
| Length | a |
| Electrical resistance | $\rho/a$ |
| Magnetic field | $I/a$ |
| Weight | $\beta a^3$ ($\beta$ is the density of wire) |

With these units, eq. (6) becomes

$$\frac{H}{\sqrt{\varepsilon R}} = \frac{\int_0^h \left\{\frac{y_1}{\sqrt{x^2+y_1^2}} - \frac{y_2}{\sqrt{x^2+y_2^2}} + \log \frac{y_2 + \sqrt{x^2+y_2^2}}{y_1 + \sqrt{x^2+y_1^2}}\right\} dx}{\left[\int_0^h (y_2^2 - y_1^2)\,dx\right]^{1/2}}, \quad (6a)$$

The weight W of this coil is

$$W/\varepsilon = 2\pi \int_0^h (y_2^2 - y_1^2)\,dx \quad (7)$$

The values of $H/\sqrt{\varepsilon R}$ and $W/\varepsilon$ are calculated for various combinations of b and h for the coils of Fig. 1. Some of the results are shown in Figs. 2-4.

Fig. 2 shows the changes in $H/\sqrt{\varepsilon R}$ and $W/\varepsilon$ for solenoid coils with various dimensions, while Fig. 3 is the same things for the coils with optimum outer shape and spherical cavity. Comparison of these two figures show that the changes in magnetic field and weight are quite similar in two different coils except that $H/\sqrt{\varepsilon R}$ is somewhat larger in optimum shape coils.

Fig. 4 shows the maximum field strength obtainable by four types of coils with various ratios of b/a. The difference in performance is very small between multi-layer solenoid and optimum shape-cylindrical cavity coils. As some special care and tools may be needed to produce coils with varying diameters, it is usually better to work with an ordinary solenoid. When the requirement on maximum field is quite severe or when the coil is anyway produced as separate thin slices for reasons of cooling, say, optimum shape coils will become useful.

The following is the recommended design process for AF demagnetizer coils.

(1) Select the type of the coil. Solenoids are usually the first choice. When field requirement is severe and when the inner cavity is spherical shape, the optimum shape coils may

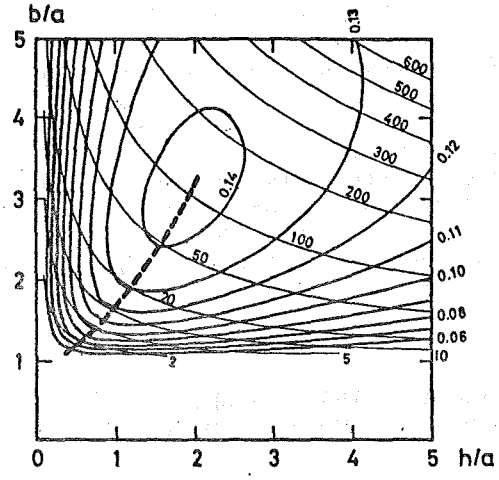


Fig. 2. Performance diagram of multi-layered solenoid. Values of $H/\sqrt{\epsilon R}$ (thick lines) and $W/\epsilon$ (thin lines) are indicated in nondimensional units. Thick broken line indicates the locus of maximum $H/\sqrt{\epsilon R}$ for given $W/\epsilon$.

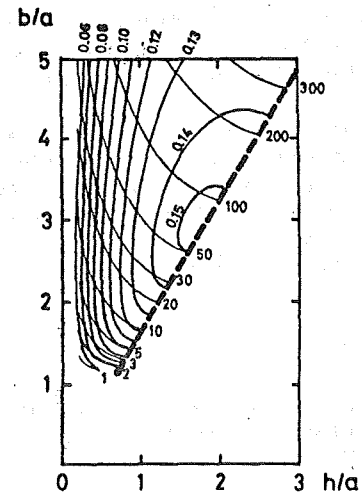


Fig. 3. Performance diagram of optimum outer shape-spherical inner cavity coil. For legend, see Fig. 2.

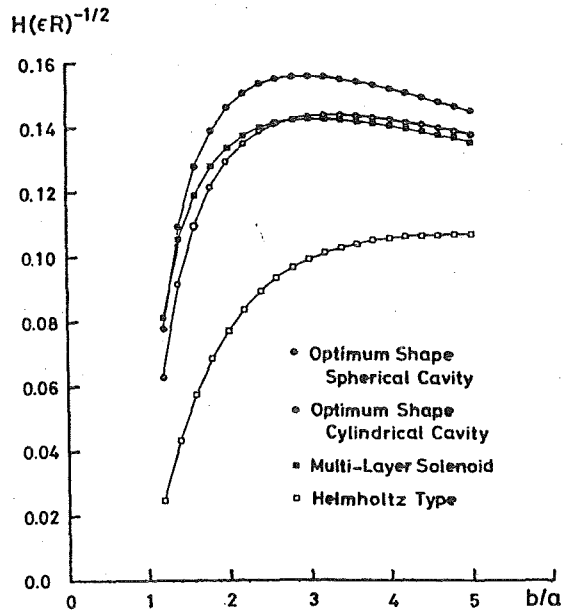


Fig. 4. Maximum magnetic field obtained by various types of coils having specified b/a values. Absolute maxima are reached in optimum shape coils and solenoid at about $b/a \sim 3$.

be chosen. If uniformity rather than magnitude of the field is required, Helmholtz type coils may be produced.
(2) Select the permissible range of weight. This, in turn, decides the outer dimensions h and b through the use of Figs. 2-3.
(3) Decide the proper diameter of wire from (1) so that the d.c. resistance matchs the given power supply as (4). Since wires are available only at discrete intervals, minor adjustment in h and b may be required after the actual wire size is selected.
(4) The maximum magnetic field may now be calculated using Figs. 2-4.

Reference

Roy, J.L., J. Reynolds, and E. Sanders (1973) Publ. Earth Phys. Branch, 44, 37, Department of Energy, Mines and Resources, Ottawa, Canada.

(Submitted to J. Geophys. Res.)

# STATISTICS OF PALEOMAGNETIC INCLINATION DATA

Masaru KONO

Geophysical Institute, University of Tokyo, Tokyo 113, Japan

## Introduction

In paleomagnetism, it is usually assumed that the directions of natural remanent magnetization (NRM) in a rock unit (lava flow, a horizon in a sediment, etc.) follow an azimuthally symmetric distribution introduced by Fisher (1953) :

$$f(\omega, \psi)\, d\omega\, d\psi = \frac{\kappa}{4\pi \sinh \kappa} e^{\kappa \cos\omega} \sin\omega\, d\omega\, d\psi \qquad (1)$$

where $\omega$ is the angular displacement from the mean, $\psi$ the azimuthal angle, and $\kappa$ the precision parameter describing how well the distribution is concentrated near the true mean direction. The Fisherian analysis can, in principle, be applied only when the complete knowledge of NRM directions are available; i.e., both the inclination I and declination D are known. However, it has become more and more important to study samples which contain only partial information of remanence directions. In deep borings such as done in Deep Sea Drilling Project (DSDP), rocks are recovered as fragmentary pieces for which only vertical is known and even "relative" declinations are not available. Briden and Ward (1966) developed statistical methods for such cases. They started from the Fisher distribution and obtained expressions relevant for paleomagnetic data of inclination only. However, their expressions contain infinite series which they calculated numerically, and interpolation in tables or graphical approach is required for the derivations of most probable values of true inclination and precision parameter. Since the precision parameter $\kappa$ changes widely, the use of their tables and figures sometimes leads to substantial errors. Because of this practical inconvenience, the method of Briden and Ward has not always been applied to real problems as it should. The main purpose of this paper is to develop Briden and Ward's analysis in such a way that all the statistical parameters can be obtained easily and exactly, without references to tables and figures, and to show a way to compare results with those from the ordinary Fisherian analysis.

## Analytical Expressions for $\theta_0$ and $\kappa$

In Fisher distribution (1), $\omega$ and $\psi$ form polar coordinates centered about the true mean direction. If we move to another polar coordinate system $\theta$, $\phi$ centered about the vertical, the two systems are related by

$$\cos\omega = \cos\theta_0 \cos\theta + \sin\theta_0 \sin\theta \cos\phi ,$$

and

$$\sin\omega\, d\omega\, d\psi = \sin\theta\, d\theta\, d\phi ,$$

where $\theta_0$ is the angular distance between the true mean direction and the vertical (Figure 1). The frequency density function (1) in the new coordinates is then

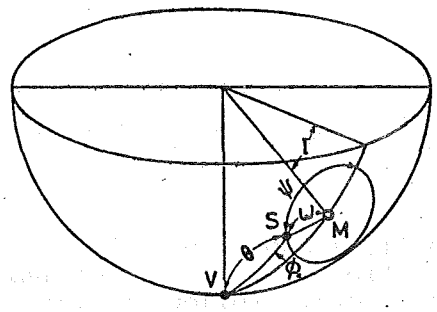


Fig. 1 Relation between two polar coordinate systems $(\omega, \psi)$ centered about the true mean direction and $(\theta, \phi)$ centered about the vertical. The true inclination is $I = \frac{\pi}{2} - \theta_0$ .

$$f(\theta,\phi) = \frac{\kappa}{4\pi\sinh\kappa} \exp(\kappa\cos\theta_0\cos\theta + \kappa\sin\theta_0\sin\theta\cos\phi)\sin\theta \quad (2)$$

Using the relation

$$\frac{1}{2\pi}\int_0^{2\pi} e^{x\cos\phi}\, d\phi = \frac{1}{2\pi}\sum_{n=0}^{\infty}\frac{x^n}{n!}\int_0^{2\pi}\cos^n\phi\, d\phi$$

$$= \sum_{n=0}^{\infty}\frac{x^{2n}}{2^{2n}(n!)^2}$$

which is the infinite-series expression of 0-th order modified Bessel function $I_0(x)$, the marginal distribution $f(\theta)$ can be obtained from (4).

$$f(\theta) = \int_0^{2\pi} f(\theta, \phi)\, d\phi \quad (3)$$

$$= \frac{\kappa}{2\sinh\kappa}\exp(\kappa\cos\theta_0\cos\theta)\, I_0(\kappa\sin\theta_0\sin\theta)\sin\theta.$$

The problem now is to determine simultaneously $\theta_0$ and $\kappa$ from observed distribution of $\theta$. Using the following integration formulas,

$$\int_0^{\pi}\sin^{2n}\theta\cos^{2m}\theta\, d\theta = \frac{\pi(2m-1)!!\ (2n-1)!!}{(2m+2n)!!}$$

$$\int_0^{\pi}\sin^{2n+1}\cos^{2m}\, d\theta = \frac{2(2m-1)!!\ (2n)!!}{(2m+2n+1)!!}$$

$$\int_0^{\pi}\sin^{n}\theta\cos^{2m+1}\theta\, d\theta = 0$$

Briden and Ward (1966) obtained expressions for the expected values of $\cos\theta$ and $\sin\theta$

$$E(\cos\theta) = \int_0^{\pi} \frac{\kappa}{2\sinh\kappa} \sum_{n=0}^{\infty}\sum_{m=0}^{\infty} \frac{(\kappa\cos\theta_0\ \cos\theta)^m}{m!} \frac{(\kappa\sin\theta_0\ \sin\theta)^{2n}}{2^{2n}(n!)^2} \sin\theta\cos\theta\, d\theta$$

$$= \frac{\kappa}{\sinh\kappa} \sum_{n=0}^{\infty}\sum_{m=0}^{\infty} \frac{(\kappa\cos\theta_0)^{2m+1}(\kappa\sin\theta_0)^{2n}}{(2m+1)!\ 2^{2n}(n!)^2} \frac{(2m+1)!!(2n)!!}{(2m+2n+3)!!} \quad (4)$$

and likewise

$$E(\sin\theta) = \frac{\pi\kappa}{2\sinh\kappa} \sum_{n=0}^{\infty}\sum_{m=0}^{\infty} \frac{(\kappa\cos\theta_0)^{2m}(\kappa\sin\theta_0)^{2n}}{(2m)!\ 2^{2n}(n!)^2} \frac{(2m-1)!!(2n+1)!!}{(2m+2n+1)!!} \quad (5)$$

Although Briden and Ward decided that equations (4) and (5) cannot be reduced to an easier form, (4) can actually be reduced rather easily. In fact, expectations of any power of cosθ or any even power of sinθ or their products can be calculated by methods similar to the following. We shall only treat the integration of $E(\cos^n\theta)$ in this paper.

The moment generating function of cosθ, $M_{\cos\theta}(t)$, is such a function that the moments of any power of cosθ about the origin can be calculated by differentiation (Carnahan et al., 1969).

$$E(\cos^n\theta) = \int_0^{\pi} f(\theta)\ \cos^n\theta\ d\theta$$

$$= \left[\frac{\partial^n M_{\cos\theta}(t)}{\partial t^n}\right]_{t=0}$$

In the present case

$$M_{\cos\theta}(t) = E(e^{t\cos\theta})$$

$$= \int_0^{\pi} e^{t\cos\theta}\ f(\theta)\ d\theta$$

$$= \frac{\kappa}{2\sinh\kappa} \int_0^{\pi} \exp(t\cos\theta + \kappa\cos\theta_0\cos\theta)\ I_0(\kappa\sin\theta_0\sin\theta)\sin\theta\, d\theta$$

$$= \frac{\kappa}{2\sinh\kappa} \sum_{n=0}^{\infty}\sum_{m=0}^{\infty} \frac{(\kappa\sin\theta_0)^{2n}}{2^{2n}(n!)^2} \frac{(\kappa\cos\theta_0+t)^m}{m!} \int_0^{\pi} \sin^{2n+1}\theta\cos^m\theta\, d\theta .$$

Using integration formulas mentioned above,

$$M_{\cos\theta}(t) = \frac{\kappa}{2\sinh\kappa} \sum_{n=0}^{\infty}\sum_{m=0}^{\infty} \frac{(\kappa\sin\theta_0)^{2n}(\kappa\cos\theta_0+t)^{2m}}{2^{2n}(n!)^2(2m)!} \frac{2(2m-1)!!(2n)!!}{(2n+2m+1)!!} .$$

$$= \frac{\kappa}{\sinh\kappa} \sum_{n=0}^{\infty}\sum_{m=0}^{\infty} \frac{(\kappa\sin\theta_0)^{2n}(\kappa\cos\theta_0+t)^{2m}(n+m)!}{n!\ m!\ (2n+2m+1)!}$$

To sum the double infinite series, we replace n + m by n, then the range of summation of m becomes from 0 to n and

$$M_{\cos\theta}(t) = \frac{\kappa}{\sinh\kappa} \sum_{n=0}^{\infty} \sum_{m=0}^{n} \frac{(\kappa\sin\theta_0)^{2n-2m}(\kappa\cos\theta_0+t)^{2m}\, n!}{(2n+1)!\; m!\; (n-m)!}$$

$$= \frac{\kappa}{\sinh\kappa} \sum_{n=0}^{\infty} \frac{(\kappa\sin\theta_0)^{2n}}{(2n+1)!} \left[1 + \left(\frac{\kappa\cos\theta_0+t}{\kappa\sin\theta_0}\right)^2\right]^n$$

$$= \frac{\kappa}{\sinh\kappa} \sum_{n=0}^{\infty} \frac{1}{(2n+1)!} \left[t^2 + 2\kappa t\cos\theta_0 + \kappa^2\right]^n.$$

Therefore, we finaly obtain the analytical form of moment generating function,

$$M_{\cos\theta}(t) = \frac{\kappa}{\sinh\kappa} \frac{\sinh[\kappa^2 + 2\kappa t\cos\theta_0 + t^2]}{\kappa^2 + 2\kappa t\cos\theta_0 + t^2} \tag{6}$$

Any moment of $\cos\theta$ can now be easily calculated from (6). In particular,

$$E(\cos\theta) = \cos\theta_0 L(\kappa), \tag{7}$$

$$E(\cos^2\theta) = \cos^2\theta_0 + \frac{1 - 3\cos^2\theta_0}{\kappa} L(\kappa), \tag{8}$$

where L is the Langevin function

$$L(x) = \coth x - \frac{1}{x}.$$

Expectation of $\sin\theta$ (5) cannot be reduced to such an elementary expression.

Since $f(\theta)$ is a two-parameter function, it can be completely specified by selecting any two of the independent moments, such as $E(\cos\theta)$, $E(\sin\theta)$, $E(\cos^2\theta)$, etc. Here, we choose the first and second moments of $\cos\theta$ and equate them with the mean values derived from the observed inclinations. The best estimates of the mean inclination ($I = \frac{\pi}{2} - \theta_0$) and the precision parameter (k) can be determined by solving the simultaneous equations

$$\sin I \left(\coth k - \frac{1}{k}\right) = \frac{1}{N} \sum_{i=1}^{N} \sin I_i \tag{9}$$

$$\sin^2 I + \frac{1 - 3\sin^2 I}{k} \left(\coth k - \frac{1}{k}\right) = \frac{1}{N} \sum_{i=1}^{N} \sin^2 I_i \tag{10}$$

where $I_i$ ($i = 1, 2, \ldots N$) are the observed inclinations ($I_i = \frac{\pi}{2} - \theta_i$). The solutions of (9) and (10) can easily be obtained by iteration. When we calculate statistics of virtual geomagnetic longitude (VGL), we can simply replace inclination by VGL in the above formulas.

## Discussion

Fig. 2 shows the error in the estimate of mean inclination

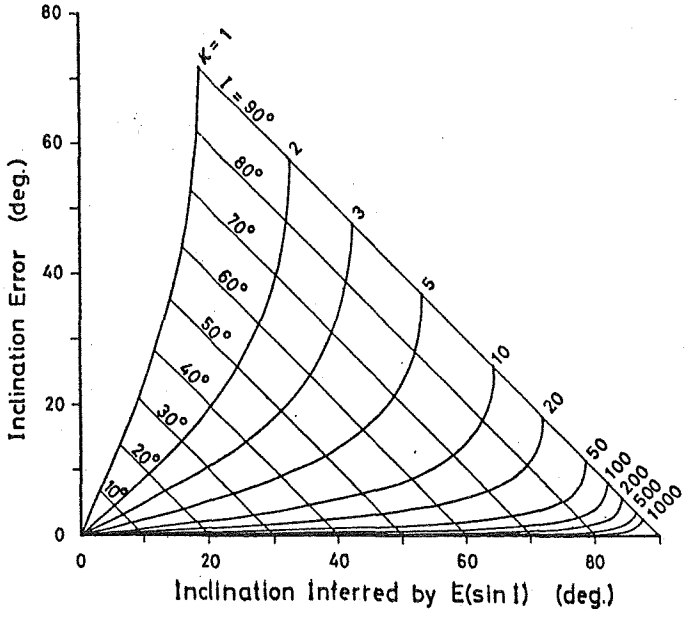


Fig. 2. Errors in the estimate of inclination when only the mean value of sin $I_i$ is known.

when the correct statistics is not used in the calculation. In this figure, the abscissa is the arcsine of the mean of observed inclinations which is quite similar to the simple mean of the inclinations, while the ordinate is the difference between the true mean and the calculated value (abscissa). As expected, the error is small when the precision parameter ($\kappa$) is large, except at very high inclinations.

Fig. 3 is a diagram which may serve as a quick reference to obtain rough estimates of the true mean inclination and the precision parameter. The abscissa and ordinate represent theoretical values of the mean and the standard deviation of sin $I_i$ for a combination of I and $\kappa$. This figure may be useful to estimate I and $\kappa$, but since the exact expressions are quite simple, it will be better to calculate these values from eqs. (9) and (10).

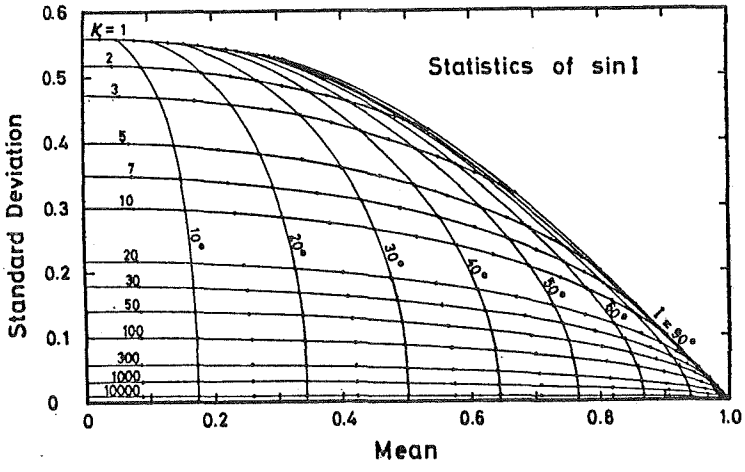


Fig. 3. Values of true inclination (I) and precision parameter ($\kappa$) corresponding to combinations of the mean and standard deviation of sin $I_i$.

# AUTHOR INDEX